A Study of the Epstein Barr Virus Nuclear Antigens EBNA3A and EBNA3C *in vitro* and *in vivo*

Christine Theresa Styles

Thesis submitted for the degree of Doctor of Philosophy

Section of Virology

Department of Medicine

Imperial College London

October 2018

Abstract

The lymphotropic γ-herpesvirus Epstein Barr virus (EBV) is ubiquitous within the human population, but it is etiologically associated with several B cell malignancies. *In vivo,* EBV infects and activates naïve B cells to differentiate into memory B cells (MBC), where viral persistence is established for the lifetime of the host. The oncogenic EBV nuclear antigens EBNA3A and EBNA3C are transcriptional regulators required for EBV-mediated oncogenic progression and cell cycle deregulation. This study encompasses *in vitro* and *in vivo* approaches to further investigate the roles of EBNA3A and EBNA3C.

To further characterise the independent and overlapping functions of EBNA3A and EBNA3C, bacterial artificial chromosome (BAC) and estrogen receptor (ER) fusion technology were used to generate a recombinant EBV where EBNA3A and EBNA3C were both conditionally expressed. Proliferation and viability analysis of primary B cells infected with this virus *in vitro* revealed the absence of EBNA3A and EBNA3C is cumulatively detrimental to cells, and activation of cell cycle regulatory factors was more profound. Protein and qPCR analysis of EBV-infected cells lacking both EBNA3A and EBNA3C also revealed elevated levels of the plasma cell (PC) differentiation factors $p18^{INK4c}$ and BLIMP-1 at 20 days post infection. Consistent with increased PC differentiation factors, flow cytometric analysis showed EBNA3A/EBNA3C-null cells had a PC-like phenotype, with increased CD138 and CD38 cell surface antigens, alongside elevated immunoglobulin production. This suggests that alongside their oncogenic functions, EBNA3A and EBNA3C have evolved to suppress the B cell to PC differentiation pathway after infection with EBV. This likely favours the alternative MBC differentiation pathway, and therefore long-term EBV latency and persistence.

To assess the roles of EBNA3A and EBNA3C *in vivo*, a mouse model with human immune system components was established. Humanised mice were infected with EBV lacking the EBNA3A and EBNA3C genes. Immunohistochemistry and qPCR for viral factors demonstrated EBV can persist in the absence of EBNA3A and EBNA3C expression for 6 weeks, and viral pathology was seen. The viability of using conditional ER-fusion recombinant EBV viruses *in vivo* was also assessed.

Declaration of Originality

I hereby declare that all of the work presented in this thesis is a result of my work and been produced by me, unless otherwise stated in the text.

Christine Theresa Styles, October 2018

Copyright Declaration

The copyright of this thesis rests with the author and is made available under a Creative Commons Attribution Non-Commercial No Derivatives licence. Researchers are free to copy, distribute or transmit the thesis on the condition that they attribute it, that they do not use it for commercial purposes and that they do not alter, transform or build upon it. For any reuse or redistribution, researchers must make clear to others the licence terms of this work.

Acknowledgments

First and foremost, I would like to dedicate this thesis to the memory of my wonderful supervisor Prof. Martin Allday. I am deeply grateful for his guidance and wisdom, and for the opportunity to do a PhD in his lab. I wish to thank Prof. Paul Farrell for taking over supervision of my PhD and helping in the writing of this thesis, and thanks go to my co-supervisor Dr. Rob White for advice and help throughout my PhD.

I would like to thank all of the members of the Allday lab. Thank you to Quentin for teaching me everything I know and for always being a supportive and helping hand, Gillian for always being there and making sure everything ran smoothly in the lab, Adam for always listening patiently during my out-loud lab decision making and Kostas for all his help and guidance. I am also grateful to the MRC for my studentship and support throughout my PhD.

I couldn't have done this PhD without the support, encouragement and love of my whole family, and I will forever be grateful to my Dad and Mum, Grandma and Grandad Cats, Grandma and Grandad Sadie and my wonderful sisters Bex, Nelly and Megan for their constant and unwavering belief in me. Thank you also to Tim, as well as the Major Family, for always being encouraging and supportive. I also wish to thank all of my wonderful friends in Essex, London and afar. Special thanks go to Bedding for always being enthusiastic about my work, and to my 57 Ongar Road housemates; Christian, Alice, Medic, James, Ed, Emily and Sam, you all made my Imperial College experience unforgettable.

Finally, I would like to express my gratitude and love for my amazing boyfriend Lloyd, I could not have done this without you. I am very thankful for you, and cannot express how grateful I am for your encouragement, assurances and support through my many years of study.

Abbreviations

3AERT2	EBV BAC with an oestrogen receptor fusion to EBNA3A
3CERT2	EBV BAC with an oestrogen receptor fusion to EBNA3C
3A3CERT2	EBV BAC with an oestrogen receptor fusion to EBNA3A and EBNA3C
3AKO	EBV BAC with deletion in EBNA3A
3BKO	EBV BAC with deletion in EBNA3B
3CKO	EBV BAC with deletion in EBNA3C
ALAS1	5'-aminolevulinate synthase 1
Amp	Ampicillin
APS	Ammonium persulphate
BAC	Bacterial artificial chromosome
BCL2	B cell lymphoma protein 2
BCL6	B cell lymphoma protein 6
BCL2L11	Gene encoding BIM
BCR	B cell receptor
BIM	BCL2-interacting mediator
BL	Burkitts lymphoma
BLIMP-1	B lymphocyte-induced maturation protein
BSA	Bovine serum albumin
CD	Cluster of differentiation
CD40-L	CD40 ligand
CDK	Cyclin-dependent kinase
CDKI	Cyclin-dependent kinase inhibitors
CDKN1A	Gene encoding cyclin-dependent kinase inhibitor 1A ($p21^{WAF1/CIP1}$)
CDKN1B	Gene encoding cyclin-dependent kinase inhibitor 1B ($p27^{KIP1}$)
CDKN1C	Gene encoding cyclin-dependent kinase inhibitor 1C ($p57^{KIP2}$)
CDKN2A	Gene encoding cyclin-dependent kinase inhibitor 2A ($p16^{INK4a}$)
CDKN2B	Gene encoding cyclin-dependent kinase inhibitor 2B ($p15^{INK4b}$)
CDKN2C	Gene encoding cyclin-dependent kinase inhibitor 2A ($p18^{INK4c}$)
cDNA	Complementary DNA
ChIP	Chromatin immunoprecipitation
ChIP-qPCR	Chromatin immunoprecipitation followed by qPCR
ChIP-seq	Chromatin immunoprecipitation followed by deep sequencing
CHK2	Checkpoint kinase 2
COBLL1	Cordon-bleu WH2 repeat protein like 1
Cm	Chloramphenicol
Cp	C promoter
CpG	Cytosine-phosphate-guanine dinucleotide
CtBP	C-terminal binding protein
ddH_20	Double distilled water
DDR	DNA damage response
DLBCL	Diffuse large B cell lymphoma
DMSO	Dimethyl sulphoxide

DNA	Deoxyribonucleic acid
DTT	Dithiothreitol
DZ	Dark zone
EBER	Epstein-Barr virus encoded small RNA
EBNA	Epstein-Barr virus nuclear antigens
EBV	Epstein-Barr virus
ECL	Enhanced chemiluminescence
E.coli	*Escherichia Coli*
EDTA	Ethylenediamine tetre-acetic acid
ERT2	4-hydroxytamoxifen-conditional oestrogen receptor
EtBr	Ethidium bromide
EZH2	Enhancer of zeste homologue-2
E3KO	EBV BAC lacking the entire EBNA3 locus
FACS	Fluorescence-activated cell sorting
FCA	Flow cytometric analysis
FCS	Foetal calf serum
FDC	Follicular dendritic cell
FTh	Follicular T helper cell
GC	Germinal centre
GFP	Green fluorescence protein
H3K27ac	Histone 3 lysine 27 acetylation
H3K27me3	Histone 3 lysine 27 trimethylation
H3K4me3	Histone 3 lysine 4 trimethylation
HAT	Histone acetyltransferase
HDAC	Histone deacetylase
HL	Hodgkins lymphoma
HPV	Human papilloma virus
HRP	Horseradish peroxidase
HT	4-hydroxtamoxifen
Hu-mice	Humanised mice
HWB	Hepatocyte wash buffer
Ig	Immunoglobulin
IL	Interleukin
IL-2Rγ	Interleukin-2 receptor common γ-chain
IRF4	Interferon-regulatory factor 4
Kan	Kanamycin
Kb	Kilobases
kDa	Kilo Daltons
KO	Knock-out
KSHV	Karposi's sarcoma associated herpes virus
LB	Luria-Bertani broth
LCL	Lymphoblastoid cell line
LCV	Lymphocrypovirus
LDB	Liver digestion buffer
LMP	Latent membrane protein

LP	Leader protein
LZ	Light zone
Kan	Kanomycin
MACS	Model-based analysis of ChIP
MBC	Memory B cell
MHC	Major histocompatibility complex
miRNA	microRNA
mQH_20	Millipore purified water
mRNA	Messenger RNA
min	Minute
NCoR	Nuclear receptor co-repressor
NHP	Non-human primate
NK cell	Natural killer cell
NOD	Non-obese diabetic
NPC	Nasopharyngeal carcinoma
NRG	NOD/Rag$^{-/-}$/IL-2Rγ^{null} humanised mouse
NSG	NOD/*scid*/IL-2Rγ^{null} humanised mouse
o/n	Overnight
ORF	Open reading frame
OriP	Origin of replication
OriL	Origin of lytic replication
pRb	Phosphorylated retinoblastoma protein
PAGE	Polyacrylamide gel electrophoresis
PBL	Peripheral blood leucocyte
PBMC	Peripheral blood mononuclear cells
PBS	Phosphate buffered saline
PBS-T	Phosphate buffered saline containing 0.1% (v/v) Tween
PC	Plasma cell
PcG	Polycomb group
PCR	Polymerase chain reaction
pi	Post infection
PMSF	Phenylmethanesulfonyl fluoride
Pol II	RNA polymerase II
PRC	Polycomb repressive complex
PTLD	Post-transplant lymphoproliferative disease
Qp	Q promoter
qPCR	Quantitative PCR
RAG	Recombinase activating gene
Rb	Retinoblastoma protein
RBPJκ/CBF1	Recombinant binding protein J kappa/C-promoter binding factor 1
REF	Rat embryonic fibroblasts
Rev	Revertant
RIPA	Radioimmunoprecipitation
RNA	Ribonucleic acid
Rp	R promoter

RT-qPCR	Reverse transcription qPCR
RUNX	RUNT-related transcription factor
SB	Super broth
SD	Standard deviation
SDS	Sodium dodecyl sulphate
Seq	Sequencing
Ser 5	Serine 5 (of Pol II)
Scid	Severe combined immunodeficiency
Sin3A	SIN3 transcription regulator family member A
SOC media	Super optimal broth with catabolite repression
STET	Solution containing sucrose, titron, EDTA and tris
SV40	Simian virus 40
TAP	Tandem affinity purification
TBE	Tris-borate-EDTA
TCR	T cell receptor
TE	Tris-EDTA
TEMED	Tetramethylethlenediamine
Tet	Tetracycline
TF	Transcription factor
Th cell	T helper cell
TMX-food	Tamoxifen impregnated mouse feed
TR	Terminal repeats
TSS	Transcription start site
v/v	Volume by volume
w/v	Weight by volume
WB	Western blot
Wp	W promoter
WT	Wild-type
XBP-1	B-box binding protein-1
Zp	Z promoter

Table of Contents

Abstract **2**

Declaration of Originality **3**

Copyright Declaration **3**

Acknowledgments **4**

Abbreviations **5**

Table of Contents **9**

List of Figures **19**

List of Tables **22**

1. Chapter I: Introduction **23**

1.1. B cell biology *23*

1.1.1. Role of B cells and antibodies in the immune system 23

1.1.2. Antigen mediated B cell activation 25

1.1.3. Germinal centre reaction 26

1.1.4. Plasma cell differentiation 29

1.2. Epstein Barr virus (EBV) *31*

1.2.2. Discovery of EBV 31

1.2.3. EBV transmission, tropisms and life cycle 32

1.2.4. EBV latency in vivo: Germinal centre model of EBV persistence 34

1.2.5. Lytic reactivation 36

1.2.6. EBV latency in vitro 37

1.2.7. Transcription of latent genes from the EBV genome 39

1.2.8. EBV latency-associated proteins 40

1.2.8.1. EBNA1 40
1.2.8.2. EBNA2 41
1.2.8.3. The EBNA3 family 43
1.2.8.4. EBNA-LP 45
1.2.8.5. Latent membrane proteins 46
1.2.8.5.1. LMP1 46
1.2.8.5.2. LMP2A and LMP2B 47
1.2.8.6. EBV RNAs and miRNAs 48
1.2.9. EBV associated diseases 49
1.2.9.1. Infectious mononucleosis 49
1.2.9.2. B cell lymphomas 49
1.2.9.2.1. Burkitts lymphoma 50
1.2.9.2.2. Hodgkins lymphoma 51
1.2.9.2.3. Immunodeficiency-associated lymphoproliferative disease 52
1.2.9.2.4. Diffuse large B cell lymphoma 52
1.2.9.3. EBV-associated carcinoma 53
1.2.9.4. EBV and autoimmune diseases 54
1.2.10. Immune responses to EBV 55
1.3. EBNA3 proteins are transcriptional regulators that affect host gene expression 57
1.3.1. Cell cycle regulation 57
1.3.1.1. The cell cycle 57
1.3.1.2. G1 phase progression and regulation 59
1.3.1.3.1. The INK4 family 61
1.3.1.3.2. The CIP/KIP family 62
1.3.1.4. The DNA damage response and cell cycle checkpoints 63
1.3.2. Control of gene regulation by polycomb proteins 64
1.3.3. EBNA3 mediated deregulation of the cell cycle 66
1.3.3.1. EBNA3 regulatory mechanisms 66

1.3.3.2. Transcriptional repression of $p16^{INK4a}$ and the INK4a-ARF-INK4b locus 69

1.3.3.3. Translational and proteasomal degradation of the CIP/KIP family 71

1.3.3.4. Anti-apoptotic functions of EBNA3A and EBNA3C 74

1.4. Recombinant EBV viruses allow analysis of EBNA3 function 76

1.4.1. Use of BAC-derived EBV 76

1.4.2. Recombinant EBV viruses available for the study of EBNA3 proteins 77

1.5. Epstein Barr virus infection in vivo 79

1.5.1. Limitations of research in vitro 79

1.5.2. In vivo mouse models of human disease 80

1.5.3. Use of tamoxifen systems for gene modification in mouse models 82

1.5.4. Mouse models with human immune system components 84

1.5.5. EBV infection of mice with human immune system components 88

1.5.5.1. Studying EBV-associated tumorigenesis in mice 88

1.5.5.2. The role of EBNA3B in vivo 90

1.5.5.3. Limitations of humanised mice in EBV research 91

1.6. Aims of this study 94

1.6.1. Aims for the study of EBNA3A and EBNA3C in vitro 94

1.6.2. Aims for the study of EBNA3A and EBNA3C in vivo 94

2. Chapter II: Materials and Methods 95

2.1. Solutions and buffers 95

2.2. Cell culture protocols 100

2.2.1. Maintenance of cell lines and culture medium 100

2.2.2. Cell line storage and thawing 102

2.2.3. Counting and harvesting cells 102

2.2.4. In vitro induction of plasma cell differentiation 103

2.3. Isolation of surface marker specific cell populations 103

2.3.1. Isolation of peripheral blood leucocytes (PBLs) from peripheral blood 103

2.3.2. Purification of $CD19^+$ primary B cells 104

2.3.3. Purification of $CD34^+$ hematopoietic stem cells 105

2.4. Cloning and techniques for DNA manipulation 106

2.4.1. Small scale preparation of plasmid DNA (mini-prep) 107

2.4.2. Large scale preparation of BAC DNA (maxi-prep) by caesium chloride density gradient 107

2.4.3. Restriction enzyme digest 108

2.4.4. Agarose gel electrophoresis 109

2.4.5. Gel extraction of DNA fragments 109

2.4.6. DNA ligation 109

2.4.7. Transformation of DNA into competent bacteria 109

2.4.8. Pulsed field gel electrophoresis (PFGE) 110

2.4.9. Klenow-mediated blunt-ending of 5' overhang 110

2.5. Generation of recombinant EBV virus 110

2.5.1. Production of competent bacteria 110

2.5.2. Homologous recombination of target constructs and EBV-BAC 111

2.5.2.1. Production of co-integrants by recombination between target constructs and EBV-BAC 111

2.5.2.2. Production of competent bacteria containing BAC co-integrant 112

2.5.2.3. Resolution of co-integrants of target constructs and EBV-BAC 112

2.5.3. Generating HEK-293 cell clones transfected with EBV-BAC 113

2.5.3.1. Transfection of HEK-293 cell with EBV-BAC 113

2.5.3.2. Isolation of 293 HEK clones transfected with EBV-BAC 114

2.5.3.3. Episome rescue by low molecular weight extraction of DNA from transfected cells to validate EBV recombinant 114

2.5.3.4. Electroporation of DNA into bacterial cells 115

2.6. Virus production and infection 116

2.6.1. Generating infectious virus from 293 HEK cells with EBV-BAC 116

2.6.2. Concentrating virus 116

2.6.3. Virus titration 116

2.6.4. Infection of primary B cells with recombinant EBV viruses 117

2.7. Gene expression analysis 118

2.7.1. RNA and DNA analysis 118

2.7.1.1. RNA extraction 118

2.7.1.2. DNA extraction 118

2.7.1.3. Reverse-transcription 119

2.7.1.4. Real-time quantitative PCR (qPCR) using SYBR Green 119

2.7.1.5. Real-time quantitative PCR (qPCR) using Taqman 120

2.7.2. Protein analysis 121

2.7.2.1. Protein extraction 121

2.7.2.2. SDS-PAGE and western blotting 122

2.8. Flow cytometric analysis 124

2.8.1. Analysis of proliferation and cell cycle distribution 125

2.8.2. Lymphocyte surface marker analysis 126

2.8.2.1. Assessing purity of $CD19^+$ purified B cells 126

2.8.2.2. Quantification of humanised mouse engraftment and lymphocyte composition 126

2.8.2.2.1. Basic analysis of human CD45 and CD19 cell engraftment in humanised mice 126

2.8.2.2.2. Analysis of human B and T lymphocyte engraftment in humanised mice 127

2.8.2.2.3. Analysis of B lymphocyte composition 127

2.8.3. Staining of intracellular and extracellular immunoglobulin 128

2.9. Generation of mice with human immune system components 128

2.9.1. Mice 128

2.9.2. Sub-lethal irradiation and injection of $CD34^+$ hematopoietic stem cells of newborn mice for establishment of human immune system components 129

2.10. Protocols for analysis of humanised mice 129

2.10.1. Infection of humanised mice with recombinant EBV viruses 129

2.10.2. Use of tamoxifen impregnated food 130

2.10.3. Venesection (blood sampling) 130

2.10.4. Terminal analysis of humanised mice 130

2.10.4.1. Cardiac puncture for analysis of peripheral blood 130

2.10.4.2. Terminal analysis of spleens from humanised mice 131

2.10.4.2.1. Immunohistochemistry 131

2.10.4.2.1.1. Spleen fixation 131

2.10.4.2.1.2. Dewaxing and antigen retrieval 131

2.10.4.2.1.3. Primary antibody staining 131

2.10.4.2.1.4. Visualisation 132

2.10.4.2.2. Mechanical disruption of splenic tissue for single cell suspension 133

2.10.4.2.3. Isolation of splenic lymphocytes 133

2.10.4.2.4. Outgrowth of EBV infected humanised mouse spleen derived LCL (mLCL) 133

2.11. Statistical analysis 134

3. Chapter III: Identifying the independent and combined functions of EBNA3A and EBNA3C 135

3.1. Introduction 135

3.2. Results 137

3.2.1. Construction and validation of the EBNA3A-ERT2/EBNA3C-ERT2 (3A3CERT2) double conditional virus 137

3.2.1.1. Construction of the EBNA3A-ERT2/EBNA3B/EBNA3C-ERT2 double conditional recombinant plasmid 137

3.2.1.2. Constructing the 3A3CERT2 double conditional recombinant EBV-BAC virus by homologous recombination 142

3.2.1.3. Confirming resolution of the 3A3CERT2 double conditional recombinant EBV-BAC 146

3.2.1.4. Transfection of double conditional recombinant 3A3CERT2-BAC into HEK-293 cells to generate EBV producer lines 149

3.2.1.5. Presence of EBNA3A and EBNA3C proteins in 3A3CERT2 conditional cell lines is dependent on continued addition of HT 156

3.2.1.6. Confirmation of EBV latency-associated protein expression in the 3A3CERT2 infected B cells ……159

3.2.2. A cumulative phenotypic effect is seen when both EBNA3A and EBNA3C are simultaneously non-functional compared to when either EBNA3A or EBNA3C are independently functional 162

3.2.2.1. Cell viability and proliferation are reduced in cells with simultaneously non-functional EBNA3A and EBNA3C compared to those with functional expression of either EBNA3A or EBNA3C 162

3.2.2.2. EBNA3A and EBNA3C target genes are regulated as predicted in cells with simultaneously conditional expression of EBNA3A and EBNA3C 165

3.2.3. EBNA3A and EBNA3C cooperatively regulate CDKI 167

3.2.3.1. Regulation of CDKI by EBNA3A and EBNA3C during primary infection 168

3.2.3.2. Regulation of CDKI by EBNA3A and EBNA3C in newly established conditional LCLs 172

3.3. Summary 179

3.4. Discussion 180

3.4.1. Co-operative functions of the EBNA3 proteins 180

3.4.2. Cell cycle regulation by EBNA3 proteins 182

3.4.3. Limits of reduced expression of modified EBNA3 proteins during ERT2 EBV infections 185

3.5. Final conclusions 186

3.6. Remaining questions 186

4. Chapter IV: EBNA3A and EBNA3C suppress the B cell to plasma cell differentiation pathway during establishment of EBV latency 188

4.1. Introduction 188

4.2. Results 189

4.2.1. EBNA3A and EBNA3C are required to prevent activation of CDKN2C ($p18^{INK4c}$) and PRDM1 (BLIMP-1) transcription after EBV infection 189

4.2.1.1. EBNA3-mediated regulation of PRDM1 (BLIMP-1) transcription resembles that of CDKN2C ($p18^{INK4c}$) 189

4.2.1.2. Activation of EBNA3A and EBNA3C reverses activation of $p18^{INK4c}$ and BLIMP-1 transcription during primary B cell infection with EBV 195

4.2.1.3. EBNA3A and EBNA3C mediated repression of $p18^{INK4c}$ and BLIMP-1 becomes irreversible in primary B cells early after infection 197

4.2.2. EBNA3A/EBNA3C-null EBV infected primary B cells express a plasma-cell like phenotype 203

4.2.2.1. Expression of $p18^{INK4c}$ and BLIMP-1 in EBNA3A/EBNA3C-null cells is physiologically comparable to the levels found in two PC models 203

4.2.2.2. BLIMP-1 target genes are differentially expressed in EBNA3A/EBNA3C-null cells 204

4.2.2.3. EBNA3A/EBNA3C-null cells express elevated levels of PC surface markers 208

4.2.2.4. EBNA3A/EBNA3C-null cells express elevated immunoglobulin levels 211

4.2.3. Lytic cycle reactivation is not evident in EBNA3A/EBNA3C-null cells 213

4.3. Summary 214

4.4. Discussion 215

4.4.1. EBNA3A- and EBNA3C-mediated repression of $p18^{INK4c}$ and BLIMP-1 215

4.4.2. Suppression of the B cell to PC pathway by EBNA3A and EBNA3C 218

4.4.3. EBV latency-associated proteins and B cell differentiation pathways 220

4.4.4. EBV lytic reactivation and the PC differentiation pathway 221

4.5. Final conclusions 223

4.6. Remaining questions 223

5. Chapter V: EBV can persist in mice with human immune system components when EBNA3A and/or EBNA3C oncogenes are non-functional, but is less pathogenic 224

5.1. Introduction 224

5.2. Results 226

5.2.1. Generating a mouse model with human immune system components 226

5.2.1.1. Establishing a humanised mouse model and assessing engraftment of human immune system components in the peripheral blood and spleen 226

5.2.1.2. Variables within the humanised mouse model 230

5.2.2. Establishing protocols for investigating recombinant EBV infection in mice with human immune system components reveals EBV can persist in the absence of functional EBNA3 proteins, but is less pathogenic. 232

5.2.2.1. Weekly and terminal analysis of humanised mice infected with EBV recombinant viruses .. 232

5.2.2.2. EBV viral load in humanised mice is greater when EBNA3 proteins are functional 235

5.2.2.3. Humanised mice infected with recombinant EBV viruses without the EBNA3A and/or EBNA3C oncogenes exhibit tumour development, but at a lower frequency than infection where EBNA3 genes are functional 239

5.2.2.4. Humanised mice infected with recombinant EBV exhibit enhanced splenomegaly and elevated levels of proliferating cells when the EBNA3 proteins are functional 241

5.2.2.5. Cell lines can only be derived ex vivo from the spleens of humanised mice infected with EBV where EBNA3A and EBNA3C are functional 245

5.2.2.6. Infection of humanised mice with recombinant EBV lacking EBNA3A and EBNA3C can lead to expansion of $CD8^{+ve}$ T cells 249

5.2.2.7. Phenotypic analysis of B cell composition in humanised mice infected with EBV 251

5.2.3. Determining the viability of using conditional ERT2 recombinant EBV viruses in humanised mice 255

5.2.3.1. Determining the viability of using tamoxifen-impregnated food 255

5.2.3.2. Weight analysis of humanised mice infected with conditional ERT2 recombinant EBV viruses 257

5.2.3.3. Splenic viral load in humanised mice infected with 3AERT2 conditional viruses is elevated when mice are exposed to tamoxifen, indicating functional EBNA3A expression 258

5.2.3.4. Tamoxifen-mediated conditional activation of EBNA3A in humanised mice infected with 3AERT2 recombinant EBV results in elevated tumour development 259

5.2.3.5. Humanised mice infected with 3AERT2 conditional recombinant EBV exhibit elevated splenomegaly when EBNA3A is activated by exposure to tamoxifen 261

5.2.3.6. Cell lines can be derived from the spleens of humanised mice infected with ERT2 conditional EBV in the presence of tamoxifen 262

5.2.3.7. T cell populations in humanised mice infected with EBV with conditional expression of EBNA3A..... 264

5.3. Summary 267

5.4. Discussion 268

5.4.1. EBV persistence in the absence of EBNA3 proteins contrasts their central roles in B cell transformation in vitro and their role in favouring latency in memory B cells 268

5.4.2. Conditional EBV in humanised mice 273

5.4.3. Expanding analysis of EBNA3-deficient EBV infection in humanised mice 276

5.5. Final conclusions 279

5.6. Remaining questions 280

6. Chapter VI: General discussion on the roles of EBNA3A and EBNA3C *in vitro* and *in vivo* 282

6.1. Translation of in vitro conclusions to results in vivo 282

6.2. Is evidence of EBNA3A- and EBNA3C-mediated suppression of PC differentiation in vitro recapitulated in vivo? 284

6.3. Thesis summary 287

7. Bibliography 290

8. Appendix 329

List of Figures

Figure 1.1. Germinal centre reaction following B cell activation by antigen
Figure 1.2. The germinal centre model of EBV persistence *in vivo*
Figure 1.3. *In vitro* infection of B cells with EBV leads to continuously proliferating lymphoblastoid cell line (LCL) development
Figure 1.4. Transcription of latency-associated genes from the EBV episome
Figure 1.5. Schematic showing the structure of homology domain between the EBNA3 family of proteins
Figure 1.6. Schematic showing cancer subtypes and the associated cell types and EBV latency stages *in vivo*
Figure 1.7. Overview of the mammalian cell cycle
Figure 1.8. EBNA3A and EBNA3C regulate CDKI at a transcriptional, translational and protein level
Figure 1.9. Overview of available EBV recombinant BAC viruses
Figure 3.1. Schematic showing construction of pCS007
Figure 3.2. Schematic showing the generation of the pCS007 plasmid
Figure 3.3. Cloning the EBNA3A-ERT2/EBNA3B/EBNA3C-ERT2 construct into the shuttle vector
Figure 3.4. Generation of EBNA3A-ERT2/EBNA3B/EBNA3C-ERT2 and E3KO EBV-BAC co-integrants by RecA-homologous recombination
Figure 3.5. Resolution of co-integrant EBNA3A-ERT2/EBNA3B/EBNA3C-ERT2 and E3KO EBV-BAC by secondary RecA-homologous recombination
Figure 3.6. Pulse field gel electrophoresis analysis for verification of 3A3CERT2-BAC DNA
Figure 3.7. Pulsed field gel electrophoresis analysis for validation of 3A3CERT2-BAC integrity following transfection of 293 cells with 3A3CERT2-BAC DNA
Figure 3.8. Production and confirmation of BAC-derived recombinant EBV virus
Figure 3.9. Validation of conditional EBNA3A-ERT2 and EBNA3C-ERT2 latent protein expression in 293 cells transfected with 3A3CERT2 BAC DNA
Figure 3.10. Expression of functional EBNA3A and EBNA3C is dependent on the continued addition of HT in 3A3CERT2 conditional LCLs
Figure 3.11. Protein levels of EBNA3A and EBNA3C can be lost or stabilised by the absence or presence of HT in 3A3CERT2 conditional LCLs
Figure 3.12. Validation of EBV latency-associated protein expression in double conditional 3A3CERT2 infected cells
Figure 3.13. Levels of EBNA3A and EBNA3C expression are lower when they have an ERT2 fusion
Figure 3.14. Cell count analysis of conditional EBNA3A, EBNA3C and EBNA3A3C LCLs
Figure 3.15. Proliferative capacity and cell viability is reduced when EBNA3A and EBNA3C are non-functional in EBV infected primary B cells and conditional LCLs
Figure 3.16. EBNA3A and EBNA3C target genes are regulated in primary B cells infected with 3A3CERT2
Figure 3.17. EBNA3A and EBNA3C regulate CDKI mRNA expression early after infection with EBV
Figure 3.18. EBNA3A and EBNA3C regulate expression of CDKI early after infection with EBV
Figure 3.19. EBNA3A and EBNA3C regulate CDKI mRNA expression in newly established conditional LCLs
Figure 3.20. EBNA3A and EBNA3C regulate CDKI in newly established conditional LCLs
Figure 3.21. Regulation of CDKI in an 3A3CERT2 LCL where EBNA3A and EBNA3C are simultaneously conditionally deactivated and reactivated

Figure 4.1. Activation of *CDKN2C* ($p18^{INK4c}$) transcription is prevented by EBNA3A and EBNA3C
Figure 4.2. Activation of *PRDM1* (BLIMP-1) transcription is prevented by EBNA3A and EBNA3C
Figure 4.3. EBNA3A and EBNA3C repress *CDKN2C* ($p16^{INK4a}$) transcription but not *ALAS1*
Figure 4.4. Activation of *CDKN2C* ($p18^{INK4c}$) and *PRDM1* (BLIMP-1) transcription is prevented by the EBNA3 proteins
Figure 4.5. Elevated mRNA levels of $p18^{INK4c}$ and BLIMP-1 in EBNA3A/EBNA3C-null cells are consistent with protein levels
Figure 4.6. Elevated transcription of *CDKN2C* ($p18^{INK4c}$) and *PRDM1* (BLIMP-1) in 3A3CERT2 infected primary B cells is reversed by activation of EBNA3A and EBNA3C
Figure 4.7. Repression of $p18^{INK4c}$ and BLIMP-1 transcription is not reversible by inactivating EBNA3A/EBNA3C in newly established conditional LCLs
Figure 4.8. Repression of BLIMP-1, but not $p18^{INK4c}$, becomes reversible by inactivating EBNA3A/EBNA3C in well-established conditional LCLs
Figure 4.9. Repression of $p18^{INK4c}$ and BLIMP-1 transcription occurs early after infection with EBV
Figure 4.10. Expression of PC differentiation associated factors in EBNA3A/EBNA3C-null cells and PC models
Figure 4.11. Differential expression of BLIMP-1 target genes in EBNA3A/EBNA3C-null cells following primary B cell infection
Figure 4.12. Expression of BLIMP-1 target genes in XBP-1, SPIB and LMO2 and in EBNA3A/EBNA3C-null cells and the plasmacytoma-derived cell line U266
Figure 4.13. IRF4 protein levels are not affected by EBNA3A/EBNA3C functionality
Figure 4.14. Flow cytometric analysis shows a plasmablast/PC-like phenotype in EBNA3A/EBNA3C-null cells
Figure 4.15. Primary B cells infected with 3A3CERT2 recombinant EBV express IgG and IgM
Figure 4.16. Evidence of activation of BZLF1 transcription is inconclusive in 3A3CERT2 infected cells
Figure 4.17. Lytic protein activation is not evident by western blot in 3A3CERT2 infected primary B cells
Figure 5.1. Schematic showing the process of humanisation of new born mice
Figure 5.2. Composition of human lymphocytes in the peripheral blood of NRG mice engrafted with human immune system components
Figure 5.3. Engraftment of human CD45 immune cells in humanised mice is elevated in the spleen compared to peripheral blood
Figure 5.4. Humanisation of NOD/$Rag^{-/-}$/IL2-$R\gamma^{null}$ (NRG) mice can lead to progressive alopecia
Figure 5.5. Engraftment of human immune system components in humanised mice is variable between $CD34^{+ve}$ cell donors
Figure 5.6. Female mice exhibit more effective engraftment of human immune system components than male mice following humanisation
Figure 5.7. Schematic showing experimental procedure for EBV infection of humanised mice
Figure 5.8. Humanised mice infected with recombinant EBV do not exhibit weight loss
Figure 5.9. Viral load in humanised NRG mice following infection with recombinant EBV
Figure 5.10. EBV DNA viral load in humanised NRG mice infected with recombinant EBV is higher in the spleen than in the peripheral blood
Figure 5.11. EBV mediated tumour development can occur in the absence of its EBNA3 oncogenes
Figure 5.12. Tumour development in EBV infected humanised mice does not correlate with engraftment of human lymphocytes

Figure 5.13. WT recombinant EBV infected humanised mice exhibit splenomegaly
Figure 5.14. Immunohistological analysis of splenic sections from humanised mice infected with recombinant EBV viruses
Figure 5.15. *Ex vivo* outgrowth of B cells derived from the spleens of humanised mice only occurs following infection with WT recombinant EBV
Figure 5.16. *Ex vivo* outgrowth occurs more frequently when B cells are derived from the spleens of WT EBV infected humanised mice with higher levels of human lymphocytes
Figure 5.17. Hu-mice infected with recombinant EBV lacking the EBNA3 oncogenes can induce a cellular immune response
Figure 5.18. Mice exhibiting EBV-mediated tumour development have elevated levels of $CD8^{+ve}$ T cells
Figure 5.19. B cell populations in humanised mice infected with recombinant EBV lacking EBNA3 proteins
Figure 5.20. Humanised mice exhibit extensive weight loss when fed tamoxifen-impregnated food
Figure 5.21. Humanised mice infected with recombinant EBV do not exhibit weight loss unless fed tamoxifen-impregnated food
Figure 5.22. Tamoxifen can induce higher viral loads in the spleen of 3AERT2 infected hu-mice
Figure 5.23. Tumour development in humanised mice infected with 3AERT2 recombinant EBV is elevated when tamoxifen is consumed
Figure 5.24. Splenomegaly in humanised mice infected with WT or 3AERT2 recombinant EBV in the presence and absence of tamoxifen
Figure 5.25. *Ex vivo* outgrowth of B cells derived from the spleens of humanised mice infected with an 3AERT2 conditional recombinant EBV virus when EBNA3A was functional
Figure 5.26. Hu-mice infected with recombinant EBV with conditional EBNA3A can induce a cellular immune response

List of Tables

Table 2.1. Primary antibodies used for western blotting.
Table 2.2. Primary antibodies used for immunohistochemistry.
Table 2.3. Secondary antibodies used in this study.
Table 2.4. Antibodies used for flow cytometric analysis.
Table 2.5. List of constructs used in this study.
Table 2.6. Composition of diagnostic and preparatory restriction enzyme digests
Table 2.7. Cell lines used in this study.
Table 2.8. Cell line specific cell culture conditions.
Table 2.9. RT-qPCR primers using SYBR Green assay.
Table 2.10. RT-qPCR primers using Taqman assay.
Table 2.11. SDS-PAGE resolving and stacking gel composition.
Table 3.1. Summary of outgrowth and viral titres of 293-3A3CERT2 EBV producer cell lines.

1. Chapter I: Introduction

This study focuses on the roles of the Epstein Barr virus (EBV) nuclear antigens 3A and 3C (EBNA3A and EBNA3C, respectively) both *in vitro* and *in vivo.* Although EBV has the capacity to infect other cell types, the biology of EBV is intimately linked with that of its primary target, the B cell. As a result, a brief introduction to B cell biology will precede an introduction to EBV, the mechanisms the virus employs to circumvent regulation of cellular genes, and the implications of EBV infection *in vivo.*

Please note that excerpts of this introduction have been directly taken from the author's previously published literature review (Styles et al., 2018), as per the Creative Commons Attribution (CC BY 4.0) License (http://creativecommons.org/licenses/by/4.0/). Sections taken from this publication are referenced accordingly.

1.1. B cell biology

1.1.1. Role of B cells and antibodies in the immune system

B cells are the principal component of the humoral immune response within the adaptive immune system. In adults they are formed in the bone marrow (BM) from haemopoietic lymphoid precursors and undergo multiple stages of sequential maturation and selection in BM before circulation in the periphery as naïve cells. Antigen-mediated activation leads to the complete differentiation of mature B cell types in secondary lymphoid organs, leading to a long-lived adaptive response.

B cells are highly specialised cells that express various immunoglobulins (Ig), which are able to bind to a practically unlimited number of antigens. Igs are glycosylated protein molecules that are either expressed in the transmembrane surface of B cells or secreted (Hoffman et al., 2016). Surface Ig are responsible for B cell selection, survival and activation. They form the B cell receptor (BCR) alongside CD79a (Ig-α) and CD79b (Ig-β) which transduce signals following antigen binding (Monroe, 2006). Secreted Ig, also referred to as antibodies, neutralize antigens leading to phagocyte involvement and complement activation. Antibodies are comprised of four protein chains, two 'light'

chains and two 'heavy' chains that are linked by disulphide bonds. The antigen binding site consists of the N-terminus of the light and heavy chains , which determines variability and specificity of the antibody molecule (Hoffman et al., 2016). The constant region, termed Fc, comprises the C-terminus regions of the heavy chains and distinguishes the five antibody isotypes; IgG, IgM, IgD, IgA and IgE. The Fc region is bound by complementary receptors on immune cells that recognise the constant region of specific antibody isotypes, which activates an appropriate immune response. B cells also participate in activation of T cells through presentation of antigen and production of cytokines (Hoffman et al., 2016).

A wide repertoire of BCRs, able to recognise a vast array of antigens, are generated during the development of B cells through the random arrangement of the Ig gene segments, which are termed the variable (V), diversity (D) and joining (J) segments. The lymphoid specific recombinase activating genes *Rag1* and *Rag2,* mediate random recombination of these genes leading to antigen receptor diversity. Stringent selection check points are employed as B cells transit through differentiation and V(D)J rearrangement, to ensure correct formation and expression of the BCR. This is followed by negative selection processes to prevent the generation of B cells that recognise self-antigens (Thomas et al., 2006). Self-reactive B cells either undergo additional V(D)J rearrangement or are eliminated. Tolerance mechanisms then permit positive selection of clones with non-autoreactive BCR enabling progression into the transitional B cell population (Hoffman et al., 2016; Wardemann et al., 2003).

The BM derived B cell population is comprised of marginal zone (MZ) B cells and follicular (FO) B cells, with the cell fate decision dependent on BRC signalling strength in secondary lymphoid organs (Pillai and Cariappa, 2009). Development of FO B cells is favoured by stronger BCR signals and they migrate to B cell follicles in secondary lymphoid organs, which are adjacent to T cell zones bordering the follicles. This permits long-lived interaction between the antigen-specific T and B cells and leads to T cell dependent B cell immune responses. FO B cells are the most numerous B cell lineage, and are the conventional B cell of the adaptive immune system (Hoffman et al., 2016; Pillai and Cariappa, 2009). In contrast to FO B cells, MZ B cell development is favoured by weaker BCR signals and requires

Notch2 mediated NFκB signalling. MZ B cells are retained in the spleen and are able to self-renew, unlike FO B cells which have a defined lifespan of a few weeks [reviewed in (Pillai and Cariappa, 2009)].

1.1.2. Antigen mediated B cell activation

Mature naïve B cells continuously circulate throughout the periphery and migrate to secondary lymphoid organs. These structures, including the spleen and lymph nodes, are strategically located such that antigens and immune cells are brought into contact efficiently. Lymphoid organs contain follicles which are densely populated with naïve B cells. These follicles are separated by an inter-follicular zone which borders a T cell zone. Naïve B cells survey lymphoid tissue until they encounter a complementary antigen that binds their cell surface BCR. Activation of naïve B cells to B blasts is initiated by BCR engagement with its antigen, alongside helper signals from antigen-specific $CD4^{+ve}$ T cells. BCR engagement with the antigen triggers gene expression programmes and results in internalization of the antigen. The antigen is degraded in the endosome compartments, and the resulting peptides are bound to major histocompatibility complex (MHC) II molecules and trafficked to the cell surface (Lanzavecchia, 1985).

Additional signals are provided by antigen-specific $CD4^{+}$ T helper (Th) cells which have been activated by the same antigen, and whose T cell receptor recognises the antigen:MHC complex on the activated B cell (Blum et al., 2013; Lanzavecchia, 1985). Th cells are induced to express the co-stimulatory cell surface protein CD40 ligand (CD40L), which is bound by surface CD40 on the B cells. This stimulates B cell activation and, consequently, proliferation and differentiation of the B blast (Armitage et al., 1992; Liu et al., 1992). B cell activation is further modulated by Th cell induced cytokines including as IL4 and IL21 (Crotty, 2015; Shulman et al., 2014).

Interaction with Th cells results in differentiation of B cells along either the extrafollicular or follicular pathways. Cells entering the follicular pathway differentiate from naïve B cells into plasma cells (PCs) or memory B cells (MBCs) in germinal centres (GCs). GCs are formed in the intrafollicular region of the lymphoid structures following expression of the transcriptional regulator B cell lymphoma 6 (BCL6), the master regulator of GC formation [(Dent et al., 1997; Nurieva et al., 2009;

Shlomchik and Weisel, 2012) see Section 1.1.3 for more detail]. The extrafollicular pathway is GC independent and involves differentiation of usually MZ B cells to short-lived IgM secreting plasmablasts. These plasmablasts have a low affinity for the invading pathogen, and act as an early protective measure (Pillai and Cariappa, 2009). Furthermore, it is also thought that a subset of naïve B cells can differentiate into unswitched MBC following strong CD40 signals provided by T cell interaction, independently of the GC reaction (Kurosaki et al., 2015; Taylor et al., 2012).

1.1.3. Germinal centre reaction

GCs are histological structures transiently formed within peripheral lymphoid organs following T cell interaction with activated B cells. The GC reaction is highly complex, and involves several distinct timed events which are compartmentalised into different areas of the GC microenvironment. However, many unknowns remain regarding the GC reaction [reviewed in(De Silva and Klein, 2015)]. Entry of antigen-activated B cells into the GC is thought to initiate differentiation of B cells into either long-lived MBC or long-lived PC, which produce high affinity, isotype switched antibodies essential for host immune defence (Hoffman et al., 2016). Antibody diversity is achieved in the GC through somatic hypermutation (SHM) and class switch recombination (CSR) of Igs, which require the DNA-editing enzyme activation-induced cytidine deaminase (AID) (Papavasiliou and Schatz, 2002). CSR replaces the isotype genes, leading to antibodies with different effector functions without losing antigen specificity. Whereas SHM introduces point mutations in Ig gene segments, leading to selection of high affinity clones (Hoffman et al., 2016).

The current GC reaction model suggests that GC structure is broadly comprised of two microenvironments referred to as the dark (DZ) and light zones (LZ). The DZ is comprised of densely packed, highly proliferating B cells undergoing clonal expansion and SHM, differentiating from B-blasts to centroblasts and loosing expression of surface Ig. As centroblasts differentiate into smaller resting centrocytes, they stop clonal expansion, re-express Ig and migrate to the LZ (Allen et al., 2007a; MacLennan, 1994). The LZ is more sparsely populated and contains several other immune cell types including antigen presenting follicular dendritic cells (FDC) and follicular T helper cells (FTh). In the LZ

antigen affinity B cell selection occurs. The BCR is tested against antigen displayed on antigen-specific FDC and the centrocytes compete for antigen-specific Th cell help (Suan et al., 2017). Low-affinity or self-reactive centrocytes can circulate between the two zones, enabling repeated rounds of mutation and selection, ultimately leading to MBC and PC expressing Ig with high affinity for the invading pathogen (Allen et al., 2007b; De Silva and Klein, 2015). Recent studies have found that there are only relatively small differences between LZ and DZ cells with regard to gene expression, dynamic behaviour and size; unsurprising due to the constant shifting of cells between these two states (Victora and Nussenzweig, 2012; Victora et al., 2010).

A large number of GC B cells die from apoptosis *in situ,* in both the LZ and DZ (Allen et al., 2007b). This is a result of negative selection due to inadequate T cell help or BCR engagement, or through the acquisition of detrimental BCR mutations, which results in the loss of pro-survival signals or activation of DNA damage response pathways (Allen et al., 2007a).

Following extensive antigen affinity positive selection, repression of BCL6 results in B cells exiting the cell cycle and subsequently committing to either MBC [reviewed in (Kurosaki et al., 2015)] or PC terminal differentiation [reviewed in (Nutt et al., 2015)]. The mechanisms behind this cell fate decision are presently unknown. It is speculated that commitment to either pathway depends on extrinsic signals such as cytokines; contact with other immune cells; affinity-based signals via the BCR; or results from random division into these subtypes (Shlomchik and Weisel, 2012). It has also been suggested that the commitment to either MBC or PC differentiation may be temporal, with early GC reaction thought to preferentially generate MBCs, whereas the late GC may be dedicated to production of PCs (Weisel et al., 2016). Alternatively, it has been suggested that strong support from T cells may drive PC differentiation (Kräutler et al., 2017; Zhang et al., 2018b). The transcription regulator B-lymphocyte-induced maturation protein 1 (BLIMP-1) has been shown to be the master transcriptional regulatory factor essential for PC differentiation [(Nutt et al., 2015) see Section 1.1.4 for more detail]. In contrast to PC, a master transcription factor for MBC differentiation has not yet been identified, hampering study into MBC precursors (Kurosaki et al., 2015; Suan et al., 2017).

Nonetheless, factors promoting MBC differentiation have been identified such as activated B cell factor 1 (ABF1), which mutually represses BLIMP-1 and therefore PC differentiation (Chiu et al., 2014). Following GC-mediated differentiation of MBC, subsequent antigen-mediated re-activation (aided by Th cells), leads to proliferation and differentiation of MBCs into PCs, allowing rapid production of class-switched high affinity antibodies upon secondary exposure to the MBC-specific antigen (Kurosaki et al., 2015).

Despite various advances in B cell biology research, there remains much to be determined about the complex and critical transition of B cells through the GC reaction. A summary schematic of the GC reaction model can be seen in Figure 1.1.

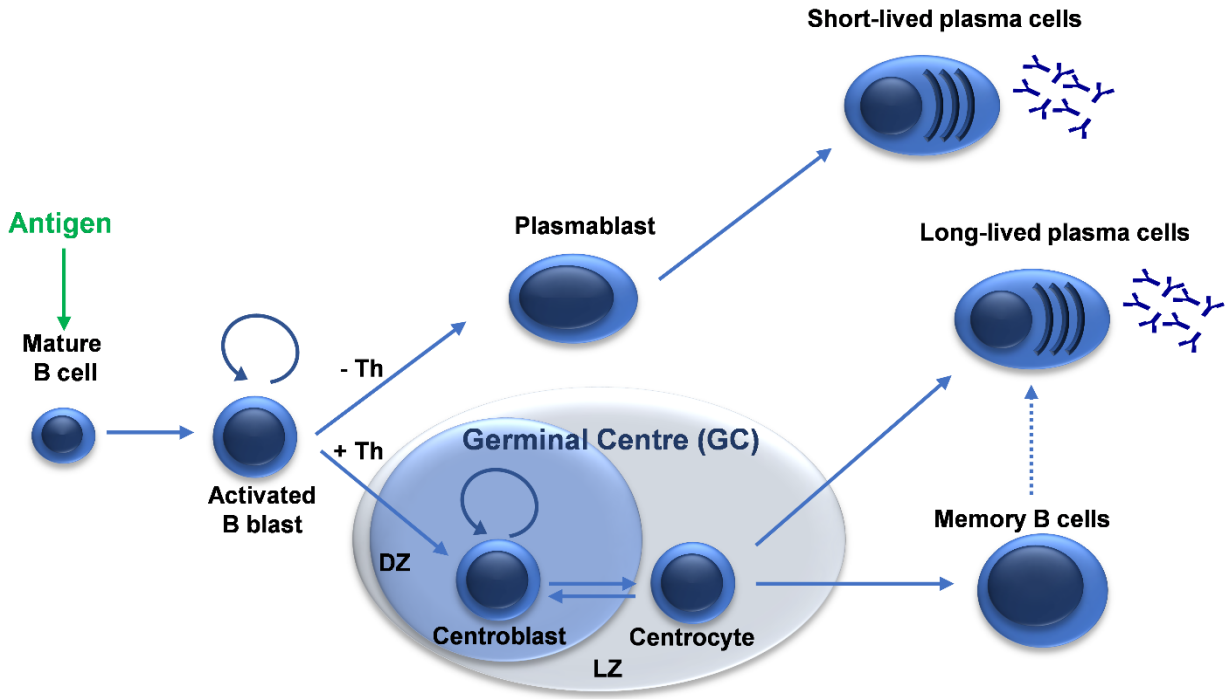


Figure 1.1. Germinal centre reaction following B cell activation by antigen. B cell activation by an antigen drives transient proliferation and B-blast activation. B-blasts can follow different B cell differentiation pathways. In the absence of T helper cells (Th-) activated B-blasts proliferate and differentiate into plasmablasts, then antibody producing short-lived plasma cells (PC). In the presence of T helper cells (Th+) activated B-blasts enter germinal centre structures where they differentiate into proliferating centroblasts in dark zone (DZ). They then differentiate into resting centrocytes and migrate to the light zone (LZ). Following extensive affinity maturation and positive selection (whereby cells recirculate back into the DZ for further somatic hypermutation and class switching of immunoglobulin genes) cells can then differentiate and exit the germinal centre either as long-lived PC or memory B cells (MBC). Upon reactivation, MBC differentiate into antibody secreting PC.

1.1.4. Plasma cell differentiation

In contrast to MBC differentiation, more is known about the processes and transcriptional profile of cells undergoing PC differentiation. Differentiation into PC occurs from different B cell populations, forming either short-lived cycling plasmablasts, long-lived post-mitotic PC or MBC derived PC, depending on the B cell precursor. This includes antigen-activated extra-follicular B cells such as MZ B cells, GC B cells and reactivated circulating MBCs (Goodnow et al., 2010; Nutt et al., 2015; Shi et al., 2015). The genome wide transcriptional profiles of these different precursor cell types are significantly different, and they each require substantial reprogramming of gene expression during the differentiation process to lead to the common transcriptional profile in resulting PC populations (Shi et al., 2015).

The process of PC differentiation is complex but at least three transcriptional regulators are considered essential for efficient differentiation of functional PCs. These factors are BLIMP-1, interferon regulatory factor 4 (IRF4) and a spliced version of X-box binding protein (XBP-1) (Nutt et al., 2011, 2015; Shi et al., 2015; Tellier et al., 2016; Yu and Lin, 2016). The PAX5, BCL6 and BACH2 transcription factors that regulate mature and GC B cells have been shown to have mutually antagonistic interactions with the PC differentiation regulatory factors BLIMP-1, IRF4 and XBP-1 in a complex regulatory network. Although low amounts of IRF4 promote GC B cells, high levels are thought to repress BCL6 and lead to activation of BLIMP-1 expression, therefore promoting PC differentiation (Sciammas et al., 2006). BLIMP-1 is thought to repress both BCL6 and PAX5, and results in upregulation of XBP-1 (Minnich et al., 2016; Shaffer et al., 2002; Tellier et al., 2016). In turn, BLIMP-1 expression has been shown to be repressed by BCL6, and BCL6 and PAX5 have been suggested to upregulate BACH2 expression which further represses BLIMP-1 (Ochiai et al., 2008; Tunyaplin et al., 2004). In addition, PAX5 has been proposed to repress XBP-1 (Reimold et al., 1996). These interactions, likely alongside others not yet demonstrated, result in separate, mutually exclusive, gene regulatory networks for B cells and differentiated antibody producing PCs (Nutt et al., 2011).

BLIMP-1 (encoded by *PRDM1*) is considered the master regulator of terminal PC differentiation, first identified using subtractive cDNA cloning to isolate late stage B cell differentiation genes. It was also found to be highly expressed in every plasmacytoma line tested (Turner et al., 1994). BLIMP-1 has been shown by microarray and RNA-seq to function primarily as a transcriptional repressor. This drives PC differentiation through repression of mature B cell or GC B cells genes such as *PAX5* and *BCL6*, and regulates cell cycle exit allowing terminal differentiation of PC (Minnich et al., 2016; Shaffer et al., 2002). *In vivo* studies using BLIMP-1 deficient mice have indicated BLIMP-1 is not required for the initiation of PC differentiation as its loss arrests PC differentiation in the pre-plasmablast stage (Kallies et al., 2007). However, ectopic expression of BLIMP-1 in mature B cells can result in plasmacytoid differentiation characteristic of early PC (Turner et al., 1994). Moreover, BLIMP-1 has been shown to be essential for the terminal differentiation of short-lived, long-lived and memory response initiated PCs, and is crucial for high level production and secretion of Ig (Kallies et al., 2007; Shapiro-Shelef et al., 2003; Tellier et al., 2016).

Alongside IRF4, BLIMP-1 and XBP-1, the cyclin dependent kinase inhibitor (CDKI) $p18^{INK4c}$ (see Section 1.3 for more detail) has been shown to be required for the generation of functional terminally differentiated PCs. This was first suggested when $p18^{INK4c}$ was shown to rescue PC differentiation *in vitro* (Morse et al., 1997). The contribution of $p18^{INK4c}$ to PC differentiation was further confirmed by the significant reduction in antibody secretion in mice deficient in $p18^{INK4c}$ during primary and secondary immune responses (Tourigny et al., 2002). Consistent with these results, increased expression of $p18^{INK4c}$ correlates with reduced proliferation and concurrent differentiation toward a PC-like phenotype in mitogen activated $CD19^{+ve}$ human B cells (O'Nions and Allday, 2004). In addition, $p18^{INK4c}$ has also been associated with enhancing survival and development of T cells (Rowell et al., 2014) and elevated $p18^{INK4c}$ levels are linked to differentiation of other cell lineages including osteoclasts and myeloid cells (Gagrica et al., 2012).

1.2. Epstein Barr virus (EBV)

1.2.1. *Overview of EBV*

Epstein Barr virus (EBV) is a lymphotropic human γ-herpes virus, belonging to the *herpesviridae* family of large dsDNA viruses. The EBV genome is comprised of a linear double stranded DNA genome, of approximately 172 kilobase pairs (kb) and the prototypical WT lab-strain B95.8 was the first herpesvirus to be cloned and sequenced (Baer et al., 1984). EBV is ubiquitous, and it persistently and asymptomatically infects the majority of the worldwide human population. Primary infection of healthy immunocompetent hosts usually progresses to a lifelong, largely benign, infection. However, if infection is delayed into adolescence then the self-limiting lymphoproliferative condition infectious mononucleosis (IM) can occur. Despite being a highly ubiquitous virus, EBV is one of the most transforming viruses identified. EBV is etiologically associated to a diverse range of lymphoid and epithelial malignancies and in 2010 contributed to nearly 2% of worldwide cancer deaths (Khan and Hashim, 2014). EBV is lymphotropic and the biology of EBV is intimately linked to that of B cell differentiation. It is thought that EBV infection drives naïve B cells to proliferate and differentiate through GCs, resulting in resting MBC that carry the EBV genome as extra-chromosomal episomes, forming long-lived reservoirs of EBV infection; a model referred to as the GC model of EBV persistence (Roughan and Thorley-Lawson, 2009; Thorley-Lawson and Babcock 1999).

1.2.2. Discovery of EBV

In 1958, a surgeon named Denis Burkitt first described a childhood malignancy prevalent in certain areas of Africa that became known as Burkitt lymphoma (BL) (Burkitt, 1958). In 1961, Burkitt presented his findings regarding BL, alongside epidemiological data suggesting a biological agent was responsible, as the disease appeared dependent upon climatic conditions. This lecture was attended by the virologist Anthony Epstein, who was greatly intrigued and a collaboration was established (Epstein, 2015). Burkitt provided BL tissue obtained from biopsies to Epstein and his colleagues, from which they were able to successfully establish a continuous suspension culture of BL cells. From this,

they were able to identify herpesvirus-like particles using electron microscopy (Epstein et al., 1964). The herpesvirus failed to react to antibodies raised against other known herpesviruses and therefore it was confirmed to be an undiscovered herpesvirus. This novel herpesvirus was called Epstein-Barr virus (EBV), after Anthony Epstein and Yvonne Barr, who had cultured the original BL cell lines (Epstein et al., 1965; Henle et al., 1968). Antibodies against EBV specific antigens were soon identified in children presenting with BL, and EBV genomes were identified in BL cell lines and nasopharyngeal carcinoma (NPC) biopsies (Gunvén et al., 1970; Hausen et al., 1970; Henle et al., 1968, 1969). Henceforth, the novel herpesvirus EBV was proposed as the first identified human tumour virus.

1.2.3. EBV transmission, tropisms and life cycle

In infected hosts, EBV is continuously shed into the saliva, and viral transmission occurs orally through salivary contact with infected individuals (Hadinoto et al., 2009). EBV then establishes life-long persistence in latently infected MBC. However, EBV also infects oral epithelial cells, which are required for the life cycle of the virus, as EBV must cross the oral mucosal epithelium to gain access to the B cell compartment (Temple et al., 2014). The dual tropism of EBV is thought to derive from differing glycoprotein content on the viral envelope, particularly the level of gp42 (Borza and Hutt-Fletcher, 2002). B cells form the pool of latently infected cells, whereas epithelial cells are thought to support replication and spread of EBV. B cells and oral epithelial cells support different patterns of EBV transcription with elevated lytic transcripts identified in epithelial cells (Shannon-Lowe et al., 2009). In addition, high levels of EBV virions have been shown to be produced by stratified epithelial cell raft cultures (Temple et al., 2014). Due to the differing glycoprotein complexes required for cell entry, epithelial cell-derived virus more efficiently infects B cells, whereas virus originating from B cells is more adept at infecting epithelial cells. This molecular mechanism is thought to alter viral tropism in an infected host, whereby virus produced by epithelium initially favours infection of B cell for the establishment latent infection, while virus produced by B cells favours infection of epithelial tissue to ensure transmission to a new host for the continuation of infection (Borza and Hutt-Fletcher, 2002).

Following salivary transmission, EBV is speculated to enter the tonsil epithelium within the Waldeyer's ring of the oropharynx. Here, the virus is thought to replicate following initiation of the lytic cycle in epithelial cells. The released virus then infects the surrounding naïve B cells within the lymphoid tissue in the Waldeyer's ring. The infected cells are driven to undergo differentiation in GCs and transition into latently infected MBCs [(Babcock et al., 1998; Laichalk et al., 2002; Roughan and Thorley-Lawson, 2009) see Section 1.2.4 for more detail]. The latently infected MBC can return to the periphery and circulate, also entering non-mucosal secondary lymphoid tissues including the spleen (Laichalk et al., 2002). Reactivation of latently infected MBC and subsequent differentiation into PC initiates viral replication and the lytic cycle (Laichalk and Thorley-Lawson, 2005). This releases virus into the saliva directly, or results in infection of surrounding epithelial cells of the oropharynx which in turn initiates production of virus from these cells. This amplifies salivary viral load and therefore enhances transmission to a new host.

The tropism of EBV for B cells results from B cell-restricted expression of the surface receptor CD21, which is the major receptor molecule for the virus and is bound by the EBV receptor gp350/220 (Young et al., 2007). Entry into epithelial cells (which lack CD21) is less well characterised. However, epithelial cell entry by EBV was recently shown to involve the Ephrin receptor A2, which interacts with the viral envelope glycoproteins gH, gL and gB to facilitate viral fusion and internalisation (Chen et al., 2018; Zhang et al., 2018a). In B cells, following attachment of CD21 to gp350/220, the human leucocyte antigen (HLA) II molecule of the B cell is bound by gp42. This triggers the process of fusion with the host cell, facilitated by gH, gL and gB (Shannon-Lowe and Rowe, 2014; Young et al., 2007). Internalisation of the virus particle follows, and the viral capsid is released. The EBV genome subsequently enters the nucleus of the infected cell, where it is maintained as an extra-chromosomal episome in the MBC.

Aside from the conventional infection route of salivary contact, transmission of EBV can also occur by solid organ transplant or blood donation from a seropositive donor. In immunosuppressed

recipients this is associated with elevated risk of post-transplant lymphoproliferative disease (Cen et al., 1991; Ho et al., 1985).

1.2.4. EBV latency in vivo: Germinal centre model of EBV persistence

EBV persistence is intimately linked with B cell biology. The widely accepted GC model of EBV persistence (shown schematically in Figure 1.2) proposes that latently infected MBC carrying the viral genome are generated through the transition and differentiation of infected B cells through the GC [reviewed in (Thorley-Lawson, 2015; Thorley-Lawson and Babcock, 1999)]. There is also evidence of direct EBV infection of unswitched GC-independent MBC, although EBV colonisation of these cells is less widespread than in GC-derived MBC (Chaganti et al., 2009).

Instead of antigen-mediated B cell activation, infection of naïve B cells with EBV *in vivo* drives them to become activated and induces proliferation, resembling antigen-activated B blasts (Thorley-Lawson and Babcock, 1999). This activation is independent of antigens and T cell interaction, and is dependent on the activity of EBV latency-associated genes (Kempkes et al., 1995). In infected B cells, the expression pattern of EBV latency-associated genes *in vivo* depends upon the differentiation stage of the B cell (Babcock et al., 2000). Differential EBV gene expression patterns were first described when some newly established BL cell lines were found to express a more restricted EBV latency-associated gene expression profile than LCLs and other BL cell lines (Rowe et al., 1986, 1987). In infected B blasts, the 'growth programme' or latency III programme is expressed. During latency III 9 latency associated proteins are expressed; six nuclear antigens (EBNA1, EBNA2, EBNA3A, EBNA3B, EBNA3C, EBNA-LP) and three latent membrane proteins (LMP1, LMP2A, LMP2B), alongside RNAs (EBER1 and EBER2) as well as several miRNAs. The latency-associated EBV proteins are described in more detail in Section 1.2.8. EBV activated cells migrate to a GC, where they undergo expansion and differentiation into centroblasts, then centrocytes. Transition through the GC corresponds with a sequential shut down of viral gene expression, such that latently infected MBC express no EBV genes, thus avoiding recognition by EBV-specific immune cells. In the GC, B cells switch from latency III, to the more restricted latency II (also known as the default programme) where most of the EBV nuclear

antigen genes are silenced such that only EBNA1, LMP1, LMP2A and LMP2B are expressed (alongside the EBERs and miRNAs) (Roughan and Thorley-Lawson, 2009). LMP1 and LMP2A are thought to provide signals necessary for the survival of infected cells in the GC, as they function as homologues of CD40 and the BCR, providing signalling required for cell survival (Caldwell et al., 1998; Dirmeier et al., 2003). This permits the continued differentiation of infected B cells along the normal differentiation pathway into MBCs. These latently infected quiescent MBCs exit the splenic follicle and enter the peripheral circulation. As no viral proteins are expressed in these MBC, this is referred to as latency 0 (Hochberg et al., 2004). It is within these latently infected MBC that EBV is able to persist for the lifetime of the infected host (Babcock et al., 1998).

Intermittent cell division of MBC, involving re-entry into the cell cycle, is not mediated by the virus and is thought to occur by homeostatic mechanisms. During cell division, EBNA1 is expressed in the MBC, which supports replication of the viral episome and segregation into daughter cells. This transcriptional profile is referred to as latency I (Hochberg et al., 2004). As EBNA1 is not recognised by CTLs its expression does not make the dividing MBC susceptible to immune surveillance (Levitskaya et al., 1995).

Reactivation of the latently infected MBC and subsequent terminal differentiation into a PC, is thought to induce the EBV lytic cycle (see Section 1.2.5 for more detail on lytic reaction). Expression of BZLF1, which begins viral replication, was shown to become active following differentiation of MBC to PC in the tonsils of healthy carriers (Laichalk and Thorley-Lawson, 2005). The tonsillar localisation of released EBV particles allows transmission via saliva.

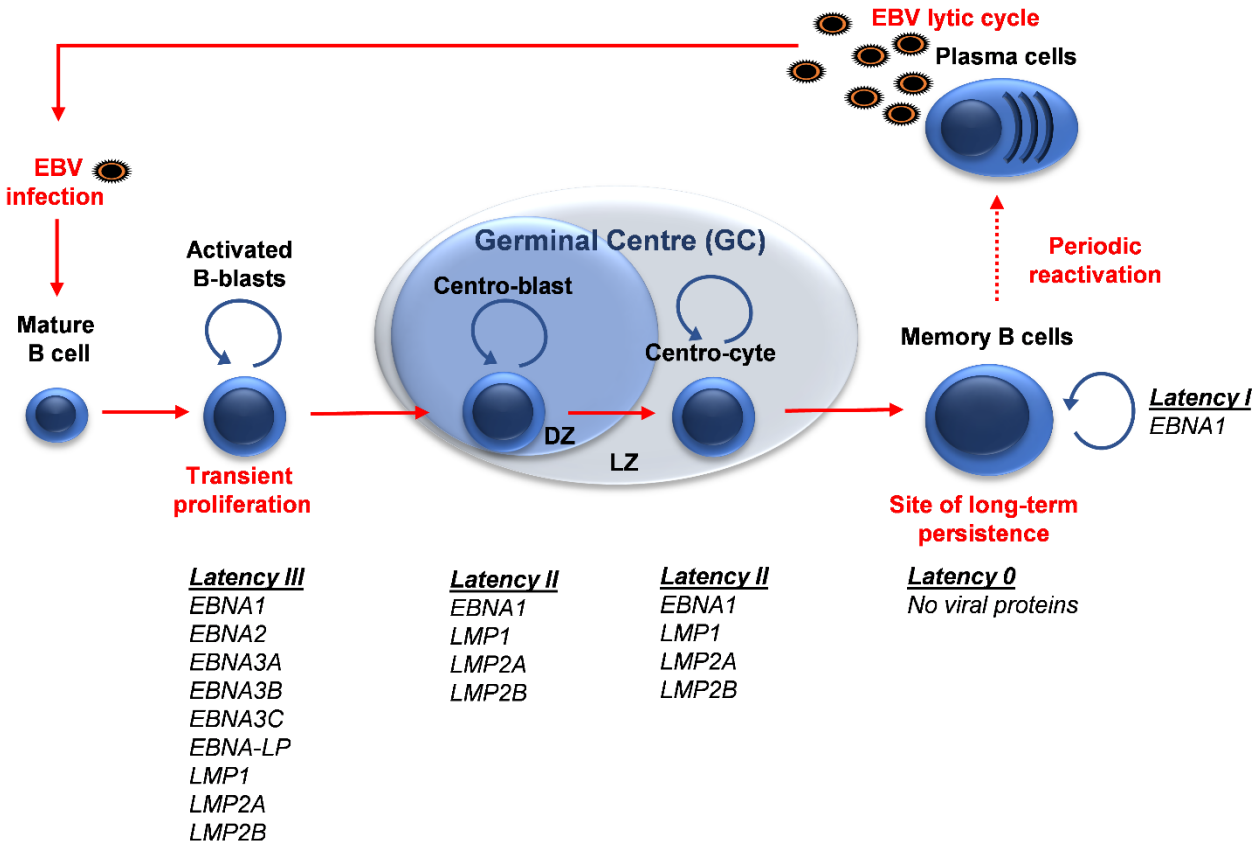


Figure 1.2. The germinal centre model of EBV persistence *in vivo*. EBV infects resting mature B cells within the tonsils via binding to CD21. Expression of the EBV latency-associated proteins comprised of 6 nuclear antigens (EBNA1, EBNA2, EBNA3A, EBNA3B, EBNA3C, EBNA-LP) and 3 membrane proteins (LMP1, LMP2A, LMP2B), known as the latency III programme, drives the infected B cells to become activated and proliferate rapidly, which resembles an antigen-activated B blast. The activated EBV infected cells enter the germinal centre and a sequential reduction of viral gene expression begins such that only EBNA1, LMP1, LMP2A and LMP2B are expressed in cells resembling centroblasts and centrocytes, known as the latency II programme. Cells further differentiate and exit the germinal centre as resting memory B cells, in which no viral gene expression is seen, known as latency 0. Upon proliferation of these cells, EBNA1 is expressed to maintain the viral genome, known as latency I. When resting memory B cells are activated to differentiate into plasma cells, the lytic cycle is induced, and live virus produced. The GC model of persistence is reviewed in (Thorley-Lawson, 2015).

1.2.5. Lytic reactivation

The EBV lytic phase is divided into three distinct sequential phases; immediate early, early and late, each with their own temporally controlled gene expression patterns. It is during the lytic cycle that the majority of EBV proteins are expressed.

Simultaneous transcription of the lytic immediate early genes *BZFL1* and *BRLF1* orchestrates transition of EBV latency into the productive lytic cycle (Hardwick et al., 1988; Rooney et al., 1989). BZLF1 is the master regulator of the switch to the lytic phase, and expression induces lytic replication in latently infected cells. BRLF1 is similarly required for the subsequent expression of viral lytic genes (Feederle, 2000). BZLF1 and BRLF1 are transcribed from the Z promoter (Zp) and R promoter (Rp) respectively, and act as transcription factors that activate each other's promoters amplifying their own expression (Liu and Speck, 2003). Together BZLF1 and BRLF1 act synergistically to induce expression of the early lytic genes, thus initiating viral replication. Following replication of the viral genome, the late genes are expressed. These genes encode structural proteins required for encapsidation of the viral genome to form infectious virions, the final stage of the lytic cycle. The lytic origin of replication (*Ori-lyt*) for the synthesis of virion DNA is independent from the plasmid DNA replication origin (*OriP*), which is used for the maintenance of the viral episome in synchrony with division of the host MBC (Hammerschmidt and Sugden, 1988).

During latency, lytic genes are silenced by chromatinization (Tempera and Lieberman, 2010). The EBV lytic cycle is thought to be induced by the differentiation of latently infected memory B cells into PC (Laichalk and Thorley-Lawson, 2005). Expression of BLIMP-1, the master regulator of PC differentiation, was recently shown to induce transcription of BZLF1 and BRLF1 from Zp and Rp in EBV-positive epithelial cell lines and some EBV-positive B cell lines, further indicating induction of PC differentiation activates the EBV lytic cycle (Reusch et al., 2015).

1.2.6. EBV latency in vitro

EBV infection of mature B cells *in vitro* establishes stable infection and forms continuously proliferating lymphoblastoid cell lines (LCLs) (Henle et al., 1967; Pope et al., 1968). LCLs express a latency III programme of genes (detailed in Section 1.2.8) and resemble activated B blasts. It is thought that due to the absence of GC within *in vitro* cell cultures differentiation of infected B blasts into MBC is not possible, and not required for sustained infection (Figure 1.3). The process of EBV transformation of B cells into LCLs is also commonly referred to as B cell immortalisation. LCLs are

widely used as a model to study latent EBV infection and the biological consequences of the latency III viral gene expression profile. *In vitro,* EBNA1, EBNA2, EBNA3A, EBNA3C, EBNA-LP and LMP1 are required for the efficient transformation of B cells (Cohen et al., 1989; Kaye et al., 1993; Lee et al., 1999; Mannick et al., 1991; Tomkinson et al., 1993).

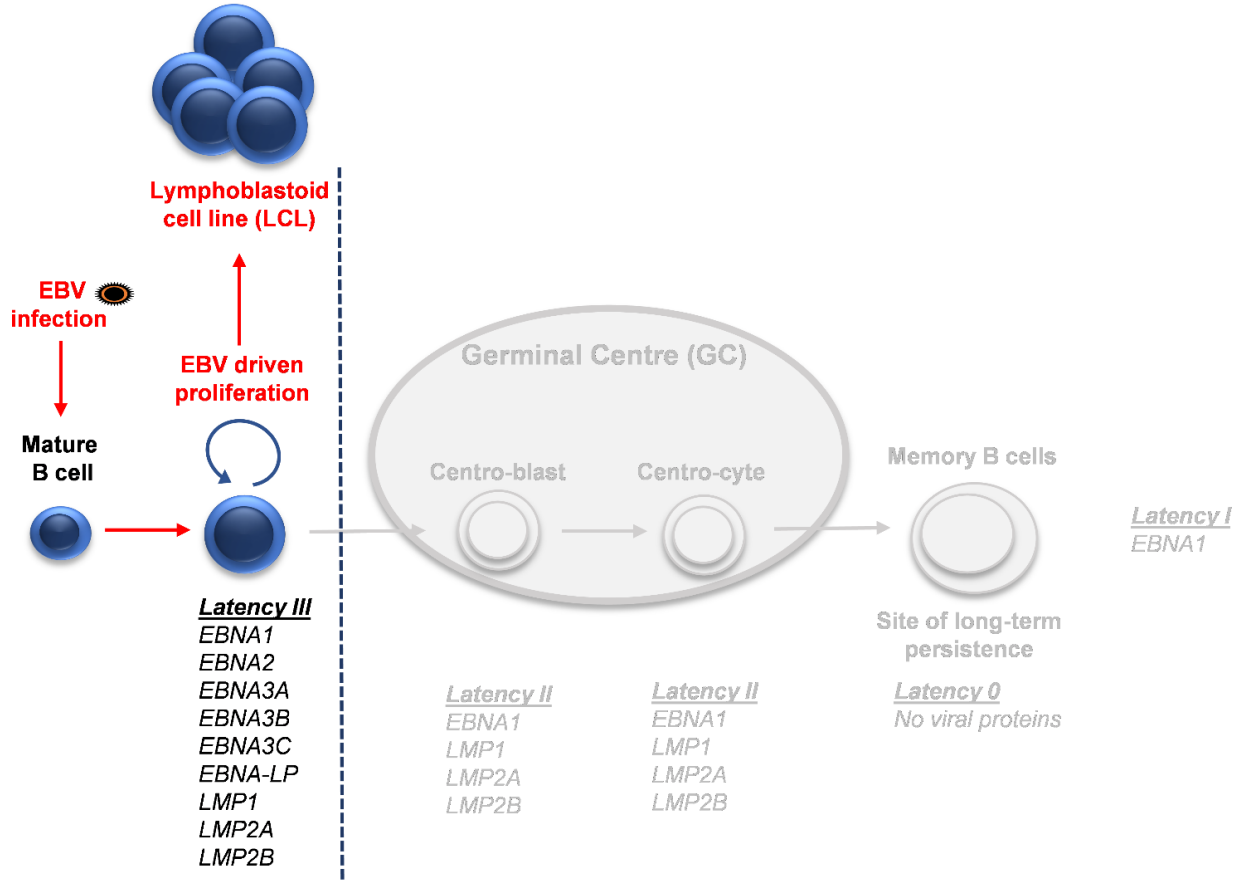


Figure 1.3. *In vitro* infection of B cells with EBV leads to continuously proliferating lymphoblastoid cell line (LCL) development. EBV infects resting mature B cells via binding to CD21. B cell activation and continuous proliferation is driven by expression of the EBV latency-associated proteins comprised of 6 nuclear antigens (EBNA1, EBNA2, EBNA3A, EBNA3B, EBNA3C, EBNA-LP) and 3 membrane proteins (LMP1, LMP2a, LMP2b). In the absence of a germinal centre and immune system *in vitro,* the sequential shut down of viral gene expression does not occur. Therefore, EBV-driven proliferation and the latency III profile is sustained, leading to the establishment of continuously proliferating lymphoblastoid cell lines (LCLs).

1.2.7. Transcription of latent genes from the EBV genome

Following infection and subsequent activation of an infected B cell, the EBV genome transitions from the linear form carried in the virion, and it circularises to form a viral episome in the B cell [(Hurley and Thorley-Lawson, 1988), Figure 1.4]. The EBV genome contains terminal repeats (TR) at each end of the linear genome, and the viral episome is formed following homologous recombination of these repeats (Raab-Traub and Flynn, 1986). In addition, the genome also contains internal repeats, referred to as the BamHI W repeats (or just W repeats). Each W repeat contains a copy of the W promoter (Wp), and the W1 and W2 exons which encode the W repeats of EBNA-LP [(Speck et al., 1986) see Section 1.2.8.4 for more detail on EBNA-LP]. Wp is the first viral promoter to be activated following B cell infection. Gene expression is then switched to the C promoter (Cp) during early infection as the infected cells proliferate and resemble B blast-like cells (Woisetschlaeger et al., 1990). Transcription from either Wp or Cp results in a very long mRNA transcript (the B cell transcription unit), which is alternatively spliced to generate the six different EBNA proteins (Rogers et al., 1990). A third promoter, the Q promoter (Qp), is used for the Latency I and II programmes, and results only in expression of EBNA1 (Schaefer et al., 1995). LMP1, LMP2A and LMP2B are transcribed independently from the EBNA proteins from a separate promoter close to the W repeats at the right-end side of the genome (Laux et al., 1988, 1989).

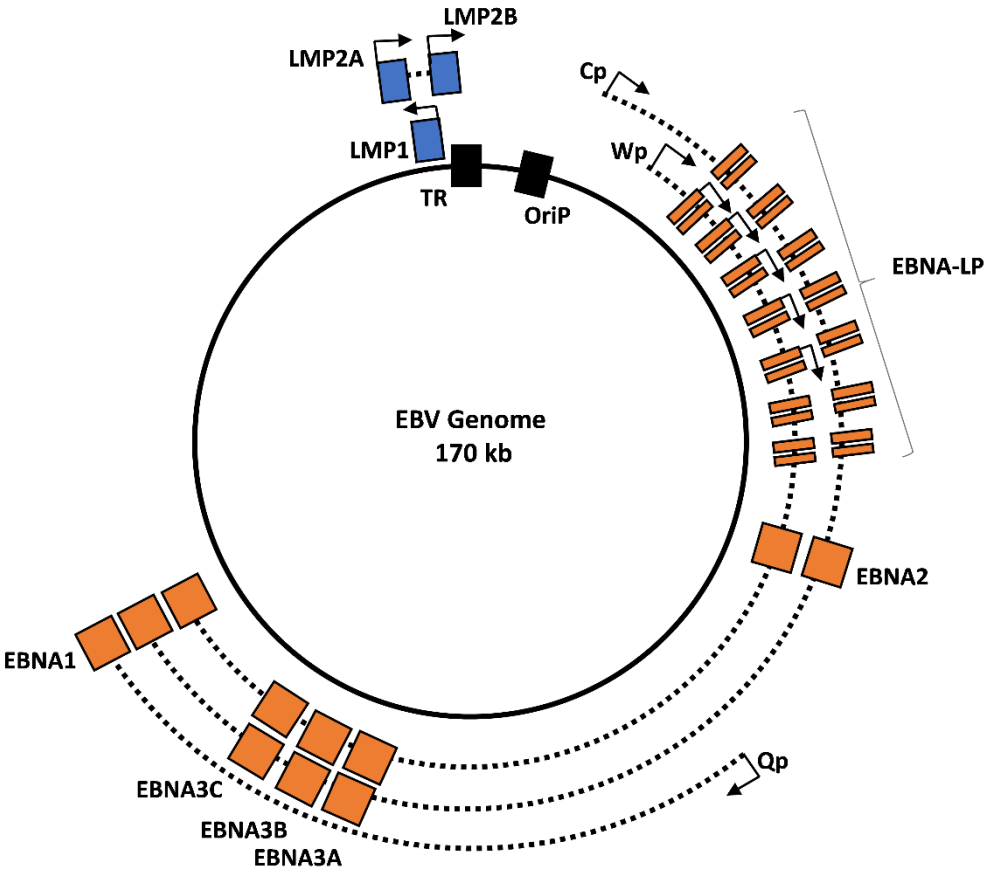


Figure 1.4. Transcription of latency-associated genes from the EBV episome. Following infection of resting B cells, the EBV genome circularises to form an episome. Gene transcription is first initiated from the W promoter (Wp) but then switches to the C promoter (Cp) in activated B blast-like infected cells. The 6 EBV nuclear antigens (EBNA1, EBNA2, EBNA3A, EBNA3B, EBNA3C, EBNA-LP, coloured in orange) are generated by alternative splicing of a long mRNA transcript and translated into the separate EBNA proteins. During latency I and II, gene expression is initiated from the Q promoter (Qp) resulting only in expression of EBNA1. The latent membrane proteins (LMP1, LMP2A and LMP2B, coloured in blue) are transcribed independently from the EBNA genes. Black boxes denote the latent origin of replication (OriP) and the terminal repeats (TR). Homologous recombination of the TR allows circularisation of the linear EBV genome. Figure adapted from (Kalla and Hammerschmidt, 2012).

1.2.8. EBV latency-associated proteins

1.2.8.1. EBNA1

EBNA1 was the first EBV latency-associated protein identified (Reedman and Klein, 1973) and is expressed in all replicating EBV infected B cells, in all forms of viral latency and in all EBV-associated malignancies. EBNA1 has various important roles during EBV infection, which is mediated by interactions with various cellular proteins as it lacks enzymatic activity (Frappier and O'Donnell, 1991).

Crucially, EBNA1 prevents the loss of the viral episome in dividing cells and is required for replication and retention of the EBV genome. EBNA1 binds within the EBV latent origin of replication (termed *OriP*) (Wysokenski and Yates, 1989; Yates et al., 1984, 1985), which contains two functional components; the dyad symmetry element (DS) and the family of repeats (FR) (Reisman et al., 1985). EBNA1 mediates replication of the EBV episome in parallel with the host genome, and EBNA1 binding to *OriP* facilitates tethering of the viral genome to cellular chromosomes during metaphase. This facilitates equal partitioning of the replicated viral episomes between the two resulting daughter cells during cell division (Grogan et al., 1983; Kanda et al., 2001). Furthermore, EBNA1 is thought to be important for transcriptional activation of the other latency-associated genes as EBNA1 binding to *OriP* transactivates transcription of the Cp and LMP promoters (Gahn and Sugden, 1995; Sugden and Warren, 1989). EBNA1 also binds down-stream of the Qp promoter which is used for expression of EBNA1 in the absence of other EBNA proteins (Nonkwelo et al., 1996). EBNA1 has a lower affinity for its recognition sites near Qp compared to the DS and FR elements of *OriP*, and therefore only binds near Qp when the other sites are saturated by high levels of EBNA1 (Ambinder et al., 1990). EBNA1 binding near to Qp is reported to repress EBNA1 levels and this is thought to be an auto-regulatory mechanism of EBNA1 to restrict its own expression levels (Sample et al., 1992).

Although EBNA1 is expressed in all latently infected cells, it is very weakly recognised by CTLs and therefore largely avoids immune surveillance. This is as EBNA1 interferes with the processing and presentation of EBNA1 by MHC class I, preventing a CTL-mediated response and thus allowing EBV to reside within the MBC population even during cell division (Levitskaya et al., 1995).

1.2.8.2. EBNA2

EBNA2 is the first viral protein detectable following primary B cell infection with EBV (alongside EBNA-LP, see Section 1.2.8.4) (Allday et al., 1989). However, expression of EBNA2 is silenced during later stages of B cell development. In cohort with EBNA-LP, EBNA2 cooperatively activates and transcriptionally regulates various viral and cellular genes (Kempkes and Ling, 2015; Peng et al., 2005). Chromatin immunoprecipitation and sequencing (ChIP-seq) analysis has identified

shared binding sites for EBNA2 and its coactivator EBNA-LP across the genome, and they largely colocalise with clusters of binding sites for B cell specific transcription factors (Portal et al., 2013). However, the relationship of EBNA2 as an enhancer and EBNA-LP as a co-activator is complicated, with recent work showing activation of some EBNA2 host target genes, thought to be transactivated by EBNA-LP, to be unaffected by the absence of EBNA-LP during primary EBV infection (Szymula et al., 2018).

EBNA2 is essential for the transformation of B cells, which was first demonstrated in the inability of the EBNA2-null P3HR-1 EBV strain to transform cells *in vitro* (Rabson et al., 1982). An important function of EBNA2 is the transactivation of Cp, inducing the switch in promoters from Wp to Cp that is observed in early B cell infection (Woisetschlaeger et al., 1991). Although, the EBNA1 and *OriP* complex is also important for the switch between Wp and Cp (Altmann et al., 2006). Both the LMP1 and LMP2 gene promoters are strongly activated by EBNA2, and EBNA2 is required to induce their expression (Abbot et al., 1990).

EBNA2 does not directly bind to DNA, instead it associates with host DNA binding factors to regulate gene expression. This includes the recombination binding protein-J kappa (RBP-Jκ, also known as Cp binding factor 1 or CBF1), early B cell factor 1 (EBF1), IRF4 and Pu.1 (Henkel et al., 1994; Jiang et al., 2014; Johannsen et al., 1996; Lu et al., 2016; Sjoblom et al., 1995). The best characterised interaction is of EBNA2 association with RBP-Jκ, (Henkel et al., 1994), and binding results in recruitment of various other transcription factors. ChIP-seq analysis has revealed extensive colocalization of EBNA2 and RBP-Jκ across the genome (McClellan et al., 2013). EBNA2 mimics intracellular cleaved Notch1, and utilizes RBP-Jκ to lead to activation of Notch1 signalling pathways involved in differentiation, proliferation and anti-apoptosis (Hofelmayr et al., 2001). EBNA2 was recently shown to induce new chromosome binding sites for RBP-Jκ and the transcription factor EBF1, and these sites strongly correlated with transcriptional activation of genes important for the function of B cells (Lu et al., 2016). EBNA2 has also been shown to deregulate the proto-oncogene c-MYC, further facilitating proliferation through cell cycle progression as a result of subsequent upregulation

of cyclins [(Kaiser et al., 1999) see Section 1.3.1.1 for cell cycle description]. Ultimately, gene activation by EBNA2 leads to activation of the resting B cells, resulting in cell cycle progression and maintenance of proliferation of transformed cells (Kempkes and Ling, 2015; Kempkes et al., 1995).

1.2.8.3. The EBNA3 family

Please note this section has been taken directly from the author's previously published review (Styles et al., 2018).

The latency-associated EBNA3 family of proteins comprises 3 large proteins called EBNA3A, EBNA3B, and EBNA3C, each composed of over 900 amino acids. These non-redundant proteins are thought to have arisen from tandem duplication events during the evolution of the old world lymphocryptoviruses. Their genes are structurally similar, with each consisting of a short 5' coding exon and long 3' coding exon and share limited but significant sequence homology. Each of the EBNA3 proteins features a proline rich region, as well as a "homology domain" of approximately 220–230 amino acids near the N-terminus, in which there is 20–30% identity between the EBNA3s [Figure 1.5, (Le Roux et al., 1994; Yenamandra et al., 2009)]. The EBNA3s are predicted to share similar secondary structures, despite having only modest homology overall (Yenamandra et al., 2009). EBNA3 mRNA transcripts are initiated from the Cp latency promoter producing large, alternatively spliced mRNAs that are only expressed in B cells. Production of EBNA3 proteins is thought to be tightly regulated, and the proteins are very stable, as protein levels and turnover are low (Davies et al., 2010; Touitou et al., 2005).

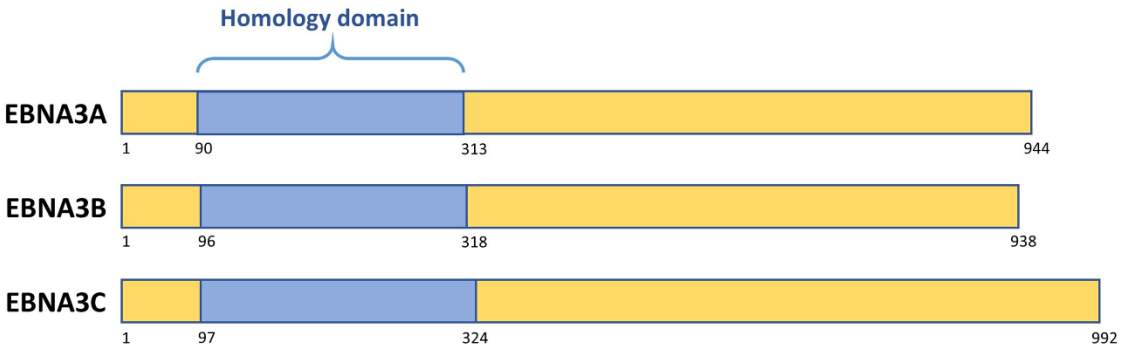


Figure 1.5. Schematic showing the structure of the homology domain between the EBNA3 family of proteins. Numbers denote amino acid position within the prototypical WT lab strain B95.8 proteins. Figure reproduced from (Styles et al., 2018).

EBNA3 proteins are well characterised regulators of transcription. Exon-microarray analysis using the EBV-negative BL cell line BL31 infected with mutant EBNA3 viruses revealed that the EBNA3 proteins transcriptionally regulate over 1000 host cell genes (White et al., 2010). A substantial number of these genes show cooperative regulation between multiple EBNA3 proteins. Most of this co-regulation involves EBNA3C working in cooperation with either EBNA3A or EBNA3B or both, with only modest cooperation between EBNA3A and EBNA3B in the absence of EBNA3C. Moreover, deletion of EBNA3C had the most significant impact on host gene regulation, with gene repression dominating differential host gene expression (White et al., 2010). ChIP analysis demonstrated that EBNA3A and EBNA3C have significant co-localisation across the genome, as do EBNA3B and EBNA3C. However, co-localisation of EBNA3A and EBNA3B in the absence of EBNA3C was extremely rare (Paschos et al., 2017). EBNA3 proteins do not bind to DNA directly, instead, transcriptional regulation is achieved through interactions with cellular DNA binding factors (See Section 1.3.3.1).

Both EBNA3A and EBNA3C are considered oncogenic. In an early demonstration of this, EBNA3C was shown to cooperate with oncogenic (Ha-)Ras during transformation of primary rat embryo fibroblasts (Parker et al., 1996). The oncogenic functions of EBNA3A and EBNA3C differ from the seemingly antagonistic EBNA3B, despite co-operative regulation of a variety of genes (Allday et al., 2015). Alongside EBNA1, EBNA2, EBNA-LP and LMP1, both EBNA3A and EBNA3C are required for

the efficient transformation of B cells (Cohen et al., 1989; Kaye et al., 1993; Lee et al., 1999; Mannick et al., 1991; Tomkinson et al., 1993). EBNA3C is essential for B cell transformation, and EBNA3A is important, with EBNA3A-null cell lines exhibiting reduced proliferative capacity (Bazot et al., 2015; Hertle et al., 2009; Maruo et al., 2003; Skalska et al., 2010). In contrast to the necessity of EBNA3A and EBNA3C for efficient B cell immortalisation, EBNA3B is completely dispensable for the transformation of B cells *in vitro,* and appears to act as a tumour suppressor *in vivo* [(White et al., 2012) see Section 1.5.5.2.2].

As EBNA3A and EBNA3C are the focus of this thesis, more detail of their functions in EBV infection and persistence can be found in Section 1.3.

1.2.8.4. EBNA-LP

Alongside EBNA2, EBNA leader protein (EBNA-LP) is one of the first viral proteins detectable after primary EBV infection and is alternatively spliced from transcripts first initiated at Wp and then later from Cp (Allday et al., 1989).The EBNA-LP protein is comprised of a variable number of repeats of a 66 amino-acid N terminal repeat domain encoded by W1 and W2 exons, and a C terminal domain encoded by the Y1 and Y2 exons. This results in expression of EBNA-LP with variable molecular weights depending on the number of W repeats contained within the virus, and EBNA-LP isoforms of different sizes are identified in early infection (Finke et al., 1987).

EBNA-LP is dispensable but important for the transformation of adult B cells (Mannick et al., 1991; Szymula et al., 2018), however it was recently shown to be essential for the transformation of naïve umbilical cord blood cells (Szymula et al., 2018). Functionally EBNA-LP is thought to support transactivation of genes by EBNA2. This includes activation of the LMP and Cp promoters (Harada and Kieff, 1997). Using ChIP-seq EBNA-LP and EBNA2 have been shown to co-localise extensively across the genome alongside various host transcription factors (Portal et al., 2013). EBNA-LP is thought to remove transcriptional repressive complexes involving the nuclear receptor co-repressor (NCoR) and RBP-Jκ from various EBNA2 sites, leading to gene activation (Portal et al., 2011). EBNA-LP was recently shown to be essential for establishing and stabilizing transcription of viral genes in cohort with EBNA2

during primary B cell infection with EBV. However, EBNA-LP was dispensable for expression of some EBNA2-activated host genes, despite EBNA-LP previously being identified as a co-activator, indicating the relationship between EBNA2 and EBNA-LP is more complicated than simply enhancer and co-activator (Szymula et al., 2018).

1.2.8.5. Latent membrane proteins

1.2.8.5.1. LMP1

LMP1 is a major oncogenic transforming protein of EBV, and transgenic mice expressing LMP1 develop B cell lymphomas (Kulwichit et al., 1998). Expression of LMP1 is induced by EBNA2 (Wang et al., 1990) and it is considered essential for the transformation of B cells (Kaye et al., 1993). However, it has been shown that LMP1 KO LCLs can be sustained on fibroblast feeder cells, although they have markedly reduced transformative ability compared to LMP1 competent WT viruses (Dirmeier et al., 2003).

LMP1 functions as a constitutively active member of the tumour necrosis factor receptor (TNFR) family and is able to activate multiple signalling pathways. Functionally, LMP1 resembles the TNFR member CD40, and can substitute for CD40, mimicking the activation processes of B cells and replacing the otherwise crucial T cell derived signals (Kieser and Sterz, 2015; Uchida et al., 1999). LMP1 activates many signalling pathways including NFκB, mitogen-activated protein kinase (MAPK) and PI3-K/AKT pathways (Cahir-McFarland et al., 2004; Dawson et al., 2003; Gires et al., 1997; Kieser et al., 1997). Mimicry of these CD40 signalling pathways by LMP1 leads to expression of essential survival signals for B cells undergoing EBV-mediated transformation. This includes expression of cell surface adhesion molecules and activation antigens, up regulation of anti-apoptotic proteins and stimulation of cytokine production [reviewed in (Kieser and Sterz, 2015)]. Moreover, LMP1 harbours immunosuppressive peptides which inhibit T cell proliferation and NK-mediated T cell cytotoxicity (Middeldorp and Pegtel, 2008). LMP1 can also disrupt function or expression of tumour suppressors such as DOK1 (Siouda et al., 2014).

1.2.8.5.2. LMP2A and LMP2B

LMP2 has two alternative, structurally similar forms; LMP2A and LMP2B, which are expressed from different promoters (Sample et al., 1989). The N-terminus of LMP2A contains immunoreceptor tyrosine-based activation motifs, which are also present in the BCR receptor factors CD79a (Ig-α) and CD79b (Ig-β), and transmit activation signals following BCR stimulation (Alber et al., 1993). LMP2A blocks BCR signal transduction by sequestering tyrosine kinases from the BCR. This prevents antigen-mediated activation of EBV infected B cells, which would otherwise lead to lytic cycle entry rather than latency (Miller et al., 1995). Binding of these tyrosine kinases also stimulates them such that they mimic BCR activation and therefore antigen-induced B cell stimulation and proliferation (Engels et al., 2012; Merchant et al., 2001). In transgenic mice, it was shown expression of LMP2A leads to survival of BCR-deficient B cells, indicating LMP2A has the ability to replace BCR-induced B cell survival signals and therefore promotes cell survival (Caldwell et al., 1998). LMP2A is also thought to alter production of the cytokine IL10 from infected B cells, which promotes tumour survival and dampens anti-viral responses (Incrocci et al., 2013).

Less is known about the functions of LMP2B. LMP2B lacks the 5'exon of LMP2A; which encodes the N-terminal cytoplasmic domain that is responsible for mimicking BCR signalling. However, LMP2B is thought to modulate distribution and function of LMP2A, thus helping maintain viral latency (Rovedo and Longnecker, 2007). Furthermore, both LMP2A and LMP2B are thought to promote spread and motility of EBV-infected epithelial cells by engaging signalling pathways (Allen et al., 2005). This likely has a role in EBV-associated NPC which has consistent expression of LMP2A and LMP2B (Busson et al., 1992).

Neither LMP2A or LMP2B are essential for the transformation of B cells *in vitro* (Speck et al., 1999), however BCR mimicking by LMP2A is thought to be essential for survival and proliferation of infected GC B cells *in vivo* (Mancao and Hammerschmidt, 2007). Exploitation of B cell biology by LMP2A in combination with the CD40-mimicking activity of LMP-1, enables survival of EBV infected B cells in the GC, such that they can differentiate into latently infected MBC (Thorley-Lawson, 2001).

1.2.8.6. EBV RNAs and miRNAs

In addition to latency-associated proteins, EBV expresses RNAs and microRNAs (miRNAs) during latency. These include the two small non-coding RNAs called EBER1 and EBER2, which are transcribed by the host RNA polymerase III, and are expressed in all forms of latency [reviewed in (Iwakiri, 2014)]. The requirement for EBERs during B cell transformation is not conclusive, as some studies using recombinant KO viruses indicate they are not essential for the transformation of B cells (Swaminathan et al., 1991), whereas other studies indicate that they are (Yajima et al., 2005). The abundance of EBER expression in latently infected cells makes them a reliable marker of EBV infection, and they are widely used as probe target in *in situ* hybridisation (Chang et al., 1992).

EBERs are thought to be oncogenic, with transfection of EBERs into EBV-negative Akata cells leading to colony formation in soft agar and tumor development in immunodeficient mice (Komano et al., 1999). EBERs also induce secretion of IL-10, thought to stimulate B cell growth and suppression of CTLs (Kitagawa et al., 2000). In addition, in BL cells EBERs were shown to facilitate resistance to RNA dependent protein kinase mediated induction of the anti-tumour IFN-α response, by aiding avoidance of the immune system they prevent its apoptotic effects (Nanbo et al., 2002).

Alongside RNAs, EBV also encodes miRNAs that are non-coding but which function in the post-transcriptional downregulation of target mRNA (Pfeffer et al., 2004). There are two clusters of miRNAs in EBV; 14 are located in the introns of *BART* and three are adjacent to *BHRF1*. These clusters appear to be differentially expressed. High levels of *BART* miRNAs are found in epithelial cells but they are rarely detected or are at very low levels in B cells. Whereas *BHRF1* miRNAs are found at high levels in latency III B cells, but are almost undetectable in stage I or II B cells or epithelial cells (Cai et al., 2006). Both BHRF1 and BART miRNAs are thought to be important in transformation, and they help prevent apoptosis of newly infected primary B cells and BL cells, favouring cell cycle progression and proliferation (Seto et al., 2010; Vereide et al., 2014). In addition, EBV miRNAs were recently shown to be immunomodulatory, and they enhance viral immune evasion during both lytic and latent infection,

from both $CD4^{+ve}$ and $CD8^{+ve}$ T cells [(Albanese et al., 2016; Tagawa et al., 2016) and reviewed in (Albanese et al., 2017)].

1.2.9. EBV associated diseases

1.2.9.1. Infectious mononucleosis

The majority of people are infected with EBV either in the first few months of life or in early childhood. Seroconversion at a young age is generally asymptomatic, however, when infection is delayed into adolescence or young adulthood the self-limiting lymphoproliferative condition infectious mononucleosis (IM, also known as glandular fever) can occur (Balfour et al., 2015). Following EBV seroconversion, these patients typically present with tonsillitis, lymphadenopathy, myalgia, fatigue and fever. The longevity of this acute illness is notable, in that it generally lasts several weeks (Balfour et al., 2013). IM is further characterised by an abnormally large expansion of EBV-specific $CD8^{+ve}$ T cells, and high viral load in the oral cavity and blood (Balfour et al., 2013; Callan et al., 1996). It remains unclear why EBV infection in childhood is asymptomatic, but primary infection during adolescence can lead to IM. It is also unknown why some adolescents present with IM, while others are asymptomatic (Kuppers, 2003). Differences between immature and adolescent immune systems may contribute to this discrepancy.

1.2.9.2. B cell lymphomas

EBV is also associated with various B cell malignancies including BL, Hodgkin lymphoma (HL) and post-transplant lymphoproliferative disease (PTLD). These different EBV-associated lymphomas are associated with specific stages of B cell differentiation and their corresponding latency gene expression programmes (shown schematically in Figure 1.6).

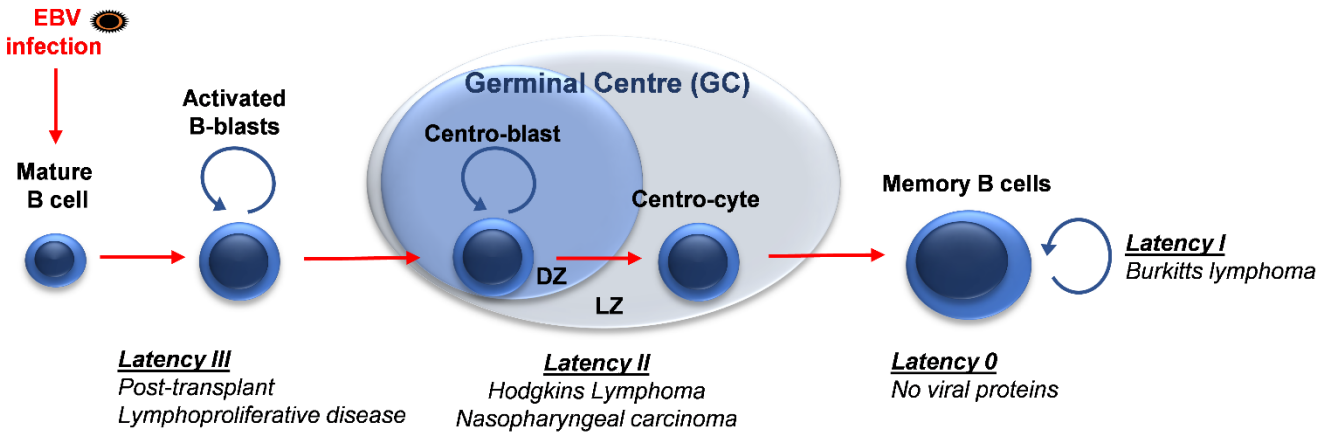


Figure 1.6. Schematic showing cancer subtypes and the associated cell types and EBV latency stages *in vivo*. Different EBV lymphomas originate from different stages of the infection process, and different latency transcription programmes. Tumours are thought to arise from the different stages of EBV biology that involve proliferation of the infected cell.

1.2.9.2.1. Burkitt lymphoma

BL is characterised as either endemic, sporadic or HIV-associated depending on geographical distribution and the presence of EBV (Brady et al., 2007). Endemic BL occurs prominently in sub-Saharan Africa and other areas where malaria is hyper-endemic. It has been established that in Africa around 95% of endemic BL is EBV positive (Brady et al., 2007), and children with the highest antibody titres against the virus are most at risk for developing BL tumours (De-Thé et al., 1978). In contrast to endemic BL, sporadic BL has lower incidence but worldwide distribution, with around 20% of sporadic BL tumours being EBV positive (Khan and Hashim, 2014). Despite histopathological similarities between endemic and sporadic EBV-positive BL, they have distinct growth characteristics and cell surface phenotypes when cultured *in vitro* (Rowe et al., 1985).

Rather than EBV, the characteristic hallmark of BL is translocation of the *c-MYC* proto-oncogene bringing it under the control of an immunoglobulin (Ig) locus, this disrupts BCL6-mediated repression and results in constitutively active expression of c-MYC in mature B cells (Manolov and Manolova, 1972; Taub et al., 1982). The over expression of c-MYC facilitates elevated proliferation of BL cells [reviewed in (Nguyen et al., 2017)]. As BL cells have somatically mutated Ig genes, they are thought to originate from post-GC MBCs (Klein et al., 1995). Furthermore, EBV positive BL exhibit a

latency I programme of viral gene expression where only EBNA1 is expressed. It is thought that in endemic BL, EBNA1 represses the tumour suppressive and apoptotic pathways that are usually activated by elevated c-MYC expression. This permits continual proliferation and survival of EBV-infected cells carrying the *c-MYC* translocation [reviewed in (Allday, 2009)]. When cultured *in vitro,* EBV-positive BL cell lines can switch from the restricted latency I programme to the latency III gene expression programme that is more characteristic of LCLs (Rowe et al., 1987).

1.2.9.2.2. Hodgkin lymphoma

HL is divided into two types: classical HL (cHL) or nodular lymphocyte predominant HL (NLP-HL). EBV association with cHL varies between 20-50% in western countries but higher rates are seen in underdeveloped countries (Chang et al., 1993; Weinreb et al., 1996). Prior presentation of IM has been linked with an elevated risk of developing EBV-associated cHL (Hjalgrim et al., 2000, 2007). In contrast to cHL, NLP-HL is more infrequent and rarely EBV-associated, although some studies suggest a proportion of NLP-HL are EBV positive (Wang et al., 2014).

cHL is characterised by the presence of multinucleated malignant Hodgkin/Reed-Sternberg (HRS) cells. HRS cells originate from mature B lymphocytes within the GC, however they aberrantly express markers of other haemopoietic cell types. They are characterised by the downregulation of global B-cell linage gene expression, resulting from the disruption of a number B cell specific transcription factors (Küppers, 2009). Lack of a functional BCR is characteristic of HL, and HRS progenitors successfully avoid the apoptosis that usually occurs in GC cells lacking BCR expression. The latency II programme (EBNA1, LMP1, LMP2A, LMP2B) is characteristically found in HL. It is thought expression of LMP1 and LMP2A, through their mimicry of the physiological functions of CD40 and BCR respectively, enables the survival and proliferation of BCR-deficient HRS cells though activation of signalling pathways and transcription factors that contribute to the rescue of infected cells from apoptosis (Murray and Bell, 2015). Indeed, almost all cases of cHL containing destructive immunoglobulin gene mutations are positive for EBV, indicating that cells carrying these mutations can only survive and lead to cancer if EBV is present (Bräuninger et al., 2006).

1.2.9.2.3. Immunodeficiency-associated lymphoproliferative disease

In healthy asymptomatic carriers, EBV infection is controlled by the immune system. However, immunosuppression either from late stage HIV infection, congenital immunodeficiency, or induced therapeutic immunosuppression increases the risk of developing B cell lymphoproliferative diseases such as PTLD. EBV-specific immune responses are impaired by the immunosuppression, allowing expansion of cells infected with the oncogenic EBV. This heterogeneous group of tumours are typically limited to lymph nodes and are commonly EBV positive (approximately 80%) (Khan and Hashim, 2014). PTLD EBV positive tumours typically exhibit the latency III programme and therefore express several viral latent proteins (Brink et al., 1997). Immunocompetent hosts would eliminate these cells, but in immunocompromised individuals, such as transplant recipients, infected cells are not eliminated and therefore can proliferate unchecked, leading to lymphoma development. When therapeutic immunosuppression is reduced, restoring T cell function, some PTLDs can be resolved (Haque et al., 1997).

1.2.9.2.4. Diffuse large B cell lymphoma

The heterogenous group of malignancies referred to as diffuse large B cell lymphomas (DLBCL) are subdivided into two major groups based on different gene expression profiles and mutagenesis signatures. These are GC B cell DLBCL (GCB-DLBCL) and activated B cell DLBCL (ABC-DLBCL) (Alizadeh et al., 2000). Approximately 10% of DLBCLs are EBV-positive, but a significantly higher incidence of EBV-positive DLBCL is found in the elderly and in immunocompromised patients (Heslop, 2005). As DLBCL is so heterogenous and can arise from different cell types, it is not associated with a single EBV latency pattern, and cells can express latency patterns II or III (or more infrequently I) depending on the origin of the infected cell. However, the majority of EBV-positive DLBCL is of the ABC type [reviewed in (Healy and Dave, 2015)].

1.2.9.3. EBV-associated carcinoma

Aside from lymphoid malignancies, EBV has also been etiologically associated with the epithelial carcinoma NPC and gastric carcinomas. In 2010, gastric cancer and NPC accounted for 92% of cancer deaths attributed to EBV, the majority of which occurred in East Asia (Khan and Hashim, 2014). The mechanisms behind NPC and GC tumorigenesis are less well characterised than in EBV-associated B cell lymphomas, with more known about the roles of EBV during NPC development than gastric carcinoma.

EBV is detected in around 10% of worldwide gastric carcinoma. EBV-associated gastric carcinoma are usually monoclonal proliferations of a single persistently infected EBV cell, usually expressing the latency I gene expression profile [reviewed in (Iizasa et al., 2012)]. In contrast, almost 100% of undifferentiated NPC are EBV positive (Khan and Hashim, 2014), and it is also thought to arise from the clonal expansion of a single proliferating EBV infected cell (Pathmanathan et al., 1995).

The link between NPC and EBV was first determined following the identification of high titres of EBV-specific antibodies in the serum of NPC patients (Gunvén et al., 1970). The discovery of EBV-positive NPC revealed EBV also infects epithelial cells, alongside its major target the B cell. EBV serology of IgA antibodies against various EBV replication derived antigens are specific markers for NPC development, reoccurrence and prognosis (Dardari et al., 2000). NPC expresses a latency II gene programme and have an abundance of EBV miRNAs (Brooks et al., 1992; Cai et al., 2006; Raab-Traub et al., 1983). The limited viral protein expression indicates the miRNAs contribute to the development of EBV-associated NPC, which largely occurs in hosts with competent immune systems (Raab-Traub, 2015). Consistent with this, BART miRNAs have been shown to potentiate tumour development and growth in a murine NPC model (Qiu et al., 2015). In addition, lack of EBNA2 and EBNA3 proteins, the major viral antigens targeted by CTLs (Hislop et al., 2007), likely contributes to immune evasion of NPC in the immunocompetent host.

Activation of NF-κB signalling pathways is thought to be important for NPC pathogenesis. Sequencing of NPC biopsy samples has shown negative regulators of NF-κB are the most frequently

mutated genes in NPC, resulting in overactive NF-κB signalling (Li et al., 2017). Similarly, LMP1 constitutively activates NF-κB signalling pathways. This indicates both host and viral selection of NF-κB activation in NPC (Li et al., 2017).

1.2.9.4. EBV and autoimmune diseases

Increasing evidence in recent years has suggested that EBV may be etiologically associated with various autoimmune conditions. Autoimmune conditions are complex disorders usually with genetic backgrounds with involvement of environmental factors, of which EBV is a plausible candidate for many syndromes. However, the most convincing epidemiological evidence supporting an etiological role for EBV in an autoimmune disorders is within multiple sclerosis (MS) and systemic lupus erythematosus (SLE), with higher disease frequency seen in those infected with EBV [reviewed in (Ascherio and Munger, 2015)].

EBV has been widely associated with MS, a chronic neurodegenerative disease, with meta-analysis of case control studies indicating that individuals who have a clinical history of IM have a 2.3 fold higher risk of MS compared to those without history of IM (Thacker et al., 2006). In addition, serum titres of antibodies targeted against EBNA proteins have also been identified as an MS risk factor, supporting an etiological role for EBV in MS development (Ascherio et al., 2001; Levin et al., 2005). Assessing anti-EBV antibodies in serial serum samples indicates MS risk is extremely low in EBV-negative individuals, but increases sharply upon infection with EBV (Levin et al., 2010).

EBV is also associated with the multisystem autoimmune condition SLE. However, in contrast to MS, no enhanced risk of SLE following clinical presentation of IM has been identified (Ulff-Møller et al., 2010). A meta-analysis of case control studies assessing EBV serology for anti-EBV capsid antigen (VCA) indicates a modest, yet significant, association between EBV infection and predisposition to SLE development (Hanlon et al., 2014). A study assessing 130 incidences of SLE indicated EBV infection preceded the onset of SLE and the presence of the autoantibodies characteristic of this condition (McClain et al., 2005). Furthermore, an approximately 40-fold increase in EBV viral load in peripheral

blood has been found in SLE patients compared to healthy controls. This is thought to be a consequence of defective immune control of EBV in SLE patients (Kang et al., 2004).

1.2.10. Immune responses to EBV

EBV achieves lifelong persistence and latency despite specific EBV-targeting immune responses, indicating EBV has evolved efficient strategies and mechanism to avoid the host immune system. EBV is controlled by both cellular and humoral immune responses. However, the immune system cannot completely eliminate the virus, allowing life-long latent infection. Consequentially, approximately 1 in 10,000-100,000 MBCs in an infected host are persistently infected with the virus (Laichalk et al., 2002). There is a delicate homeostasis of viral persistence and host immune control, with the absence of viral protein expression in latently infected MBC making them immunologically silent.

Adaptive immune responses are crucial for robust anti-EBV immune responses, with severe EBV-mediated disease evident in patients with defective T cell development or function [reviewed in (Palendira and Rickinson, 2015)]. Much of the knowledge regarding anti-EBV immunity is derived from the study of patients with the self-limiting EBV-mediated lymphoproliferative disease IM, following primary infection during adolescence. A rigorous cellular response is seen during IM, with up to 50% of $CD8^{+ve}$ cells in the peripheral blood identified as cytotoxic and directed against EBV-infected replicating cells. These EBV epitope-specific $CD8^{+ve}$ T cells can persist for at least 3 years at high levels (Callan et al., 1998). T cell responses are thought to predominantly target EBV lytic antigens, with up to 50% of the $CD8^{+ve}$ T cell population responding to individual lytic epitopes (Abbott et al., 2013; Quinn et al., 2014). Alongside lytic proteins, EBV latency-associated proteins, particularly the EBNA3 family, also provide immunodominant epitopes targeted by T cell immune responses [reviewed in (Hislop et al., 2007)]. *In vivo* infection of mice with human immune system components with EBV has further demonstrated primary infection results in expansion of EBV-specific $CD8^{+ve}$ T cells (Melkus et al., 2006; Strowig et al., 2009). Furthermore, severe EBV-mediated lymphoproliferative disease in the absence of T cell surveillance following therapeutic immunosuppression, can be reversed by infusion

of EBV-specific T cells (Haque et al., 2002). This highlights the importance of T cell mediated immune responses against EBV. Alongside the $CD8^{+ve}$ T cell response, there is a much smaller $CD4^{+ve}$ T cell response against lytic and latent antigens during IM, leading to $CD4^{+ve}$ memory B cells (Amyes et al., 2003; Long et al., 2011).

EBV also induces adaptive humoral immune responses, and serology is widely used for diagnosis of EBV-mediated diseases. Soon after the discovery of EBV, viral antigens were shown to interact with serum antibodies in the majority of individuals (Henle et al., 1974). Elevated IgG levels against the EBV lytic protein VCA first indicated a link between the virus and Hodgkin's lymphoma (Mueller et al., 1989) and NPC patients are characterised by elevated levels of IgG and IgA against EBV complexes, and a lack of EBV IgM (Cheng et al., 2002; Ji et al., 2007). Interaction of human antibodies with various immunodominant EBV proteins have been identified. This includes antibodies against viral capsid proteins, alongside latent and lytic proteins. EBNA1 is the major antigenic component of EBNA complexes that are reactive to human antibodies [reviewed in (Middeldorp, 2015)]. Elements of humoral responses against EBV have begun to be recapitulated within humanised mice models (Seung and Tager, 2013; Yajima et al., 2008).

Aside from EBV-specific adaptive immune responses, it is thought NK cells may play a role in anti-EBV immunity during the innate immune response. In a cohort of IM patients, significantly elevated levels of NK cells were identified at diagnosis and during the first month of EBV infection, and a higher proportion of NK cells correlated with significantly reduced viral loads (Williams et al., 2005). Furthermore, mice with immune system components with depleted NK cells exhibit enhanced tumorigenesis and pathogenesis compared to their NK-competent counterparts following EBV infection (Chijioke et al., 2013).

1.3. EBNA3 proteins are transcriptional regulators that affect host gene expression

Transition through the cell cycle is maintained by the stringent cooperation of cyclins, cyclin dependent kinases (CDK) and their inhibitors (CDKI), and retinoblastoma (Rb) protein pathways. Together they form a complex network of phosphorylation and feedback loops with distinct checkpoints that act as an intrinsic barrier against aberrant cellular transformation. EBV has evolved to manipulate various aspects of these cell cycle pathways. In particular, the concerted activity of EBNA3A and EBNA3C, predominantly through transcriptional regulation by polycomb protein mediated gene silencing, has been shown to deregulate the cell cycle. This allows sustained EBV-mediated cell proliferation, enabling efficient B cell transformation and consequently viral persistence.

1.3.1. Cell cycle regulation

1.3.1.1. The cell cycle

The cell cycle is a strictly controlled sequence of molecular events that govern the growth and duplication of all eukaryotic cells. Exact progression through the cell cycle is crucial and it is stringently regulated by an intricate and complex network of factors. Deregulation of the cell cycle is a common feature of oncogenesis, resulting from aberrant proliferation, as well as genomic and chromosomal instability. Correct progression through the cell cycle is monitored at specific checkpoints that assess possible defects during synthesis of DNA and chromosome segregation.

The cell cycle is comprised of four defined stages; the G1 phase, the S phase where DNA is replicated and synthesised, the G2 phase, and the mitotic (M) phase where the cell divides into two daughter cells. During the G1 and G2 gap phases, the cell prepares for the subsequent phases and RNA and protein synthesis occurs. Progression through each stage occurs in an orderly fashion and is tightly controlled by various regulatory proteins. This includes the CDKs 1,2 4 and 6, their substrate proteins referred to as cyclins and comprised of types A, B D and E, as well as the negative regulators

CDKI. Cyclins D and E mediate progression through the G1 and S phases, whereas cyclins A and B mediate transition through the S, G2 and M phases [(Figure 1.7), see (Becker, 2007) for a comprehensive review of the cell cycle].

CDK activity requires the binding of regulatory cyclins, this leads to the phosphorylation of target proteins that promote cell cycle progression. Cyclins are synthesised and degraded at distinct times during the cell cycle, therefore temporally control kinase activity. Fluctuations in cyclin expression results in oscillation of CDK activity, co-ordinating cell cycle phase transition. CDK and CDK-cyclin complexes are negatively regulated by CDKI that inhibit specific CDK-cyclin complexes, which prevent progression of the cell cycle. There are two major families of CDKI; the inhibitor of CDK4 (INK4) family and the CDK2-interaction protein (CIP)/CDK-inhibitory protein (KIP) family (see Section 1.3.1.3). The concerted activity of the cell cycle promoting CDK-cyclin complexes, relative to the CDKI cell cycle inhibitors govern progression through the cell cycle [reviewed in (Sherr and Roberts, 1999)].

Critical checkpoints are present at the interfaces between G1 and S phases, and between the G2 and M phases. Cell cycle arrest or senescence (permanent withdrawal from the cell cycle) is induced through modulation of CDK activity, mediated by CDKI regulation, if these checkpoints are activated (Becker, 2007).

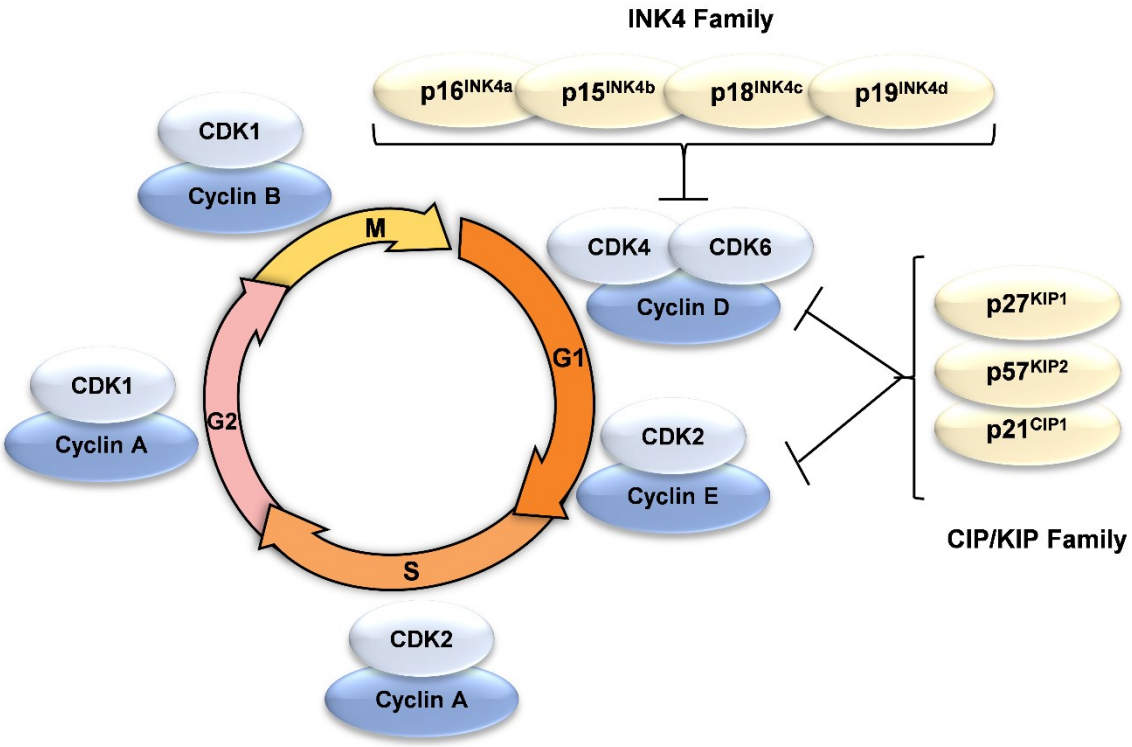


Figure 1.7. Overview of the cell cycle. The cell cycle progresses from the G1 phase, into the S phase where DNA is replicated, and then into the G2 phase and into mitosis (M), where cell division occurs. The G1-S and G2-M cell cycle checkpoints ensure correct completion of DNA replication and chromosome segregation before cell cycle progression, which is regulated by various feedback loops. Progression through the cell cycle is governed by the cyclins (A, B, D and E), cyclin dependent kinases (CDK 1, 2, 4 and 6) and the cyclin dependent kinase inhibitors (CDKI) comprised of the INK4 family ($p15^{INK4b}$, $p16^{INK4a}$, $p18^{INK4c}$, $p19^{INK4d}$) and the CIP/KIP family ($p27^{KIP1}$, $p57^{KIP2}$, $p21^{WAF1/CIP1}$). Figure adapted from (Dehay and Kennedy, 2007).

1.3.1.2. G1 phase progression and regulation

G1 is a critical phase, whereby the cell responds to extracellular cues to commit to cell division or withdraw from the cell cycle (G0) to progress instead along differentiation pathways (Sherr and Roberts, 1995). There are various controls during transition through G1 to ensure the integrity of DNA prior to the S phase, and ultimately cell division. Notably, there is a restriction point during late G1 phase, which represents a major control point for the regulation of cells entering the cell cycle. Once beyond this point, cell division becomes independent of growth signals and cells will invariably complete the cell cycle [reviewed in (Blagosklonny and Pardee, 2002)].

Upon entry of quiescent resting cells into the cell cycle, mitogenic signals induce expression of D-type cyclins, which assemble with CDK4 and CDK6 and lead to progression through the G1 phase. During the G1 phase, complexes of cyclin D with either CDK4 or CDK6 initiate phosphorylation and subsequently inactivation of members of the tumour suppressor Rb protein family; comprised of Rb/p105, p107 and Rb/130 (Giacinti and Giordano, 2006). Following this, CDK2-cyclin E complexes become active and phosphorylate Rb at additional sites. CDK mediated phosphorylation of Rb (pRb) leads to disassociation of pRB from transcriptional regulators, collectively termed E2F, which control the expression of genes required for G1 to S phase transition and DNA synthesis. Activation of cyclin A- and B-dependent CDK during later cell cycle stages, following E2F induced expression, maintains the hyper-phosphorylated from of pRb, until cells finish undergoing mitosis. At this point, pRb is returned to a hypo-phosphorylated state where it blocks the transactivation domain of E2F, and is therefore primed for the next G1 phase (Weinberg, 1995). The Rb protein plays a pivotal role during cell cycle transition, and correct expression is crucial for control of the major G1 restriction check point, leading to either cell cycle transition or the prevention of S phase entry [reviewed in (Giacinti and Giordano, 2006)].

Expression of CDKIs inhibits CDK4-and CDK6-induced phosphorylation of Rb and therefore prevents transition of the cell cycle from G1 to the S phase, causing cell cycle arrest. The CDKI $p16^{INK4a}$ has been widely shown to inhibit Rb phosphorylation and promote pRB:EF2 repressive complexes by binding CDK4 and CDK6, thus inhibiting cyclin D catalytic activity and leading to arrest of the cell cycle (Lukas et al., 1995; Serrano et al., 1993).

Conversely, loss of CDKI function can result in hyper-phosporylation of Rb, therefore allowing continued release of the E2F transcription factor. This checkpoint deregulation allows continued aberrant transition through the cell cycle. Inactivation of Rb regulation by continued hyper-phosphorylation is widely associated with cancer development, which is well characterised following loss of $p16^{INK4a}$ function (Sherr, 1996).

1.3.1.3. Cyclin-dependent kinase inhibitors (CDKI)

1.3.1.3.1. The INK4 family

The INK4 family of CDKI is comprised of $p15^{INK4b}$ [*CDKN2B* (Hannon and Beach, 1994)], $p16^{INK4a}$ [*CDKN2A* (Serrano et al., 1993)], $p18^{INK4c}$ [*CDKN2C* (Guan et al., 1994)], and $p19^{INK4d}$ [*CDKN2D* (Okuda et al., 1995)]. Each INK4 protein binds to CDK4 and CDK6, inhibiting their kinase activity by interfering with their association with the D-type cyclins. This can block cell cycle progression as inhibition of CDK4 and CDK6 leads to accumulation of hypo-phosphorylated pRb and subsequent G1 arrest of the cell cycle (Lukas et al., 1995).

$p16^{INK4a}$ is the most studied INK4 family member and was first identified as a binding partner of CDK4 and CDK6 by yeast two hybrid screening (Serrano et al., 1993). It has long been thought to act as a tumour suppressor (Lukas et al., 1995), with the altered activity of cyclin-CDK complexes during G1 exhibiting oncogenic potential (Hunter and Pines, 1994). The $p16^{INK4a}$ encoding gene *CDKN2A* in humans is adjacent to the *CDKN2B* gene which encodes the highly similar $p15^{INK4b}$ protein, of which $p16^{INK4a}$ shares 44% amino acid identity. The CDKI $p15^{INK4b}$ was first identified at high levels by immunoprecipitation of CDK4 and CDK6 in human keratinocytes undergoing G1 cell cycle arrest following treatment with transforming growth factor-β (Hannon and Beach, 1994). The adjacent *CDKN2A* and *CDKN2B* loci are also commonly referred to as the INK4a-ARF-INK4b locus. In addition to $p16^{INK4a}$, the *CDKN2A* gene also encodes $p14^{ARF}$ by an alternative reading frame. In contrast to $p15^{INK4b}$ and $p16^{INK4a}$, which target CDK, $p14^{ARF}$ modulates the tumour suppressive p53 pathway by promoting degradation of MDM2 (Zhang et al., 1998).

Following discovery of $p16^{INK4a}$ and $p15^{INK4b}$, a yeast interaction screen for proteins interacting with CDK6 identified the INK4 family member $p18^{INK4c}$, which was also demonstrated to weakly bind CDK4 (Guan et al., 1994). Aside from being a CDKI, $p18^{INK4c}$ has additionally been shown to be required for the differentiation of B cells to PCs [(Morse et al., 1997; Tourigny et al., 2002) see Section 1.1.4].

The least characterised of the INK4 proteins is $p19^{INK4d}$. Human $p19^{INK4d}$ was identified by a cDNA library screen using a probe obtained by cloning the previously identified murine $p19^{INK4d}$ (Hirai et al., 1995; Okuda et al., 1995). It was found $p19^{INK4d}$ shares around 86% identity with murine $p19^{INK4d}$ and around 44% homology with the other human INK4 proteins. Periodic expression of $p19^{INK4d}$ through the cell cycle indicated it also inhibits cyclin D kinases and their catalytic partners CDK4 and CDK6, consistent with $p16^{INK4a}$ (Okuda et al., 1995).

Each INK4 CDKI can lead to cell cycle arrest during G1 following interactions with CDK4 and CDK6, with aberrant expression of INK4 proteins widely associated with oncogenesis (Sherr and Roberts, 1999). The INK4 proteins all share a similar structure, comprised of several anykyrin repeats, suggesting evolution from a shared ancestral gene. However, they do show unique expression patterns depending on the cell and tissue, suggesting independent non-redundant functions [reviewed in (Thullberg et al., 2000)].

1.3.1.3.2. The CIP/KIP family

The CIP/KIP family is comprised of $p21^{CIP1/WAF1}$ [*CDKN1A,* (Gu et al., 1993; Xiong et al., 1993)], $p27^{KIP1}$ [*CDKN1B,* (Polyak et al., 1994a)] and $p57^{KIP2}$ [*CDKN1C* (Lee et al., 1995)]. This family of CKDI exhibit a broader spectrum of regulation and kinase selectivity than the INK4 family, and interact with both cyclins and CDK subunits. The CIP/KIP members are able to modulate the activity of CDK in complex with cyclins D, E, A and B. The CIP/KIP family share a common N terminal domain which mediates the binding of these CDKI to cyclins and CDK, but the remaining sequence diverges indicating distinct regulation and functions [see (Besson et al., 2008) for comprehensive review of the CIP/KIP family].

$p21^{WAF1/CIP1}$ was the first recognised CDKI, and was first shown to target CDK2 activity (Gu et al., 1993). Following screening of cDNA libraries with $p21^{WAF1/CIP1}$ probes, it was soon shown $p21^{WAF1/CIP1}$ was a potent inhibitor of all cyclin-CDK complexes, and a target of transcriptional activation by p53 (Xiong et al., 1993). Anti-proliferative effects of $p21^{WAF1/CIP1}$ are also facilitated through formation of a

quaternary structure with the proliferating-cell nuclear antigen (PCNA) alongside cyclins and CDKs, which blocks the DNA replication and synthesis needed for S phase progression (Waga et al., 1994).

The CDKI $p27^{KIP1}$ was identified first as an inhibitor of CDK2 complexes in G1, and subsequently cyclin D-CDK4 complexes (Polyak et al., 1994b, 1994a). It was soon shown to inhibit all G1 cyclin-CDK complexes (Cheng et al., 1998). Expression of $p27^{KIP1}$ is usually elevated in quiescent cells including mitogen starved cells (Besson et al., 2006), and in the absence of $p27^{KIP1}$expression, mice exhibit multiple organ hyperplasia and elevated tumorigenesis (Fero et al., 1996).

In addition to its role in repressing G1 and S phase CDKs-cyclin complexes, the CIP/KIP family member $p57^{KIP2}$ is thought to be the only CDKI required for embryonic development, and exhibits a higher level of tissue specific distribution compared to $p21^{WAF1/CIP1}$ and $p27^{KIP1}$ (Lee et al., 1995; Yan et al., 1997). It is thought $p57^{KIP2}$ has an important role in the cell fate decision to exit the cell cycle during development and differentiation. This is demonstrated by the severity of deletions in $p57^{KIP2}$ in mice, with embryos exhibiting hypoplasia and delayed differentiation, preventing the generation of $p57^{KIP2}$-null adult mice (Zhang et al., 1997).

Alongside their cell cycle inhibitory functions, the CIP/KIP family proteins have also been recognised to be regulators of transcription. It has been shown that $p21^{WAF1/CIP1}$ interacts with various transcription factors with broad functions [reviewed in (Besson et al., 2008)]. In particular, it is directly associated with inhibition of E2F, complementing the inhibition of CDK:cyclin complexes by enhancing repression of E2F targeted genes resulting in cell cycle arrest (Dimri et al., 1996). Furthermore, $p27^{KIP1}$ was shown to localize at gene promoters with p130-E2F enhancing recruitment of transcriptional co-repressors including SIN3A and histone deacetylases (Pippa et al., 2012).

1.3.1.4. The DNA damage response and cell cycle checkpoints

The DNA damage response (DDR) functions within the cell cycle process. It detects chemically and physically induced DNA damage and can signal growth arrest, DNA repair, DNA replication or cell death by apoptosis [reviewed in (Jackson and Bartek, 2010)]. The key DDR signalling components are the ataxia-telangiectasia mutated (ATM) and ATM- and RAD3-related (ATR) protein kinases, which

become activated by DNA damage such as double strand breaks and DNA replication fork arrest (Cimprich and Cortez, 2008; Shiloh, 2003). ATM/ATR orchestrate phosphorylation of hundreds of targets in signalling cascades, the best characterised of which are checkpoint kinase 1 and 2 (CHK1 and CHK2, respectively) (Bartek and Lukas, 2003). Together with CHK1 and CHK2, ATM/ATR act to reduce CDK activity by various mechanisms, some of which are mediated by the tumour suppressor and transcription factor p53. For example, activation of the CDKI $p21^{WAF1/CIP1}$ by p53 results in inhibition CDK4 and CDK2 activity, therefore preventing cell cycle progression and leading to G1 arrest (He et al., 2005).

ATM/ATR and CHK1/CHK2 mediated targeting of CDK results in slower cell cycle progression or cell cycle arrest, at both the G1- S phase and G2-M phase cell cycle checkpoints. This allows time for DNA repair mechanisms before S phase replication or M phase mitosis. ATM/ATR simultaneously trigger signalling cascades which induce DNA-damage repair protein expression, recruitment and activation. Successful DNA repair results in DDR inactivation and continued progression through the cell cycle (Jackson and Bartek, 2010). Alternatively, if the DNA damage cannot be resolved, chronic DDR signalling leads to apoptosis or cell senescence. This prevents passage of incorrect DNA into daughter cells and potential DNA damage induced oncogenesis (Bartkova et al., 2005, 2006). The DDR is crucial to correct cell cycling and defects in DDR associated factors are oncogenic [reviewed in (Kastan and Bartek, 2004)].

1.3.2. Control of gene regulation by polycomb proteins

Eukaryotic DNA within the cell nucleus exists in complex with histone proteins, which form nucleosomes, nucleosomes then form chromatin structures. Modification of chromatin structure can be achieved by covalent modification of specific residues within histones, including acetylation, phosphorylation, methylation or ubiquitination. These modifications can alter gene expression by facilitating active or inactive transcription. This is achieved by the unwinding or compacting of nucleosome structure, thus allowing or blocking the access of DNA binding proteins and transcription

factors, and preventing assembly of the RNA polymerase II complex [reviewed in (Felsenfeld and Groudine, 2003)].

The polycomb group (PcG) of proteins repress gene expression by inducing histone modifications which keeps chromatin in a transcriptionally inactive state. There are two core PcG complexes, comprised of multiple subunits with catalytic activity, and they are referred to as the polycomb repressive complexes 1 and 2 (PRC1 and PRC2, respectively). Broadly, PRC2 establishes repressive marks on chromatin, that are recognised by PRC1, which then stabilizes the repressive inactive state [for a review of PRC1 and PRC2 see (Aranda et al., 2015)].

PRC2 is comprised of three core proteins; enhancer of zeste 2 (EZH2), embryonic ectoderm development (EED) and the suppressor of zeste homolog 2 (SUZ12). But it can be found in complex with various other proteins [reviewed in (Vizán et al., 2015)]. PRC2 contains methytransferase activity, mediated by the EZH2 subunit, and is involved with inducing trimethylation, dimethylation and monomethylation on the lysine 27 of histone H3 (H3K27me3/me2/me1) (Ferrari et al., 2014; Kuzmichev et al., 2002). H3K27me3 is considered a repressive chromatin mark. PRC2 di- and mono-methylation of H3K27 is less well characterised, but has been suggested to be involved in gene activation (Ferrari et al., 2014).

PRC1 contains four core proteins; polycomb (PC), posterior sex combs (PSC), polyhomeotic (PH), RING1 and sex comb onmidleg (SCM), but many other proteins can be co-purified with these core proteins [reviewed in (Su et al., 2014)]. In contrast to the methyltransferase activity of PRC2, PRC1 complexes instead have E3 ligase activity mediated by the RING1 proteins (RING1a or RING1b). The best characterised substrate of PRC1 is the monoubiquitinated form of histone H2A at lysine 119 (H2AK119ub) (de Napoles et al., 2004; Wang et al., 2004). Following the association of the core PRC1 complex with CBX proteins, PRC1 is able to recognise the H3K27me3 repressive marks established by PRC2. PRC1 then monoubiquitinates H2AK119, which prevents RNA polymerase II elongation and therefore silences gene expression (Aranda et al., 2015; Zhou et al., 2008). The polycomb system has

been shown to be hijacked by EBV to induce transcriptional silencing of target genes (see Section 1.3.3).

1.3.3. EBNA3 mediated deregulation of the cell cycle

EBV has evolved various mechanisms to circumvent cell cycle pathways through interference with intrinsic cell cycle associated factors that induce anti-proliferative and suicide response signalling pathways. The best characterised example of this is EBNA3A- and EBNA3C-mediated repression of CDKIs (Allday et al., 2015). It is likely the concerted activities of the oncogenic EBNA3A and EBNA3C in the deregulation of the complex and tightly controlled molecular organisation of the cell cycle plays a crucial role in EBV persistence and transformation (Allday, 2013; Skalska et al., 2013).

1.3.3.1. EBNA3 regulatory mechanisms

Please note this section has been adapted from the author's previously published literature review (Styles et al., 2018).

EBNA3 proteins regulate many target genes and robustly associate with chromatin, but they do not directly bind DNA. Instead, the EBNA3 proteins bind and utilize many cell transcription factors to facilitate viral regulation of host genes. Detailed ChIP analyses and chromosome conformation capture techniques have begun to illuminate the intricacies of EBNA3 chromatin binding and the mechanisms of gene regulation employed by these EBV nuclear antigens. However, interactions between EBNA3C and various transcription factors and the regulatory mechanisms involved are much better characterised than those of EBNA3A, and especially EBNA3B, with the lack of an EBNA3B conditional system limiting investigation.

EBNA3-mediated gene silencing through association with transcription factors often involves localising polycomb repressive complexes to target genes. However, whether this is due EBNA3 recruitment or is a result of default gene repression mechanisms is largely unknown. The involvement of PRC2 in repression of EBNA3 target genes is well established, and has been shown to frequently result in deposition of the histone repressive mark H3K27me3, catalysed by the EZH2 methyltransferase subunit (Bazot et al., 2018; Harth-Hertle et al., 2013; Kalchschmidt et al., 2016a;

Kuzmichev et al., 2002; McClellan et al., 2012; Paschos et al., 2012; Skalska et al., 2010; Styles et al., 2017).

The EBNA3 proteins recruit transcription factors to chromatin to facilitate differential gene regulation. They all bind the notch signalling pathway DNA-binding factor RBP-Jκ via their homology domain (Kalchschmidt et al., 2016a; Robertson et al., 1996; Young and Rickinson, 2004; Zhao et al., 1996). RBP-Jκ is also competitively bound by the EBV transactivator EBNA2. The relationship between RBP-Jκ and EBNA2 and the EBNA3s is mutually exclusive, indicating co-operative and/or antagonistic functions (Wang et al., 2015; West, 2017). It was shown that interaction of RBP-Jκ with EBNA3A and EBNA3C is required to achieve the genetic reprogramming of B cells that allows the continuous proliferation of LCLs (Lee et al., 2009; Maruo et al., 2005). EBNA3A repression of the *CXCL9/CXCL10* locus is dependent on RBP-Jκ binding, leading to PRC recruitment and deposition of H3K27me3 (Harth-Hertle et al., 2013). Similarly, EBNA3C has been shown to recruit RBP-Jκ to the *COBLL1* and *ADAM28-ADAMDEC1* loci also leading to PRC2-mediated H3K27me3 deposition and repression (Kalchschmidt et al., 2016a). Interaction of EBNA3C with the histone lysine demethylase KDM2B was also recently shown to be important for EBNA3C-mediated repression of the *COBLL1* and *ADAM28-ADAMDEC1* loci, as it facilitates the removal of the H3K4me3 activation-associated histone mark prior to deposition of H3K27me3 (Gillman et al., 2018).

EBNA3C and EBNA3B (and to a lesser extent EBNA3A), have also been shown to bind to core binding factor β (CBFβ), which heterodimerizes with the transcription factor RUNX3 to form the core binding factor (CBF). EBNA3 binding to target gene loci was reduced when CBF was depleted by shRNA against CBFβ, indicating its importance for EBNA3 recruitment to chromatin (Paschos et al., 2017). EBNA3C has also been shown to interact with other transcriptional co-factors involved in histone modification and gene repression including histone deacetylases (HDACs), the co-repressor CtBP, the SIN3 transcription regulator family member A (SIN3A), the nuclear receptor co-repressor (NCoR) and the interferon regulatory factors IRF4 and IRF8 (Hickabottom et al., 2002; Jiang et al., 2014; Knight et al., 2003; Skalska et al., 2010; Touitou et al., 2001). Interestingly, IRF4 was found to be essential for

only EBNA3C binding to specific sites, not EBNA3A or EBNA3B, possibly indicating specific transcription factors contribute to the complexity of co-operative gene regulation by the different EBNA3 proteins (Wang et al., 2015). However, of proteins reported to interact with EBNA3s, only CtBP has been confirmed to be directly involved in gene repression by genetic analysis using recombinant EBV viruses in B cells. Here, the requirement for CtBP interaction was demonstrated for EBNA3-mediated repression of $p16^{INK4a}$ in B cells (Skalska et al., 2010).

Although EBNA3 proteins extensively bind across the genome and co-localise with various similar transcription factors, only a small proportion of binding sites are located near to the transcription start site of target genes. Instead EBNA3 binding sites are predominantly located at regulatory regions, classed as enhancer elements (McClellan et al., 2013; Paschos et al., 2017; West, 2017). These are characterised by high levels of H3 acetylation and histone modifications, alongside multiple transcription factor binding sites and can be intronic, upstream or downstream of genes (Heintzman and Ren, 2009; Whyte et al., 2013). The significant presence of EBNA3 proteins at enhancer regulatory elements indicates that long distance chromatin interactions are a prominent feature of EBNA3-mediated gene regulation (McClellan et al., 2013; Paschos et al., 2017; West, 2017). Specifically, EBNA3C, and in part EBNA3A, are thought to facilitate repression of the *ADAM28-ADAMDEC1* locus by promoting a long range interaction between an intergenic enhancer and their respective promoters leading to PRC2 mediated H3K27me3 deposition (Kalchschmidt et al., 2016a; McClellan et al., 2013). Additionally, EBNA3C promotes chromatin interactions between the downstream enhancer and promoter of *WEE1,* leading to gene repression (McClellan et al., 2013). In contrast, *BCL2L11* (BIM) and *CTBP2* repression are thought to result from EBNA3-mediated disruption of enhancer-promoter interactions (McClellan et al., 2013; Wood et al., 2016). Furthermore, it has been demonstrated that EBNA3A and EBNA3C can also activate transcription by promoting long distance chromatin interactions between distal enhancer elements and the transcription start site of the pri-miRNA of the miRNA 221/222 cluster (Bazot et al., 2015). Together, these observations suggest that EBNA3C, and probably EBNA3A, can both engage and disrupt long range chromatin interactions,

and that these structural changes can both enhance or repress gene transcription, likely in ways that can only be ascertained on a gene-by-gene basis.

Using microarray analysis, EBNA3A and EBNA3C have been demonstrated to both up- and down-regulate genes (White et al., 2010). EBNA3A and EBNA3C binding sites have been identified within 'contact domains' (genomic regions with shared proximity and consequently likely subject to some connected regulatory processes) of both up- and down-regulated target genes. It has been shown that EBNA3A and EBNA3C (Bazot et al., 2015), and EBNA3C independently (Kalchschmidt et al., 2016a) direct transcriptional activation of host genes. In contrast, direct association of EBNA3B binding near target genes is only evident for down-regulated EBNA3B targets, suggesting that EBNA3B functions directly only as a repressor. Therefore, any genes activated by EBNA3B are probably activated indirectly (Paschos et al., 2017). The molecular mechanisms responsible for EBNA3 mediated gene activation are poorly understood. However, EBNA3C has been shown to associate with the histone acyltransferase transcriptional co-activator p300, suggesting that acetylation may be involved with EBNA3C-mediated activation (Cotter and Robertson, 2000).

Epigenetic reprogramming of genes by EBNA3 proteins is imperative to permit B cell transformation and subsequent viral latency. The complexity of EBNA3 gene regulatory mechanisms likely relates to the wealth of transcription factors they can interact with. Despite recent insights, there remains much to be determined regarding the intricate and complicated molecular mechanisms employed by the EBNA3 proteins to regulate gene expression, especially regarding the basis of co-operative gene regulation by EBNA3 proteins, a phenomenon that is largely uncharacterised.

1.3.3.2. Transcriptional repression of $p16^{INK4a}$ and the INK4a-ARF-INK4b locus

Please note this section is taken directly from the author's previously published literature review (Styles et al., 2018).

EBV-mediated repression of the CDKI and tumour suppressor $p16^{INK4a}$ was first shown using a recombinant virus containing EBNA3C fused to estrogen receptor (ER). This showed that functional EBNA3C is essential to restrain expression of $p16^{INK4a}$ (Maruo et al., 2006). Inactivation of EBNA3C in

conditional LCLs leads to progressively increased levels of $p16^{INK4a}$ mRNA and protein, with correspondingly reduced levels of hyper-phosphorylated forms of Rb, a cessation of proliferation, and more cells in the G1 phase of the cell cycle (Maruo et al., 2006; Skalska et al., 2010, 2013). Increased $p16^{INK4a}$ levels were ablated by transfection of a plasmid expressing EBNA3C and by stabilisation of the conditional EBNA3C (Maruo et al., 2006). The *CDKN2A* gene encodes $p16^{INK4a}$, and also (by an alternative reading frame) encodes $p14^{ARF}$, which is also repressed by EBNA3C (Maruo et al., 2011). However, the consequences are functionally distinct. The $p16^{INK4a}$ protein interacts with the cyclin dependent kinases CDK4 and CDK6, preventing phosphorylation of the Rb protein leading to cell cycle arrest, whereas $p14^{ARF}$ interacts with MDM2, resulting in p53 activation and subsequent cell cycle arrest or apoptosis (Popov and Gil, 2010). Analysis of EBNA3A knockout and conditional LCLs has demonstrated that EBNA3A also plays a role in repressing both $p16^{INK4a}$ and $p14^{ARF}$ (Hertle et al., 2009; Maruo et al., 2011; Skalska et al., 2010). The importance of $p16^{INK4a}$ repression during B cell transformation by EBV was highlighted by evidence that EBNA3C becomes unnecessary for transformation and sustained proliferation when $p16^{INK4a}$ is functionally inactive. In an elegant experiment, Skalska *et al*. showed that EBNA3C-null LCLs can be readily produced from B cells derived from an individual with a homozygous deletion in *CDKN2A* that inhibits all known $p16^{INK4a}$ functions. This demonstrated that EBNA3C-mediated repression of $p16^{INK4a}$ plays a crucial role in the transformation of B cells by EBV (Skalska et al., 2013).

ChIP analysis indicates EBNA3A and EBNA3C directly repress $p16^{INK4a}$ through epigenetic chromatin modification, via deposition of the polycomb-associated repressive mark H3K27me3, and reduction of the activation mark H3K4me3 at the *CDKN2A* locus (Maruo et al., 2011; Skalska et al., 2010). Moreover, epigenetic regulation of *CDKN2A* by EBNA3s is maintained in the absence of functional $p16^{INK4a}$, further indicating *CDKN2A* is a direct target of EBV (Skalska et al., 2013). The chromatin remodelling of *CDKN2A* by EBNA3A and EBNA3C was shown to require interaction with the transcriptional co-repressor CtBP (Skalska et al., 2010). CtBP is the collective term for the proteins CtBP1 and CtBP2, which promote cell survival and are associated with repression of various tumour

suppressors [reviewed in (Chinnadurai, 2009)]. EBNA3A and EBNA3C, but not EBNA3B, have been shown to interact with CtBP, and they are readily immunoprecipitated together from LCL extracts (Hickabottom et al., 2002; Touitou et al., 2001). Mutating the CtBP binding sites within EBNA3A and EBNA3C compromises transformation of primary B cells infected with recombinant EBV, and similarly compromises transformation of rodent embryo fibroblasts following transfection with EBNA3A or EBNA3C (Hickabottom et al., 2002; Skalska et al., 2010; Touitou et al., 2001). In B cells, mutation of CtBP binding sites within EBNA3A and EBNA3C correlates with significantly reduced H3K27me3 at the *CDKN2A* locus, alongside increased H3K4me3. The resulting increases in $p16^{INK4a}$ mRNA and protein are thought to contribute to the impaired outgrowth of primary B cells infected with EBV containing mutated CtBP binding sites in EBNA3A and EBNA3C, and the reduced proliferative capacity of resulting LCLs (Skalska et al., 2010).

Alongside *CDKN2A*, EBNA3 proteins have also been shown to repress the adjacent gene *CDKN2B.* This gene encodes the related INK4 family protein $p15^{INK4b}$, which performs similar functions to $p16^{INK4a}$ (Popov and Gil, 2010). EBNA3A-mediated transcriptional repression was shown to occur via interactions with the transcriptional factor MIZ1, leading to subsequent deposition of the repression histone mark H3K27me3 in close proximity to the transcription start site, as seen with $p16^{INK4a}$ repression (Bazot et al., 2014; Skalska et al., 2013). Furthermore, increased $p15^{INK4b}$ mRNA transcription has been reported following EBNA3C inactivation in conditional systems, demonstrating EBNA3C involvement in $p15^{INK4b}$ repression (Jiang et al., 2017; Styles et al., 2017). As with *CDKN2A,* ChIP analyses have indicated EBNA3A and EBNA3C bind near the transcription start sites of the *CDKN2B* locus, suggesting EBNA3A and EBNA3C play a direct repressive role (Jiang et al., 2014, 2017; Skalska et al., 2013).

1.3.3.3. Translational and proteasomal degradation of the CIP/KIP family

Please note this section is taken directly from the author's previously published literature review (Styles et al., 2018).

As well as directly repressing genes of the CDKI INK4 family, EBNA3A and EBNA3C can indirectly repress cell cycle components through transcriptional activation of repressive miRNAs. EBNA3A and EBNA3C were recently shown to mediate transactivation of the oncogenic miRNA cluster miR221 and miR222 (miR221/222), leading to repression of the CDKI $p57^{KIP2}$ and, to a lesser extent, $p27^{KIP1}$ (Bazot et al., 2015).

Screening LCLs, where EBNA3A and EBNA3C were either conditionally expressed or knocked out, identified modified expression of various miRNAs by the EBNA3 proteins. Expression of the oncogenic miR221/222 cluster was shown to be reduced when either EBNA3A or EBNA3C was non-functional, with a significant increase in miR221/222 mRNA when EBNA3A and EBNA3C were conditionally activated. ChIP analysis confirmed EBNA3A and EBNA3C binding sites within an enhancer element of the pri-miR221/222 loci from which miR221 and miR222 are processed. ChIP analysis further revealed an altered epigenetic profile in which the transcriptional activation markers H3K4me3, H3K9ac, H3K27ac, and phospho-Ser5 Pol II were elevated at the transcription start site only when EBNA3A and EBNA3C were functionally expressed. Furthermore, chromosome confirmation capture established that long range chromatin interactions between EBNA3A and EBNA3C binding sites within the predicted enhancer site of pri-miR221/222 and its promoter only occur when EBNA3A and EBNA3C are functionally active. The miRNA221/222 cluster targets the CDKIs $p57^{KIP2}$ and $p27^{KIP1}$; transcriptional activation of the miRNAs by EBNA3A and EBNA3C leads to repression of $p57^{KIP2}$ and, to a lesser extent, $p27^{KIP1}$. This provides a novel indirect method of cell cycle regulation mediated by EBNA3A and EBNA3C gene activation (Bazot et al., 2015).

Alongside indirect repression of $p27^{KIP1}$ and $p57^{KIP2}$, EBNA3A and EBNA3C have also been associated with repression of the CDKI and CIP/KIP family member $p21^{WAF1/CIP1}$ (Banerjee et al., 2014; Tursiella et al., 2014). In contrast to the direct polycomb-mediated transcriptional repression of the INK4 proteins, or miRNA-mediated translational regulation of $p57^{KIP2}$ and $p27^{KIP1}$, EBNA3C works directly though interactions with the oncogenic kinase Pim-1 to result in proteasomal degradation of $p21^{WAF1/CIP1}$ (Banerjee et al., 2014).

There is compelling evidence that transcriptional repression of $p16^{INK4a}$ is the dominant factor in EBNA3A- and EBNA3C-mediated cell cycle control during B cell transformation by EBV (Skalska et al., 2013). However, EBNA3A and EBNA3C have been shown to target many CDKIs, employing diverse mechanisms that encompass regulation at the transcriptional, translational, and protein level (summarised in Figure 1.8). This suggests the EBNA3 proteins function to achieve a specific molecular balance that allows control of the cell cycle by EBV, enabling establishment of viral latency.

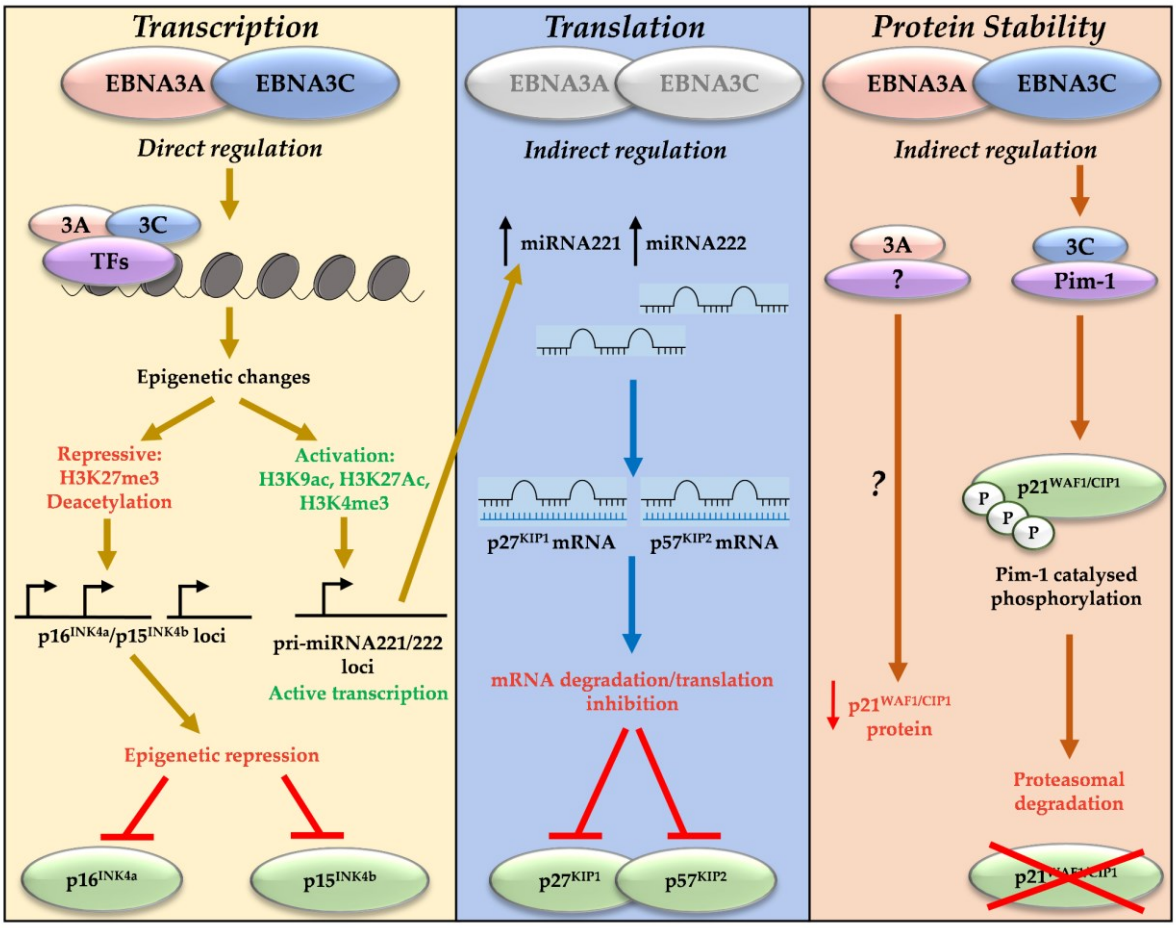


Figure 1.8. EBNA3A and EBNA3C regulate CDKI at a transcriptional, translational and protein level. EBNA3A and EBNA3C bind cell transcription factors (TFs) including RBP-Jκ, CBF, and IRF4. This results in polycomb complex recruitment and deposition of chromatin marks on the loci of target genes. These chromatin marks can either repress transcription (the CDKIs $p16^{INK4a}$ and $p15^{INK4b}$) or activate transcription (miRNA221/222). EBNA3-mediated activation of miRNA221/222 leads to subsequent repression of the CDKI $p27^{KIP1}$and $p57^{KIP2}$ via translation inhibition. EBNA3A and EBNA3C can also repress CKDI by targeting them for degradation. EBNA3A mechanisms are unclear, but EBNA3C has been shown to mediate Pim-1 catalysed phosphorylation and subsequent proteasomal degradation of $p21^{WAF1/CIP1}$. Figure reproduced from (Styles et al., 2018).

1.3.3.4. Anti-apoptotic functions of EBNA3A and EBNA3C

Please note this section is taken directly from the author's previously published literature review (Styles et al., 2018).

Concurrent with manipulation of CDKI and cell cycle control, EBNA3A and EBNA3C further facilitate virally-induced proliferation and oncogenesis by repressing apoptotic responses to viral infection and transformation. Using a panel of EBNA3KO viruses in BL31 BL-derived cells, EBNA3A and EBNA3C were found to cooperatively repress the tumour suppressor and pro-apoptotic BCL-2-family member BIM (Bcl-2-interacting mediator of cell death) encoded by *BCL2L11* (Anderton et al., 2008). EBNA3-mediated regulation of BIM was also observed in LCLs, with repression shown to be reversible using an EBNA3C conditional system, whereby inactivating EBNA3C for three weeks led to elevated BIM mRNA levels (Paschos et al., 2012; Skalska et al., 2013). BIM becomes upregulated during unscheduled cellular proliferation and directly initiates apoptosis through inhibition of BCL2 and other pro-survival proteins. This is particularly important during the development of lymphocytes, as BIM mediates negative selection of auto-reactive B cells, and initiates programmed cell death in B cells expressing low-affinity antibodies in the GC (Enders et al., 2003; Fischer et al., 2007; Strasser, 2005). Furthermore, BIM is activated by the proto-oncogene *c-MYC*, which is expressed by B cells following EBV infection and induces hyper-proliferation. A hallmark of BL is translocation of *c-MYC* and subsequently constitutively elevated expression (Dang et al., 2005). BIM is the effector of one of the accumulative apoptotic pathways triggered by c-MYC overexpression (the other being the $p14^{ARF}$–MDM2–p53 pathway) and it has been shown that even loss of a single *BIM* allele accelerates B cell lymphomagenesis (Egle et al., 2004). The epigenetic mode of BIM repression by EBNA3A and EBNA3C may be important for BL development, since it can create an environment permissive for c-MYC overexpression even after EBNA3A and EBNA3C expression is shut down, as the virus progresses through different stages of latency (Anderton et al., 2008; Paschos et al., 2009; Thorley-Lawson and Allday, 2008).

Analogous with the epigenetic repression of INK4 family proteins, detailed ChIP analysis of EBV-positive B cells indicated that EBNA3-mediated repression of BIM involves modification of chromatin marks. This includes a reduction of histone acetylation and deposition of the H3K27me3 repressive mark within the *BCL2L11* locus, facilitating transcriptional repression (Paschos et al., 2009). Direct participation of EBNA3 proteins in repression of BIM was subsequently demonstrated when binding of EBNA3C to sites proximal to the *BCL2L11* transcriptional start site was confirmed by ChIP analysis, with later studies showing concurrent EBNA3A binding sites (Paschos et al., 2012; Wood et al., 2016). Furthermore, EBNA3A and EBNA3C were found to recruit the PRC2 subunits SUZ12 and EZH2 to BIM regulatory elements, facilitating H3K27me3 deposition (Paschos et al., 2012). A requirement for the polycomb system in EBV-mediated repression of BIM was further confirmed as BIM repression was found to be disrupted by lentiviral delivery of shRNA against PRC2 components, and reversed by an EZH2 inhibitor (Paschos et al., 2012; Wood et al., 2016). EBNA3A- and EBNA3C-mediated repression of BIM was also recently shown to involve long range chromatin interactions between the BIM promoter and enhancers bound by EBNA3A and/or EBNA3C (Wood et al., 2016).

In addition to EBNA3A- and EBNA3C-mediated repression of the important tumour suppressors $p16^{INK4a}$ and BIM and various CDKI, EBNA3C has been shown to attenuate the DDR, which functions to limit aberrant proliferation by inducing senescence or apoptosis (Nikitin et al., 2010). The DDR is transiently activated in response to the hyper-proliferation of EBV infected cells during primary infection. However, EBNA3C was shown to attenuate this response by inhibiting the DDR kinases CHK2 and ATM (Nikitin et al., 2010). Induction of the DDR temporally correlates with the transient increase in $p16^{INK4a}$ expression seen following primary infection (Skalska et al., 2013). This is associated with oncogene activation, but is also speculated to be a consequence of DNA damage due to hyperproliferating cells inappropriately entering the cell cycle S phase (Allday, 2013; Skalska et al., 2013). The continuation of the DDR, as well as $p16^{INK4a}$ and BIM activation, is prevented by the expression of functional EBNA3C and EBNA3A. This prevents the apoptosis and cell cycle arrest pathways that would be activated by EBV infection (Allday, 2013; Nikitin et al., 2010; Skalska et al.,

2013). Furthermore, EBNA3C has also been associated with the repression of other factors involved in the cell cycle, DDR, apoptotic pathways and the oncogenic stress response, including MDM2, p53, H2AX, pRb, E2F1, Cyclin A, Cyclin D1, Cyclin D2, ubiquitin ligase SCF^{SKP2} and c-MYC (Bajaj et al., 2008; Jha et al., 2014; Knight and Robertson, 2004; Knight et al., 2005b, 2005a; Pei et al., 2018; Saha et al., 2009, 2012; Yi et al., 2009).

EBNA3A and EBNA3C mediated regulation of CDKI and the DDR is extensive. Regulation of these host factors and pathways is achieved through a variety of molecular mechanisms including transcription regulation, regulation via translation inhibition and through protein:protein interactions, demonstrating the broad activities of these oncogenic proteins.

1.4. Recombinant EBV viruses allow analysis of EBNA3 function

1.4.1. Use of BAC-derived EBV

Bacterial artificial chromosome (BAC) vectors are based on the *E. coli* fertility factor (F-factor) replicon and are used in cloning of large DNA fragments. This replicon is stably maintained in the bacterial host as a circular supercoiled extrachromosomal single copy plasmid and can be easily modified (Hall et al., 2012; O'Connor et al., 1989). As BACs can carry insets of up to 300 Kb they are able to accept the genome of dsDNA viruses. Use of BACs enables the study of mutagenesis of a viral genome using highly versatile genetic tools developed in bacteria. Lucklow and colleagues were the first to demonstrate cloning of a complete genome of a large dsDNA virus into a BAC vector (Luckow et al., 1993). This technology was extended into herpesvirus research when the complete genome of murine cytomegalovirus was cloned into a BAC. This allowed recovery of infectious virus following introduction of the BAC virus into susceptible cells (Messerle et al., 1997).

Both the B95.8 EBV genome and Akata genome have now been cloned into BAC constructs (Delecluse et al., 1998; Kanda et al., 2004). In the Allday Laboratory we focused on the use of the B95.8 strain, this prototypical laboratory adapted stain is hereafter referred to as WT. To generate modified recombinant EBV for the study of specific viral proteins, mutations or modifications have been made

within the B95.8 BACs. However, it must be noted that the B95.8 strain was selected for study due to its transformative ability in the lab and it has been passaged through marmoset lymphocytes (Miller et al., 1972). Furthermore, it contains a genomic deletion, resulting in the lack of most EBV encoded miRNAs as well as a lytic origin of replication (Parker et al., 1990; Raab-Traub et al., 1980).

The use of this BAC technology has permitted the generation of various recombinant EBV viruses using DNA manipulation within *E.coli* (Delecluse et al., 1998). Homologous recombination between wild type and mutant versions of a gene of interest can be used to construct recombinant EBV BACs, allowing study into the host phenotype and transcriptome associated with individual EBV latent genes. A target vector is used containing a mutated version of the gene of interest flanked by sequences homologous to the wild type version in the genome. This can be used to both introduce mutations and also to achieve deletions of specific genes. Eukaryotic and prokaryotic resistance cassettes, including antibiotic resistance and the green fluorescent protein (GFP), have also been introduced into the BAC constructs to allow manipulation and selection of specific genetic sequences [reviewed in (Feederle et al., 2010)].

1.4.2. Recombinant EBV viruses available for the study of EBNA3 proteins

BAC technology has been used to generate various EBV recombinant viruses containing EBNA3 genetic modifications. This has permitted detailed study of each of the EBNA3 proteins within the context of infection, transformation of B cells, establishment of LCLs and maintenance of viral latency. An overview of the EBNA3 modified recombinant viruses used in this study can be found in Figure 1.9.

Recombinant EBNA3 knockouts (KO), for EBNA3A, EBNA3B and EBNA3C independently, have been generated using truncating mutations, as well as a KO lacking the entire EBNA3 locus (Anderton et al., 2008; White et al., 2010). All KO also have a corresponding revertant, in which the deleted genes were reintroduced to control for off-target secondary mutations resulting from the homologous recombination that may differ from WT.

Conditional systems for the EBNA3 proteins have also been established. These systems use a modified murine estrogen receptor (ER) fused to the open reading frames of EBNA3A or EBNA3C. This renders functional expression of the resulting fusion protein dependent on the presence of estrogen, or its related analogue 4-hydroxytamoxifen (HT). The introduction of HT to the culture of cells infected with a conditional virus stabilises the EBNA3-fusion protein, allowing nuclear localisation and functional expression. In the absence of HT, the conditional fusion proteins are retained in the cytoplasm where they are inactive and degraded (Maruo et al., 2003, 2006; Skalska et al., 2010). Recently, a more modified estrogen receptor (ERT2) has been utilized for the generation of conditional viruses for EBNA3A and EBNA3C independently (Bazot et al., 2015; Styles et al., 2017).This modified ERT2 receptor contains a G400V/M543A/L544A triple mutation, which makes the receptor insensitive to endogenous mouse estrogen permitting use of these viruses *in vivo*. In addition, it is more sensitive to HT than previously used ER fusions (Feil et al., 1997). Thus far, a virus with HT-dependent conditional expression of EBNA3B has not been established.

Recombinant EBV with epitope-tagged EBNA3 proteins have also been developed, including using a FLAG-STREP II Tandem Affinity Purification (TAP) tag (Gloeckner et al., 2007) fused to EBNA3A, EBNA3B or EBNA3C (Paschos et al., 2017). These epitope-tagged EBNA3 BAC viruses have been widely used in ChIP-seq experiments and have enabled identification of thousands of EBNA3 binding sites across the genome (Jiang et al., 2014; McClellan et al., 2012, 2013, Paschos et al., 2012, 2017; Schmidt et al., 2015).

Transfection of modified recombinant EBV BACs into 293-HEK cells establishes virus producer lines. Inducing the lytic cycle by transient expression of BZLF1 and BALF4 lytic genes results in the production and secretion of infectious EBV virions into the culture supernatant. This supernatant can then be used to infect peripheral blood leucocytes or $CD19^{+ve}$ purified primary B cells. Together, EBNA3-modified BAC-derived recombinant EBV viruses have enabled robust genetic analysis of the contribution of each EBNA3 protein to the biology of EBV.

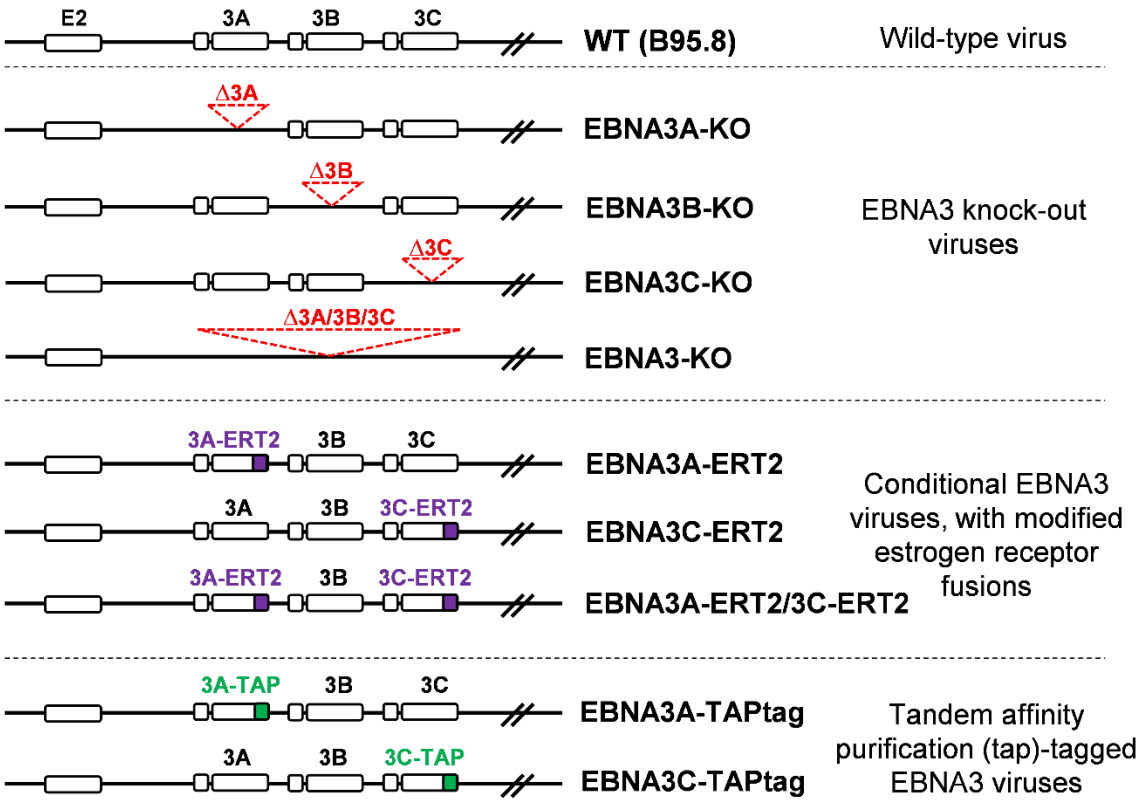


Figure 1.9. Overview of available EBV recombinant BAC viruses. Overview of EBV recombinant viruses derived from the prototype WT stain B95.8 BAC used in this project. Knock-out viruses contain deletions for EBNA3A (Δ3A), EBNA3B (Δ3B), EBNA3C (Δ3C) or all 3 EBNA3 proteins (Δ3A/Δ3B/Δ3C) (Anderton et al., 2008; White et al., 2010). Conditional viruses contain a C-terminal fusion to a modified oestrogen receptor for either EBNA3A, (EBNA3A-ERT2), EBNA3C (EBNA3C-ERT2) or both EBNA3A and EBNA3C (EBNA3A-ERT2/3C-ERT2) [see Chapter III for further description (Bazot et al., 2015; Skalska et al., 2010; Styles et al., 2017)]. Tandem affinity purification (TAP)-tag were fused to either EBNA3A or EBNA3C and contain a Flag-2X Strep tags utilized in chromatin immunoprecipitation (Paschos et al., 2012).

1.5. Epstein Barr virus infection in vivo

1.5.1. Limitations of research in vitro

Although an invaluable and essential tool in biological research, results gained from research using *in vitro* cell culture systems have inherent limitations regarding extrapolation of results to the complexity of living organisms. *In vitro* research is largely performed in cancerous cell lines which are continuously passaged. Cancer cells can have substantially abnormal functions, potentially making extrapolation to normal cells misleading. *In vitro* cell lines also do not exhibit cytokine and chemokine

interactions or immunomodulation of infection. Furthermore, *in vitro* cell cultures are limited by a lack of biokinetics and metabolism pathways, the absence of the 3-dimensional tissue architecture found *in vivo* and by the lack of interaction between different cell types (Shetab-Boushehri and Abdollahi, 2012).

Extrapolation of *in vitro* research to the effect in humans has inherent limitations, whereas *in vivo* research in animal models have the advantage of assessing infection within the context and complexity of a living organism. In contrast to *in vitro* cell lines, *in vivo* animal models allow investigation of the mechanisms of diseases alongside subsequent immunological responses, which can then be used to predict human outcomes (Eynon and Flavell, 1999; Kohnken et al., 2017). However, although a valuable resource, there are ethical issues around the use of animals for *in vivo* research, with an important emphasis on reduction of animals being used, refinement of experiments and replacement of animal research where possible for *in vitro* systems (Russell WMS, 1992). There also remain drawbacks with regards to extrapolation of *in vivo* results to that of humans, with differences in physiological and biological parameters. Additionally, it should be noted that *in vivo* models can represent specific characteristics of human infections, but are unlikely to cover all aspects of diseases (Johnson et al., 2001; Rezaee and Abdollahi, 2017). Nonetheless, the use of *in vivo* models is an invaluable asset to biological research in which to expand biomedical knowledge.

1.5.2. In vivo mouse models of human disease

Mice have long been considered the animal model of choice for biomedical research and are a significant and powerful research tool for mimicking clinical behaviour of human disease (Kohnken et al., 2017). Mice are appealing models of human disease for a variety of reasons. These include the relative similarity of human and mouse genetics, with over 90% gene homology between the species and the ability to comprehensively experimentally manipulate mouse genetics (Waterston et al., 2002). Mice also have similar anatomical characteristics to humans, providing ability to assess organ systems. The small size of mice, ease of handling, short life span, breeding reliability and commercial abundance makes them a convenient and practical option compared to larger and more expensive

animal models (Kohnken et al., 2017). In addition, due to their extensive use over decades there is a wealth of antibodies and reagents available to use with these model systems. In particular, the field of immunology has benefitted immeasurably from the use of mouse models and much of the workings of the immune system has been derived from research in mice. However, inherent differences between mice and humans create difficulties in their use as models of infectious diseases (Coers et al., 2009).

Some infectious agents are able to infect both humans and rodents enabling the use of simple mouse models, for example mice can be used to study the diseases caused by *Yersinia pestis* bacteria (Ngampasutadol et al., 2008) or influenza virus (Groves et al., 2018). However, in many cases co-evolution of hosts and pathogens has led to strict host tropisms which limits the use of mice for the study of human diseases. Alternatives such as the use of homolog infectious diseases can act as models of human infection. However, the extrapolation of results to that of the human phenotype can be difficult. For example, the murine γ-herpesvirus 68 (MH-68) acts as model to human herpesvirus diseases, in particular Karposi's sarcoma-associated herpesvirus (KSHV), and has led to insights into the pathogenesis and biology of γ-herpesviruses (Blackman and Flaño, 2002).

For diseases lacking murine homologs, the use of transgenic mice with genetic modifications to permit infection with human infectious agents can allow the study of human diseases within mouse models. The introduction of transgenes expressing the receptors for human tropic viruses, such as adenoviruses (Wang et al., 2012), measles virus (Sellin and Horvat, 2009) and coronavirus (Lassnig et al., 2005), permits murine infection. However, this is not feasible for all viruses. Alternatively, insight into the functions, phenotype and immunological changes associated with the expression of specific pathogen genes can also be gained through the introduction of specific pathogen genetic material into mice. For example, transgenic mice expressing the EBV latent protein LMP1 can be used to study EBV-induced immune surveillance and lymphomagenesis (Zhang et al., 2012). To avoid the possible consequences of gene alteration during development, conditional models have been developed to allow spatially and temporally controlled gene alterations. This can be achieved by cross-breeding

mice carrying Cre-recombinase effector genes with mice carrying target genes incorporating a *loxP-stop* cassette (Kohnken et al., 2017; Rosenthal and Brown, 2007).

Over the last decade there has been extensive development regarding the use of severely immuno-compromised mice engrafted with human immune system components. These humanised mouse models more closely mimic human disease and have enabled investigation into infectious agents with strict tropisms to human immune cells, particularly viruses such as EBV (described in detail in Section 1.5.4). Humanisation of specific target organs has also been performed, for example human liver-chimeric mice. For this, severely immunocompromised mice are transplanted with human hepatocytes leading to up to 95% human liver chimerism. This makes them permissible to pathogens such as hepatitis B and C, permitting study into the biological mechanisms of these viruses (Bissig et al., 2010). In addition, different model systems can be combined. For example, mice harbouring human hepatocytes alongside human immune system components have been shown to recapitulate HCV-specific pathogenesis, as well as HCV-associated immune responses (Washburn et al., 2011).

Although mouse models of human infection and cancer permit extensive advances to our knowledge of human diseases, it must be noted that these models require extensive validation and careful consideration in the extrapolation of data to a human phenotype. Alongside differences in the tropism of infectious diseases, immunological, environmental and physiological differences remain. For example, this includes the predominance of lymphocytes in white blood cell composition in mice, whereas in humans neutrophils are dominant (Doeing et al., 2003). The extent of which human disease can be recapitulated within the mouse model must be considered. However, animal models remain and invaluable tool for scientific research of human disease.

1.5.3. Use of tamoxifen systems for gene modification in mouse models

Modified ER systems for conditional expression of proteins in mice can be used to temporally activate or deactivate gene expression, in a temporal or spatial manner *in vivo*. The most prominent use of inducible tamoxifen systems in mice is within Cre-recombinase systems in transgenic mice. Here, mice are bred to contain Cre fused to a modified ER rendering functional expression of Cre

dependent on the presence of the activating ligand HT, which can be delivered via tamoxifen. Stabilisation of the Cre-ER fusion protein by addition of HT allows expression of Cre-recombinase, which specifically excises target genes flanked by loxP sites leading to gene activation or deactivation (Feil et al., 1997; Whitfield et al., 2015; Wilson et al., 2014). Cre-ER systems can also be used in a tissue specific manner, with transgenic mice expressing Cre-ER under the control of a liver specific promoter enabling specific genetic study of liver pathology (Zhu et al., 2003).

The reversible aspects of HT induced systems, which require continuous HT for gene stabilisation, have been widely used in the study of cancer (Whitfield et al., 2015). Oncogenes, such as c-MYC, fused to mutated ER have been used to establish whether sustained gene activation is required to maintain a cancerous phenotype (Murphy et al., 2008). Similarly, inducible HT systems in combination with tumour suppressors such as p53 have revealed aspects of their biology, for example the kinetics and reversibility of p53-mediated responses *in vivo* (Christophorou et al., 2005).

Various routes of administration can be used for HT. Most prominently used is intraperitoneal injection of HT or use of tamoxifen impregnated food, which is then metabolised to HT in the mouse liver (Wilson et al., 2014). The demand for tamoxifen usually defines usage, as some models require continual administration of tamoxifen whereas others require only one dose. Despite the aversion to tamoxifen impregnated food leading to weight loss, this method is less stressful and more humane when continuous tamoxifen is required, as it does not involve daily injection of a HT-oil emulsion (Kiermayer et al., 2007; Wilson et al., 2014).

At the time of writing the use of an exogenous ER fusion system in mice, such as infection with a recombinant ER conditional virus, was not documented in the literature. However, the ability to temporally activate or deactivate pathogen genes following infection would be a valuable tool in biomedical research. For example, the use of reversible ER-fusion conditional recombinant EBV in the hu-mice model would enable detailed analysis of the specific roles of EBV proteins during *in vivo* infection.

1.5.4. Mouse models with human immune system components

Mice carrying genetic modifications that result in severe immunodeficiency can be engrafted with human immune system components (hu-mice) following the introduction of human hemopoietic cells. These hu-mice provide immeasurable benefits to medical research of human diseases as models of human tropic diseases. The strict tropism of EBV for B cells (alongside oral epithelia) has previously limited research to *in vitro* models, due to the absence of a small animal model and the inherent costs and difficulties associated with non-human primate models. At present, there are several variants of humanized mouse models, of which only some will be discussed here. Each model has its own strengths and weaknesses but there remains a need for further advanced hu-mouse models that can more accurately recapitulate a human immune system and its associated responses.

Mice with human immune system components were first described by three independent groups in 1988 (Kamel-Reid and Dick, 1988; McCune et al., 1988; Mosier et al., 1988). CB17 mice, carrying mutations to render them immunodeficient, were engrafted with either adult human PBLs (Kamel-Reid and Dick, 1988; Mosier et al., 1988) or human foetal tissues (McCune et al., 1988) leading to the presence of human immune system components in the mice.

These early models have been advanced and improved significantly over the last three decades. The non-obese diabetic (NOD) genetic background is now commonly used in the generation of hu-mice as it confers superior engraftment of human progenitor cells than mice of BALB or CB17 genetic backgrounds (Greiner et al., 1995). This is attributed to NOD mice carrying a polymorphism in the gene encoding SIRPα which confers support for human hematopoiesis. The interaction between CD47 and SIRPα has been associated with regulation of phagocytosis-mediated clearance of leukocytes, whereby CD47 expression inhibits macrophage phagocytosis. The SIRPα carried on macrophages in NOD mice has enhanced binding to human CD47 ligand rather than mouse CD47 (Takenaka et al., 2007). This induces mouse macrophage phagocytic tolerance of human cells, thus supporting engraftment. It is also speculated that the SIRPα-CD47 interaction may induce signalling

pathways in the human hemapoetic cells, supporting survival alongside engraftment (Takenaka et al., 2007).

NOD mice are commonly bred to contain either the *scid* mutation (NOD/scid) or a deletion in the recombinase activating genes (Rag) 1 or 2 (NOD/Rag$^{-/-}$) to achieve immunodefiency. Scid mice commonly refers to those carrying a mutation in *Prkdc^{scid},* the catalytic polypeptide of the DNA-activated protein kinase essential for recombination of B and T cells. This causes severe combined immunodeficiency (scid) in the mouse, and was originally identified as a spontaneous mutation in a litter of CB17 mice (Bosma et al., 1983). Alternatively, mice can be genetically engineered to contain targeted mutations in *Rag1* or *Rag2* (Mombaerts et al., 1992; Shinkai et al., 1992). Both genetic alterations were shown to impair T and B lymphocyte maturation and abolish the development of adaptive mouse lymphocytes. The presence of either of these mutations in the NOD background enhances immune deficiency (Rongvaux et al., 2013). The *Prkdc^{scid}* mutation found in scid mice is widely involved in DNA repair, whereas *Rag1* and *Rag2* expression is limited to DNA recombination in haemopoietic cells (Pearson et al., 2008). Therefore scid mice are more sensitive to radiation induced DNA damage, whereas Rag mice are more tolerant to the sub-lethal irradiation commonly preceding introduction of human cells into immunodeficient mice (Fulop and Phillips, 1990; Pearson et al., 2008; Shultz et al., 2007).

Further developments have led to the introduction of an additional mutation in the Interleukin-2 receptor common γ-chain (IL-2Rγ) to NOD mice carrying either *scid* or *Rag* mutations (referred to as NSG and NRG mice respectively) resulting in a higher engraftment rate (DiSanto et al., 1995; Ito et al., 2002; McDermott et al., 2010; Pearson et al., 2008). The IL-2Rγ is a cytokine receptor chain shared by many cytokines (including IL-2, IL-4, IL-7, IL-9, IL-15 and IL-21) and therefore the mutation in IL-2Rγ impairs innate immune signalling (Leonard, 2001; Shultz et al., 2007). The lack of IL-7 signalling also impairs the development of innate lymphoid cell precursors (Kang and Coles, 2012). In addition, NK development and maintenance requires IL-15 signalling, therefore deletion of IL-2Rγ further impairs NK mediated elimination of human xenografts (DiSanto et al., 1995). The combination

of mutations in either *scid* or *Rag* with IL-2Rγ, alongside the already immunodeficient NOD background results in severely immunocompromised mice permissive to significant human immune cell engraftment (Shultz et al., 2007). The level of human immune cell engraftment in the blood, spleen and bone marrow of NOD mice with IL-2Rγ mutation carrying either *scid* or *Rag* mutations is comparable between the two models (Pearson et al., 2008).

These severely immunocompromised mice are engrafted with human immune system components through the introduction of human hemopoietic cells isolated from different sources. Cells are usually administered intravenously to adult recipient mice or intra-hepatically to new born recipient mouse. More efficient engraftment of human hemopoietic cells is seen in new born mice compared to adult mice (Drake et al., 2012; Traggiai et al., 2004). Commonly, human haemopoietic $CD34^{+ve}$ cells are isolated either from foetal liver (Strowig et al., 2009; White et al., 2012), cord blood (Ito et al., 2002; Traggiai et al., 2004), adult peripheral blood or adult bone marrow (Drake et al., 2012; Pearson et al., 2008). The engraftment of mice with human immune system components is elevated when $CD34^{+ve}$ cells are derived from foetal liver or cord blood, compared to cells obtained from adults (Drake et al., 2012; Matsumura et al., 2003). However, availability and ethical considerations of cord blood or foetal liver derived cells can be limiting. The introduction of human haemopoietic cells into severely immunocompromised mice has been shown to result in engraftment of mouse tissues with multiple lineages of human immunological cells including B cells, T cells, NK cells, dendritic cells and macrophages (Pearson et al., 2008; Traggiai et al., 2004).

A further improvement within the field of hu-mice models is the BLT (bone-liver-thymus) hu-mice model. This NOD/*scid* model uses surgical introduction of foetal liver and thymus tissue fragments under the renal capsule, preceding intravenous injection of HSC isolated from the same donor liver (Brainard et al., 2009; Lan et al., 2006; Melkus et al., 2006). This provides a human microenvironment enabling robust intrathymic selection and development of human T cells subsequently providing T cell help for efficient antibody production with class switching, supporting more representative human T and B cell immunological activity. In addition, rudimentary immune

lymphoid structures can be observed in these mice (Brainard et al., 2009; Lan et al., 2006; Melkus et al., 2006). Although this is the only method that results in the generation of a human-like mucosal immune system, the use of this model is limited by the requirement of surgical knowledge and facilities, as well as foetal tissues (Shultz et al., 2012).

Further methods to improve hu-mouse models are ongoing, such as introduction of human cytokines to enhance innate immune cell development, with introduction of recombinant human IL-15 shown to enhance human NK cell development and maturation in hu-mice (Drake et al., 2012; Huntington et al., 2009). Enhancement of humoral responses is also required to better model the human immune system and is a focus for development. It has been shown that B cell development can be improved in BLT humanized mice through transgenic expression of human stem cell factor (SCF), granulocyte-macrophage colony-stimulating factor (GM-CSF) and IL-3, leading to the generation of antigen-specific antibody responses to Dengue infection (Jangalwe et al., 2016). In addition, NSG mice have been transgenically engineered to express human HLA class I heavy and light chains, which overcomes the lack of thymic human T-cell selection through HLA class I molecule interaction. This permitted functional human T cells expressing cytotoxic molecules and cytokines in hu-mice (Shultz et al., 2010).

Mice carrying human immune system components permit infection of viruses with tropisms for human immune cells such as EBV and HIV. These small animal models have allowed an expanse of knowledge of human tropic pathogens and the improvement of the models bring immeasurable benefit to biomedical research (Fujiwara et al., 2013). The mice used in this study carry *Rag* and *IL2-Rγ* mutations in the NOD background and are referred to as NOD/Rag$^{-/-}$/IL2-Rγ^{null} (NRG) mice. Hereafter NRG refers to these mice following the humanization process.

1.5.5. EBV infection of mice with human immune system components

1.5.5.1. Studying EBV-associated tumorigenesis in mice

Many hu-mice models have been shown to support EBV infection with EBV associated diseases and lymphomagenesis recapitulated in these systems. These models have enabled various insights into EBV pathogenesis and viral mechanisms (Berges and Tanner, 2014; Fujiwara et al., 2015; Gujer et al., 2015; Traggiai et al., 2004).

EBV positive tumours have been identified in various organs in infected hu-mice, including the spleen, liver, lymph nodes and kidney (Traggiai et al., 2004; Yajima et al., 2008). As B cells in hu-mice are predominantly characterised as naïve, there appears to be a bias for latency III EBV infection. Lymphoproliferative lesions following approximately 4-6 weeks of infection predominantly express a latency III phenotype (Ma et al., 2011; Strowig et al., 2009; Yajima et al., 2008). In line with a latency III phenotype, EBV-transformed cells can be isolated from infected mice and grow out into continuously proliferating LCL (Strowig et al., 2009; White et al., 2012). Interestingly, even in the absence of tumour development, in some hu-mice the bone marrow and spleen contain detectable EBV DNA and have been shown to express EBNA1, EBNA2, LMP1 and LMP2a viral gene expression, indicative of a latency III programme (Yajima et al., 2008). In humans, the latency III phenotype is commonly found in PTLD and AIDS-associated DLBCL, therefore making these hu-mice attractive models for these diseases (Gujer et al., 2015).

Hu-mice have also been shown to exhibit latency I and II phenotypes with reduced latent protein expression, representative of BL and HL in humans (Cocco et al., 2008; Islas-Ohlmayer et al., 2004; Lee et al., 2015). The composition of lymphocytes within hu-mice is thought to affect the development of EBV-induced lymphoma subtypes following infection. B cell dominant mice were shown to be more likely to exhibit a more DLBCL phenotype, compared to mice with elevated T cell levels, which were more likely present with to HL-like pathology. These HL-like tumours had a latency II viral protein expression phenotype, but B cells exhibiting a latency III phenotype were shown to coexist in these mice (Lee et al., 2015). It is yet to be determined why hu-mice present with different

clinical manifestations following EBV infection. However, it may be reflective of the different hu-mice models used in the studies and their respective biological variation, the time frames of infection used, or the use of different virus strains or virus quantities administered.

Hu-mice have expanded the study of immune responses against EBV. Antibody mediated T cell depletion has been shown to result in enhanced EBV mediated lymphomagenesis and elevated viral loads in EBV infected NSG mice (Strowig et al., 2009). BLT mice have been shown to support EBV infection and have been shown to mount EBV specific adaptive MHC restricted T cell immune responses (Melkus et al., 2006). Furthermore, depletion of NK cell activity in hu-mice indicated the importance of the innate response against the virus, with elevated lymphomagenesis and pathogenesis following EBV infection of hu-mice lacking NK activity (Chijioke et al., 2013).

Hu-mice have allowed detailed study of the *in vivo* biology and roles of specific EBV lytic and latent proteins, through infection with genetically engineered recombinant KO viruses. Infection of BLT hu-mice with replication defective recombinant EBV lacking the lytic BZLF1 gene indicated that BZLF1 enhances lymphomagenesis through induction of abortive lytic infection (Ma et al., 2011). Using a novel hu-mouse model whereby haemopoietic cord blood cells were infected with EBV lacking LMP1 before introduction into adult severely immunocompromised mice, LMP1 was shown to be dispensable for EBV persistence *in vivo*, with T cell help speculated to substitute for the functions of LMP1 (Ma et al., 2015). Furthermore, LMP1 was shown to collaborate with LMP2A to promote lymphomagenesis using recombinant viruses with independent or simultaneous deletions in these two latent proteins. In addition, both LMP1 and LMP2A were shown to be non-essential for *in vivo* EBV infection (Ma et al., 2017). Furthermore, the tumour suppressive role of EBNA3B was also determined in hu-mice models using a KO recombinant virus [(White et al., 2012) described in detail in Section 1.5.5.2], and EBNA3A and EBNA3C were recently shown to be dispensable for persistence of EBV *in vivo* using recombinant viruses with deletions of these proteins [(Murer et al., 2018) described in detail in Chapter V]. Analysis of hu-mice infected with recombinant EBV containing

deletions in viral genes of interest reveals the functions and requirements of these genes within in the life cycle and pathogenesis of EBV.

1.5.5.2. The role of EBNA3B in vivo

Please note this section is taken directly from the author's previously published literature review (Styles et al., 2018).

Infection of hu-mice with a recombinant EBV virus lacking the EBNA3B gene, revealed great insight into the functions and roles of this EBNA3 protein. Despite structural and partial sequence homology, EBNA3B has distinctly different functions from those of the oncogenic EBNA3A and EBNA3C. It is completely dispensable *in vitro*, and B cells infected with EBV in the absence of EBNA3B exhibit elevated proliferative capacity compared to WT (Allday et al., 2015; Tomkinson and Kieff, 1992; White et al., 2012). This phenotype contrasts with that of the reduced efficiency of B cell transformation by EBNA3A-null EBV and the inability of EBNA3C-null EBV to cause LCL outgrowth (Hertle et al., 2009; Maruo et al., 2003; Skalska et al., 2013; Tomkinson et al., 1993).

In contrast to the oncogenic functions of EBNA3A and EBNA3C, EBNA3B appears to have tumour suppressive activity *in vivo* (White et al., 2012). In NSG mice engrafted with human immune system components, those infected with EBNA3B-KO exhibited increased splenomegaly and a higher frequency of large tumour masses than WT and EBNA3B-revertant infections after four weeks. These tumours destroyed splenic architecture, and by immunohistochemistry were monomorphic and highly proliferative, resembling the activated B cell (ABC) subtype of DLBCL. Furthermore, tumours derived from EBNA3B-deficient infections lacked infiltrating T cells. This was despite these infections priming a stronger systemic immune response compared to WT and revertant virus infections, with a higher percentage of splenic T cells, including $CD8^{+ve}$ T cells capable of killing EBV-positive cells *in vitro* (White et al., 2012). This is potentially a result of an absence of EBNA3B-mediated activation of the T cell migratory chemokine CXCL10, although microarray studies have identified other chemokine, chemokine receptor, and integrin genes whose expression is altered in EBNA3B-KO LCLs that could also contribute to the exclusion of T cells from the tumour (White et al., 2010, 2012). Together, this

indicates that EBNA3B plays a role in immunological trafficking and T cell surveillance of tumours. Furthermore, EBV-positive ABC-DLBCL with non-sense mutations in the EBNA3B gene, and BL and HL with in frame deletions in EBNA3B, have also been identified in humans; suggesting that EBV mutations can contribute to occurrence of these cancers (White et al., 2012).

The roles of EBNA3A and EBNA3C *in vivo* and persistence of EBV in the absence of these oncogenic proteins in hu-mice was investigated through the course of this PhD and is discussed in Chapter V.

1.5.5.3. Limitations of humanised mice in EBV research

Although the technical advances in mice with human immune system components are extensive, there remain limitations for the study of human diseases in these models. These limitations must be deliberated when considering the translation of *in vivo* results into the phenotype within humans.

There remain constraints to overcome to further the humanisation of the immune system in mouse models to enhance biomedical research of human immune cell tropic pathogens. This includes the homing of human immune cells to haematopoietic tissues, the use of human cytokine support, the presence of secondary lymphoid tissue and a thymic microenvironment for maturation of B and T cells, alongside further increasing the deficiency of mouse innate immune systems. These are all required to better model the human immune system (Shultz et al., 2007). Overall, increasing human engraftment and particularly lineage differentiation will aid more accurate recapitulation of human diseases in hu-mice.

The B cell compartment within hu-mice is largely comprised of transitional B cells and naïve B cells. The lack of secondary lymphoid tissue prevents the GC reaction, therefore resulting in poor development of CSR and SHM, preventing maturation and differentiation of B cells (Rongvaux et al., 2013). The use of IL-2Rγ mutations prevents IL-7 signalling which is required for the development of innate lymphoid precursor development; a prerequisite of lymphoid tissue induced cell differentiation and GC establishment (Lane et al., 2012). EBV infection of naïve B cells presents with a latency III

phenotype, however the impaired GC reactions in most hu-mice prevents MBC differentiation, hindering research into long term latency of EBV disease (Rongvaux et al., 2013; Roughan and Thorley-Lawson, 2009). Aside from the BLT model, a lack of secondary lymphoid tissues in hu-mice models needs to be overcome to further investigate EBV long-term latency and persistence.

In terms of humoral responses to infection and the stages of EBV latency, the poor development of secondary lymphoid tissues at mucosal sites and GCs in mice with human immune system components impedes the study of antibody responses to EBV *in vivo,* as differentiation of PC is impaired (Rongvaux et al., 2013; Seung and Tager, 2013). Enhanced T cell help for class switching and the development of GCs would enhance study in this area (Shultz et al., 2012).

Alongside limits in the human immune system composition of hu-mice, the lack of human epithelial tissue, and therefore infection via the oropharyngeal physiological route, also limits the study of EBV, as transmission of the virus cannot be modelled.

Considering the frequency of EBV-associated malignancies in immunocompetent hosts worldwide, the presence of EBV induced tumours is comparatively higher in humanised mice following infection with EBV (Ma et al., 2017; White et al., 2012). This must be considered when extrapolating results in humanised mice to disease in humans whereby only a fraction of hosts exhibit tumour development. This also prevents assessment of why only in some hosts does infection with highly ubiquitous EBV lead to cancer progression. Instead, hu-mice infection with EBV is more representative of infection of immuno-compromised human hosts (Strowig et al., 2009; Yajima et al., 2008).

Finally, hu-mice are commonly reconstituted with HSC isolated from foetal liver or cord blood that subsequently produce human lymphocytes in hu-mice. However, typically *in vitro* EBV studies use B cells isolated from adult peripheral blood, which have been exposed to various pathogens over their lifetime. This could lead to further potential discrepancies between results gained *in vitro* and *in vivo*. The variation in the age and developmental environment of these two cell populations could potentially lead to differences in immunological activation and maturation. Consequentially, these cell populations may exhibit differential expression and regulation of cell cycle regulatory factors. For

example, level of the CDKI $p16^{INK4a}$, the crucial barrier for EBV mediated B cell transformation, has been suggested to increase with age and is therefore comparatively low in foetal tissues compared to adults (Skalska et al., 2013; Sorrentino et al., 2014).

1.6. Aims of this study

The primary aim of this PhD project was to further characterise the roles and functions of the EBV oncoproteins EBNA3A and EBNA3C in EBV persistence and latency *in vitro* and *in vivo.* The specific aims for these two lines of investigation are detailed below.

1.6.1. Aims for the study of EBNA3A and EBNA3C in vitro

1. Use BAC and ER technology to generate a conditional recombinant EBV virus in which functional expression of EBNA3A and EBNA3C can be simultaneously regulated by the activating ligand HT
2. To use the newly constructed double conditional virus, alongside previously generated viruses where EBNA3A and EBNA3C are independently regulated, to further characterise the overlapping and independent roles of EBNA3A and EBNA3C in cell cycle deregulation and viral latency
3. To investigate whether EBNA3A and EBNA3C regulate the CDKI and plasma cell differentiation factor $p18^{INK4c}$, and explore whether this has implications regarding the B cell to plasma cell differentiation pathway

1.6.2. Aims for the study of EBNA3A and EBNA3C in vivo

1. To establish a mouse model system with human immune system components, and subsequently infect the mice with recombinant EBV viruses
2. Establish protocols for the analysis of EBV latency in the humanised mice model
3. Investigate the outcome of infection of humanised mice with EBV in the absence of the EBNA3A and EBNA3C oncoproteins, and the absence of the entire EBNA3 locus, to assess the roles of these proteins in EBV persistence and lymphomagenesis
4. To determine the viability of using conditional ERT2 HT-dependent recombinant EBV viruses *in vivo,* by infection of humanised mice with and without exposure to the activating ligand HT through the selective use of tamoxifen-impregnated food

2. Chapter II: Materials and Methods

2.1. Solutions and buffers

All solutions and buffers were made up with Milli-Q® water (mQH_20) unless stated otherwise. Ethylenediamine tetre-acetic acid (EDTA) was neutralised to pH 8.0 with NaOH unless stated otherwise.

Agarose gel loading buffer (6x)

25% (w/v) Ficoll 400

25 mM EDTA

0.1% (w/v) Bromophenol blue

0.1% (w/v) Xylene cyanol

Alkaline SDS

1% (w/v) SDS

0.2 M NaOH

Ammonium acetate (7.5 M)

500 g of ammonium acetate (Sigma Aldrich) was made up to 800 ml with mQH_20

Ammonium persulphate (10%)

1 g of ammonium persulphate was made up to 10 ml in mQH_20

Blocking solution for western blot

5% (w/v) of skim milk powder (Sigma Aldrich) in PBS-Tween

CD34 selection buffer

2% FCS (v/v) in PBS

Filter sterilised, stored at 4°C.

GTE

50 mM glucose

50 mM Tris-HCl, pH 8.0

50 mM EDTA

Autoclaved and stored at RT.

Hepatocyte wash buffer

2 mM L-glutamine

25 mg Gentamicin sulfate

100 units/ml penicillin

0.1 mg/ml streptomycin

Added to a 500 ml bottle of GIBCO® Williams E medium (Thermo Fisher)

4-hydroxytamoxifen

4 mM stock (10,000x) prepared by resuspending 5 mg of 4-hydroxytamoxifen (Sigma) to a total of 3.22 ml of 100% ethanol. Aliquots were stored at -20^{oC} in the dark and diluted 1:10 in 100% ethanol for use in cell culture.

KPB (20x)

340 mM KH_2PO_4

1.4 M K_2HPO_4

Filter sterilised and stored at RT.

LB-Broth

1% (w/v) Bacto-tryptone

0.5% (w/v) Yeast extract

1% (w/v) NaCl

Autoclaved and stored at room temperature.

LB-Agar

1% (w/v) Bacto-tryptone

0.5% (w/v) Yeast extract

1% (w/v) NaCl

1.5% (w/v) Agar

Autoclaved and cooled before pouring into plates. Plates stored at 4°C.

LB-Agar with 5% sucrose (w/v)

Autoclaved in 90% of required volume; then 10% volume of 50% sucrose solation was added after cooling to 60°C in a waterbath.

Liver digestion buffer

0.1% (w/v) collagenase

40 mM HEPES pH 7.0

2 mM $CaCl_2$

2 U/ml DNAse I (Sigma Aldrich)

Made up to 50 ml with GIBCO® HBSS +/+ medium (Thermo Fisher).

MACS Running buffer

PBS supplemented with 2 mM EDTA, 0.5% (w/v) BSA, filter sterilised and stored at 4°C.

MACS Rinsing buffer

PBS supplemented with 2 mM EDTA, filter sterilised and stored at RT.

Phosphate buffered saline (PBS)

10 mM phosphate buffer (pH7.4)

2.7 mM KCl

137 mM NaCl

PBS/BSA

1% BSA (w/v) dissolved in PBS.

Filter sterilised and stored at 4°C.

PBS-Tween

PBS supplemented with 0.1% (v/v) Tween-20 (Sigma).

Peptide 6

50 mg of peptide 6 resuspended in 50 ml OptiMEM I (Invitrogen). Stored at -80° C in aliquots.

PMSF

100 mM (phenylmethanesulfonyl fluoride) PMSF resuspended in isopropanol and stored at -20°C in aliquots.

RIPA buffer (5x)

250 mM Tris-HCl, pH 8.0

750 mM NaCl

5% (v/v) NP40

2.5% (w/v) Sodium deoxycholate

0.5% (v/v) SDS

RIPA lysis buffer

1x RIPA buffer

4% protease inhibitor cocktail

1 mM PMSF

Made up in distilled H_2O

SDS-PAGE Running buffer (10x)

250 mM Tris-Base

1.92 M Glycine

1% (w/v) SDS

SDS-PAGE sample loading buffer (5x)

250 mM Tris-HCl, pH 6.8

50% (v/v) Glycerol

10% (w/v) SDS

5% (v/v) β-mercaptoethanol

0.1% (w/v) Bromophenol blue

SDS-PAGE Transfer buffer

10% 10x SDS-PAGE running buffer

23.3% (v/v) Ethanol

STET

8% (w/v) Sucrose

50 mM Tris-Base, pH 8.0

50 mM EDTA

0.1% Triton X-100

Superbroth

1.2% (w/v) Bactotryptone

2.4% (w/v) Yeast extract

0.4% (v/v) Glycerol

Water added to 95% of intended volume. Autoclaved and stored at RT, 5% (v/v) of autoclaved 20x KPB was added before use.

TBE Buffer (10x)

0.89 M Tris-Base

0.89 M Boric acid

20 mM EDTA

TE Buffer

10 mM Tris-HCl, pH 8.0

1 mM EDTA, pH 8.0

$T_{10}E_{25}$ Buffer

10 mM Tris-HCl, pH 8.0

25 mM EDTA, pH 8.0

TE saturated butanol

1:2 solution of TE and n-butanol made up in 50 ml falcon tubes and mixed by shaking then centrifuged at 1600 xg for 5 minutes. Only the top (organic) layer was used.

2.2. Cell culture protocols

2.2.1. Maintenance of cell lines and culture medium

A summary of cell lines used in this study can be found in Table 2.1. Cell lines were maintained in a humidified incubator at 37°C and 10% CO_2. Cell lines were cultured in RMPI 1640 medium (Gibco) supplemented with 10% FCS (Gibco) and penicillin (100 units/ml) and streptomycin (0.1 mg/ml). Additional cell line specific supplements are summarised in Table 2.2.

Suspension cell lines were passaged 2 to 3 times a week. Cells were homogenised by pipetting and approximately two thirds of the culture removed by vacuum aspiration before diluting the remaining cells in pre-warmed fresh media according to cell density requirements. Suspension cell cultures were maintained at approximately 10 ml and expanded as required for experiments.

Adherent cell lines were cultured in T75 cm^2 flasks and split every 5-7 days as required. For this, medium was removed and cells gently washed once with 10 ml pre-warmed PBS. Cells were then detached by incubation with 3 ml of warmed 0.05% Trypsin-EDTA (Gibco) for 5 minutes at room temperature (RT). Then 5 ml of fresh medium was added, and cell clumps broken up by pipetting before transfer of a fraction of the cells to a fresh flask as per the cell density requirements. For EBV-293 producer lines this was usually ¼ of the cell culture. Adherent cells were then maintained with 20 ml of growth medium within a T75 cm^2 flask.

Table 2.1. Cell lines used in this study.

Cell Line	Cell Type	Description	Reference
WT A4	HEK 293	EBV WT producer line	Generated by Adam Gillman
3AKO M16	HEK 293	EBV 3AKO producer line	(Anderton et al., 2008)
3CKO M9	HEK 293	EBV 3CKO producer line	(Anderton et al., 2008)
E3KO JY6-C2	HEK 293	EBV E3KO producer line	(White et al., 2010)
3AERT2 NL1	HEK 293	EBV conditional 3AERT2 producer line	(Bazot et al., 2015)
3CERT2 NL4	HEK 293	EBV conditional 3CERT2 producer line	(Styles et al., 2017)

3A3CERT2 C9	HEK 293	EBV conditional 3A3CERT2 producer line	This study, generated by Christine Styles [Chapter III, (Styles et al., 2017)]
U266	B cell lymphoma	EBV negative	(Nilsson et al., 1970)
Raji	BL	EBV positive	(Epstein et al., 1966)
Namalwa	BL	EBV positive	(Klein et al., 1972)
WT LCL	LCL	BAC B95.8, EBV positive	Produced in this study from $CD19^{+}$ primary B cells from different independent donors
3AERT2 LCL	LCL	LCL with conditional expression of EBNA3A	Produced in this study from $CD19^{+}$ primary B cells purified from different independent donors
3CERT2 LCL	LCL	LCL with conditional expression of EBNA3C	Produced in this study from $CD19^{+}$ primary B cells purified from different independent donors
3A3CERT2 LCL	LCL	LCL with conditional expression of EBNA3A and EBNA3C	Produced in this study from $CD19^{+}$ primary B cells purified from different independent donors

Table 2.2. Cell line specific cell culture conditions.

Cell Line	**Basic culture medium**	**Supplements**
Established LCLs (including Raji and Namalwa)	• RPMI 1640 medium (containing L- glutamine) • 10% FCS • Penicillin (100 units/ml) • Streptomycin (0.1 mg/ml)	N/A
U266		N/A
Newly infected $CD19^{+ve}$ primary B cells		- 15% FCS for the first 30 days after infection, before reduction to 10% as per LCLs - Additional 2mM L-glutamine
Lymphocytes derived from the spleen of EBV infected humanised mice		- 15% FCS for the first 30 days post isolation, before reduction to 10% as per LCLs

		- Additional 2mM L-glutamine - Cyclosporine A at 500 ng/ml
Adherent HEK-293		- Additional 2mM L-glutamine
Adherent HEK-293 producer lines		- Additional 2mM L-glutamine - 100 µg/ml Hygromycin B (Roche)

2.2.2. Cell line storage and thawing

For long term storage, cells lines were stored in liquid nitrogen. Suspension cell lines were seeded at $3x10^5$/ml one day prior to freezing, and adherent cells were frozen when they reached confluence. Adherent cells underwent Trypsin-EDTA detachment as detailed in 2.2.1 prior to harvest. Cells were homogenised by pipetting and then centrifuged at 215 xg for 10 minutes at 4°C. Cells were then resuspended in RPMI 1640 medium (Gibco) supplemented with 20% FCS (Gibco) and 10% dimethyl sulfoxide (DMSO, VWR Chemicals) and 1 ml transferred to a cryovial (Thermo Scientific). Cryovials were placed into an isopropanol-filled Mr Frosty™ freezing container (Thermo Scientific) and stored at -80°C for approximately 24 hours until transfer to liquid nitrogen.

For cell line recovery from liquid nitrogen storage, cells were rapidly thawed in a water bath at 37°C before dilution in 10 ml growth medium. Cells were then centrifuged at 300 xg for 4 minutes at 4°C before resuspension in an appropriate volume of growth medium, usually 10 ml for suspension cells and 20 ml for adherent cells. Cells were left to recover for at least 1 week before being used in experiments.

2.2.3. Counting and harvesting cells

Cells were counted using a haemocytometer and light microscope. Cells were homogenised by vigorous pipetting, 10 µl of cells was then diluted 1:1 in 0.4% trypan blue (Sigma-Aldrich). Live cells that did not incorporate the blue dye in a defined region of the haemocytometer grid were counted. For cell count experiments, cells were counted as described on day 0 and seeded at $3x10^5$/ml and

incubated for 2-3 days. Cells were then counted and again seeded to $3x10^5$/ml in fresh medium. This was repeated for up to 30 days.

Unless stated, suspension cells were seeded at $3x10^5$/ml 1 day before harvesting, and adherent cells harvested when confluent. Media was removed from adherent cells and they were washed once in 10 ml pre-warmed PBS. A cell scraper was then used to detach cells into 1 ml PBS and the suspension homogenised by pipetting. Cells were then centrifuged at 300 xg for 4 minutes at 4°C. Suspension cells were homogenised by pipetting and were centrifuged at 300 xg for 4 minutes at 4°C and washed once in cold PBS. Both cells types were then pelleted again as before, and if not already in one, transferred to a 1.5 ml Eppendorf in 1 ml cold PBS. Cells were pelleted at 376 xg for 5 minutes at RT and the supernatant removed. Cells were then either snap frozen, by placing into dry ice and transferred to -80°C until further extraction, or analysis performed immediately.

2.2.4. In vitro induction of plasma cell differentiation

$CD19^+$ primary B cells were isolated as detailed in Section 2.3.2. Purified $CD19^+$ primary B cells were seeded at $2x10^6$/ml in 2ml of growth medium supplemented with 15% FCS, 100 units/ml Penicillin and 0.1 mg/ml streptomycin. For induction of plasma cell differentiation, 50 ng/ml CD40-Ligand (Enzo Life Science) and 100 ng/ml IL21 (Preprotech) were then added to the culture. Cells were incubated for 5-7 days and harvested as described in Section 2.2.3 for analysis.

2.3. Isolation of surface marker specific cell populations

2.3.1. Isolation of peripheral blood leucocytes (PBLs) from peripheral blood

Buffy coat residues derived from anonymous donors were obtained from the UK Blood transfusion service. Individual buffy coats contained approximately 100-120 ml of peripheral blood. The blood was diluted to 200 ml with cold sterile PBS. Then 25 ml of diluted blood was carefully layered over 25 ml of Ficoll-Paque (GE Healthcare) at RT. This was then centrifuged at 339 xg with both acceleration and brake off for 30 minutes at RT. The lymphocyte fraction, identified as a grey/white interface in the centre of each tube was carefully removed and pooled into 100 ml wash buffer (RPMI,

1% FCS). This was centrifuged for 5 minutes, at 339 xg with the brake off at 4°C. The supernatant was removed and the pellet containing peripheral blood leucocytes (PBLs) was resuspended in 200 ml wash buffer (RPMI, 1% FCS) before centrifuging for 5 minutes as before. The pellet was then resuspended in 50 ml growth medium and passed through a 70 nm cell strainer to remove cell aggregates.

Murine peripheral blood was obtained by cardiac puncture, as detailed in Section 2.10.4.1. Peripheral blood obtained from mice infected with the same recombinant EBV virus were pooled and diluted to 7 ml in PBS. This diluted blood was then layered over 7 ml ficoll at RT. This was then centrifuged at 339 xg, with both acceleration and brake off for 30 minutes at RT. The PBL fraction was then collected as described above and washed twice in 10 ml of wash buffer (RPMI, 1% FCS) before being resuspended in 10 ml full growth medium and passed through a 70 nm cell strainer.

PBLs were then counted as described in Section 2.2.3, and either seeded at $2x10^6$/ml or subject to $CD19^{+ve}$ primary B cell purification.

2.3.2. Purification of $CD19^+$ primary B cells

Primary B cells were purified from PBLs (isolated as described in Section 2.3.1) by magnetic sorting using an AutoMACS Separator (Miltenyi Biotec). Up to 10^9 PBLs were pelleted at 215 xg for 5 minutes at 4°C. The supernatant was then removed and cells resuspended in 8 ml MACS running buffer containing 500 µl CD19 selection microbeads (Miltenyi Biotec). Cells were incubated for 15 minutes at 4°C to allow magnetic labelling of the $CD19^+$ primary B cells. Following incubation, the volume was made up to 50 ml with PBS/BSA before centrifugation as before. Cells were then resuspended in 5 ml MACS running buffer. Resuspended cells were run on an AutoMACS Separator (Miltenyi Biotec) and $CD19^+$ magnetically labelled cells were positively sorted according to the manufacturers protocol, referred to as the 'possel' programme.

Purified $CD19^+$ B cells were resuspended in full growth medium at $2x10^6$/ml and placed in an incubator at 37°C and 5% CO_2. The next day purity was assessed by flow cytometry (See Section 2.8.2.1) and cells infected with recombinant EBV viruses (see Section 2.6.4).

2.3.3. Purification of CD34^{+} hematopoietic stem cells

CD34^{+} haemopoietic stem cells were purified from foetal livers obtained from Advanced Bioscience Resources Inc, and isolated using CD34-specific magnetic beads and an EasySep Magnet (Stem Cell Technologies) as follows.

Liver tissue was mechanically disrupted in a 10 cm dish using sterile curved scissors and then digested in 20 ml Liver Digestion Buffer (LDB) in a 37°C incubator on a rocker for 30 minutes. Digested homogenised liver was then passed through a 70 μm cell strainer. This was performed in 5 ml batches and a plunger from a sterile 5ml syringe was used to gently push fragments through the strainer. The strainer was repeatedly rinsed with 5 ml hepatocyte wash buffer (HWB) following each 5 ml of digested liver. The volume of the cell suspension was then increased to 50 ml with HWB. The cell suspension was centrifuged at 20 xg for 5 minutes at RT to pellet hepatocytes, and the supernatant (containing 'smaller' cells including CD34^{+ve} cells) removed to a fresh tube. Cells were then spun at 524 xg for 5 minutes at RT, and then resuspended in 50 ml HWB. Cells were then filtered through a 40 μm cell strainer and counted (see Section 2.2.3). Cells were then spun at 524 xg for 5 minutes at RT and resuspended in CD34 selection buffer (PBS with 2% FCS) at 5x10^{8}/ml. Cells were then transferred to 5ml polystyrene tubes, at 1 ml per tube and 100 μl/ml EasySep human CD34 positive selection cocktail (Stem Cell Technologies) added. This was then incubated for 15 minutes at RT. Then 50 ul/ml EasySep magnetic particles (Stem Cell Technologies) was added and cells incubated for a further 10 minutes at RT. The 1 ml of cells per tube was then diluted to 3 ml with CD34 selection buffer and the tubes placed into an immunomagnetic column-free magnet for 5 minutes on ice. Following incubation, excess liquid was poured out of the tube, while said tube remained within the magnet, retaining the CD34^{+ve} cells on the side of the tube. The tube was them removed from the magnet and the sides gently rinsed with 3 ml CD34 selection buffer. Tubes were then returned to the magnet for a further 5 minutes, on ice. This was repeated 4 times. After the 5th wash, cells were resuspended 3ml HWB, pelleted by centrifugation and then frozen down at 2x10^{6}/ml in 90% FCS/10% DMSO.

2.4. Cloning and techniques for DNA manipulation

Vector NTI® Advance software (Invitrogen) was used to establish cloning strategies and aided construct design and diagnosis. Briefly, plasmids containing DNA fragments with the required sequences and exons were identified and restriction enzymes used to excise the desired fragments. Digested DNA fragments were run on agarose gels, and the separated DNA fragment was cut from the gel and then DNA purification and ligation performed. The constructs were transformed into bacteria and those successfully transformed were selected based on engineered antibiotic resistance. Constructs were further selected on temperature sensitivity with some (pKovKanΔCm; pDF25-Tet) containing TS origins that only grow at 30°C, while others (eg the whole EBNA3 locus) that are large and/or contain repeats than can be unstable, were grown at 30°C to improve construct stability. Construct DNA was extracted from bacteria and purified by mini-prep before confirmation by diagnostic restriction digest, followed by conventional agarose gel electrophoresis and/or pulsed field gel electrophoresis (PFGE). Successfully cloned constructs were used for further sub-cloning or transfection. A list detailing the constructs used in this study can be found in Table 2.3, and construct maps can be found in the Appendix.

Table 2.3. List of constructs used in this study.

Name	Description	Source
p4487.1	pKovKanΔCm	(White et al., 2003)
pDF25-Tet	RecA gene + tetracyclineresistance, temperature sensitive replication origin	(Lalioti and Heath, 2001)
pQB-01	Source of ERT2 and EBNA3B	(Bazot et al., 2015)
pQB-02	Source of EBNA3C-ERT2	Dr Quentin Bazot
pJY07.1	Contains EBNA3 locus used for reverting E3KO	(Yee et al., 2011)
pJY06+3.2	E3KO BAC	(Yee et al., 2011)
p8195	Minimal pBR322-based plasmids with multiple cloinng sites and ampicillin resistance	Dr Rob White
pRP004.7	Minimal pBR322-based plasmids with multiple cloinng sites and ampicillin resistance	Dr Rob White

2.4.1. Small scale preparation of plasmid DNA (mini-prep)

Bacterial colonies were grown at 37°C overnight (o/n) on agar with required antibiotics. Following incubation, individual bacterial colonies were picked using a p200 tip and placed into 1.5 ml super-broth (SB) with required antibiotics and grown o/n at 37°C with agitation. The resulting bacterial culture was then centrifuged at 1503 xg for 5 min, and the pellet resuspended in 70 µl STET. Then 200 µl alkaline SDS was added while vortex mixing. During further vortexing, 150 µl 7.5 M ammonium acetate was added and samples placed on ice for 5 minutes. The samples were then centrifuged at 4°C and 9391 xg for 15 minutes. The DNA-containing supernatant was then recovered, and 240 µl isopropanol added to precipitate the DNA. DNA was then isolated by centrifugation at 9391 xg for 5 minutes. The supernatant was removed and the resulting pellets were washed in 200 µl of 70% ethanol. Samples were then spun at 9391 xg for 3 minutes and the supernatant removed. After 5-15 minutes air drying, DNA was resuspended in 50 µl Tris-EDTA buffer (TE).

2.4.2. Large scale preparation of BAC DNA (maxi-prep) by caesium chloride density gradient

Bacterial colonies were grown o/n on agar with their required antibiotics. Following incubation individual bacterial colonies were picked using a p200 tip and placed into 1ml SB with required antibiotics and grown for 8 hrs at 30-37°C (depending on construct) with agitation. Cells were then transferred into 500 ml SB with required antibiotics and grown o/n at 37°C with agitation. The next day bacteria were centrifuged for 15 min at 4000 rpm in an SLA-1500 rotor. The resulting pellet was then resuspended in 40 ml GTE. Then 80 ml alkaline SDS was added, and the samples were mixed by inversion. Then 60 ml ammonium acetate was added, the samples mixed and then placed on ice for 15 minutes. Bacterial samples were then centrifuged at 6000 rpm, 4°C for 30 minutes (SLA-1500 rotor). The resulting supernatant was harvested and filtered through a 70 µm strainer to remove cell debris. To precipitate the DNA, 105 ml isopropanol (approximately 0.6-0.7 volumes) was added to the DNA-containing supernatant, this was then mixed and left for 5-10 minutes at RT. Samples were then

centrifuged at 6500 rpm (SLA-1500 rotor), for 25 minutes at RT. The resulting pellet was then washed with 5 ml 70% ethanol and resuspended in 4 ml T_{10} E_{25}.

4.3g of CsCl was dissolved in 4 ml of the resulting DNA solution and 200 µl Ethidium Bromide (EtBr) added. Samples were transferred by pouring through a syringe and 19G blunt needle into a quick-seal polyallomer tube. The DNA solution was then centrifuged overnight in a Beckman NVT65.2 rotor at 60,000 rpm (Optima ultracentrifuge, Beckman Coulter), with maximum acceleration and no brake at 20°C. The next day, a 19G needle was used to extract supercoiled DNA (the lower DNA band as visualised on a blue light transilluminator) from the resulting gradient. Extracted DNA was made up to volume of 5.2 ml with CsCl mix (36.9 g CsCl resuspended in 37.7 ml $T_{10}E_{25}$) and centrifuged as before. The next day, approximately 500 µl of supercoiled DNA was recovered as before and divided between two 2 ml Eppendorf tubes. To remove the EtBr, the tube was filled with 1ml TE-saturated butanol and inverted vigorously. The sample was then centrifuged for 10 seconds in a microcentrifuge and the pink layer removed. This was repeated until two extractions after the solution was appearing clear. The DNA was then precipitated by addition of 0.5 volume of NH_4Ac. The samples were then split into two 2 ml Eppendorf tubes each and then 2.5 volumes of 100% ethanol was added to both tubes. Samples were then centrifuged at 15,871 xg for 10 minutes and the resulting pellets washed with 200 µl of 70% ethanol before centrifugation at 15,871 xg for 3 minutes. The resulting pellets were then air dried and then resuspended in 50 µl TE.

2.4.3. Restriction enzyme digest

Restriction digests were performed using enzymes from New England Biolabs (NEB), using their suggested buffers, and according to the manufacturer's protocols. Digests using 2 different restriction enzymes used the most appropriate buffer. Digests were performed for 3 hours at 37°C, with a 10-20 fold excess of restriction enzyme to aid complete digestion of DNA. Volumes used for diagnostic digests and preparatory digests are shown in Table 2.4.

Table 2.4. Composition of diagnostic and preparatory restriction enzyme digests

Digest Component	Diagnostic digest	Preparatory digest
DNA	1 µl	3 µl
10X enzyme buffer	1.5 µl	3 µl
20X BSA	0.75 µl	1.5 µl
Restriction enzyme	0.1 µl	0.1 µl
ddH_2O	11.75	22.5
Total volume	15 µl	30 µl

2.4.4. Agarose gel electrophoresis

DNA fragments were separated by migration through gels made with 1% agarose dissolved in 1X TBE and containing 1X SYBRsafe (Thermo Scientific). Samples were mixed with 6X agarose gel loading buffer before loading and a 1 Kb DNA ladder (NEB) was used to assess band sizes of samples. Gels were run in 1X TBE at 80 V for 1-2 hours in Hoeffer HE33 apparatus. Gels were then visualised with blue light conversion screen and the images captured on a Molecular Imager® Gel Doc™ XR System (Bio-Rad).

2.4.5. Gel extraction of DNA fragments

Gels were visualised using a blue light transilluminator and the desired plasmid fragments were excised from the gel using a scalpel. DNA was then purified using a QIAquick gel extraction kit according to the manufacturer's instructions (Qiagen).

2.4.6. DNA ligation

Ligation of two restriction digest purified DNA fragments was performed using approximately 1-5 µl of DNA, aiming for a 1:3 ratio of vector DNA to insert DNA. Ligation reactions were run with 0.5 µl T4 DNA Ligase as per the manufacturer's instructions (NEB) at RT for at least 2 hours. The resulting ligated DNA was then subject to further sub-cloning or transformed into competent bacteria.

2.4.7. Transformation of DNA into competent bacteria

For this 50 µl of competent DH5α bacterial cells (made competent for transformation in the lab) was added to ligated DNA constructs (see Section 2.4.6) and placed on ice for 20 minutes. Samples

were then heat shocked at 42°C in a water bath, for 45 seconds. Tubes were immediately returned to ice, and then 900 µl LB was added to each sample. Samples were then incubated for 1 hour with shaking at 30-37°C depending on the construct. The bacteria were then plated onto agar containing the required antibiotics, and incubated o/n at 30-37°C (depending on construct).

2.4.8. Pulsed field gel electrophoresis (PFGE)

Pulse field gel electrophoresis (PFGE) was performed to separate larger DNA fragments and was performed on a Bio-Rad CHEF DR II system. Gels were made with 1% agarose dissolved in 0.5X TBE and run for 14 hrs at 14°C, with running conditions of 6 V/cm, with a start switch time of 1s and end switch time of 10s. To evaluate band sizes 15 ng of a 1:1 mixture of two size standards (λ DNA-BstEII Digest and λ DNA-Mono Cut Mix; both NEB) was used. Gels were stained with 12 µl EtBr in 300 ml 0.5X TBE for 30-60 minutes before visualisation under UV illumination. Gel images were then captured on a Molecular Imager® Gel Doc™ XR System (Bio-Rad).

2.4.9. Klenow-mediated blunt-ending of 5' overhang

Following restriction digest, 33 µM dNTP and 1 unit of Klenow enzyme (DNA pol I) was added to the DNA. This was incubated for 15 minutes at 25°C, then stopped by addition of EDTA to a final concentration of 10 mM, and the solution incubated at 75°C for 20 minutes. The modified restriction digest fragment was run on an agarose gel (Section 2.4.4), and then ligated (described in Section 2.4.6, due to blunt-ending the reaction was incubated for 4 hours).

2.5. Generation of recombinant EBV virus

2.5.1. Production of competent bacteria

Bacteria cells were grown in 10 ml LB with required antibiotics o/n at 37°C with agitation. Then 1 ml of the resulting culture was added to 100 ml LB with required antibiotics and grown at 37°C with agitation for 3 hours. Following incubation, bacterial cells were placed on ice for 30 minutes and subsequent work was performed in a cold room to keep the bacteria cold. Bacteria was centrifuged at 2844 xg for 15 minutes at 4°C and the resulting pellet resuspended in 20 ml $CaCl_2$ (100 mM) and left

on ice for 30 minutes. Bacteria was then centrifuged for 15 minutes at 2844 xg at 4°C and resuspended in 2 ml $CaCl_2$ (100mM) with 15% glycerol. Bacteria was then snap cooled on dry ice and 100 µl aliquots stored at -80°C. Competent bacteria were defrosted on ice immediately before transformation.

2.5.2. Homologous recombination of target constructs and EBV-BAC

Briefly, recombinant EBV-BACs were generated by RecA-mediated homologous recombination of an established EBV-BAC (containing a positive selection cassette; chloramphenicol [Cm] resistance) and a shuttle vector (pKovKan∆Cm) containing a sequence of interest (eg a C-terminal fusion of EBNA3A or EBNA3C to the modified oestrogen receptor ERT2) alongside a cassette for positive selection (kanamycin [Kan] resistance) and negative selection (SACBII). RecA recombinase was introduced by pDF25-Tet which also contains a tetracycline (Tet) resistance gene. The differing antibiotic resistance across constructs allowed selection following incorporation and excision of DNA fragments during the recombination process. Furthermore, both pDF25-Tet and pKovKan∆Cm have temperature-sensitive origins of replication therefore can propagate at 30-33°C but not 43°C. This allows controlled transient expression of these plasmids due to loss of unintegrated pDF25-Tet and pKovKan∆Cm at higher temperatures.

2.5.2.1. Production of co-integrants by recombination between target constructs and EBV-BAC

Target constructs (the region to be incorporated into the EBV-BAC flanked by regions of homology) were cloned into the pKovKan∆Cm shuttle vector. The resulting construct was confirmed by restriction digest (see Section 2.4.3) and 1 µl of mini-prepped DNA was added to 100 µl of competent bacteria carrying the desired BAC construct for recombination, alongside 5 µl of mini-prepped DNA of the RecA recombinase expressing plasmid pDF25-Tet. Samples were then kept on ice for 30 minutes then heat shocked at 42°C in a water bath for 1 minute and returned to ice. Then 1 ml LB was added to the bacteria which was then incubated at 30°C for 1.5 hour with agitation. 100 µl of the resulting culture was then plated onto agar containing Cm, Kan and Tet and incubated o/n at 30°C.

Bacterial colonies were then picked and diluted in 1 ml LB, of which 200 µl was immediately plated on Cm and Kan and grown o/n at 43°C to select for co-integrant BACs that had recombined with the target construct carrying pKovKanΔCm shuttle vector. DNA from resulting colonies was isolated by mini-prep (see Sections 2.4.1) and analysed by restriction digest (Section 2.4.3) and PFGE (Section 2.4.8) to confirm recombination between the BAC and the target construct carrying pKovKanΔCm shuttle vector. There are 2 possible independent co-integrants from recombination of the BAC and target constructs due to the two different recombination half sites between the parental BAC and the target construct.

2.5.2.2. Production of competent bacteria containing BAC co-integrant

Bacterial colonies confirmed to carry intact BAC co-integrants were picked using a p200 tip and grown o/n in 1 ml LB with required antibiotics at 37°C. The next day 100 µl of the resulting culture was diluted into 10 ml LB and incubated at 43°C for 3 hours. Cells were then placed on ice for 30 minutes, and the subsequent steps were performed in a cold room to keep the bacteria cold. Bacteria were then centrifuged at 2844 xg for 15 minutes at 4°C and then resuspended in 2 ml $CaCl_2$ (100 mM) and left on ice for 30 minutes. Cells were then centrifuged for 15 minutes at 2844 xg at 4°C and then resuspended in 200 µl $CaCl_2$ (100mM) containing 15% glycerol and 50 µl aliquots were stored at -80°C.

2.5.2.3. Resolution of co-integrants of target constructs and EBV-BAC

50 µl of competent co-integrant-containing bacteria was defrosted on ice and 2 µl of the RecA expressing pDF25-Tet was added. Samples were then kept on ice for 30 minutes then heat shocked at 42°C in a water bath for 1 minute. Then 1 ml LB was added to the bacteria and the culture incubated at 30°C for 1.5 hours with agitation. 100 µl of the resulting culture was then plated onto agar containing Cm and Tet and incubated o/n at 30°C. Bacterial colonies were then individually picked and diluted into 1 ml LB containing Cm and Tet as well as 5% sucrose and incubated at 30°C for 8 hours for selection of colonies where recombination has resulted in removal of the pKovKanΔCm backbone. Following incubation, 20 µl of this culture was then streaked using a serial dilution method onto a 14 cm diameter agar plate containing Cm with 5% sucrose and incubated o/n at 43°C. Replica plating of

colonies onto Cm only and Cm/Kan-containing agar plates was then performed to distinguish colonies containing a resolved co-integrant BAC containing the insert carried by pKovKan∆Cm from co-integrants that survived sucrose selection due to SacB mutations. DNA from resulting resolved co-integrant colonies was purified by mini-prep (see Sections 2.4.1) and analysed by restriction digest (Section 2.4.4) and PFGE (2.4.8) to confirm co-integrant resolution. Resolved co-integrants can either be the incorporation of the target construct into the EBV-BAC, or the homologous recombination results in a reversion to the original BAC construct.

2.5.3. Generating HEK-293 cell clones transfected with EBV-BAC

2.5.3.1. Transfection of HEK-293 cell with EBV-BAC

Prior to transfection with recombinant EBV-BAC DNA, a T75cm^2 flask of confluent HEK-293 cells was seeded in a 6 well plate and incubated for 24 hours. For one well of cells, 1.5 µl Lipofectin® Reagent (Invitrogen) and 80 µl of 1 ml/mg peptide 6 were mixed and incubated for 5 minutes at RT. Meanwhile, maxi-prepped EBV-BAC DNA was added to 200 µl OptiMEM (Invitrogen) to a concentration of 2 µg. This DNA solution was then added to the lipid/peptide mix and incubated for 20-40 minutes at RT, before addition of OptiMEM to a final volume of 1 ml. Culture medium was removed from the cells and the transfection mix added. Cells were incubated with the transfection mix for 6-10 hours at 37°C, before the transfection mix was removed and replaced with growth medium.

24 hours later, medium was removed from the cells and they were washed gently with 1 ml of warmed PBS. Cells were then trypsinised in 0.5 ml Trypsin-EDTA (Invitrogen) as described in Section 2.2.3. Cells were then detached by agitation and were resuspended in 48 ml of medium supplemented with 150 µg/ml hygromycin for selection of successfully transfected cells. Suspended cells were then seeded into four 10 cm dishes, each containing 12 ml of cell culture. Cells were incubated untouched for 10 days before changing the media. After 2-3 weeks transfected cells had formed distinct colonies suitable for isolation.

2.5.3.2. Isolation of 293 HEK clones transfected with EBV-BAC

Approximately 2-3 weeks after transfection of HEK-293 cells with EBV-BAC DNA (Section 2.5.3.1), cells formed small colonies within the dishes. Depending on their number and density, approximately 20 colonies were picked for expansion and subsequent analysis. EBV-BAC constructs contain green fluorescent protein, therefore fluorescent microscopy was used to identify bacterial colonies containing EBV-BAC episomes and these were subsequently preferentially picked.

For colony picking, medium was removed and cells were washed once with 5 ml warmed RPMI 1640 medium (Gibco) without additives. The thin end of a yellow p200 tip was removed and discarded leaving a 'cloning ring' from the thicker end of the tip. These were autoclaved before use and the larger end dipped into autoclaved vacuum grease before being securely placed over a single colony. Then 40 µl of warmed 0.05% Trypsin-EDTA (Invitrogen) was added to the cloning ring and incubated for 3 min. Following incubation, 60 µl of growth medium was added to the cloning ring and cells were detached by gentle pipetting. Clones were transferred to independent wells on a 6 well plate containing 4 ml of warmed growth medium. Colonies were incubated to allow expansion, before transfer into a T75cm^2 flask as required. Colonies were tested for ability to generate high viral titres (see Section 2.6.3) and the integrity and identity of EBV-BAC DNA was confirmed by episome rescue (see Section 2.5.3.3).

2.5.3.3. Episome rescue by low molecular weight extraction of DNA from transfected cells to validate EBV recombinant

Low molecular weight DNA extraction was performed to isolate EBV-BAC DNA episomes from mammalian cells (LCLs and EBV recombinant virus producing HEK-293 cell lines). Cells were harvested as described in Section 2.2.3. Cell pellets were resuspended in 60 µl STET. While vortex mixing, 130 µl alkaline SDS was then added to samples, followed by addition of 110 µl ammonium acetate (7.5 M) while vortexing. The resulting cell lysate was placed on ice for 10-20 minutes and then centrifuged for 30 minutes at 4°C at 15,781 xg. The resulting DNA-containing supernatant was recovered and placed into a MaXtract high density tube (Qiagen) and 200 µl of TE-saturated phenol:chloroform:isoamyl

alcohol (25:24:1) was added. Tubes were then vigorously inverted continuously for 1 minute to homogenise the solution. Tubes were then centrifuged for 6 minutes at 9391 xg. The MaXtract high density tube contains a gel that forms a barrier between an aqueous phase containing nucleic acid at the top of the tube and the bottom of the tube containing the phenol:chlorophorm and contaminants. Following centrifugation, 200 µl chlorophorm was added to the top layer and tube inversion and centrifugation repeated. A following 200 µl chlorophorm was added to the top layer and tube inversion and centrifugation repeated once more. The top layer (containing the DNA) was then removed to a fresh microcentrifuge tube and the DNA precipitated as described in Section 2.4.1 and resuspended in 50 µl TE containing 5 µg/ml RNAse A. Viral DNA was then electroporated into competent bacteria (see Section 2.5.3.4). Bacteria was then grown and underwent mini-prep to isolate DNA (see Section 2.4.1) and BAC structure was confirmed by restriction digest (see Section 2.4.4) and PFGE (see Section 2.4.8).

2.5.3.4. Electroporation of DNA into bacterial cells

For this process 19 µl of electrocompetent ElectroMAX DH10B bacterial cells (Invitrogen) were added to 1 µl DNA (typically purified by low molecular weight extraction, described in Section 2.5.3.3) on ice. This was transferred to a chilled Gene Pulser Electroporation Cuvette (0.1 cm gap, Bio-Rad) before electroporation using a Gene Pulser Electroporator (Bio-Rad) using these conditions: Capacitance 25 µF, Resistance 200 Ω and voltage 1800 V. Cells were then immediately flushed out of the cuvette and into a 6 ml round bottomed tube with 400 µl SOC medium (Invitrogen) and placed in an incubator with agitation for 1 hour at 37°C. The resulting bacterial suspension was then plated onto selective agar plates (typically 14 cm places containing Cm) and incubated o/n at 37°C. EBV-BAC DNA was then isolated by mini-prep (see Section 2.4.1) and BAC structure was confirmed by restriction digest (see Section 2.4.4) and PFGE (see Section 2.4.8).

2.6. Virus production and infection

Following confirmation of BAC integrity by PFGE, EBV recombinant virus producing HEK-293 cells (referred to as a 293-EBV producer cell lines) were transfected to facilitate production of infectious virus particles.

2.6.1. Generating infectious virus from 293 HEK cells with EBV-BAC

Virus production was performing by transfection of expression plasmids for BZLF1 and BALF4 (provided by Dr Rob White) with GeneJuice reagent. Confluent 293-EBV producer cells in a T75 cm^2 flask were trypsinised (see Section 2.2.3) and seeded into five 10cm dishes. Two days later, for each plate 500 µl of Opti-MEM (Invitrogen) was incubated with 12 µl GeneJuice for 5 minutes. Then 2µg of each of pBZLF1 and pBALF4 was added to the solution and it was then incubated again for a minimum of 10-30 minutes. During incubation, the media of the 293-EBV producer cells was exchanged for 10 ml of growth medium without hygromycin. The 516 µl transfection mixture was then added to each plate and they were incubated for 3-5 days. The virus-containing supernatant from the same 293-EBV producer line was removed from the 10 cm dishes and pooled. This was then filtered through a 0.5 µm filter (Millipore) and stored at 4˚C.

2.6.2. Concentrating virus

To increase viral titres for *in vivo* infection 0.1 mg/ml Bacitracin (Company) was added to virus-containing supernatant before they were centrifuged at 30,000 xg for 2 hours. The supernatant was removed and the virus particles were then resuspended overnight in 1 ml cold PBS and stored at 4˚C.

2.6.3. Virus titration

The titre of virus-containing supernatant was determined by serial dilution of virus in Raji cell cultures. In a well of a 24 well plate, 111.1 viral supernatant was added to 1 ml growth medium. This was then serially diluted 10x, by serial transfer of 111.1 µl of this virus-containing medium into further wells containing 1 ml growth medium. This led to wells containing 100, 10, 1 and 0.1 µl of virus respectively. To these wells 0.5 ml of Raji cells at $1x10^5$ was then added and the plates returned to the

incubator. After 2 days, a final concentration of 20 nM TPA and 5 mM sodium butyrate was added to each well of culture along with 0.5 ml growth medium and the cells were incubated for a further 24 hours to enhance the GFP expression in the infected cells. The viral titre was then determined using fluorescence microscopy to count GFP-expressing cells per well to calculate the number of Raji green cells infected per µl of virus, referred to as green Raji units (GRU).

2.6.4. Infection of primary B cells with recombinant EBV viruses

Approximately 24 hours after purification, 1.5 ml of $CD19^{+ve}$ purified primary B cells at $2x10^6$/ml were seeded in 24 well plates. Then 500 µl of virus-containing supernatant with the lowest titre was added to the cells a final volume of 2 ml culture. The volume of other virus-containing supernatant used for that experiment were then normalised across the infection to GRU of the lowest titre and made up to a final culture volume of 2 ml with growth medium.

When viral titres were less than 100 GRU, $3x10^6$ primary B cells were centrifuged for 5 minutes at 300 xg and resuspended in 2 ml of virus-containing supernatant and placed into a well of a 24 well plate. As before, the volume of other virus-containing supernatant for that experiment were then normalised across the infection to GRU of this titre.

For large scale analyses of primary B cell infections, cell numbers and virus amounts were increased with ratios consistent with those mentioned. For example, 2 ml of viral supernatant would be added to 6 ml of $CD19^+$ cells at $2x10^6$/ml in a T25 cm^2 flask.

Following infection, cells were cultured in an incubator at 37°C with 5% CO_2. Approximately 25% of the culture was then harvested (see Section 2.2.3) every 3-7 days for analysis, and fresh medium added to the previous volume. When cells reached high density (namely medium acidification after 3 days), culture volume was increased with fresh medium and then maintained at 10 ml in a T75 cm^2 flask and then expanded as required for use in experiments.

2.7. Gene expression analysis

2.7.1. RNA and DNA analysis

2.7.1.1. RNA extraction

For RNA extraction, cells were harvested as described previously (Section 2.2.3) and resuspended 350 μl RLT buffer (Qiagen) with additional β-mercapatolethanol as per the manufacturer's instructions. Cells were then either snap frozen on dry ice and stored at -80°C before extraction, or RNA extracted immediately using the RNeasy Mini Kit (Qiagen) according to the manufacturer's protocol and including the optional genomic DNA digestion step using the RNase-free DNase set (Qiagen). RNA was eluted in RNAse free water and all extracted RNA was quantified by measuring absorbance at 260nm on a short path spectrophotometer (Denovix DS-11 FX+) prior to reverse transcription (Section 2.7.1.3) and real time quantitative PCR (qPCR) using SYBR-Green (Section 2.7.1.4).

2.7.1.2. DNA extraction

DNA extraction from cell culture

5 x 10^6 cells were pelleted by centrifugation at 300 xg for 5 minutes. Cell pellets were then resuspended in 200 μl PBS prior to DNA extraction.

DNA extraction from murine blood

Peripheral blood was collected from mice (as described in Section 2.10.3 and 2.10.4.1) and approximately 50-100 μl diluted to 200 μl with PBS prior to DNA extraction.

DNA extraction from the spleen

DNA was extracted from splenic tissue and splenic lymphocytes. Spleens were mechanically disrupted (see Section 2.10.4.2.2) to achieve a single cell suspension in 3 ml. Then 30 μl of this suspension was added to lysis buffer ATL from the DNeasy Blood and Tissue Kit (Qiagen) according to the manufacturers protocol for digestion of splenic tissue.

Following these harvesting steps, DNA was extracted using a DNeasy Blood and Tissue Kit (Qiagen) according to the manufacturers protocol. DNA was eluted in 30 μl of elution buffer AE and concentration quantified by measuring absorbance at 260nm on a short path spectrophotometer (Denovix DS-11 FX+).

2.7.1.3. Reverse-transcription

Reverse transcription was performed on 300 ng to 1 μg mRNA using a Superscript III First-Strand Synthesis SuperMix (Invitrogen), according to the manufacturers protocol. cDNA was treated with RNAse H and diluted to 5 ng/μl in RNAse free water, assuming complete conversion of RNA to DNA, for normalisation purposes.

2.7.1.4. Real-time quantitative PCR (qPCR) using SYBR Green

To analyse RNA abundance, real-time quantitative PCR (qPCR) was performed on cDNA using SYBR Green qPCR SuperMix-UDG Kit (Invitrogen). For this process, 10 ng of cDNA was used in a final reaction mix of 10 μl containing 200 nmoles of primers (Primers detailed in Table 2.5). Reactions were set up in MicroAmp® Optical 384-well reaction plates and qPCR was performed on a QuantStudio 7 Flex (Life Technologies). The qPCR cycling conditions were as follows: an initial denaturation step for 2 min at 95°C, followed by 40 PCR cycles with denaturation for 3 seconds at 95°C and primer annealing and elongation for 30 seconds at 60°C. Melt curve analysis was performed at the end of every qPCR to assess specificity of PCR products. Every sample was assayed in triplicate and *GNB2L1* was used as an endogenous control for each sample. Relative gene expression was calculated using the comparative Ct method (ΔΔCt, Schmittgen and Livak, 2008). Error bars in graphs represent standard errors from the triple qPCR reactions for each sample, unless stated otherwise. Primer efficiency was assessed by serial dilution of pooled cDNA samples.

Table 2.5. qPCR primers using SYBR Green assay.

Target gene	Primer sequence (5'-3')	Reference
GNB2L1	F: GTTGCAGTTAGCCAGGTTC	(Skalska et al., 2010)
	R: GAGTGTGGCCTTCTCCTCTG	
ALAS1	F: TCCACTGCAGCAGTACACTACCA	(Skalska et al., 2010)
	R: ACGGAAGCTGTGTGCCATCT	
p15^{INK4b}	F: CGGAGTCAACCGTTTCGG	(Bazot et al., 2014)
	R: GGTGAGAGTGGCAGGGTCT	
p16^{INK4a}	F: CCCCTTGCCTGGAAAGATAC	(Skalska et al., 2010)
	R: AGCCCCTCCTCTTTCTTCCT	
p18^{INK4c}	F: GGAGCCACACAAATCTTCAATAAACG	(Styles et al., 2017)
	R: GTCAGGAGAGCTACTCAGT	
p21^{WAF1}	F: CTGGAGACTCTCAGGGTCGAA	(Skalska et al., 2010)
	R: GCGGATTAGGGCTTCCTCTT	
p27^{KIP1}	F: GGAGCAATGCGCAGGAATAA	(Lindberg et al., 2008)
	R: TGGGGAACCGTCTGAAACAT	
p57^{KIP2}	F: GGCGATCAAGAAGCTGTCC	(Bazot et al., 2015)
	R: GACTTCTCAGGCGCTGATCT	
BLIMP-1	F: TACATACCAAAGGGCACACG	(Desai et al., 2009)
	R: TGAAGCTCCCCTCTGGAATA	
LMO2	F: GGCGGCGCCTCTACTACA	(Malumbres et al., 2011)
	R: CCAAAAAGCCTGAGATAGTCTCT	
SPIB	F: GCATACCCCACGGAGAACT	(Dontje et al., 2006)
	R: GGCTGTCCAACGGTAAGTCT	
XBP1	F: CCTGGTTGCTGAAGAGGAGG	(Mimura et al., 2012)
	R: CCATGGGGAGATGTTCTGGAG	
BZLF1	F: AAATTTAAGAGATCCTCGTGTAAAACATC	(Loebel et al., 2014)
	R: CGCCTCCTGTTGAAGCAGAT	

2.7.1.5. Real-time quantitative PCR (qPCR) using Taqman

For analysis of EBV viral load qPCR was performed on DNA using a Taqman® assay using primers for the viral protein BALF5, with Beta-2-Microglobulin (β2M) acting as an endogenous control.

DNA was extracted (see Section 2.7.1.2.) and levels normalised in nuclease free water depending on the lowest concentration of the samples. 4 μl of DNA assayed with 5 μl of Takyon™ Low ROX Probe 2X MasterMix dTTP blue (Eurogentec) and made up to a final reaction volume of 10 μl with primers diluted in nuclease-free water (primer concentrations detailed in Table 2.6). Assays were performed in MicroAmp® Optical 384-well reaction plates on a Quantstudio 7 Flex (Life Technologies) using Fast Mode. The cycling conditions were as follows: one activation step at 95°C for 3 min, followed by 40 cycles with denaturation at 95°C for 3 seconds, followed by primer annealing and extension at 60°C for 30 seconds. Every sample was assayed in triplicate. The cell line Namalwa, which has been established to contain 2 EBV genomes per cell, was used to establish EBV DNA copy number standards.

Table 2.6. RT-qPCR primers using Taqman assay.

Target gene	**Primer sequence (5'-3')**	**Final Concentration**
BALF5	F: CTTTGGCGCGGATCCTC	200 nM
	R: AGTCCTTCTTGGCTAGTCTGTTGA C	200 nM
	PROBE: **FAM**-CATCAAGAAGCTGCTGGCGGCC-**TAMRA**	200 nM
β2M	F: GGAATTGATTTGGGAGAGCATC	60 nM
	R: CAGGTCCTGGCTCTACAATTTACTAA	80 nM
	PROBE: **VIC-**AGTGTGACTGGGCAGATCATCCACCTTC-**TAMRA**	100 nM

2.7.2. Protein analysis

2.7.2.1. Protein extraction

Protein was extracted from cell pellets (see Section 2.2.3) and lysed in an approximately equivalent volume of 1x RIPA lysis buffer supplemented with 1mM PMSF and complete protease inhibitor cocktail (Roche). Lysates were left on ice for 30 minutes and then centrifuged at 9391 xg for 10 minutes at 4°C and the supernatant removed to a fresh tube. The concentration of the protein was determined using a detergent compatible (DC) protein assay (Bio-Rad), and measured at 750 nm on a

Helios spectrophotometer (Thermo Scientific) using bovine serum albumin to generate a standard curve from which protein concentrations were deduced.

2.7.2.2. SDS-PAGE and western blotting

The concentration of quantified protein samples were normalised in sterile water, usually to 20-30 μg depending on concentration of the samples. Following normalisation, samples were mixed with with SDS-PAGE sample loading buffer (5x final concentration) and heated at 100°C for 5 minutes to denature proteins. SDS-PAGE gels were made with an appropriate concentration of polyacrylamide required to identify the molecular weight of the relevant protein of interest as described in Table 2.7. Gels were placed in a Mini-PROTEAN® II Electrophoresis cell (Bio-Rad) containing 1x SDS-PAGE running buffer and samples were loaded. A Spectra Multicolour Broad Range Protein Ladder (Thermo Scientific) was used on each gel as a reference of the molecular weight of protein samples. Gels were then run for approximately 1.5 hours at 150 volts.

After SDS-PAGE, samples were transferred onto a nitrocellulose membrane (GE Healthcare) for 70 minutes at 100V using a Mini Trans-Blot® Electrophoretic Transfer Cell (Bio-Rad) filled with western transfer buffer. Following transfer, membranes were blocked with blocking solution (5% milk powder in PBS-Tween) for 1 hour at room temperature with rocking. Primary antibodies were diluted in PBS-Tween with 5% milk powder as detailed in Table 2.8 and incubated with membranes over night at 4°C with rocking. In most cases membranes were cut to allow analysis of multiple proteins with different molecular weights. Following primary antibody incubation, the next day membranes were washed four times for 10 minutes in PBS-Tween and then incubated at room temperature for 1 hour with the appropriate horseradish peroxidase (HRP)-conjugated secondary antibody (see Table 2.9). Membranes were washed in PBS-Tween as before and incubated for 2 minutes with enhanced chemical luminescence (ECL™, Amersham; GE Healthcare). Luminescence on the membranes was detected by exposure on Amersham Hyperfilm™ (GE Healthcare) autoradiography films, which were subsequently developed on an automatic X-ray film processor JP-33 (JPI).

Table 2.7. SDS-PAGE resolving and stacking gel composition. 30% Acrylamide/Bis solution obtained from Bio-Rad; TEMED obtained from BDH Chemicals (VWR). 10 ml of resolving gel is suitable for one gel of 1.5 mm thickness.

	Resolving Gel (10 ml)					**Stacking Gel (5 ml)**
Component	**7.50%**	**10%**	**12%**	**15%**	**Component**	
1.5 M Tris, pH 8.8	2.5 ml	2.5 ml	2.5 ml	2.5 ml	1 M Tris, pH 6.8	630 µl
30% Acrylamide/Bis solution 37.5:1	2.5 ml	3.3 ml	4 ml	5 ml	30% Acrylamid/Bis solution 37.5:1	830 µl
ddH20	4.7 ml	4 ml	3.3 ml	2.3 ml	ddH20	3.4 ml
10% SDS	100 µl	100 µl	100 µl	100 µl	10% SDS	50 µl
10% APS	100 µl	100 µl	100 µl	100 µl	10% APS	50 µl
TEMED	6 µl	4 µl	4 µl	4 µl	TEMED	5 µl

Table 2.8. Primary antibodies used for western blotting.

Antibody	**Description**	**Working dilution**	**Source**
anti-EBNA3A	Sheep polyclonal	1:1000	Abcam, ab16126
anti-EBNA3B	6C9, Rat monoclonal TC supernatant	1:10	(White et al., 2010)
anti-EBNA3C	A.10 hybridoma, mouse monoclonal, TC supernatant	1:10	Hybridoma from Prof. Martin Rowe (Maunders et al., 1994)
anti-EBNA1	Human serum	1:100	Gift from Prof. Paul Farrel
anti-EBNA2	PE2, mouse monoclonal	1:500	Abcam, ab90543
anti-EBNA-LP	JF-186, mouse monoclonal	1:100	(Finke et al., 1987)
anti-LMP1	CS1-4, mouse monoclonal	1:1000	DAKO, CS1-4
anti-γ-tubulin	Mouse monoclonal	1:10,000	Sigma-Aldrich, T6557
anti-$p15^{INK4b}$	Rabbit polyclonal	1:1000	Abcam, 53034
anti-$p16^{INK4a}$	Mouse monoclonal	1:10	JC8, Gift From Dr G. Peters
anti-$p18^{INK4c}$	Mouse monoclonal	1:1000	Cell Signalling, DCS118,
anti-$p21^{WAF1/CIP1}$	Rabbit monoclonal	1:1000	Cell Signalling, 29475
anti-$p27^{KIP1}$	Mouse monoclonal	1:1000	BD Transductions, 610242
anti-$p57^{KIP2}$	Rabbit monoclonal	1:500	Abcam, ab133531

anti-BLIMP-1	Rabbit monoclonal	1:1000	Cell Signalling, C14A4
anti-IRF4	M-17, Goat polyclonal	1:4000	Santa Cruz, sc-6059
anti-BZLF1	Mouse monoclonal	1:500	Gift from Prof. Paul Farrel
anti-BALF2	OT13N, Mouse monoclonal	1:1000	Gift from Jaap Middledorp
anti-p18VCA	Rabbit serum	1:100	Gift from Jaap Middledorp
anti-gp220/350	OT6, Mouse monclonal	1:1000	Gift from Jaap Middledorp

Table 2.9. Secondary antibodies used for western blotting.

Antibody	**Description**	**Working dilution**	**Application**	**Source**
anti-mouse (HRP conjugated)	Sheep polyclonal	1:2000	WB	GE Healthcare
anti-rabbit (HRP conjugated)	Polyclonal goat		WB	DAKO
anti-human (HRP conjugated)	Polyclonal rabbit		WB	DAKO
anti-sheep (HRP conjugated)	Polyclonal rabbit		WB	DAKO
anti-rat (HRP conjugated)	Polyclonal rabbit		WB	DAKO
anti-goat (HRP conjugated)	Polyclonal rabbit		WB	DAKO

2.8. Flow cytometric analysis

Flow cytometry was performed on either a Fortessa B (Beckon Dickinson) or LSRII (BD) flow cytometer. Where appropriate, compensation beads were used to ensure compensation between different fluorescent channels. One drop of both negative and positive compensation beads was combined independently with 1 µl of the antibodies of interest to create single stains. These were incubated for 30 minutes at RT and washed twice in PBS as per cellular samples and used to create a compensation control for each multiple-antibody experiment. All new antibodies were titrated for optimisation within multi-antibody flow cytometric panels and antibodies were purchased from BD Biosciences unless noted otherwise. Analysis was performed using FlowJo software, and gating was used to ensure only live, single cells were analysed. Antibodies used in this study are detailed in Table 2.10.

Table 2.10. Antibodies used for flow cytometric analysis. Working dilutions regarding different flow cytometry assays are described in the text.

Antibody	Flurochrome	Source
anti-human CD3	PE-Cy7	BD Biosciences
anti-human CD4	PerCP-Cy5.5	BD Biosciences
anti-human CD8	Alexa Fluor 700	BD Biosciences
anti-human CD19	PE	BD Biosciences
anti-human CD20	RPE	DAKO
anti-human CD20	Alexa Fluor 700	BD Biosciences
anti-human CD27	BV650	BD Biosciences
anti-human CD38	PE-Cy7	BD Biosciences
anti-human CD45	BV510	BD Biosciences
anti-mouse CD45	BV421	BD Biosciences
anti-human CD138	APC	BD Biosciences
anti-human IgG	PE	BD Biosciences
anti-human IgM	BV605	BD Biosciences
anti-human IgD	PerCP-Cy5.5	BD Biosciences

2.8.1. Analysis of proliferation and cell cycle distribution

For the analysis of cells during primary B cell infection with EBV, approximately 500 µl of cell culture was transferred to a fresh 24 well plate and 500 µl growth medium added. 24 hours later an additional 500 µl growth medium was added alongside EdU to a final concentration of 5 µM. These cells were then returned to an incubator and allowed to grow for 2 hours before the culture was harvested. For analysis of established cell lines, cells were seeded at $3x10^5$/ml in 4 ml. After 20 hours 1 ml of medium containing EdU for a final concentration of 10 µM was added. Cells were then returned to an incubator and allowed to grow for 2 hours before the culture was harvested.

Following EdU incubation, cells were washed in 1-5 ml of cold PBS and resuspended in 1 ml cold PBS containing 0.5 µl Violet Fixable Dead Cell Stain (Life Technologies) and incubated for 30 minutes on ice. Cells were then washed once in 1 ml PBS, then again in 1 ml PBS/BSA before being resuspended in 100 µl PBS/BSA. Cells were then fixed by addition of 400 µl 100% ethanol at -20˚C

while vortex mixing. Cells were then incubated on ice for 1 hour before being centrifuged at 376 xg for 5 minutes. The supernatant was then removed and cells were rehydrated in 500 µl PBS/BSA for 15 minutes. The cells were then centrifuged for 5 minutes at 1500 xg and resuspended in 100 µl PBS/BSA. EdU was then labelled using Click chemistry. Cells were incubated with a 500 µl of reaction mix containing 438 µl PBS/BSA, 10 µl $CuSO_4$, 2.5 µl Alexa488 Azide and 50 µl 1x additive G, for 30 minutes at RT. Following incubation, 800 µl PBS/BSA was added to cells before pelleting at 1500 xg for 5 minutes. Cells were then resuspended in 500 µl PBS/BSA containing 10 ug/ml RNAse and 1 µl/ml FxCycle Far Red and incubated for 30 minutes at RT. Cells were then analysed by flow cytometry.

2.8.2. Lymphocyte surface marker analysis

2.8.2.1. Assessing purity of $CD19^+$ purified B cells

To analyse purity of isolated $CD19^+$ cells, $5x10^5$ purified $CD19^{+ve}$ B cells, and $5x10^5$ cells from a sample of the PBLs from which they were isolated, was added to 1 ml PBS/BSA. Cells were then centrifuged at 350 xg for 5 minutes and the supernatant removed. Cells were resuspended in 50µl PBS/BSA with 1µl of human IgG and incubated for 15 minutes at RT. Then 1ml PBS/BSA was added straight to the antibody mixture and the cells were centrifuged at 350 xg for 5 minutes. Cells were then resuspended in 100µl PBS/BSA with 1 µl of CD20-RPE antibody and incubated for 30 minutes at 4°C. Cells were then washed twice in 1 ml PBS, then resuspended in 400 µl PBS containing 4 µl DRAQ7 Live/Dead stain (BioStatus) and assessed by flow cytometry.

2.8.2.2. Quantification of humanised mouse engraftment and lymphocyte composition

2.8.2.2.1. Basic analysis of human CD45 and CD19 cell engraftment in humanised mice

Peripheral blood was collected from mice as described in Sections 2.10.3 and 2.10.4.1. Approximately 50 or 100 µl blood was resuspended in red blood cell (RBC) lysis buffer (Biolegend) to 3 ml or 6 ml respectively. The solution was then gently vortexed to mix and incubated for 10-15 minutes at RT. The cells were then centrifuged for 5 min at 350 g and then washed in 1 ml cold PBS, followed by washing in 1 ml cold PBS/BSA. Cells were then centrifugated as before and resuspended

in 50 µl PBS/BSA containing 1 µl hum-CD45-BV510 antibody, 1 µl mouse-CD45-BV421 antibody and 1 µl hum-CD19-PE antibody and incubated for 30 minutes at 4˚C. Following incubation, cells were washed twice more in 1 ml PBS. The cells were then resuspended in 400 µl PBS containing 4 µl DRAQ7 Live/Dead stain (BioStatus) and assessed by flow cytometry. Engraftment of a human immune system components in humanised mice was calculated as the %hCD45$^+$ cells / (%mCD45$^+$ cells + % hCD45$^+$ cells).

2.8.2.2.2. Analysis of human B and T lymphocyte engraftment in humanised mice

Peripheral blood was collected from humanised mice as described in Sections 2.10.3 and 2.10.4.1. Approximately 50 or 100 µl blood was resuspended in red blood cell (RBC) lysis buffer (Biolegend) to 3 ml or 6 ml respectively. The solution was then gently vortexed to mix and incubated for 10-15 minutes. The cells were then centrifuged for 5 min at 350 g and washed in 1 ml cold PBS, cells were centrifuged as before and then resuspended in 1ml PBS containing 0.5 µl Fixable Viability Stain 780 (BD Biosciences) and incubated for 15 minutes at RT. Following incubation, cells were pelleted and washed in 1 ml PBS/BSA. Cells were then centrifuged again as before and resuspended in an antibody mastermix containing 1 µl hum-CD45-BV510 antibody, 1 µl mouse-CD45-BV421 antibody, 1 µl hum-CD19-PE, 1 µl hum-CD3 antibody, 1 µl hum-CD4-PerCP-Cy5.5 antibody and 2 µl hum-CD8-AF700 antibody in 100 µl 1% PBS/BSA and incubated for 30 minutes at 4˚C. Following incubation, cells were washed twice in 1 ml PBS. Cells were then resuspended in 400 µl PBS and assessed by flow cytometry. Engraftment of a human immune system components in humanised mice was calculated as the %hCD45$^+$ cells / (%mCD45$^+$ cells + % hCD45$^+$ cells).

2.8.2.2.3. Analysis of B lymphocyte composition

Approximately 10^6 cells were pelleted by centrifugation at 350 xg for 5 minutes and washed in 1 ml PBS. Cells were centrifuged again and then resuspended in 1ml PBS containing 0.5 µl Fixable Viability Stain 780 (BD Biosciences) and incubated for 15 minutes at RT. Following incubation, cells were centrifuged as before and washed in 1 ml PBS/BSA. Cell were then centrifuged as before and

then resuspended in a 100 µl PBS/BSA antibody mastermix containing 10 µl CD19-PE antibody, 2.5 µl CD20-AF700 antibody, 2.5 µl CD38-PE-Cy7 antibody, 5 µl CD138-APC antibody, 2.5 µl CD27-BV605 and 5 µl IgD-PerCP-Cy5.5. If cells were derived from humanised mice then the antibody mastermix was also supplemented with 1 µl hum-CD45-BV510 antibody and 1 µl mouse-CD45-BV421 antibody. Cells were incubated with the antibodies for 30 minutes at 4˚C. Following incubation, cells were washed twice in 1 ml PBS and then resuspended in 500 µl PBS and analysed by flow cytometry.

2.8.3. Staining of intracellular and extracellular immunoglobulin

A Cytofix/Cytoperm kit (BD Biosciences) was used for intracellular staining of immunoglobulins (Ig) as per the manufacturer's instructions. Cultured cells were centrifuged at 350 xg for 5 minutes and then washed twice in 1 ml PBS. Following the washes, cells were resuspended in 1ml PBS containing 0.5 µl Fixable Viability Stain 780 and incubated for 15 minutes at RT. Cells were then washed in 1.5 ml PBS/BSA and then resuspended in antibody mastermix of surface marker antibodies containing 5 µl CD138-APC, 2.5 µl CD38-PE-Cy7 and 5 µl CD20-AF700 made up to 100 µl with PBS/BSA, and incubated for 30 minutes at 4˚C. Following incubation, cells were washed twice in 1 ml PBS/BSA and resuspended in 250 µl of Fixation/Permeabilization buffer and incubated for 20 minutes at 4˚C. Cells were then washed twice in 1 ml Permeabilization/Wash buffer and then resuspended in an antibody mastermix containing 5 µl IgM-BV605 and 20 µl IgG-PE, made up to 100 µl with PBS/BSA, and incubated for 30 minutes at 4˚C**.** Following incubation, cells were washed twice in 1 ml Permeabilization/Wash buffer and then resuspended in 500 µl PBS for flow cytometric analysis.

2.9. Generation of mice with human immune system components

2.9.1. Mice

All mice used in this study were of the NOD/Rag$^{-/-}$/IL2-γR^{null} (NRG background) and were obtained from Jackson Laboratories. Mice were raised under specific pathogen free conditions. All animal protocols were conducted according to the UK Animals (Scientific Procedures) Act 1986. Animal protocols were performed by Christine Theresa Styles under the personal license I10FA9E48

according to the project license authority of Imperial College London. Work was performed under the project license PPL: 708219 (Development of humanised mice for HIV), held by Dr Marcus Dorner.

2.9.2. Sub-lethal irradiation and injection of CD34⁺ hematopoietic stem cells of newborn mice for establishment of human immune system components

Pups between 0-4 days old were sub-lethally irradiated with 100 cGy. Mice were then left for 3-6 hours before intrahepatic injection of $CD34^+$ cells (on the same day). $CD34^+$ cells were removed from liquid nitrogen and thawed (see Section 2.2.2). Once thawed, cells were centrifuged at 300 xg for 3 minutes and then washed in 10 ml regular growth medium. Cells were centrifuged again and resuspended in the appropriate volume of regular growth medium such that there was 50 µl per mouse within the litter to be humanised, with approximately 100 µl excess to account for loss in syringes. Cell numbers were such that each mouse received approximately 10^5-10^6 cells respectively. Mice were appropriately restrained and 50 µl of cells was injected into the liver of each mouse using a 0.3 ml microfine U-100 insulin needle (BD Biosciences). Engraftment of human immune system components was assessed at approximately 3 months of age, as detailed in section 2.8.2.2.

2.10. Protocols for analysis of humanised mice

2.10.1. Infection of humanised mice with recombinant EBV viruses

Mice were infected by intra-peritoneal injection with $1x10^5$ GRU recombinant EBV virus resuspended in 100-200 µl PBS (depending on viral titre), using a 0.3 ml microfine U-100 insulin needle (BD Biosciences). Mock infected mice were administered with 100 µl PBS via intra-peritoneal injection. Mice were distributed as evenly as possible across different EBV recombinant infections with regards to sex, age, $CD34^+$ cell donor, level of engraftment and percentage of $CD19^+$ cells. Mice were weighed and health and wellbeing was assessed a minimum of twice a week to ensure project license end points were adhered to. E45 cream was applied using a cotton bud to mice exhibiting fur loss and dry skin as required.

2.10.2. Use of tamoxifen impregnated food

Where noted, mice were fed tamoxifen-impregnated food (Envigo). Regular food and tamoxifen-impregnated food were mixed with water to obtain a wet food mix, these were mixed 1:1 and given to mice. Since mice had an aversion to the tamoxifen-impregnated food, regular food was administered on weekends and when mouse weight dropped by 10-15% to avoid breaching weight loss end points as per the animal license.

2.10.3. Venesection (blood sampling)

Blood sampling was performed by venesection. EMLA cream was applied directly to mouse tails and left to become numb for at least 15 minutes. Mice were appropriately restrained and a scalpel used to lightly nick a tail vein. Then 50 µl of blood was collected using a minivette POCT capillary tube (Sarstedt), and pressure applied immediately afterwards to cease bleeding. Blood was immediately transferred into a 1.5 ml eppendorf tubes pre-coated with EDTA to prevent blood clotting. DNA extraction or flow cytometic analysis was subsequently performed as required (see Section 2.7.1.2 and 2.8.2).

2.10.4. Terminal analysis of humanised mice

2.10.4.1. Cardiac puncture for analysis of peripheral blood

Mice were anaesthetised using isoflurane in combination with oxygen. Following confirmation of anaesthetisation by assessment of pedal reflexes, a 26-gauge needle was used to perform a cardiac puncture enabling harvest of up to 1 ml of blood. Mice were humanely culled by cervical dislocation before regaining consciousness. Blood was immediately transferred into a 1.5 ml Eppendorf tube pre-coated with EDTA to prevent blood clotting. DNA extraction (Sections 2.7.1.2), flow cytometic analysis (Section 2.8.2) or lymphocyte isolation was subsequently performed on harvested blood as required (Section 2.3.1).

2.10.4.2. Terminal analysis of spleens from humanised mice

Spleens were removed from mice post mortem and assessed visually for tumour development and weighed to assess splenomegaly. They were then placed on ice in 1 ml PBS for same day analysis.

2.10.4.2.1. Immunohistochemistry

2.10.4.2.1.1. Spleen fixation

Following post mortem extraction of spleens and initial assessment, spleens were cut in half using a scalpel and a section immediately placed into formalin and fixed for 24 hours (the other section was used within alternative protocols). Spleens were then placed into 70% EtOH until being embedded in paraffin wax. 5 µM sections were then mounted onto slides.

2.10.4.2.1.2. Dewaxing and antigen retrieval

Slide mounted sections were dewaxed using a Leica immunohistochemistry machine, employing use of 100% Aquaclear for 15 minutes, 90% Aquaclear for 15 minutes, followed by 30 seconds in 100% EtOH then 30 seconds in 90% EtOH. Following dewaxing, slides were immediately placed into 100% methanol containing hydrogen peroxide at a ratio of 100:1 for 10 minutes at room temperature, to block endogenous peroxide activity. Slides were then removed to tap water for 10 minutes. Antigen retrieval was performed by heat treatment using a microwave to boil slides in 1 M Tri-sodium citrate buffer at pH 6 for 10-20 minutes, before cooling in tap water for 10 minutes.

2.10.4.2.1.3. Primary antibody staining

Antibodies and concentrations can be seen in Table 2.11. All primary antibodies were appropriately titrated considering their respective antibody isotype.

Mouse primary antibodies

The Mouse-On-Mouse kit (MOM kit, Vector Labs) was used for all mouse derived antibodies, essentially as per the manufacturer's instructions. First, to block endogenous biotin, biotin receptors and avidin binding sites, an avidin-biotin blocking kit (Vector labs) was used as per the manufacturer's instructions. Sections were then washed for 2 minutes in PBS 3 times, before for blocking with mouse

Ig blocking reagent for 1 hour at room temperature. Following a 5 minute incubation with the MOM kit protein dilutent, sections were incubated with approximately 150 μl of appropriately diluted primary antibody overnight at 4°C.

Non-mouse primary antibodies

Sections were blocked with 5% goat serum in PBS for 1 hour at room temperature, then washed for 2 minutes in PBS, 3 times. Avidin-biotin blocking was then performed as above, before overnight incubation at 4°C with primary antibody appropriately diluted in PBS with 5% goat serum.

Table 2.11. Antibodies used for immunohistochemistry.

Antibody	**Description**	**Working dilution**	**Source**
anti-EBNA2	Mouse monoclonal	1:8000	Abcam, ab90543
anti-CD20	Mouse monoclonal	1:100	Abcam, ab9475
anti-Ki67	Rabbit monoclonal	1:160	ThermoFisher, SP6
anti-mouse (Biotin conjugated)	Component of 'Mouse On Mouse' (MOM) kit	1:500	Vector Labs
anti-rabbit (Biotin conjugated)	Polyclonal goat	1:500	Stratech

2.10.4.2.1.4. Visualisation

The following day, slides were washed for 5 minutes PBS-Triton (0.1% v/v), 3 times. Sections were then incubated with their respective secondary biotinylated antibody. Antibodies and concentrations can be found in Table 2.11. Following secondary antibody incubation slides were washes in PBS-Triton as before, and an Avidin-Biotin Complex kit (Vector Labs) was used as per the manufacturer's instructions. Immobilized antibodies were detected using a Diaminobenzidine (DAB)-HRP kit (Vector Labs) and sections counterstained in hematoxylin. A cover slip was applied to each slide and samples were visualised using a light microscope.

2.10.4.2.2. Mechanical disruption of splenic tissue for single cell suspension

Following post-mortem extraction of the spleen from mice, the splenic tissue was mechanically disrupted to obtain a single cell suspension. Spleens were disrupted by gently pushing the tissue through a 70 μM cell strainer using the plunger of a sterile 5 ml syringe. Strainers were rinsed twice with 1 ml of PBS to release cells and resuspend them in a total of 3 ml PBS. Cells were then homogenised with a 5 ml pipette. DNA was then extracted for analysis of splenic viral load (see Section 2.7.1.2).

2.10.4.2.3. Isolation of splenic lymphocytes

A single cell suspension of splenic cells within 3 ml PBS (obtained as described in Section 2.10.4.3.1) was layered over 3 ml of Ficoll-Paque (GE Healthcare) in a 15 ml falcon tube. Tubes were then centrifgued for 30 minutes at 339 xg, with both break and acceleration off. The lymphocyte fraction, identified as the white/grey interface in the centre of the tube, was removed using a 1 ml Gilson pipette into 10 ml wash buffer (RPMI, 1% FCS). Cells were pelleted by centrifugation at 339 xg for 5 minutes with the break off and then resuspended in 10 ml wash buffer. The cells were then centrifugated as before and resuspended in 2 ml growth medium with 15% FCS and counted (see Section 2.2.3).

Cells then underwent flow cytometic analysis (Section 2.8.2) or were assessed for the outgrowth of humanised mouse-derived LCL (mLCL, see Section 2.10.4.2.4).

2.10.4.2.4. Outgrowth of EBV infected humanised mouse spleen derived LCL (mLCL)

Splenic lymphocyte cells were isolated as described in Section 2.10.4.2.3 and 10^7 cells were seeded in 3 ml growth medium containing 15% FCS and 500 ng/ml cyclosporine A. Cultures were visually inspected for LCL clumping by light microscopy. When cells reached high density (namely medium acidification and cell abundance), culture volume was increased with fresh medium. Cell lines were maintained at 10 ml in a T75 cm^2 flask and then expanded as required for use in experiments. Outgrowth of mouse derived LCL (mLCL) was quantified as expansion of an individual cell cultures to 10 ml of continuously proliferating culture.

2.11. Statistical analysis

Statistical analysis was performed using Prism Software (Graphpad). Unpaired two-tailed students t-test with Welch's correction or Fishers exact test were used, as appropriate. A p value of <0.05 was considered statistically significant, a p value of <0.01 was considered very significant.

3. Chapter III: Identifying the independent and combined functions of EBNA3A and EBNA3C

3.1. Introduction

The EBV oncogenes EBNA3A and EBNA3C support EBV persistence and latency by differentially regulating various host genes. Microarray and ChIP analyses have shown that EBNA3A and EBNA3C co-operatively regulate many target genes and co-localise extensively across the genome, indicating shared functions (Paschos et al., 2017; White et al., 2010). For example, both EBNA3A and EBNA3C have been shown to target various cell cycle regulatory factors, including CDKI, resulting in cell cycle deregulation (see Chapter I, Section 1.3). The origin of EBNA3A and EBNA3C from a single ancestral gene, still found in a New World lymphocryptovirus of Marmosets (Rivailler et al., 2002), and their shared structure and sequence homology (Le Roux et al., 1994; Yenamandra et al., 2009) further suggests duplicated functions. However, despite sharing a number of target genes (White et al., 2010), and therefore complementary activity, both EBNA3A and EBNA3C are required for efficient B cell transformation and subsequent viral persistence (Tomkinson et al., 1993). The conserved nature of these oncogenes during EBV evolution further suggests they perform non-redundant functions. Furthermore, host genes independently regulated by either EBNA3A (Bazot et al., 2018) or EBNA3C (Kalchschmidt et al., 2016a) have been identified. There remains much to be established regarding the complexities of the shared and independent functions of EBNA3A and EBNA3C, and their combined requirement during EBV infection.

The cloning of the B95.8 EBV strain into an F factor derived plasmid (Delecluse et al., 1998) has allowed our lab and others to introduce deletions and fusion tags into the EBV genome [(reviewed in (Feederle et al., 2010), see (Styles et al., 2018) for recent review of studies using recombinant EBV viruses constructed in the Allday laboratory]. This EBV-BAC system allows propagation and manipulation of the EBV genome within bacteria. Purification of EBV-BAC produces large amounts of

DNA that can be transfected into mammalian cells, allowing production of infectious virus. Recently, recombinant BAC-derived EBV viruses with genetic modifications within the EBNA3 proteins have allowed detailed genetic analysis of the roles of EBNA3A and EBNA3C within B cell transformation and viral latency (see Chapter I, Section 1.4).

To further characterise the independent and combined activity of the EBNA3A and EBNA3C oncoproteins, RecA-mediated recombineering of the EBV-BAC was used to generate a conditional recombinant virus where both EBNA3A and EBNA3C can be simultaneously regulated. Recombinant viruses with conditional expression of either EBNA3A and EBNA3C independently have been generated by our lab as well as others (Bazot et al., 2015; Maruo et al., 2003; Skalska et al., 2010), and infecting cells with these recombinant viruses has illuminated many aspects of EBNA3A and EBNA3C gene regulation [reviewed in (Allday et al., 2015; Styles et al., 2018)]. To generate a double conditional virus, a HT-sensitive ERT2 domain was introduced to the C-terminal of both EBNA3A and EBNA3C using a RecA-mediated homologous recombination system adapted by White *et al* (White et al., 2003). The use of ERT2 fused to both EBNA3A and EBNA3C makes functional expression of both EBNA3A and EBNA3C simultaneously dependent on the activating ligand HT. In the absence of HT, the fusion protein is targeted for degradation and the conditional protein is non-functional. The addition of HT to cells infected with conditional recombinant viruses stabilises the fusion protein, this allows nuclear translocation and functional expression.

Both EBNA3A and EBNA3C are required for efficient B cell immortalisation (Tomkinson et al., 1993). EBNA3C is essential for transformation (Skalska et al., 2013), and EBNA3A-null cells exhibit reduced proliferative capacity (Bazot et al., 2015; Hertle et al., 2009). Therefore, using the double conditional recombinant EBV virus, I wanted to address whether cells with simultaneously non-functional EBNA3A and EBNA3C would exhibit a more extreme phenotype (with further reduced proliferative capacity and elevated cell cycle arrest) compared to cells where EBNA3A or EBNA3C was independently expressed.

Furthermore, EBNA3A and EBNA3C have been associated with deregulation of various cell cycle associated factors, including the CDKI $p15^{INK4b}$, $p16^{INK4a}$, $p21^{WAF1/CIP1}$ $p27^{KIP1}$ and $p57^{KIP2}$ (see Chapter I, Section 1.3.1). Therefore, regulation of these CDKI, as well as the $p16^{INK4a}$/$p15^{INK4b}$ related CDKI $p18^{INK4c}$, was assessed in cells with conditional expression of both EBNA3A and EBNA3C. Alongside the hypothesis that inactivation of both EBNA3A and EBNA3C may result in a more extreme phenotype, it was thought regulation failure may be more profound when both EBNA3A and EBNA3C are simultaneously non-functional as they share various target genes.

3.2. Results

3.2.1. Construction and validation of the EBNA3A-ERT2/EBNA3C-ERT2 (3A3CERT2) double conditional virus

3.2.1.1. Construction of the EBNA3A-ERT2/EBNA3B/EBNA3C-ERT2 double conditional recombinant plasmid

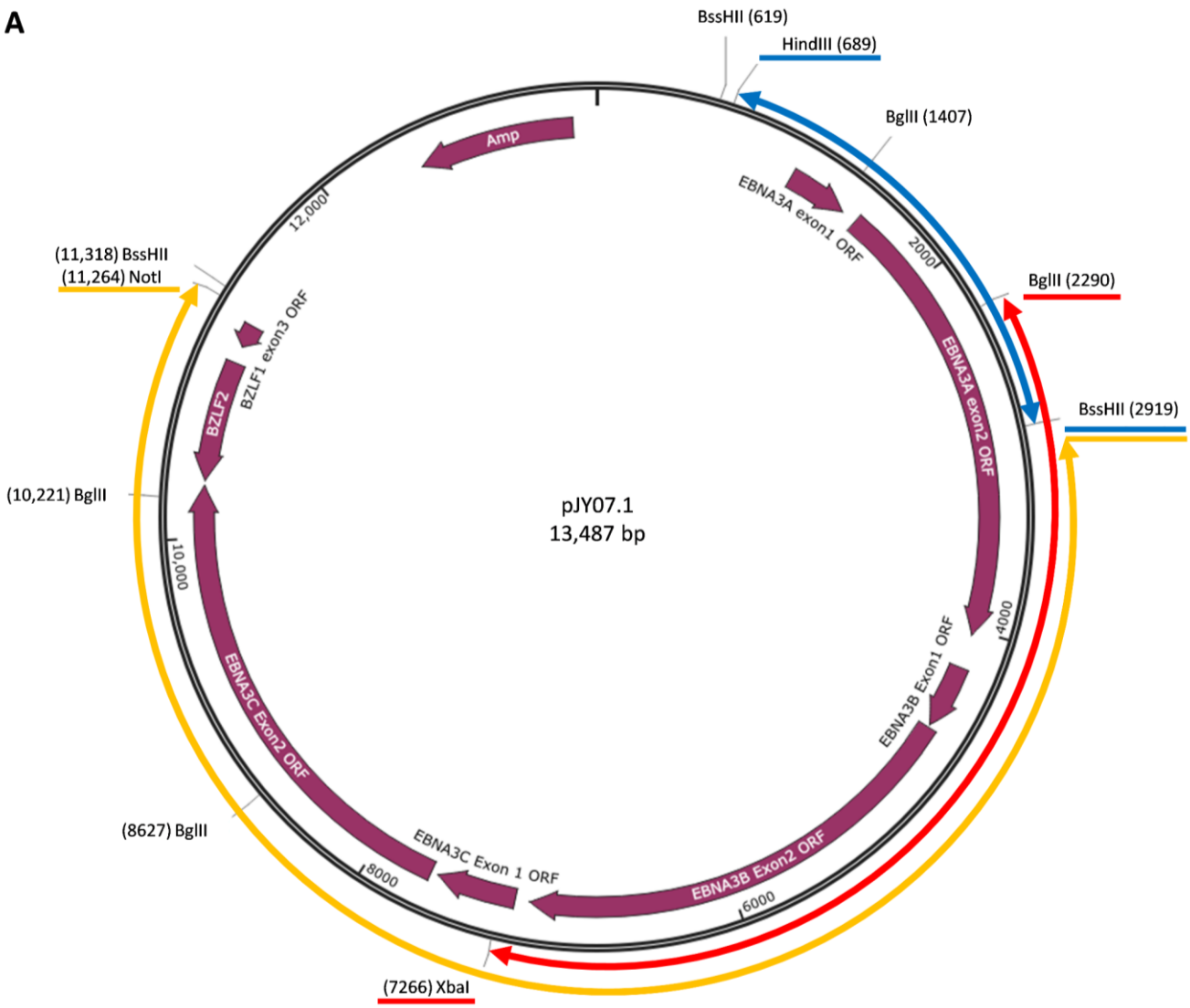
Prior to the start of this project, Dr Jade Yee had generated the recombinant EBV-BAC virus E3KO, in which the entire EBNA3 locus had been removed, as well as a revertant EBV-BAC where the EBNA3 locus was re-introduced [(White et al., 2010), Dr J Yee, PhD Thesis]. As a cloning intermediate for producing the revertant of E3KO (E3REV), she generated a plasmid containing all the EBNA3 proteins (pJY07.1), which was used as the source of all of the EBNA3 proteins during the cloning process detailed in this thesis. In addition, Dr Quentin Bazot had generated EBNA3A-ERT2 and EBNA3C-ERT2 EBV-BAC viruses with conditional expression of either EBNA3A or EBNA3C (Bazot et al., 2015; Styles et al., 2017). These viruses were constructed with an ERT2 receptor, as this is better than the ER that was used in previously constructed viruses (Maruo et al., 2003, 2006; Skalska et al., 2010) because it is more estrogen-resistant. Use of ERT2 recombinant viruses enables the use of these recombinant EBV-BAC viruses *in vivo*. As intermediates in this process, Quentin constructed the pQB-

01 and pQB-02 plasmids containing ERT2 genes, and these were used as the source of ERT2 constructs. Plasmid maps can be found in the Appendix.

Using restriction digest and ligation techniques (as detailed in the Materials and Methods, Section 2.4) the EBNA3 proteins were cloned alongside ERT2 genes. Briefly, plasmids were digested with restriction enzymes as required, and fragments separated on agarose gels. Specific DNA fragments were isolated from gels and fragments were ligated together. Ligated DNA constructs were transformed into competent DH5α bacteria, which were then grown on selective antibiotics. DNA was isolated from the bacteria by mini-prep and the resulting plasmid constructs confirmed by diagnostic restriction digest, and visualised on an agarose gel, before use in subsequent cloning steps. To obtain fragments of the EBNA3 genes, restriction enzymes were used to digest pJY07.1 (detailed schematically in Figure 3.1A). In a series of steps (summarised in Figure 3.1B) the pCS007 construct was created, which contained the EBNA3 genes with ERT2 genes at the C-termini of both EBNA3A and EBNA3C.

The BglII/XbaI fragment of pJY07.1 containing from inside EBNA3A to the start of EBNA3C was cloned into a p8195 vector digested with BamHI and NheI to generate pCS001. An ERT2 gene was then sub-cloned from pQB-01 into pCS001 following digestion with BssHII and NheI to generate pCS004. A fragment of pJY07.1 from digestion with HindIII and BssHII containing the start of EBNA3A was inserted into pRP004 digested with the same restriction enzymes, producing pCS002. pCS002 was then digested with HindIII, and the klenow enzyme introduced to blunt the ends of the DNA fragment. The DNA fragment was then ligated, which resulted in a NheI restriction digest site in place of the HindIII site, producing pCS005. The NotI/BssHII fragment of pJY07.1 containing from inside EBNA3A to the end of the EBNA3 fragment was cloned into NotI/BssHII-digested pRP004 to produce pCS003. The end of EBNA3C-ERT2 was then sub-cloned from pQB-02 into pCS003 with NsiI and NdeI digestion to produce pCS006. Finally, the fragments were reassembled into the pCS007 construct, following digestion of pCS004, pCS005 and pCS006 with SfiI/BssHII, ClaI/BssHII or SfiI/ClaI, respectively (shown schematically in Figure 3.2). All constructs were confirmed by diagnostic restriction digest.

The pCS007 construct carries the EBNA3 locus with ERT2 fused to the C-terminal of both EBNA3A and EBNA3C. pCS007 also contains an Amp resistance cassette for selection of clones, and a BZLF1 exon 3 upstream of EBNA3C. This acts as a homology region required for the subsequent recombination of the EBNA3 locus and ERT2 construct into the E3KO EBV-BAC, which lacks the EBNA3 locus.


A
BssHII (619)
HindIII (689)
BglII (1407)
BglII (2290)
BssHII (2919)
(7266) XbaI
(8627) BglII
(10,221) BglII
(11,318) BssHII
(11,264) NotI
Amp
EBNA3A exon1 ORF
EBNA3A exon2 ORF
EBNA3B Exon1 ORF
EBNA3B Exon2 ORF
EBNA3C Exon 1 ORF
EBNA3C Exon2 ORF
BZLF1 exon3 ORF
BZLF2
pJY07.1
13,487 bp
2000
4000
6000
8000
10,000
12,000

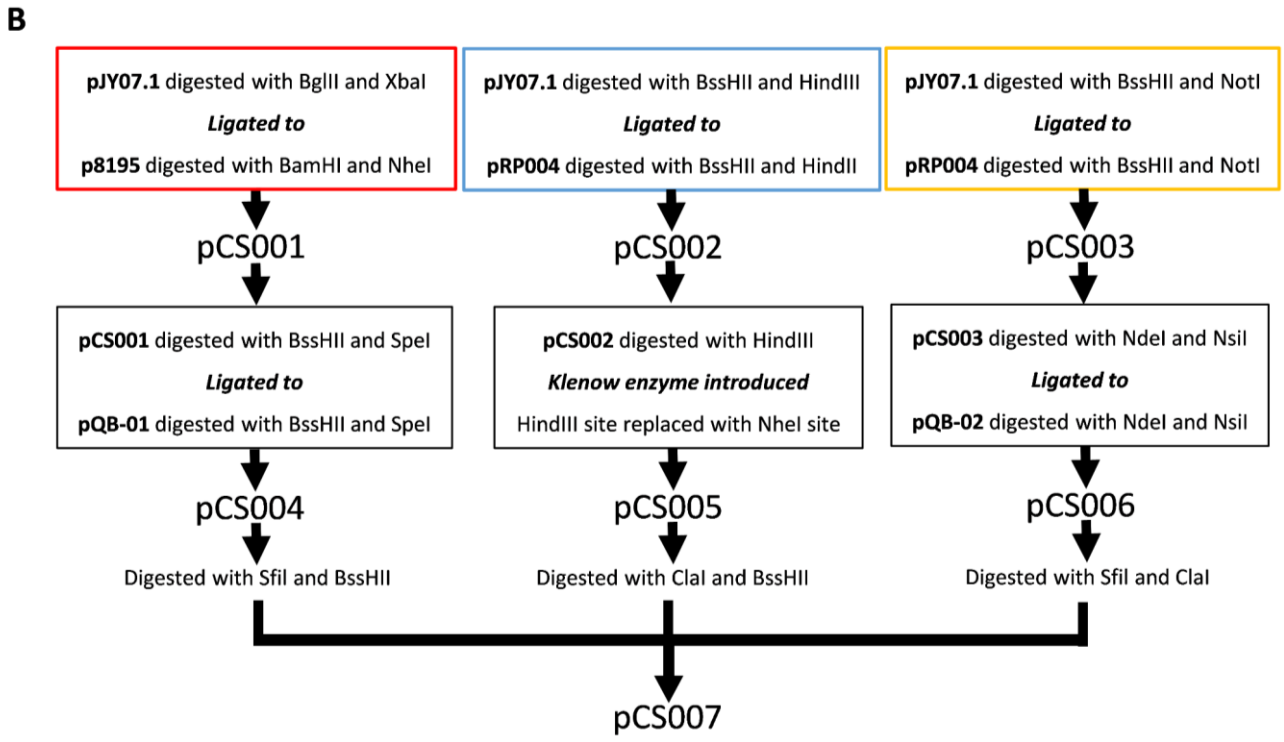

B
pJY07.1 digested with BglII and XbaI
Ligated to
p8195 digested with BamHI and NheI
pJY07.1 digested with BssHII and HindIII
Ligated to
pRP004 digested with BssHII and HindII
pJY07.1 digested with BssHII and NotI
Ligated to
pRP004 digested with BssHII and NotI
pCS001
pCS002
pCS003
pCS001 digested with BssHII and SpeI
Ligated to
pQB-01 digested with BssHII and SpeI
pCS002 digested with HindIII
Klenow enzyme introduced
HindIII site replaced with NheI site
pCS003 digested with NdeI and NsiI
Ligated to
pQB-02 digested with NdeI and NsiI
pCS004
pCS005
pCS006
Digested with SfiI and BssHII
Digested with ClaI and BssHII
Digested with SfiI and ClaI
pCS007

Figure 3.1. Construction of pCS007. (**A**) pJY07.1 was digested with either BglII and XbaI, HindIII and BssHII or BssHII and NotI restriction enzymes to obtain fragments of EBNA3 genes for the construction of pCS007. (**B**) Flow chart summarising the subsequent steps in the construction of pCS007, detailing intermediate plasmid identification and restriction enzymes used.

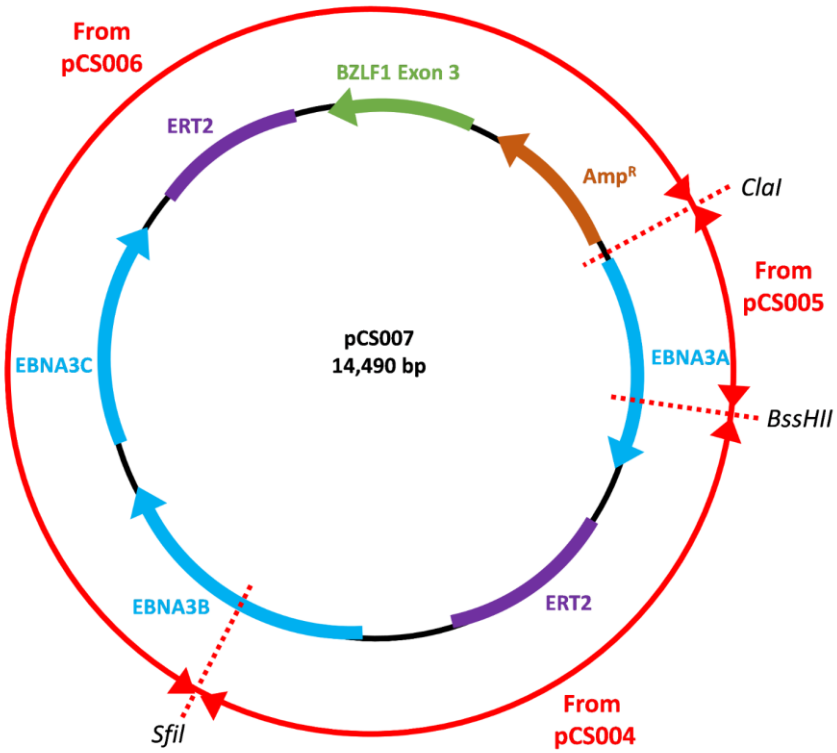


Figure 3.2. Schematic showing the generation of the pCS007 plasmid. pCS004 was digested with SfiI and BsHII restriction enzymes and ligated to fragments obtained from pCS005 digested by Cla and BsHII and pCS006 digested with ClaI and SfiI. The resulting ligated plasmid, called pCS007, contains EBNA3A-ERT2, EBNA3B, EBNA3C-ERT2 as well as a BZLF1 exon and Ampicillin (Amp^R) resistance cassette.

To recombine the pCS007 construct with an EBV-BAC, a pKovKanΔCm construct (p4487) was used as a shuttle vector (White et al., 2003). The pKovKanΔCm shuttle vector carries a Kan resistance cassette for positive selection of clones and a levansucrase gene (SACBII) for negative selection, which causes the death of the transformed bacteria when plated on sucrose. The pKovKanΔCm shuttle vector also contains a temperature sensitive origin of replication such that it can propagate at 30°C but is unable to replicate at 43°C. Fragments obtained by digesting pCS007 with MluI and NheI, and p4487 with BssHII and XbaI, were ligated together, resulting in insertion of pCS007 into the

pKovKanΔCm vector (shown schematically in Figure 3.3). The structure of the resulting plasmid (pCS008) was confirmed by diagnostic restriction digest.

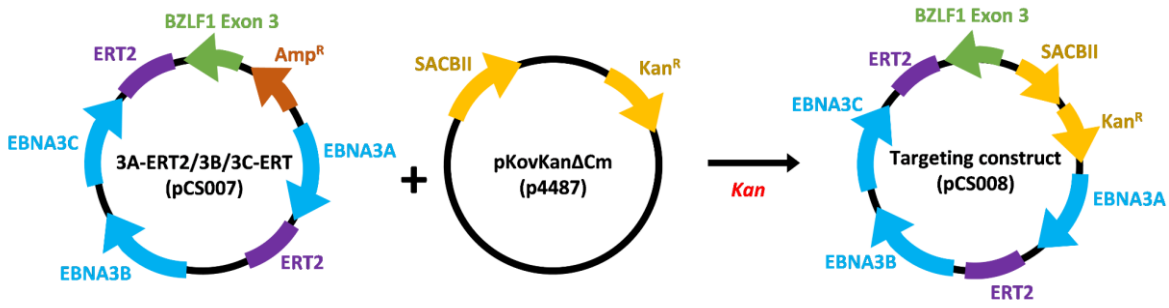


Figure 3.3. Cloning the EBNA3A-ERT2/EBNA3B/EBNA3C-ERT2 construct into the shuttle vector. The EBNA3A-ERT2/EBNA3B/EBNA3C-ERT2 containing plasmid (pCS007) was digested with MluI and NheI and ligated into the BssHII/XbaI-digested pKovKanΔCm shuttle vector (White et al., 2003). The resultant construct was selected on LB-agar containing Kanamycin (Kan) at 30°C.

3.2.1.2. Constructing the 3A3CERT2 double conditional recombinant EBV-BAC virus by homologous recombination

The pCS008 construct was then recombined with the E3KO EBV-BAC (JY06+3.2, hereafter referred to as JY6) from which the EBNA3 locus has been deleted, with the exception of a fragment of EBNA3A exon 1 for use as a homology region for the reintroduction of the EBNA3 locus. The BZLF1 exon 3 acts as the second homology region. E3KO EBV-BAC carries a Cm resistance cassette for selection. pCS008 was co-transformed with pDF25-Tet into bacteria carrying the E3KO EBV-BAC. The pDF25-Tet plasmid carries a Tet resistance gene and a RecA recombinase gene, and like pKovKanΔCm has a temperature sensitive origin. To select for transformed bacteria carrying the parental EBV-BAC, pCS008 and pDF25-Tet, bacteria were grown in the presence of Cm, Kan and Tet overnight at 30°C, and then re-plated on Cm/Kan at 43°C to select for co-integrant BACs: those in which pCS008 had incorporated into the E3KO-BAC by RecA-mediated homologous recombination.

RecA catalyses homologous recombination between either the BZLF1 exon 3 region (at the end of the EBNA3C-ERT2 insert) or the remaining EBNA3A region in the parental E3KO EBV-BAC, and the complementary homologous regions contained within pCS008. Recombination at either of these sites results in different co-integrant configurations, depending on which homologous site was recombined, either producing a co-integrant at the EBNA3A exon 1 region (co-integrant I, Figure 3.4A), or a co-integrant at the BZLF1 exon 3 region (co-integrant II, Figure 3.4B).

Diagnostic restriction digestion and PFGE were used to identify the co-integrant constructs and assess the integrity of resulting EBV-BACs. Diagnostic digestion of DNA isolated from sixty independent transformed bacterial clones identified only one bacterial colony carrying the co-integrant orientation I (pJY6+CS8.53), however, multiple bacterial colonies carrying co-integrant orientation II were identified (pJY6+CS8.3a/15/17/21/22). This indicates that recombination at the BZLF1 exon 3 region (upstream of EBNA3C-ERT2) was more efficient.

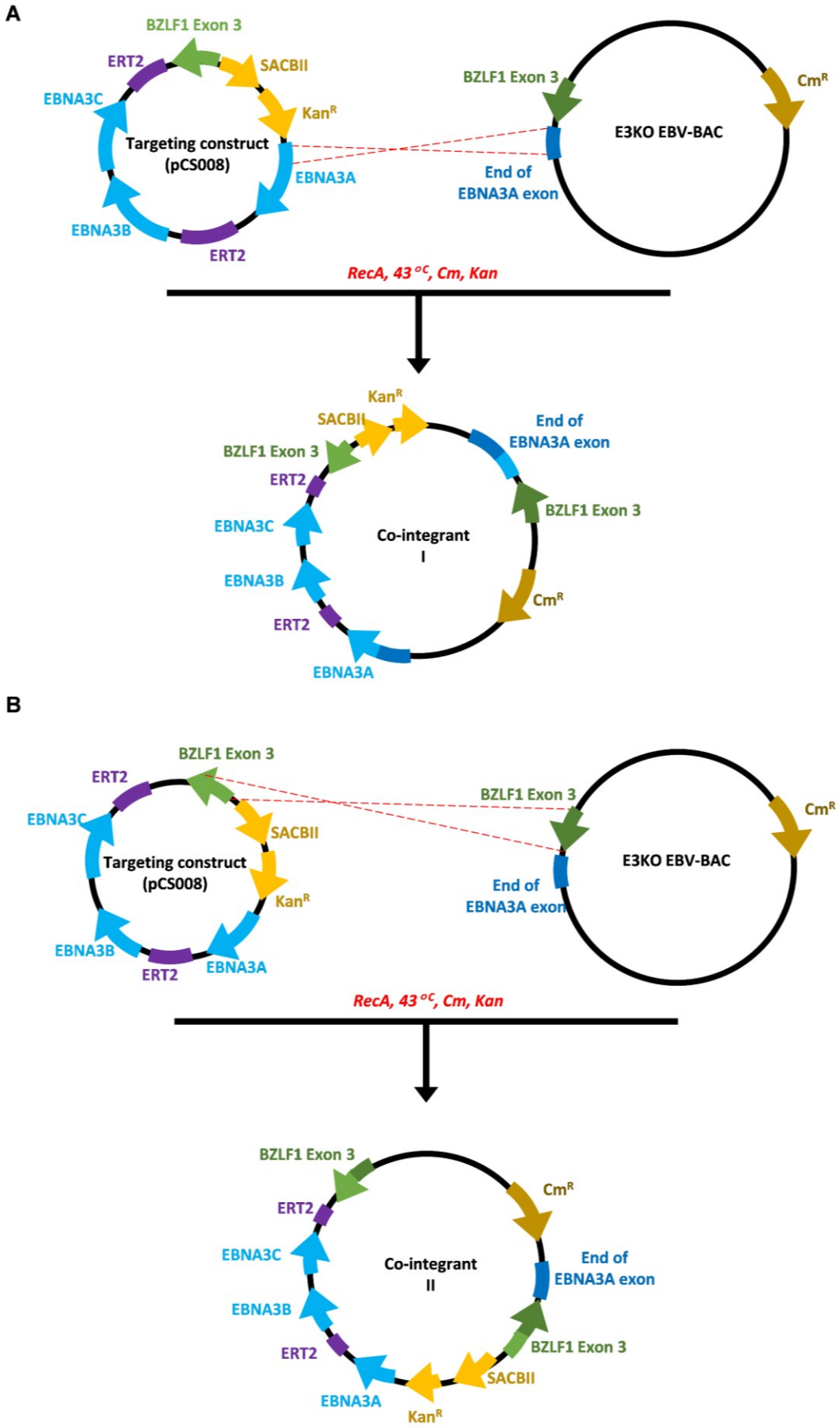

A
BZLF1 Exon 3
ERT2
SACBII
EBNA3C
Kan^R
Targeting construct
(pCS008)
EBNA3A
EBNA3B
ERT2
BZLF1 Exon 3
Cm^R
E3KO EBV-BAC
End of
EBNA3A exon
RecA, 43 °C, Cm, Kan
Kan^R
SACBII
End of
EBNA3A exon
BZLF1 Exon 3
ERT2
BZLF1 Exon 3
EBNA3C
Co-integrant
I
EBNA3B
Cm^R
ERT2
EBNA3A
B
BZLF1 Exon 3
ERT2
BZLF1 Exon 3
Cm^R
EBNA3C
SACBII
Targeting construct
(pCS008)
E3KO EBV-BAC
End of
EBNA3A exon
Kan^R
EBNA3B
ERT2
EBNA3A
RecA, 43 °C, Cm, Kan
BZLF1 Exon 3
Cm^R
ERT2
EBNA3C
Co-integrant
II
End of
EBNA3A exon
EBNA3B
BZLF1 Exon 3
ERT2
SACBII
EBNA3A
Kan^R

Figure 3.4. Generation of EBNA3A-ERT2/EBNA3B/EBNA3C-ERT2 and E3KO EBV-BAC co-integrants by RecA-homologous recombination. pCS008 containing EBNA3A-ERT2/EBNA3B/EBNA3C-ERT within a pKovKanΔCm shuttle vector backbone, and RecA-containing pDF25-Tet were co-transformed into competent bacteria containing the E3KO EBV-BAC. Homologous recombination occurs either (**A**) at the start of end of the EBNA3A exon (co-integrant I) or (**B**) at the BZLF1 exon 3 after EBNA3C-ERT2 (co-integrant II) forming co-integrant BACs.

Following confirmation of co-integrants by diagnostic restriction digest and PFGE, the single bacterial colony carrying the co-integrant EBV-BAC of orientation I (pJY6+CS8.53) and a colony carrying co-integrant EBV-BAC of orientation II (pJY6+CS8.3a) were subjected to a secondary homologous recombination reaction by the reintroduction of pDF25-Tet.

The second homologous recombination stage induced by reintroduction of RecA to co-integrant carrying bacteria can result in two different structures. First, if the recombination occurs at the same site of the original homologous recombination it can excise the entire target construct (including the EBNA3-ERT2 fusions) resulting in reversion to the parental E3KO EBV-BAC. Alternatively, if the homologous recombination occurs at the second homologous site then the pKovKanΔCm shuttle vector is excised (along with the deleted EBNA3 locus region containing the EBNA3A exon 1 fragment), and the modified EBNA3 genes remain in the EBV-BAC (3A3CERT2 BAC, shown schematically for co-integrant orientation I in Figure 3.5). To select for bacteria carrying resolved EBV-BAC, bacteria were grown on Cm with 5% sucrose at 43°C. Only successful recombinants or revertant BAC would survive on Cm plates containing 5% sucrose, unless bacteria carrying co-integrant EBV-BAC have mutated the SACBII gene. To exclude these colonies, bacteria were replica plated on Cm and Kan, where only bacteria carrying co-integrant EBV-BAC would survive. Diagnostic digest and PFGE was used to identify correctly resolved 3A3CERT2-BAC from the parental E3KO revertants.

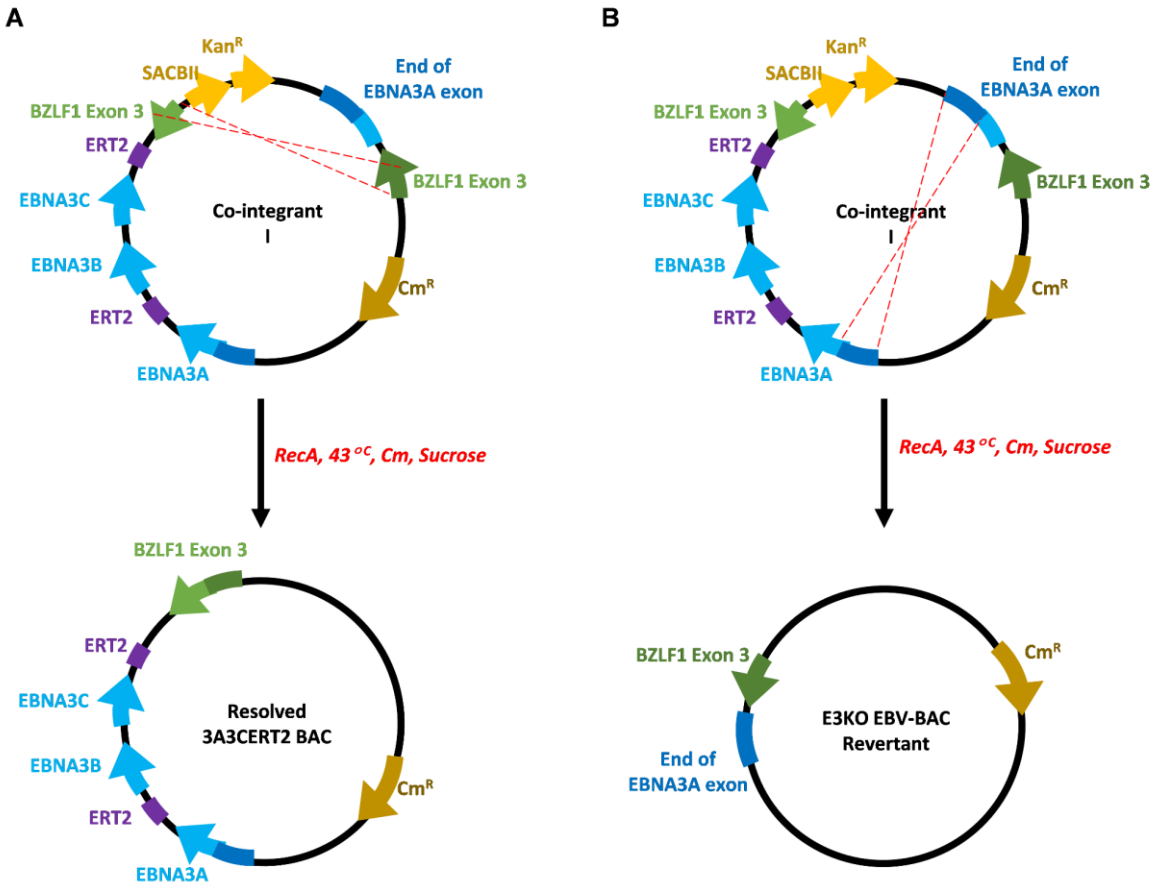


Figure 3.5. Resolution of co-integrant EBNA3A-ERT2/EBNA3B/EBNA3C-ERT2 and E3KO EBV-BAC by secondary RecA-homologous recombination. Co-integrant BACs were resolved by a second RecA-mediated recombination and formed either (**A**) the EBNA3A-ERT2/EBNA3B/EBNA3C-ERT2 (3A3CERT2) EBV-BAC or (**B**) reverted to the original E3KO EBV-BAC. Only co-integrant I is shown here.

3.2.1.3. Confirming resolution of the 3A3CERT2 double conditional recombinant EBV-BAC

Two bacterial colonies were identified (by mini-prep and diagnostic digest) as carrying resolved 3A3CERT2-BACs from co-integrant orientation I (pJY6+CS8+53.1 and pJY6+CS8+53.4). DNA was then maxi-prepped for further analysis.

Further diagnostic digests were performed on maxi- and mini-prepped DNA from pJY6+CS8.53.1 and pJY6+CS8.53.4 3A3CERT2-BACs, to further confirm that the co-integrant I had been successfully resolved to form a 3A3CERT2-BAC with the presence of EBNA3 genes and ERT2 fusions to both EBNA3A and EBNA3C. NotI restriction sites within the ERT2 domains in the EBV-BAC resulted in

visible changes in band sizes on the pulsed field gel confirming the introduction of EBNA3A-ERT2, EBNA3B and EBNA3C-ERT2 within the parental JY6 E3KO-BAC backbone (Figure 3.6A).

EcoRI, AgeI and BamHI cut throughout the EBV genome, and these digests were used to ensure there were no gross changes to BAC integrity, and to scrutinise the size of specific repeat regions that may be altered by exposure to the recombinase. Restriction digest fragment sizes were compared to the parental JY6 E3KO-BAC (Figure 3.6B-D). Although the EcoRI digestion of JY6 did not result in identifiable bands, the band sizes of pJY6+CS8.53.1 and pJY6+CS8.53.4 did correspond to bands digested JY6 fragments on alternative pulsed field gels (not shown). AgeI digestion identified an aberrant band in the maxi-prepped DNA of pJY6+CS8.53.1, therefore this BAC was discarded (Figure 3.8C). No gross changes or aberrant repeat regions were identified in the maxi- or mini-prepped DNA of the pJY6+CS8.53.4 3A3CERT2-BAC. This 3A3CERT2-BAC was therefore transfected into mammalian cells for production of infectious virus (Section 3.2.1.4).

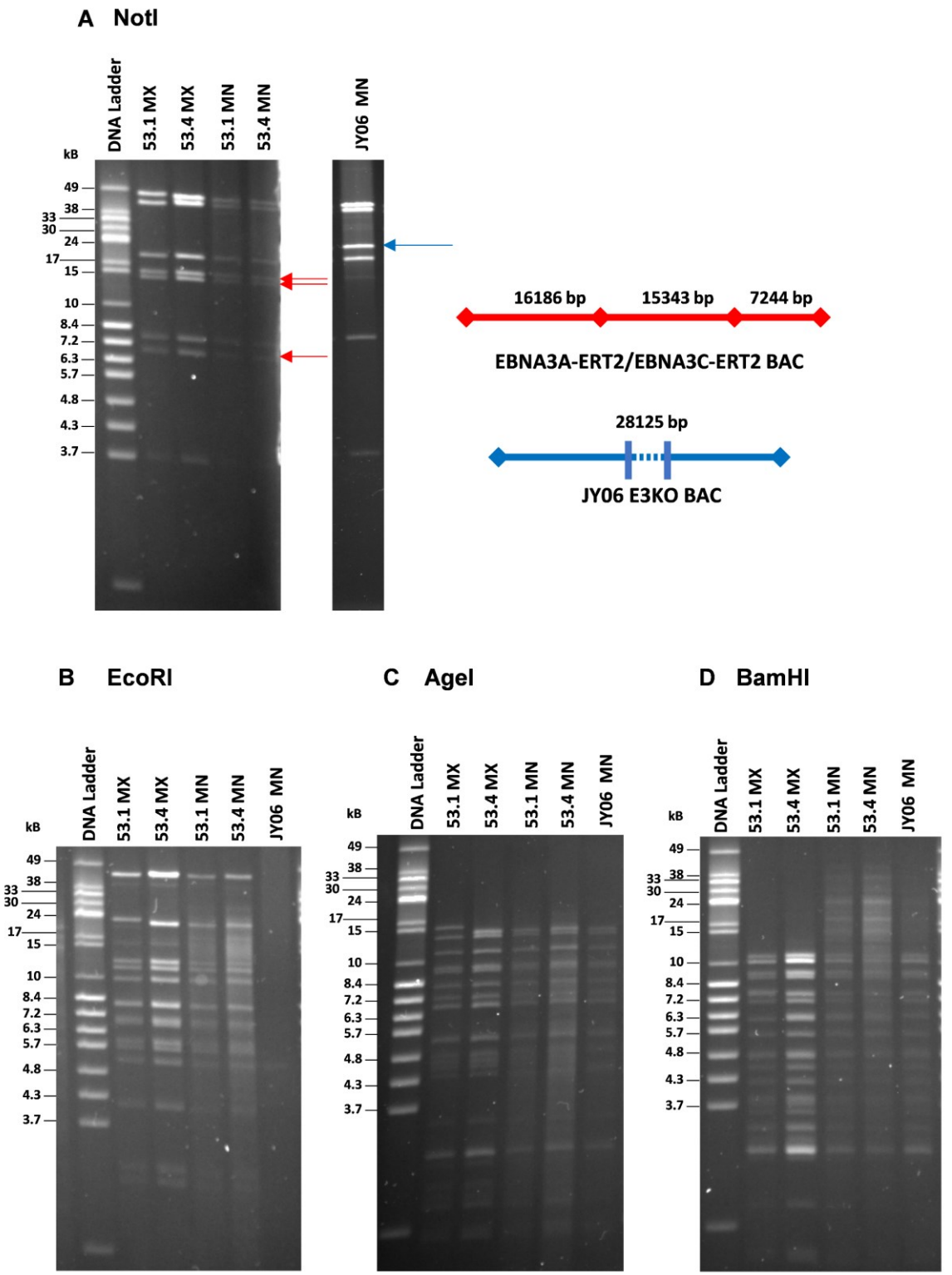


Figure 3.6. Pulse field gel electrophoresis analysis for verification of 3A3CERT2-BAC DNA. Mini- (MN) and maxi-prepped (MX) DNA of the pJY6+CS8.53.1 (53.1) and pJY6+CS8.53.4 (53.4) 3A3CERT2 EBV-BAC and mini-prepped DNA of the parental E3KO EBV-BAC (JY06) was digested with NotI to identify the ERT2 fusions to EBNA3A and EBNA3C. The C-terminus of both ERT2 sequences contains a NotI site which causes the 28125 bp band of JY06 EBV-BAC (blue arrow) to cut into 3 bands of the sizes indicated in the EBNA3A-ERT2/EBNA3C-ERT2 EBV-BAC (red arrows) as a result of recombineering. NotI band

sizes are shown schematically (**A**). DNA was also digested with EcoRI (**B**), AgeI (**C**), and BamHI (**D**) restriction enzymes to check EBV-BAC integrity.

Following the second homologous recombination stage of the alternative co-integrant orientation II (pJY6+CS8.3a), only nine bacterial colonies grew on the appropriate selection, two of which carried resolved 3A3CERT2-BAC, however diagnostic digestion indicated issues with this EBV-BAC. A further second secondary homologous recombination reaction was then subsequently performed on bacteria carrying pJY6+CS8.3a. Although this second reaction yielded twenty-three colonies carrying successfully recombined EBV-BAC, diagnostic digest identified either revertant E3KO-BAC or indicated gross changes in the resolved 3A3CERT2-BAC. Therefore, the second homologous recombination stage was performed on two different independent bacterial colonies carrying the co-integrant orientation II (pJY6+CS8.17 and pJY6+CS8.21). Diagnostic digestion indicated the resulting colonies (thirteen and eight respectively) were either revertant E3KO-BAC or indicated gross changes in the resolved 3A3CERT2-BAC. The bacteria carrying pJY6+CS8.3a were therefore revisited, and a third secondary homologous recombination reaction of was performed. Analysis of a further forty bacterial colonies led to the identification of two correctly resolved 3A3CERT2-BAC (pJY6+CS8+3aIII.31 and pJY6+CS8+3aIII.33) with no identifiable changes in the BAC integrity or repeat regions. Maxi-prep was performed, and further diagnosis digest confirmed the pJY6+CS8+3aIII.31 3A3CERT2-BAC carried the modified EBNA3 genes without gross changes to the BAC structure and repeat regions (data not shown). However, transfection of the pJY6+CS8+3aIII.31 3A3CERT2-BAC into mammalian cells was not successful, with no outgrowth of transfected HEK-293 cells.

3.2.1.4. Transfection of double conditional recombinant 3A3CERT2-BAC into HEK-293 cells to generate EBV producer lines

Maxi-prep DNA of the pJY6+CS8.53.4 3A3CERT2-BAC (hereafter referred to as 3A3CERT2-BAC) was transfected into HEK-293 cells by a lipofectin-based method (see Materials and Methods, Section 2.5.3.1). Following transfection, HEK-293 cells were cultured at low density with hygromycin to select for successfully transfected cells carrying the 3A3CERT2 EBV-BAC (293-3A3CERT2). After 2-3 weeks

the transfected cells established discrete colonies; these were visualised under a fluorescent microscope to screen for GFP expression (contained within the EBV-BAC). Thirty-two colonies were then isolated for expansion and validation.

Of the thirty-two 293-3A3CERT2 colonies isolated, seventeen maintained GFP expression and expanded to levels suitable for assessment (Table 3.1). To confirm the cell lines could produce virus, 293-3A3CERT2 cells were transiently transfected with BZLF1 and BALF4 expression plasmids to induce the lytic cycle and consequently production of virus particles. The resulting virus-containing supernatant was then titrated, which allowed for identification of the cell lines with the highest viral titre. Of the seventeen cell lines titrated, fifteen produced identifiable EBV virus, although some were extremely low (see Table 3.1 for values).

Virus Clone Identifier	Outgrowth?	Viral Titre (GRU)
M1	N	-
M2	N	-
M3	N	-
M4	N	-
M5	N	-
M6	Y	20
M7	Y	40
M8	Y	30
C1	Y	3.8
C2	Y	16.5
C3	N	-
C4	N	-
C5	Y	0
C6	N	-
C7	N	-
C8	Y	17
C9	Y	850
C10	N	-
C11	N	-
C12	Y	60
C13	Y	75
C14	N	-
C15	N	-
C16	Y	10
C17	Y	0
C18	Y	10
C19	Y	10
C20	Y	290
C21	N	-
C22	Y	3.4
C23	Y	3.5
C24	N	-

Table 3.1 Summary of outgrowth and viral titres of 293-3A3CERT2 EBV producer cell lines.

To ensure the 3A3CERT2-BAC DNA in the producer cell lines was stable following transfection into mammalian cells, viral episomes were isolated by low-molecular weight extraction (see Materials and Methods, Section 2.5.3.3) from the three 293-3A3CERT2 cell lines with the highest viral titres (C9,

C13 and C20). DNA was then transformed back into bacteria and several colonies mini-prepped for diagnostic digests and PFGE.

Digestion of the 3A3CERT2-BAC with NotI confirmed the presence of EBNA3A-ERT2 and EBNA3C-ERT2 in the 3A3CERT2-BAC rescued from each of the 293-3A3CERT2 EBV producer lines. However, this also identified a gain of DNA in one of the mini-preps of bacteria transformed with DNA isolated from the C13 293-3A3CERT2 EBV producer line (C13.6, Figure 3.7A). This gain of DNA was also evident following digest with EcoRI (Figure 3.7D). BAC DNA isolated from the C9 and C20 293-3A3CERT2 EBV producer lines had no detectable alterations to the DNA structure (Figure 3.7). The C13 293-3A3CERT2 cell line was therefore discarded, and virus-containing supernatant obtained from the C9 and C20 293-3A3CERT2 EBV producer lines was used to infect cells. The validation process for the 293-3A3CERT2 EBV producer lines is shown schematically in Figure 3.8.

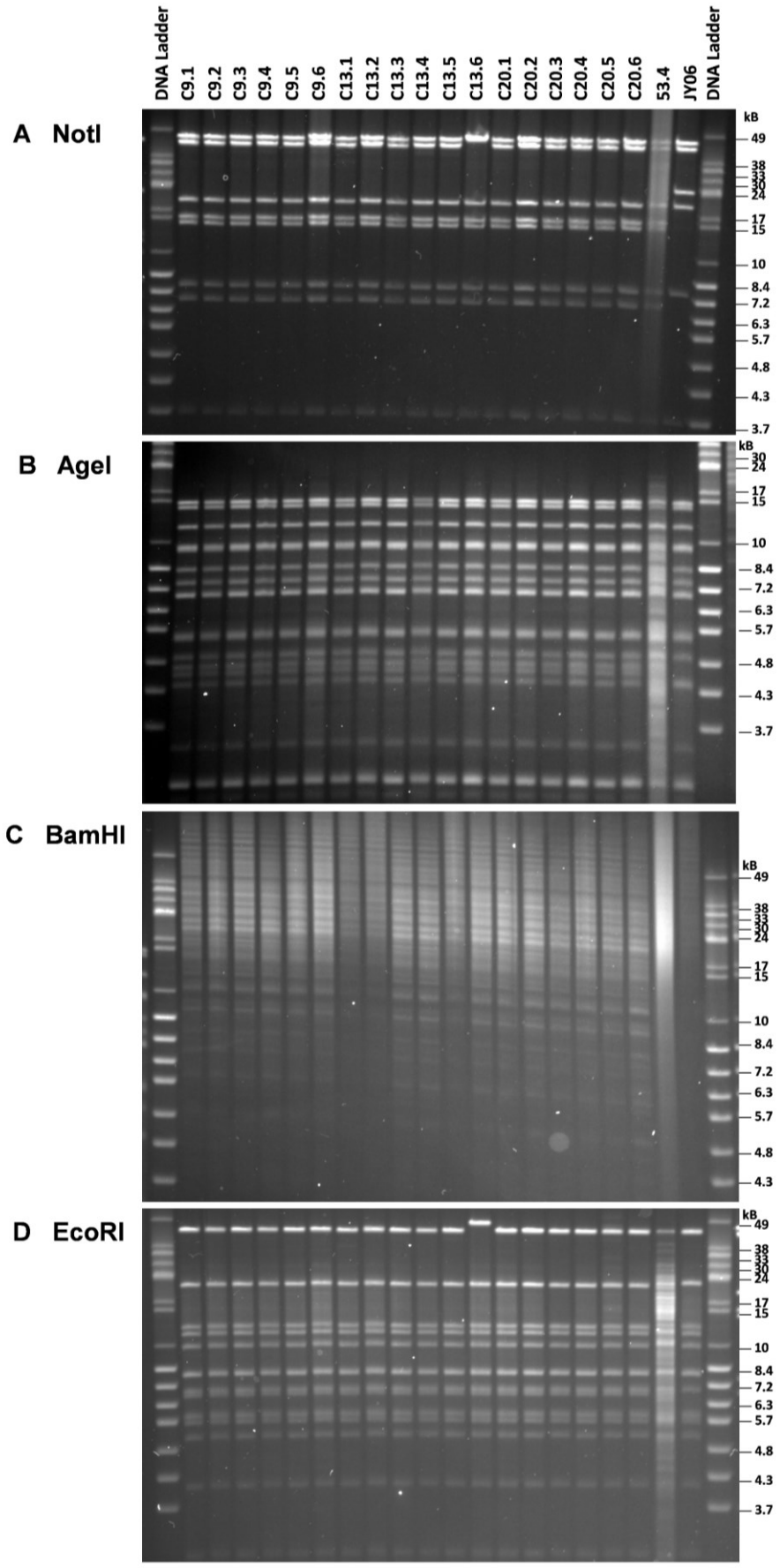

DNA Ladder
C9.1
C9.2
C9.3
C9.4
C9.5
C9.6
C13.1
C13.2
C13.3
C13.4
C13.5
C13.6
C20.1
C20.2
C20.3
C20.4
C20.5
C20.6
53.4
JY06
DNA Ladder
A NotI
B AgeI
C BamHI
D EcoRI
kB
49
38
33
30
24
17
15
10
8.4
7.2
6.3
5.7
4.8
4.3
3.7

Figure 3.7. Pulsed field gel electrophoresis analysis for validation of 3A3CERT2-BAC integrity following transfection of 293 cells with 3A3CERT2-BAC DNA. Mini-prepped DNA purified from bacteria transformed with BAC DNA isolated from three 293-3A3CERT2 EBV producer cell lines (C9, C13 and C20) digested with the restriction enzymes Not I (**A**), AgeI (**B**), EcoRI (**C**), and BamHI (**D**) and subject to pulse field gel electrophoresis. 6 representative colonies (.1 through .6) of 12 assessed are shown. The parental E3KO EBV-BAC and original 3A3CERT2-BAC pJY6+CS8.53.4 are also shown for comparison.

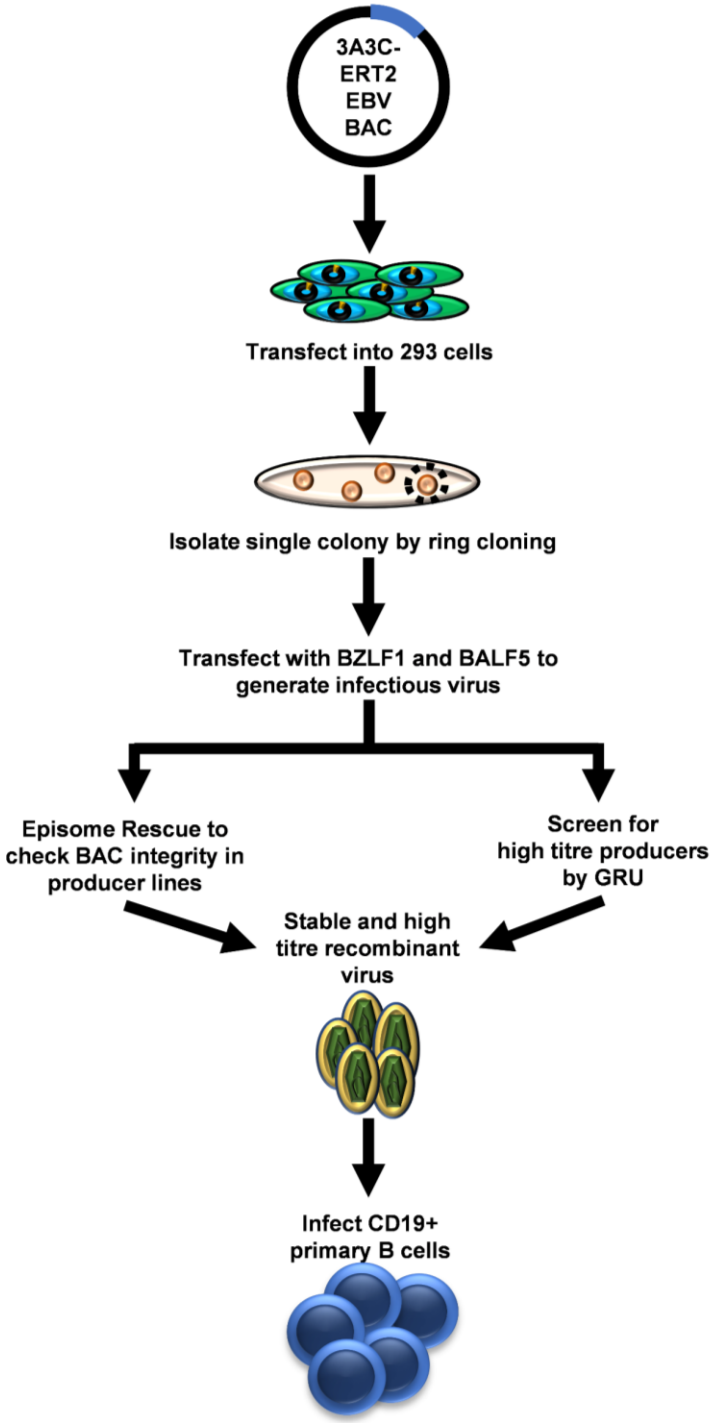


Figure 3.8. Production and confirmation of BAC-derived recombinant EBV virus. Verified 3A3CERT2 EBV-BAC DNA was transfected in 293 cells forming producer cell lines. Single 293-producer cell colonies were isolated and expanded. 293-producer cells carrying EBV-BAC DNA were transfected with BZLF1 and BALF5 to induce virus production; subsequent virus was titrated for green Raji units (GRU). EBV-BAC DNA was recovered from 293-producer cells and transfected back into bacteria to verify integrity of the EBV-BAC. High titre virus from 293-producer cell lines with verified BAC integrity were used to infect $CD19^{+ve}$ primary B cells.

As a quick diagnostic test to confirm the conditional activity of the 3A3CERT2 EBV-BAC (that the conditional EBNA3A-ERT2 and EBNA3C-ERT2 proteins would be stabilised only in the presence of the activating ligand) HT was added to the 3A3CERT2 293-producer cell line for 7 days. Protein was then harvested and analysed by western blotting (Figure 3.9). This confirmed that in 3A3CERT2 293-producer cells, EBNA3A-ERT2 and EBNA3C-ERT2 protein expression can be induced by HT, but EBNA3A-ERT2 and EBNA3C-ERT2 were not expressed in the absence of HT. As expected, EBNA3B was expressed under both conditions. This experiment was performed for the two 293-3A3CERT2 EBV producer cell lines (C9 and C20), but only one representative shown.

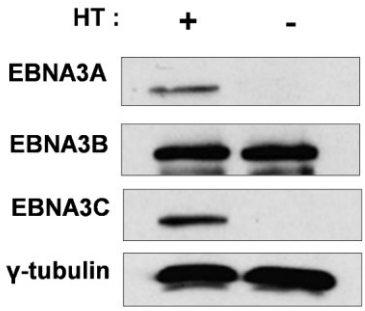


Figure 3.9. Validation of conditional EBNA3A-ERT2 and EBNA3C-ERT2 latent protein expression in 293 cells transfected with 3A3CERT2 BAC DNA. Expression of the EBV latency-associated proteins EBNA3A-ERT2, EBNA3B and EBNA3C-ERT2 was demonstrated by western blotting extracts from the 3A3CERT2 293 producer line cultured with (+) or without (-) 4-hydroxytamoxifen (HT) for 7 days. In each blot γ-tubulin was used as a loading control and was similarly consistent across all blots.

3.2.1.5. Presence of EBNA3A and EBNA3C proteins in 3A3CERT2 conditional cell lines is dependent on continued addition of HT

To validate that EBNA3A and EBNA3C would be simultaneously conditionally expressed in cells infected with the 3A3CERT2 conditional virus, $CD19^{+ve}$ B cells were purified and infected with the 3A3CERT2 virus generated from a validated 293-producer cell line. Infected cells were cultured in the continuous presence of HT for at least 1 month to establish conditional LCLs. LCLs were then split, and either HT addition continued or ceased. Protein was then sampled weekly for western blotting. This

experiment was performed in independent LCLs derived from infection of $CD19^{+ve}$ B cells with virus obtained from both 293-3A3CERT2 EBV producer cell lines (C9 or C20) to validate HT-dependent expression of EBNA3A and EBNA3C, but only one representative shown.

In 3A3CERT2 LCLs where HT is added continuously, EBNA3A and EBNA3C are expressed. However, if the addition of HT is stopped, then levels of EBNA3A and EBNA3C progressively reduce, so much so that by 34-40 days without addition of HT expression of both EBNA3A and EBNA3C is barely detectable (Figure 3.10). This is consistent with the progressive reduction or loss of HT as it is diluted in medium during cell maintenance. This indicates that HT is required continuously to maintain expression of EBNA3A and EBNA3C.

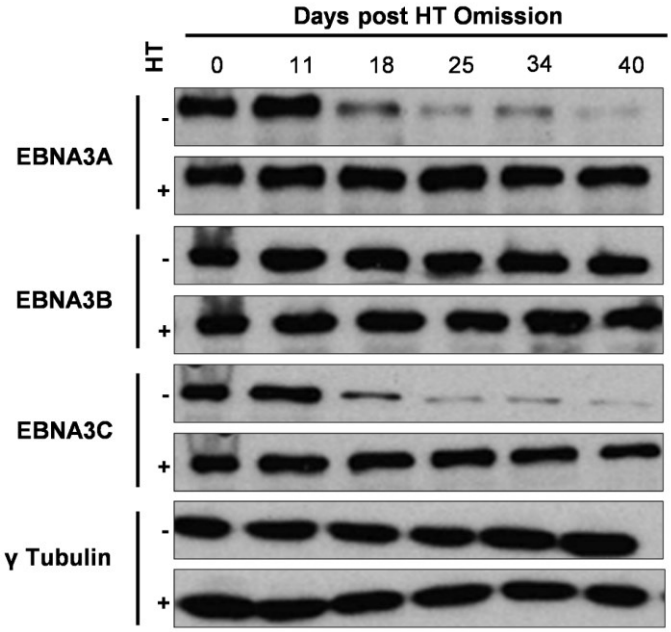


Figure 3.10. Expression of functional EBNA3A and EBNA3C depends on the continued addition of HT in 3A3CERT2 conditional LCLs. Expression of EBNA3A, EBNA3B and EBNA3C was demonstrated by western blotting extracts from a 3A3CERT2 lymphoblastoid cell lines (LCL). Cells were grown continuously with 4-hydroxytamoxifen (HT) (+) or HT addition was ceased at day 0 (-) and cultured for 40 days. Samples were taken at the time points post cessation of HT addition indicated. In each blot γ-tubulin was used as a loading control and was similarly consistent across all blots.

To further validate whether the EBNA3A and EBNA3C ERT2 fusion proteins in 3A3CERT2 LCLs respond to the addition or omission of HT, a 3A3CERT2 LCL was split and half washed to remove HT

from the culture medium, and the cells re-cultured in fresh medium in the absence of HT. This differs from the previous experiment, as HT was specifically withdrawn, rather than progressively diluted.

After 30 days HT was re-added to the culture to induce functional expression of the fusion proteins. After HT was removed by washing and re-culturing in fresh medium the expression of EBNA3A and EBNA3C progressively reduced such that by 20-30 days post-washing, levels of EBNA3A and EBNA3C were largely undetectable (Figure 3.11). The reduction of EBNA3A and EBNA3C in washed cells where HT was specifically withdrawn occurred at a swifter rate than where HT addition was simply stopped (compare Figures 3.10 and 3.11). Addition of HT to the culture resulted in a swift recovery of functional expression of both EBNA3A and EBNA3C (Figure 3.11). This confirms that the presence of EBNA3A and EBNA3C protein is simultaneously dependent on the presence of the activating ligand HT, and activation is reversible. As expected EBNA3B is constitutively expressed in the 3A3CERT2 LCL and is unaffected by the presence or absence of HT, or the switch in EBNA3A and EBNA3C stability (Figures 3.10 and 3.11).

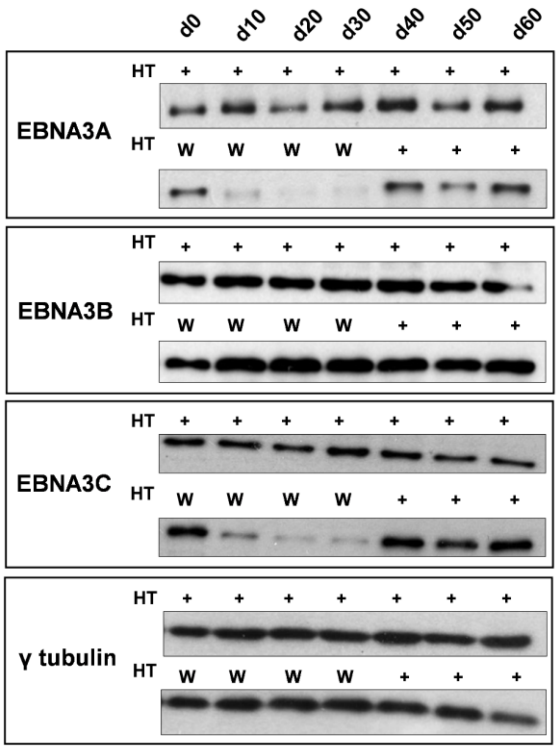


Figure 3.11. Protein levels of EBNA3A and EBNA3C can be lost or stabilised by the absence or presence of HT in 3A3CERT2 conditional LCLs. Expression of EBNA3A, EBNA3B and EBNA3C was demonstrated by western blotting extracts from an 3A3CERT2 lymphoblastoid cell line (LCL). Cells

were grown with 4-hydroxytamoxifen (HT) (+) or washed and grown without HT for 30 days (W) and then HT re-added to the culture for a further 30 days (+). Samples were taken at the times post washing as indicated. In each blot γ-tubulin was used as a loading control, and was similarly consistent across all blots. One representative experiment shown of two independent 3A3CERT2 LCL assessed.

3.2.1.6. Confirmation of EBV latency-associated protein expression in the 3A3CERT2 infected B cells

Having established that EBNA3A-ERT2 and EBNA3C-ERT2 protein levels vary as expected in 3A3CERT2 LCLs in response to addition or omission of HT, the next step was to ensure that other EBV latency-associated proteins were not being affected by the presence or absence of HT. 3A3CERT2 conditional LCLs were generated by infection of $CD19^{+ve}$ primary B cells isolated at the same time from buffy coats provided by three independent donors (LCL D1, LCL D2, LCL D3) and cultured with HT continuously. HT was removed from the culture medium by washing and cells resuspended in fresh media and cultured for 30 days in the absence of HT. Western blot analysis of these cells showed that other latency-associated proteins are expressed in these conditional LCLs and they are not affected by the presence or absence of HT, or by the switch in EBNA3A and EBNA3C stability (Figure 3.12A).

Consistent with the results from LCLs, the same pattern of EBV latency-associated protein expression can be seen in $CD19^{+ve}$ B cells infected with 3A3CERT2 (1°B D1) when cultured with or without HT for 20 days (Figure 3.12B). This confirms that cells infected with 3A3CERT2 recombinant EBV have simultaneously conditional expression of EBNA3A and EBNA3C during primary B cell infection and in established LCLs, while maintaining the expression of other latency-associated EBV proteins.

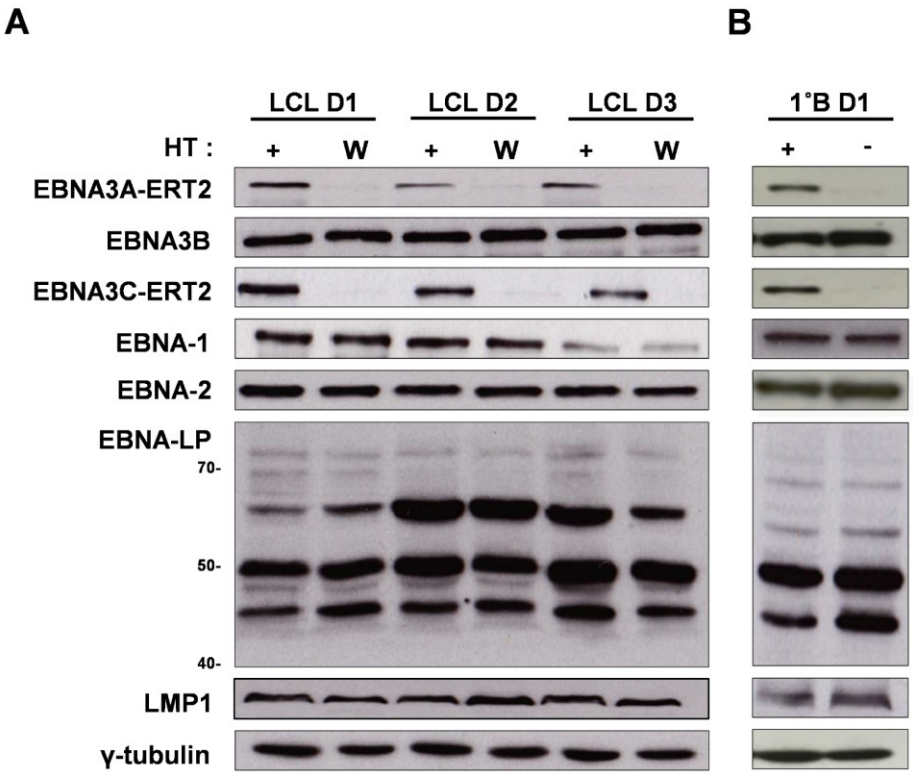


Figure 3.12. Validation of EBV latency-associated protein expression in double conditional 3A3CERT2 infected cells. Expression of EBV latency-associated proteins EBNA1, EBNA2, EBNA3A, EBNA3B, EBNA3C, EBNA-LP and LMP-1 was demonstrated by western blotting extracts from 3A3CERT2 lymphoblastoid cell lines (LCLs) derived from 3 independent donors (3A3CERT2 LCL D1, 3A3CERT2 LCL D2, 3A3CERT2 LCL D3) cultured with 4-hydroxytamoxifen (HT) (+) or washed and grown without HT for 30 days (W) (**A**) and primary $CD19^{+ve}$ B cells 20 days post infection with 3A3CERT2 recombinant EBV (1˚B D1) cultured with (+) or without (-) HT (**B**). In each blot γ-tubulin was used as a loading control and was similarly consistent across all blots.

The protein levels of conditional EBNA3A-ERT2 and EBNA3C-ERT2 in infected cells were compared to the levels in EBV infected cells where EBNA3A and EBNA3C were not fused to ERT2 (WT expression). For this, $CD19^{+ve}$ B cells from the same donor were infected with 3A3CERT2 recombinant EBV (where both EBNA3A and EBNA3C contain an ERT2 fusion), 3AERT2 recombinant EBV (conditional expression of EBNA3A-ERT2 but untagged WT expression of EBNA3C), or 3CERT2 recombinant EBV (conditional expression of EBNA3C-ERT2 but untagged WT expression of EBNA3A). Cells were grown with or without HT and protein samples taken at 20 days pi (1°B). Cells were then cultured with HT for

2 months to establish LCLs. LCLs were split and half washed to remove HT and cultured for 30 days before protein samples were harvested. Western blot analysis was then performed.

The expression of conditional EBNA3A (3AERT2 and 3A3CERT2) in newly infected cells and the corresponding LCLs, was considerably lower than the untagged WT levels found in 3CERT2 infected cells (Figure 3.13). Expression of conditional EBNA3C was also lower than that of untagged WT EBNA3C in 3AERT2 cells, although expression was more comparable than for EBNA3A-ERT2. The lower expression levels of both EBNA3A-ERT2 and EBNA3C-ERT2 must be considered when assessing the effects of EBNA3A- and EBNA3C-mediated gene regulation in cells with conditional expression of these proteins, as the consequences of regulation may be less profound than in cells with untagged WT expression of EBNA3 proteins.

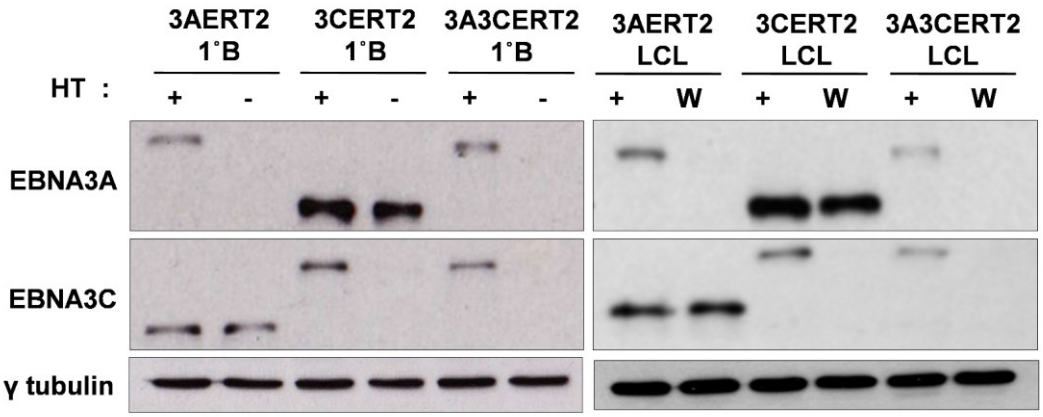


Figure 3.13. Levels of EBNA3A and EBNA3C expression are lower when they have an ERT2 fusion. Expression of the EBV latency-associated proteins EBNA3A, EBNA3B and EBNA3C was demonstrated by western blotting extracts from $CD19^{+ve}$ B cells infected with 3AERT2, 3CERT2 and 3A3CERT2 recombinant EBV and cultured for 20 days with (+) or without (-) 4-hydroxytamoxifen (HT), and from conditional 3AERT2, 3CERT2 and 3A3CERT2 lymphoblastoid cell lines (LCLs) derived from the same donor and cultured with (+), or washed and grown without HT for 30 days (W). In each blot γ-tubulin was used as a loading control and was similarly consistent across all blots.

3.2.2. A cumulative phenotypic effect is seen when both EBNA3A and EBNA3C are simultaneously non-functional compared to when either EBNA3A or EBNA3C are independently functional

3.2.2.1. Cell viability and proliferation are reduced in cells with simultaneously non-functional EBNA3A and EBNA3C compared to those with functional expression of either EBNA3A or EBNA3C

The proliferative capacity of cells is impaired when either EBNA3A or EBNA3C are independently non-functional: a reduced proliferative capacity is seen in EBNA3A-null cell lines compared to WT, and EBNA3C-null cells are unable to produce LCLs (Bazot et al., 2015; Hertle et al., 2009; Skalska et al., 2013). Therefore, the viability and levels of proliferation were assessed in cells where EBNA3A and EBNA3C were simultaneously non-functional by cell count analysis and by EdU incorporation, and compared to cells where EBNA3A or EBNA3C were independently conditionally expressed. Purified $CD19^{+ve}$ cells isolated from the same donor were infected with either 3AERT2, 3CERT2 or 3A3CERT2 recombinant EBV. Cells were grown with HT continuously to produce LCLs with conditional expression of EBNA3A, EBNA3C or both EBNA3A and EBNA3C.

Once LCLs had been established, the conditional EBNA3 proteins were inactivated by removal of the activating ligand HT from each culture by washing. Over the 30 days following HT withdrawal, cells were seeded at specific densities and then counted after 2-3 days to assess proliferation (see Materials and Methods, Section 2.2.3). Confirming previous observations, cell proliferation was decreased when either EBNA3A or EBNA3C were non-functional due to the removal of HT from cell culture, with fewer EBNA3C-null proliferating cells than EBNA3A-null proliferating cells [(Maruo et al., 2003; Skalska et al., 2010), Figure 3.14A/B]. However, the least proliferation was seen in cells where both EBNA3A and EBNA3C were simultaneously non-functional (Figure 3.14C/D).

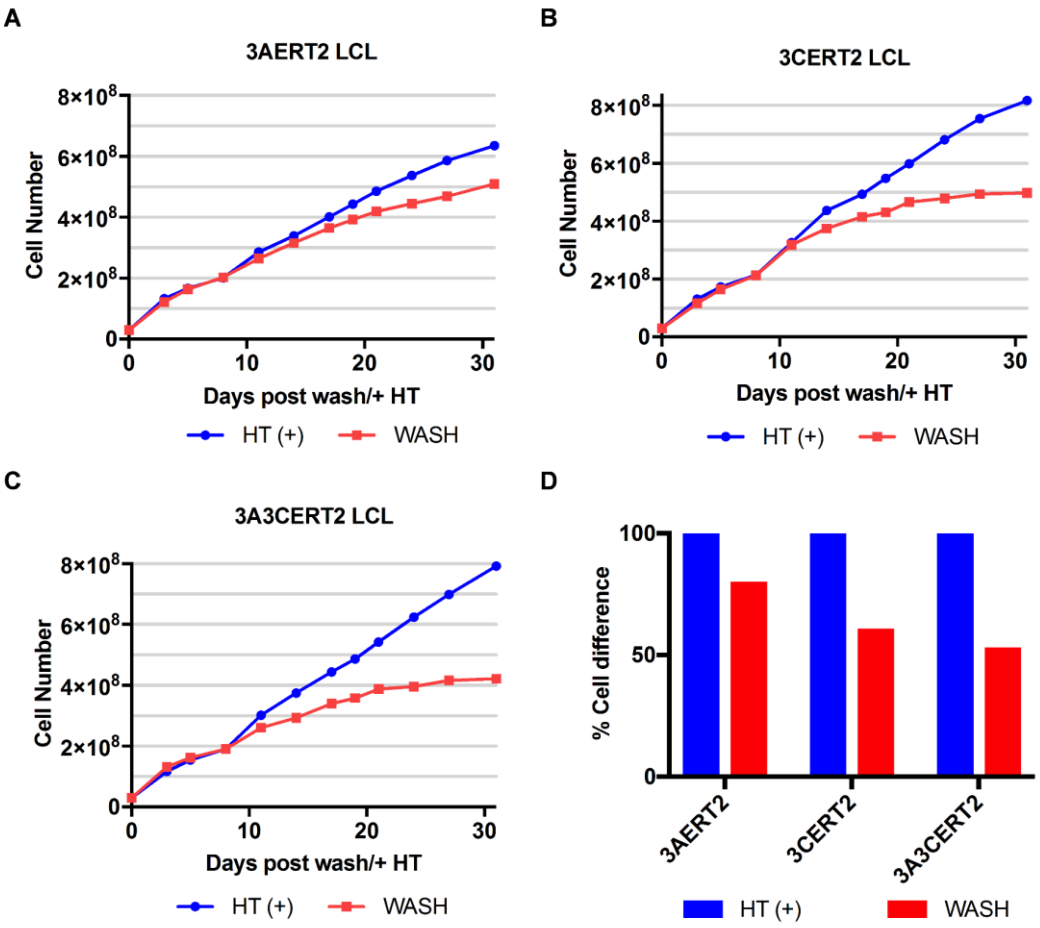


Figure 3.14. Cell count analysis of conditional EBNA3A, EBNA3C and EBNA3A3C LCLs. Cell expansion was analysed in 3AERT2 (**A**), 3CERT2 (**B**) and 3A3CERT2 (**C**) conditional lymphoblastoid cell lines (LCLs) derived from the same donor cultured with 4-hydroxytamoxifen (HT) (+, blue) or washed and grown without HT (WASH, red) for 30 days. Cell expansion was determined by trypan blue exclusion at the days post washing as indicated and total cell expansion was plotted. (**D**) Percentage difference of the cells of **A**, **B** and **C** grown without HT (WASH) for 31 days shown relative to cells grown with HT (+). This experiment was performed once.

Cell viability was assessed by live-dead staining, and a more precise measure of cell proliferation was conducted by measuring EdU incorporation, in both newly infected primary B cells and conditional LCLs. In each experiment $CD19^{+ve}$ cells were isolated from the same independent donor and infected with either 3AERT2, 3CERT2 or 3A3CERT2. Newly infected cells were grown in the presence or absence of HT and were assessed at 21 days pi. LCLs derived from the same independent donor (as described above, Figure 3.14) were split and half of the culture washed and removed to fresh media in the absence of HT for 30 days to inactive the conditional proteins (WASH).

In both newly infected cells and conditional LCLs, live cell staining revealed increased levels of dead cells when both EBNA3A and EBNA3C were non-functional (3A3CERT2 HT-/WASH), compared to cells with inactivation of EBNA3A or EBNA3C alone (3AERT2 HT-/WASH, 3CERT2 HT-/WASH) (Figure 3.15A/C). Incorporation of EdU was used as a measure of cells undergoing or entering the S phase over a 2-hour exposure period, therefore indicating cells undergoing preparation for division and proliferation. As was the case for cell proliferation when assessed by cell count analysis, the percentage of cells in S phase was reduced when either EBNA3A or EBNA3C were inactive but was reduced more in the simultaneous absence of both EBNA3A and EBNA3C (Figure 3.15B/D).

The absence of both EBNA3A and EBNA3C in EBV infected cells appears to be more detrimental to proliferation and viability than when either EBNA3A and EBNA3C are independently absent. Together, this data suggests an additive effect when both EBNA3A and EBNA3C are simultaneously non-functional. This implies EBNA3A and EBNA3C have non-redundant independent functions, alongside their overlapping roles.

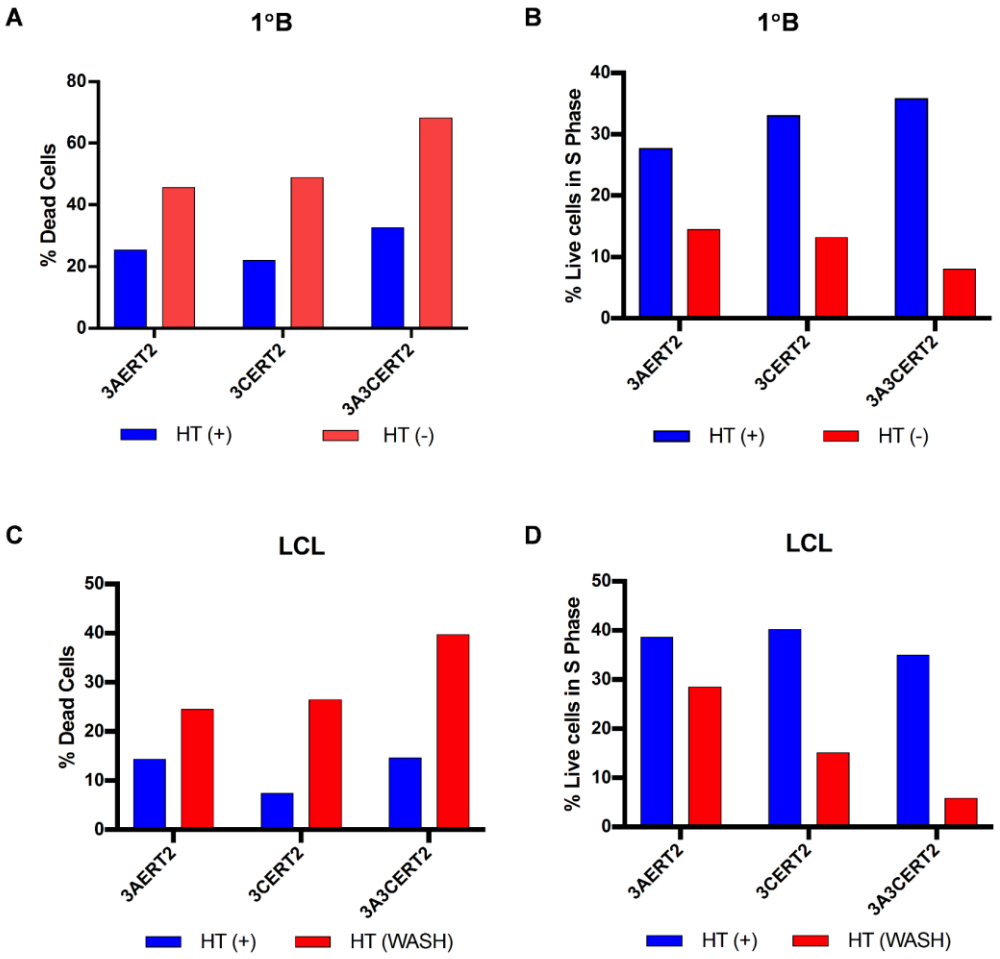


Figure 3.15. Proliferative capacity and cell viability is reduced when EBNA3A and EBNA3C are non-functional in EBV infected primary B cells and conditional LCLs. Cell viability of CD19^{+ve} purified B cells isolated from the same donor and infected with 3AERT2, 3CERT2 or 3A3CERT2 recombinant EBV virus cultured with (+) or without (-) 4-hydroxytamoxifen (HT) for 21 days (**A**) and 3AERT2, 3CERT2 and 3A3CERT2 conditional LCLs derived from the same donor cultured with (+) or washed and grown without HT (WASH) for 28 days (**C**) was evaluated by live/dead staining. Proliferation of the live cells described in A and C was assessed by EdU incorporation (5 µM) over 2 hours and determined by flow cytometry. The percentage of live single cells that have entered the S phase are summarised (**B** and **D**). Representative experiment of two independent CD19^{+ve} cell donors analysed.

3.2.2.2. EBNA3A and EBNA3C target genes are regulated as predicted in cells with simultaneously conditional expression of EBNA3A and EBNA3C

Quantitative PCR was used to assess whether the conditional inactivation of EBNA3A and EBNA3C by absence of HT would result in an absence of regulation of target genes. CD19^{+ve} cells were isolated from an independent donor and infected with 3AERT2, 3CERT2 or 3A3CERT2 recombinant

EBV. Cells were cultured for with (+) or without (-) the activating ligand HT and mRNA harvested at 20 days pi.

Messenger RNA levels of the EBNA3A target gene CXCL10 (Hertle et al., 2009) rose in the absence of EBNA3A independently (3AERT2-) and in the absence of both EBNA3A and EBNA3C (3A3CERT2-, Figure 3.16A) as predicted. Similarly, the EBNA3C-repressed gene COBLL1 (Kalchschmidt et al., 2016a) was de-repressed in cells with lacking EBNA3C function (3CERT2- and 3A3CERT2-) (Figure 3.16B). *CDKN2A* encodes $p16^{INK4a}$, which is repressed by both EBNA3A and EBNA3C (Skalska et al., 2010). As previously established, levels of $p16^{INK4a}$ mRNA was elevated when either EBNA3A or EBNA3C are independently conditionally inactivated. When both EBNA3A and EBNA3C are simultaneously inactive (3A3CERT2-) there appeared to be a greater effect with mRNA levels of $p16^{INK4a}$ exceeding those seen in 3AERT2- or 3CERT2- cells. Regulation of the housekeeping control gene ALAS1 was unaffected by EBNA3 activity showing that HT-associated regulation is an EBNA3-specific effect and not a consequence of cell differences (Figure 3.16D). This shows that EBNA3A and EBNA3C target are regulated as expected, as regulation was lost in cells with simultaneously conditional inactivation of EBNA3A and EBNA3C. Furthermore, these results indicate a potential additive effect on genes targeted by both EBNA3A and EBNA3C.

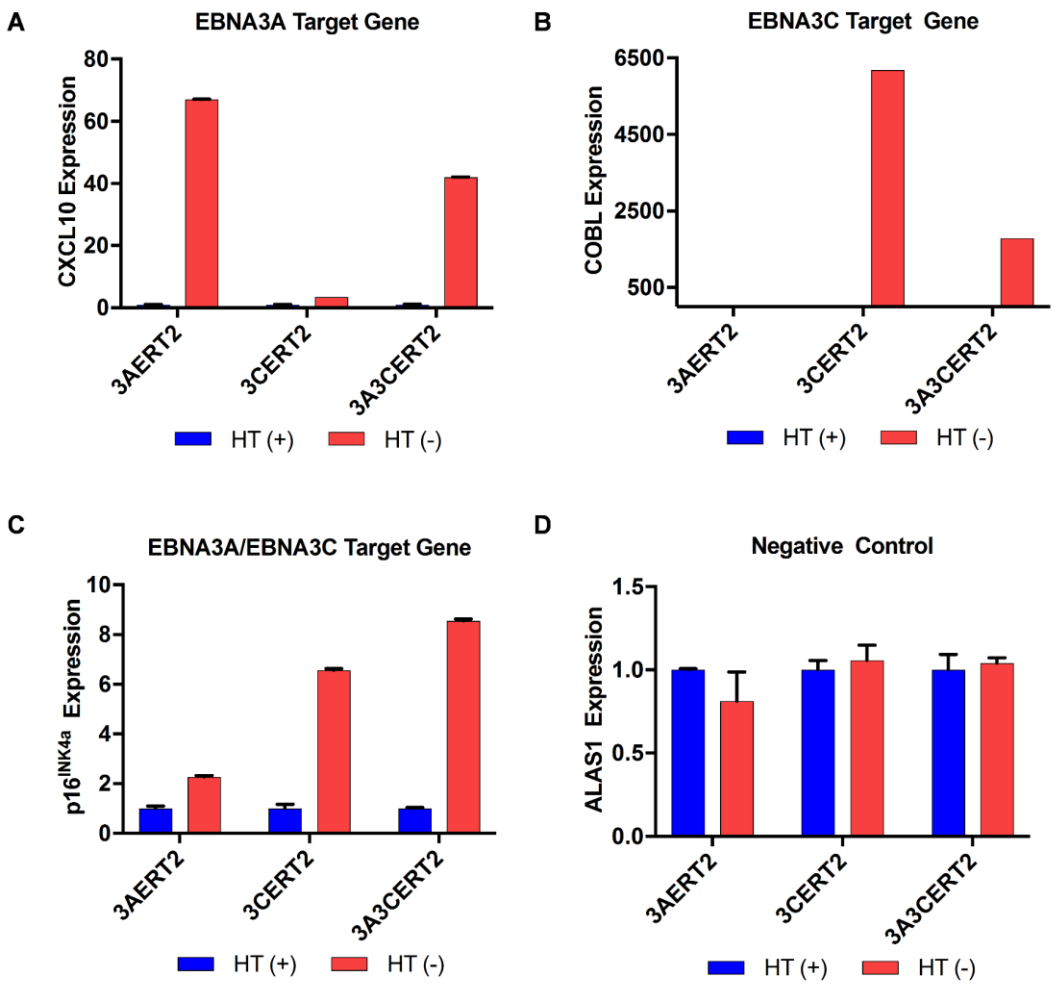


Figure 3.16. EBNA3A and EBNA3C target genes are regulated in primary B cells infected with 3A3CERT2. Primary B cells infected with 3AERT2, 3CERT2 and 3A3CERT2 recombinant EBV were cultured with (+) or without (-) 4-hydroxtamoxifen (HT) for 20 days. Analysis of expression of *CXCL10* (**A**)*, COBLL1* (**B**) *CDKN2A* ($p16^{INK4a}$, **C**) and *ALAS1* (control housekeeping gene, **D**) mRNA was performed by quantitative PCR (qPCR) and relative mRNA expression was normalised to the endogenous control *GNB2L1,* with fold change shown relative to cells grown with (+) HT for each cell line. Error bars indicate the standard deviation of qPCR triplicates for each sample. Representative experiment of three independent $CD19^{+ve}$ cell donors analysed.

3.2.3. EBNA3A and EBNA3C cooperatively regulate CDKI

EBNA3A and EBNA3C have been shown to regulate various cell cycle regulatory factors, particularly CDKIs [reviewed in (Allday et al., 2015; Styles et al., 2018)]. This is likely a mechanism to circumvent cell cycle regulatory pathways that act to prevent aberrant cell proliferation and induce

suicide response pathways, that would otherwise be stimulated by EBV-mediated transformation. Therefore, differential regulation of CDKIs was assessed in cells with simultaneously conditionally inactive EBNA3A and EBNA3C, and compared to cells derived from the same donor where either EBNA3A or EBNA3C alone were conditionally inactive.

3.2.3.1. Regulation of CDKI by EBNA3A and EBNA3C during primary infection

Assessing differential gene regulation during infection of primary B cells with EBV allows the study of EBV regulation during early infection and the transformation of B cells in a polyclonal population. Therefore, the transcriptional regulation of CDKI by EBNA3A and EBNA3C was assessed in $CD19^{+ve}$ cells from an independent donor infected with 3AERT2, 3CERT2 and 3A3CERT2 and cultured as described for Figure 3.16.

EBNA3C, and to a lesser extent EBNA3A, have been shown to transcriptionally regulate the adjacent genes encoding the INK4 family members $p15^{INK4b}$ and $p16^{INK4a}$ by initiating deposition of the repressive histone mark H3K27me3 on the *CDK2NA* and *CDKN2B* locus (Jiang et al., 2017; Skalska et al., 2010, 2013). Consistent with these findings, elevated levels of $p15^{INK4b}$ and $p16^{INK4a}$ mRNA were seen when EBNA3C was inactive. However, when both EBNA3A and EBNA3C were inactive, levels of $p15^{INK4b}$, and to a lesser extent $p16^{INK4a}$, were even more elevated (Figure 3.17A/B). This suggests a possible additive effect of losing both EBNA3A and EBNA3C function (Figure 3.17A/B).

Regulation of the INK4 CDKI family member $p18^{INK4c}$ by EBNA3A and EBNA3C has not been previously assessed. Interestingly, at 20 days pi $p18^{INK4c}$ transcription was elevated only when both EBNA3A and EBNA3C are non-functional, but remained largely repressed when either EBNA3A or EBNA3C alone were active (Figure 3.17C). This suggests that either EBNA3A or EBNA3C is sufficient to repress the CDKI $p18^{INK4c}$. As $p18^{INK4c}$ has a set of B cell specific functions, which EBV primarily infects, further investigation into EBNA3A and EBNA3C-mediated repression of $p18^{INK4c}$ was performed and is described in Chapter IV.

It has been suggested that EBNA3A and EBNA3C regulate expression of $p21^{CIP1/WAF1}$ by targeting it for proteasomal degradation (Banerjee et al., 2014; Tursiella et al., 2014). Consistent with

this, there was little difference in $p21^{WAF1/CIP1}$ transcript levels when EBNA3A or EBNA3C were both conditionally inactive (Figure 3.17D).

EBNA3A and EBNA3C have been shown to transcriptionally activate expression of miR221 and miR222, which subsequently leads to repression of $p57^{KIP2}$, and to a lesser extent $p27^{KIP1}$ (Bazot et al., 2015). There was no considerable difference in $p27^{KIP1}$ mRNA when both EBNA3A and EBNA3C were simultaneously or independently inactive (Figure 3.17E). However, a substantially elevated level of $p57^{KIP2}$ was seen in the absence of functional EBNA3A (in both EBNA3A-null and EBNA3A/EBNA3C-null cells), and to a lesser extent in the absence of EBNA3C (Figure 3.17F).

As expected, transcriptional expression of the control housekeeping gene ALAS1 was unaffected by the differing activity of the EBNA3A and EBNA3C oncogenes during primary B cell infection (Figure 3.17G)

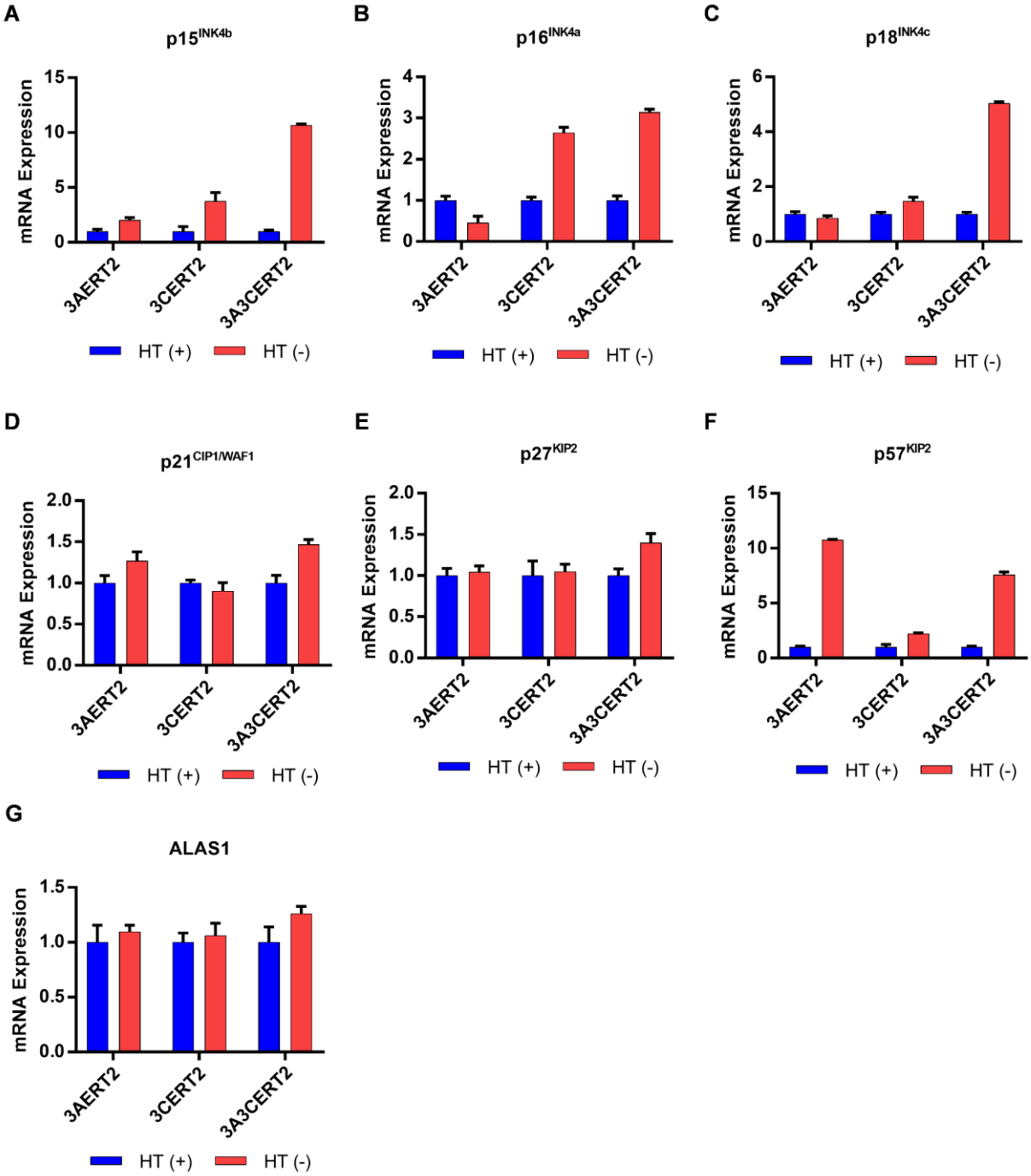


Figure 3.17. EBNA3A and EBNA3C regulate CDKI mRNA expression early after infection with EBV. CD19^{+ve} primary B cells infected with 3AERT2, 3CERT2 and 3A3CERT2 recombinant EBV were cultured with (+) or without (-) 4-hydroxtamoxifen (HT) for 20 days. Analysis of expression of *CDKN2B* (p15^{INK4b}; **A**), *CDKN2A* (p16^{INK4a}; **A**), *CDKN2C* (p18^{INK4c}; **C**), *CDKN1A* (p21$^{CIP1/WAF1}$; **D**), *CDKN1B* (p27^{KIP1}; **E**), *CDKN1C* (p57^{KIP2}; **E**) and *ALAS1* (control housekeeping gene; **G**) mRNA was performed by quantitative PCR (qPCR) and relative mRNA expression was normalised to the endogenous control *GNB2L1,* with fold change shown relative to cells grown with (+) HT. Error bars indicate the standard deviation of qPCR triplicates for each sample. Representative experiment of three independent CD19^{+ve} cell donors analysed.

To corroborate these findings at a protein level, western blot analysis was performed. $CD19^{+ve}$ cells were isolated from a second independent donor and infected with the same recombinant viruses and grown under the same conditions. Protein was harvested 20 days pi and CDKI protein levels assessed. Cell extracts were previously described in Figure 3.13.

Western blot analysis of $p15^{INK4b}$ and $p16^{INK4a}$ protein levels in $CD19^{+ve}$ B cells infected with the same viruses and grown under the same conditions were consistent with the elevated mRNA levels seen in cells with inactive EBNA3 proteins (Figure 3.18). In addition, consistent with the mRNA results, elevated protein levels of $p18^{INK4c}$ were only seen in cells with simultaneously conditionally inactive EBNA3A and EBNA3C (Figure 3.18).

Analysis of $p21^{WAF1/CIP1}$ transcripts did not show any considerable difference in $p21^{WAF1/CIP1}$ mRNA expression when EBNA3A and EBNA3C were active or inactive. However, elevated levels of $p21^{CIP1/WAF1}$ were seen by western blotting in cells with inactive EBNA3A and simultaneously inactive EBNA3A and EBNA3C (Figure 3.18). This supports previous work, which has suggested EBNA3A and EBNA3C are regulating $p21^{CIP1/WAF1}$ in a post-transcriptional manner (Banerjee et al., 2014; Tursiella et al., 2014).

In contrast to the absence of differential mRNA expression of $p27^{KIP1}$ depending on EBNA3A and EBNA3C stability, proteins levels were modestly elevated in cells with simultaneously inactive EBNA3A and EBNA3C (Figure 3.18). Consistent with EBNA3A- and EBNA3C- mediated repression of $p57^{KIP2}$ (Bazot et al., 2015), and elevated mRNA levels when they are inactivated (Figure 3.17F), increased levels of $p57^{KIP2}$ were seen by western blot in cells with inactive EBNA3A and EBNA3C. As with $p15^{INK4b}$ and $p16^{INK4a}$, there appeared to be an additive effect of the absence of both EBNA3A and EBNA3C, with increasingly higher $p57^{KIP2}$ protein levels (Figure 3.18). However, this additive effect was not evident at the mRNA level (Figure 3.17). Furthermore, $p57^{KIP2}$ transcript levels were higher in EBNA3A-null cells compared to EBNA3C-null cells whereas the protein levels of $p57^{KIP2}$ were higher in EBNA3C-null cells compared to EBNA3A-null cells. This is possibly a result of donor dependent

variation in the relative contributions of EBNA3A and EBNA3C to gene regulation, as mRNA and protein levels were assessed in different CD19^{+ve} B cell donors.

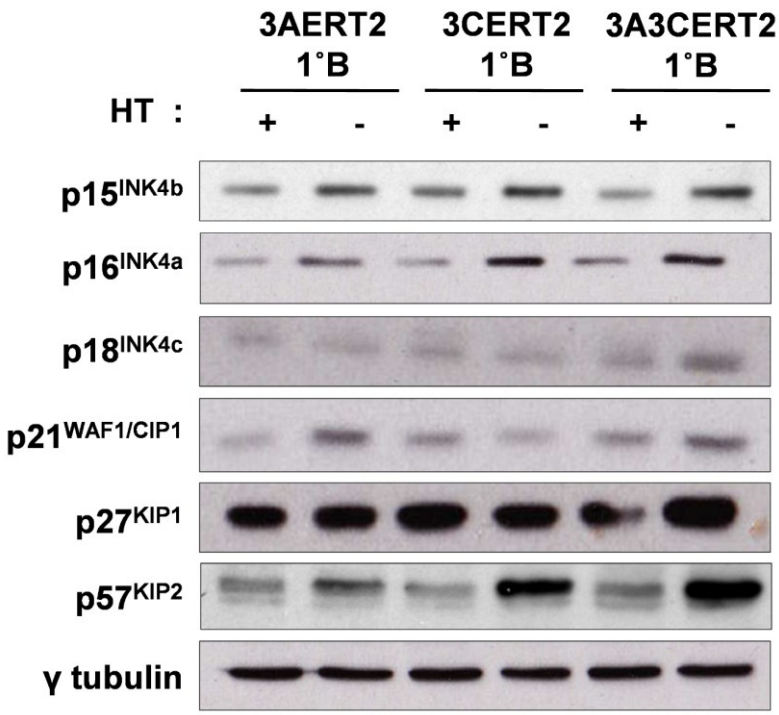


Figure 3.18. EBNA3A and EBNA3C regulate expression of CDKI early after infection with EBV. Expression of the EBV latency-associated proteins EBNA3A and EBNA3C, and the CDKI p15^{INK4b}, p16^{INK4a}, p18^{INK4c}, p21$^{CIP1/WAF1}$, p27^{KIP1} and p57^{KIP2} was demonstrated by western blotting extracts from CD19^{+ve} primary B cells from an independent donor infected with 3AERT2, 3CERT2 or 3A3CERT2 recombinant EBV and cultured for 20 days with (+) or without (-) 4-hydroxytamoxifen (HT). In each blot γ-tubulin was used as a loading control and was similarly consistent across all blots.

3.2.3.2. Regulation of CDKI by EBNA3A and EBNA3C in newly established conditional LCLs

Following assessment of EBNA3A- and EBNA3C-mediated regulation of CDKI during primary B cell infection, regulation of CDKI in conditional LCLs was assessed. The 3AERT2, 3CERT2 or 3A3CERT2 infected CD19^{+ve} B cells grown with HT from Figure 3.18 were cultured for two-months to establish LCLs. They were then split, and half of the culture was washed and re-cultured in media without HT. After 30 days, mRNA and protein samples were harvested for assessment of CDKI transcript and proteins levels by qPCR and western blotting. Cell extracts were described previously in Figure 3.13.

Consistent with EBNA3A- and EBNA3C-dependent reversible regulation of $p15^{INK4b}$ and $p16^{INK4a}$ as described previously (Jiang et al., 2017; Skalska et al., 2013; Styles et al., 2017), mRNA and protein levels were elevated 30 days after withdrawal of HT from conditional LCLs (Figure 3.19A/B). However, the level of $p18^{INK4c}$ (which was substantially de-repressed in 3A3CERT2-infected primary B cells lacking HT) was only very modestly elevated, with less than a 2-fold increase in $p18^{INK4c}$ mRNA (Figure 3.19C). This indicates that while initiating repression of $p18^{INK4c}$ requires either EBNA3A or EBNA3C, it may not require them for its continued repression (see Chapter IV).

Elevated levels of $p21^{CIP1/WAF1}$ were evident only at a protein level when EBNA3A and EBNA3C were inactivated in newly infected cells. This was mirrored in conditional LCLs, with no considerable differences in mRNA expression when EBNA3A and EBNA3C were inactivated (Figure 3.19D).

Regulation of $p27^{KIP2}$ by EBNA3A and EBNA3C is thought to occur at a lesser extent than $p57^{KIP1}$ (Bazot et al., 2015) and, as seen in $CD19^{+ve}$ cells newly infected with conditional EBV viruses, there was no notable difference in $p27^{KIP1}$ mRNA levels following inactivation of EBNA3A and/or EBNA3C for 30 days (Figure 3.19E). In contrast to $p18^{INK4c}$, and consistent with $p15^{INK4b}$ and $p16^{INK4c}$, reversible regulation of $p57^{KIP2}$ in conditional LCL was consistent with regulation during primary B cell infection. However, inactivation of EBNA3A, EBNA3C and both EBNA3A and EBNA3C simultaneously led to comparably elevated levels of $p57^{KIP2}$ mRNA. This contrasts with the apparently dominant effect of EBNA3A in newly infected cells (Figure 3.19F, Figure 3.17F). This is possibly reflective of the involvement of miRNA in repression of $p57^{KIP2}$, rather than direct transcriptional repression by EBNA3A and EBNA3C.

Expression of the control housekeeping gene ALAS1 mRNA was not affected by the inactivation of EBNA3A and EBNA3C proteins in the conditional LCLs (Figure 3.19G).

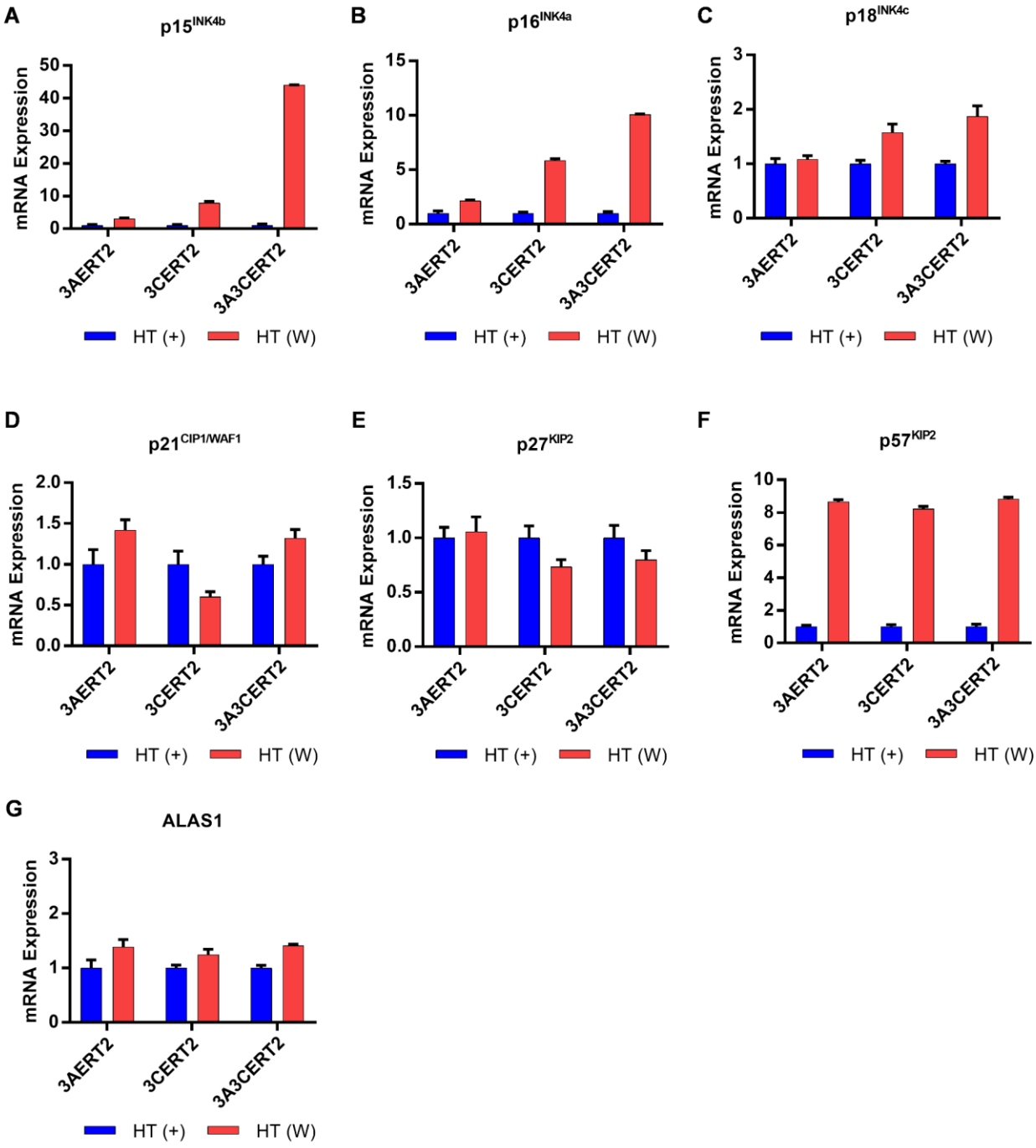


Figure 3.19. EBNA3A and EBNA3C regulate CDKI mRNA expression in newly established conditional LCLs. CD19^{+ve} B cells from the same donor were infected with either 3AERT2, 3CERT2 or 3A3CERT2 recombinant EBV and were cultured with 4-hydroxytamoxifen (HT) to establish conditional lymphoblastoid cell lines (LCLs). LCLs were grown either with HT (+) or washed and grown without (W) 4-hydroxtamoxifen (HT) for 30 days. Analysis of expression of *CDKN2B* (p15^{INK4b}; **A**), *CDKN2A* (p16^{INK4a}; **B**), *CDKN2C* (p18^{INK4c}; **C**), *CDKN1A* (p21$^{CIP1/WAF1}$; **D**), *CDKN1B* (p27^{KIP1}; **E**), *CDKN1C* (p57^{KIP2}; **E**) and *ALAS1*

(control housekeeping gene; **G**) mRNA was performed by quantitative PCR (qPCR) and relative mRNA expression was normalised to the endogenous control *GNB2L1,* with fold change shown relative to cells grown with (+) HT. Error bars indicate the standard deviation of qPCR triplicates for each sample. Representative experiment of three independent $CD19^{+ve}$ cell donors analysed.

To confirm these findings at a protein level, western blotting analyses were performed on protein extracts from the same cells, harvested on the same day as the mRNA samples. These cell extracts were previously described in Figure 3.13.

Protein levels of $p15^{INK4b}$ and $p16^{INK4a}$ were consistent with the mRNA results, and the results of the newly infected cells, further indicating reversible regulation of these CDKI. These all showed elevated levels of $p15^{INK4b}$ and $p16^{INK4a}$ when EBNA3C and (to a lesser extent) EBNA3A were independently inactivated, with the highest levels seen in cells with simultaneously inactivated EBNA3A and EBNA3C (Figure 3.20). Furthermore, consistent with only a very modest increase in $p18^{INK4c}$ mRNA, at a protein level there was no notable difference in $p18^{INK4c}$ expression when HT was withdrawn (Figure 3.20).

Consistent with the cells newly infected with conditional EBV viruses, there was no notable difference in $p21^{WAf1/CIP1}$ expression at an mRNA level when EBNA3A, EBNA3C or both were inactivated for 30 days in conditional LCL. However, there was an increase in $p21^{WAF1/CIP1}$ protein (Figure 3.20), further indicating EBNA3A and EBNA3C are post-transcriptionally regulating $p21^{WAF1/CIP1}$ as has been suggested previously (Banerjee et al., 2014; Tursiella et al., 2014).

No notable difference in $p27^{KIP1}$ protein expression was evident in conditional LCLs (Figure 3.20), consistent with the mRNA results. However, this contrasts the newly infected cells where EBNA3A/EBNA3C-null cells had elevated levels of $p27^{KIP1}$ protein (Figure 3.18). Although mRNA levels of $p57^{KIP2}$ were comparably elevated at an mRNA level, the protein levels were not consistent, with an elevated increase seen in EBNA3A-null cells compared to cells where EBNA3C or EBNA3A and EBNA3C were inactivated for 30 days (Figure 3.20).

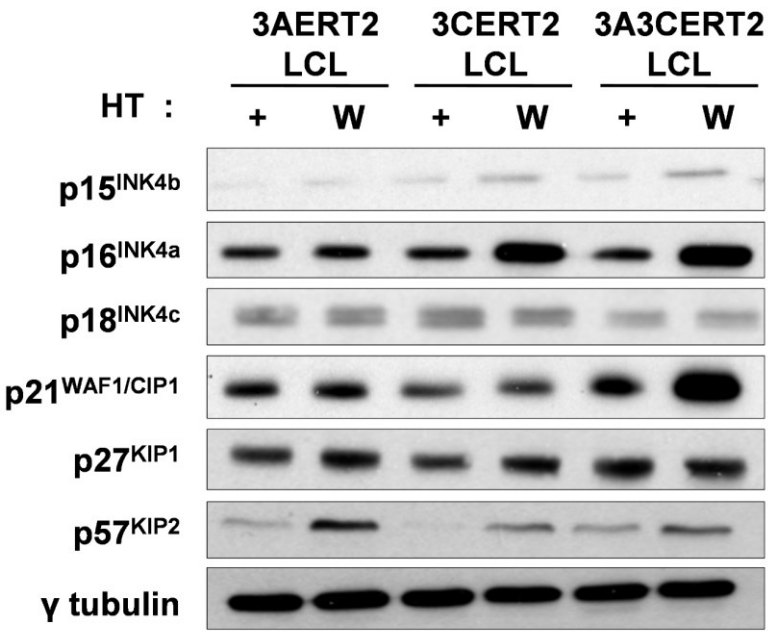


Figure 3.20. EBNA3A and EBNA3C regulate CDKI in newly established conditional LCLs. Expression of the CDKIs p15^{INK4b}, p16^{INK4a}, p18^{INK4c}, p21^{WAF1}, p27^{KIP1} and p57^{KIP2} was demonstrated by western blotting extracts from an 3AERT2, 3CERT2 and 3A3CERT2 lymphoblastoid cell lines (LCLs) derived from the same donor and cultured with 4-hydroxytamoxifen (+,HT), or washed and grown without HT for 30 days (W). In each blot γ-tubulin was used as a loading control and was similarly consistent across all blots.

Regulation of CDKIs in an LCL with conditional expression of both EBNA3A and EBNA3C simultaneously was further analysed by western blotting over a 60-day time course, whereby EBNA3A and EBNA3C were inactivated for 30 days and then re-activated for 30 days. Cell extracts were previously shown in Figure 3.11 and described in Section 3.2.1.4.

As seen in EBV infected primary B cells, protein levels of p15^{INK4b}, p16^{INK4a}, p21$^{CIP1/WAF1}$ and p57^{KIP2} responded to the differential state of EBNA3A and EBNA3C stability. Levels of these CDKIs were elevated following inactivation of EBNA3A and EBNA3C, with re-addition of HT restoring their repression (Figure 3.21). Restoring the repression of the INK4 family CDKI p15^{INK4b} and p16^{INK4a} appeared to take well over 10 days. In contrast, repression of the CIP/KIP members p21$^{CIP1/WAF1}$ and p57^{KIP2} was nearly complete following 10 days of HT re-addition. This is potentially reflective of the different mechanisms employed by EBNA3A and EBNA3C in regulation of these CDKI. Consistent with

the previous results, there was no notable difference in $p27^{KIP1}$ when EBNA3A and EBNA3C were inactivated and sequentially reactivated.

However, as was also seen in the previous LCL experiment (Figure 3.17), expression of $p18^{INK4c}$ did not consistently increase and decrease in response to changing EBNA3A and EBNA3C activation state. However, the levels of $p18^{INK4c}$ were erratic over the 60 days in the washed population, with slightly elevated levels at 10- and 20-days post washing and at 60 days (30 days after HT re-addition). These levels do not correlate with EBNA3A and EBNA3C presence or absence, and the consistent levels of expression of the control γ-tubulin demonstrates protein levels were the same in each well. Furthermore, $p18^{INK4c}$ levels in LCLs where HT was added continuously, where EBNA3A and EBNA3C were continually functional, also fluctuate, suggesting that these variations reflect normal changes in p18 levels, irrespective of EBNA3A and EBNA3C stability.

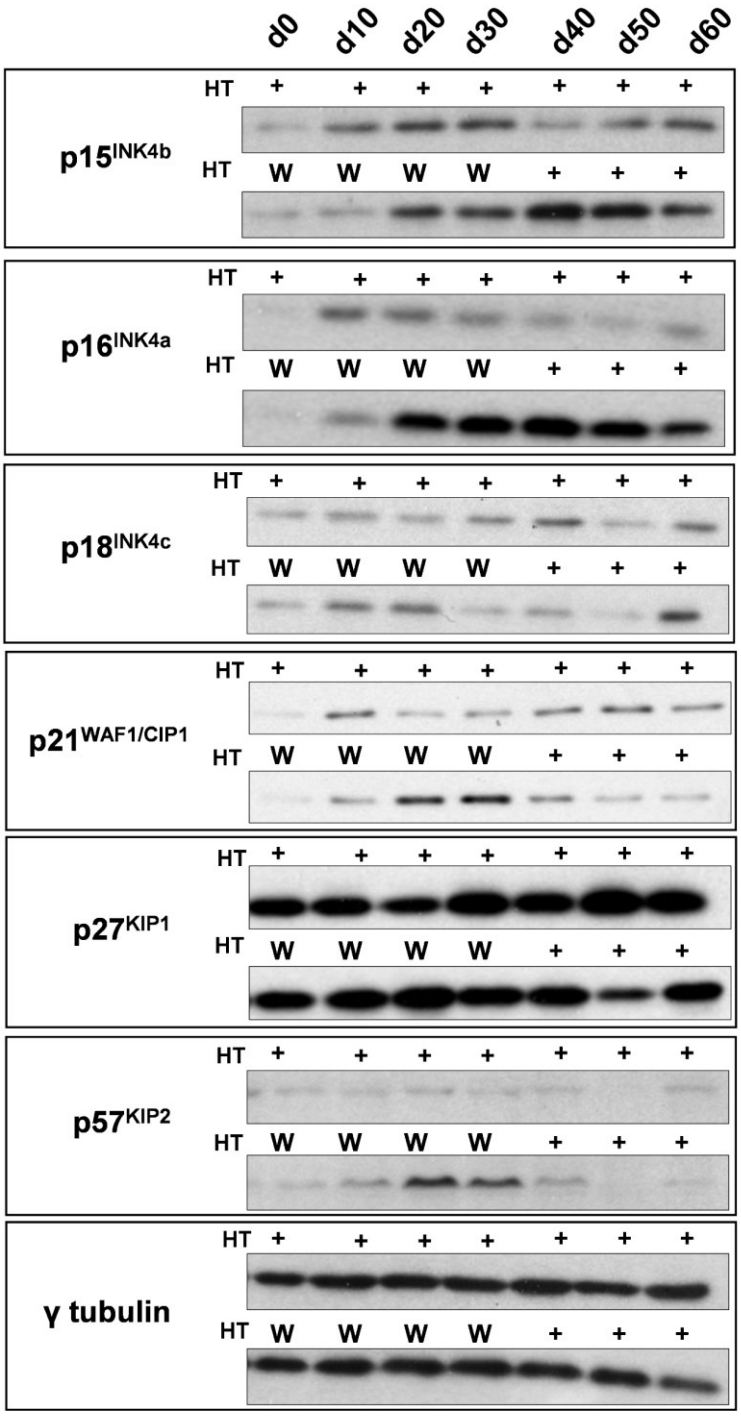


Figure 3.21. Regulation of CDKI in an 3A3CERT2 LCL where EBNA3A and EBNA3C are simultaneously conditionally deactivated and reactivated. Expression of $p15^{INK4b}$, $p16^{INK4a}$, $p18^{INK4c}$, $p21^{WAF1}$, $p27^{KIP1}$ and $p57^{KIP2}$ was demonstrated by western blotting extracts from an 3A3CERT2 lymphoblastoid cell line (LCL). Cells were grown continuously with 4-hydroxytamoxifen (HT) (+), or HT was washed out of the culture for 30 days (W) and then re-added to the culture for a further 30 days (+). Samples were taken at the indicated times point post washing. In each blot γ-tubulin was used as a loading control and was similarly consistent across all blots.

3.3. Summary

This chapter details the construction and validation of a recombinant EBV virus with simultaneously conditional expression of EBNA3A and EBNA3C; the 3A3CERT2 virus. EBNA3 proteins were cloned alongside ERT2 genes to create an EBV-BAC with ERT2 fused to both EBNA3A and EBNA3C, with the aim of making expression of both EBNA3A and EBNA3C simultaneously conditional on the presence of the activating ligand HT. This EBV-BAC was transfected into mammalian cells allowing production of infection virus following transient activation of the EBV lytic cycle. Infection of $CD19^{+ve}$ B cells with the newly constructed 3A3CERT2 virus validated that expression of EBNA3A and EBNA3C protein in these cells was dependent on the continuous presence of HT, and the expression of EBNA3A and EBNA3C responded to sequential omission or addition of HT.

Using this newly constructed virus, cells with simultaneously non-functional EBNA3A and EBNA3C were shown to exhibit enhanced cell death and reduced proliferation compared to cells where EBNA3A or EBNA3C were independently inactive.

Furthermore, qPCR and western blot analysis confirmed differential regulation of the CDKI $p15^{INK4b}$, $p16^{INK4c}$ and $p57^{KIP2}$ in cells newly infected with 3A3CERT2 and in double conditional LCLs. This also indicated an additive effect when EBNA3A- and EBNA3C-mediated regulation was simultaneously absent or lost. Although regulation of $p27^{KIP1}$ by EBNA3A and EBNA3C was not confirmed, post-transcriptional regulation of $p21^{WAF1/CIP1}$ by EBNA3 proteins was indicated by western blot analysis. Analysis of cells with simultaneously inactive EBNA3A and EBNA3C also revealed repression of the CDKI and B cell differentiation factor $p18^{INK4c}$, with loss of regulation only evident when both EBNA3A and EBNA3C were inactive in newly infected cells. However, in contrast to the other CDKI analysed, there were inconsistencies between newly infected cells and conditional LCLs, indicating repression may not require continuous expression of active EBNA3A and EBNA3C.

3.4. Discussion

3.4.1. Co-operative functions of the EBNA3 proteins

EBNA3A and EBNA3C share a diverse array of overlapping functions, yet retain some individual functions and are conserved genes within the EBV genome. The conserved nature of these genes over the history of EBV evolution indicates the vital nature of the genes, and requirement of the transcriptional profile they facilitate. Despite the differing functions of the oncogenic EBNA3A and EBNA3C, compared to the tumour suppressive EBNA3B, all three EBNA3 proteins cooperatively regulate numerous genes (White et al., 2010). EBNA3 proteins have been observed to substantially co-localise across the genome of LCLs and they can be readily co-precipitated from cell extracts (Allday et al., 2015; McClellan et al., 2013; Paschos et al., 2012, 2017; Schmidt et al., 2015). ChIP and microarray analysis has revealed there is only modest co-operation and rare co-localisation between EBNA3A and EBNA3B across the genome, with the majority of co-localisation involving EBNA3C cooperating with either EBNA3A or EBNA3B, or both (Paschos et al., 2017; White et al., 2010). Moreover, repression of host genes dominates differential gene expression, and deletion of EBNA3C most significantly affects host gene regulation (White et al., 2010).

Transcriptional regulation by the EBNA3 proteins is essential for efficient B cell transformation and persistence of EBV. Although EBNA3A and EBNA3C mediated gene regulation has substantial overlap and they appear to perform seemingly redundant functions, such as repression of $p16^{INK4a}$ and BIM (Maruo et al., 2011; Paschos et al., 2017; Skalska et al., 2010), they also independently repress specific genes. EBNA3C is thought to independently repress COBLL1 and AICDA (Kalchschmidt et al. 2016a, 2016b), and EBNA3A was recently shown to target *STK39* independently of EBNA3C (Bazot et al., 2018).

To further assess the combined and independent functions of the oncogenic EBNA3A and EBNA3C oncogenes, BAC and recombineering technology was employed to generate a recombinant EBV virus with conditional expression of both EBNA3A and EBNA3C simultaneously (3A3CERT2).

Infecting primary B cells isolated from the same donor with this newly constructed double conditional virus, alongside previously constructed recombinant EBV where either EBNA3A or EBNA3C are conditionally expressed, permitted investigation of the combined and independent functions of EBNA3A and EBNA3C during both primary B cell infection and within LCLs.

The phenotype of cells with simultaneously inactive EBNA3A and EBNA3C appeared more extreme than in cells where only EBNA3A or EBNA3C was inactive. Elevated levels of dead cells and decreased proliferating live cells, were observed in cells infected with 3A3CERT2 compared to cells infected with the single conditional viruses (3AERT2 or 3CERT2, Figures 3.14 and 3.15). This indicates that EBNA3A and EBNA3C (when expressed independently of the other), enhance cell survival, although, not for much longer than EBNA3C-null cells.

The intricacies of the cooperative behaviour of the EBNA3 proteins have not yet been completely characterised. It would therefore be interesting to generate a recombinant virus with conditional expression of EBNA3A and EBNA3C, alongside a deletion in EBNA3B to further assess the roles and contradicting functions of the oncogenic EBNA3 proteins. This would enable the conclusive exclusion of EBNA3B in transcriptional regulation of processes attributed to the EBNA3A and EBNA3C oncogenes. Furthermore, considering the extensive cooperation of EBNA3C with EBNA3B, suggested by extensive co-localization across the genome and co-operative gene regulation (Paschos et al., 2017; White et al., 2010), it may be interesting to generate a double conditional virus for EBNA3C and EBNA3B to further reveal the consequences of this cooperative behaviour. However, production of an EBNA3B-ERT2 virus has thus far been unsuccessful in the Allday Laboratory (Dr G. Ho, PhD Thesis), so an EBNA3C-ERT2/EBNA3B-KO may be more technically feasible. Although technically challenging, a recombinant virus with differential conditional expression of EBNA3A and EBNA3C proteins using different systems, such as ERT2 conditional proteins as well as a DOX-inducible system in the same recombinant virus, could also help untangle the complexities of EBNA3 cooperative gene regulation by allowing controlled expression of different EBNA3 proteins in a temporal manner.

3.4.2. Cell cycle regulation by EBNA3 proteins

EBNA3A and EBNA3C have previously been shown to regulate various cell cycle regulatory factors including $p15^{INK4b}$ and $p16^{INK4c}$ by transcriptional regulation (Jiang et al., 2017; Skalska et al., 2010), $p27^{KIP1}$ and $p57^{KIP2}$ by transactivation of inhibitory miRNA (Bazot et al., 2015) and have been associated with proteasomal degradation of $p21^{CIP1/WAF1}$ (Banerjee et al., 2014; Tursiella et al., 2014) . Therefore, regulation of these factors in cells where EBNA3A and EBNA3C were simultaneously inactivated was assessed by qPCR and western blotting, and compared to cells from the same donor where either EBNA3A and EBNA3C were inactivated independently.

As predicted, this revealed that when both EBNA3A and EBNA3C were simultaneously inactive in newly infected cells or conditionally inactivated in LCLs, there was an increase of $p15^{INK4b}$ and $p16^{INK4c}$ mRNA and protein. There appeared to be an elevated level of both $p15^{INK4b}$ and $p16^{INK4c}$ when both EBNA3A and EBNA3C were non-functional, compared to when they were individually expressed (Figures 3.17, 3.18, 3.19. 3.20). This was reflected in the increased levels of $p57^{KIP2}$ in EBNA3A/EBNA3C-null primary B cells. The levels of $p15^{INK4b}$, $p16^{INK4c}$ and $p57^{KIP2}$ similarly responded to sequential inactivation and activation of both EBNA3A and EBNA3C (Figure 3.21), confirming regulation of these CDKI by EBNA3A and EBNA3C is reversible. Although $p27^{KIP1}$ has been shown to be regulated by EBNA3A and EBNA3C, following transcriptional activation of inhibitory miRNA (Bazot et al., 2015), this was not evident at an mRNA level in newly infected cells or conditional LCLs. However, concurrent with $p57^{KIP2}$, there were increased levels in the absence of both EBNA3A and EBNA3C in newly infected cells.

Due to EBNA3-mediated repression of various CDKI, the INK4 family member $p18^{INK4c}$ was also investigated in cells with conditional expression of EBNA3A and EBNA3C. Western blot and qPCR analysis of primary B cells newly infected with EBV indicated $p18^{INK4c}$ is a target of both EBNA3A and EBNA3C, with expression of either EBNA3 protein sufficient to restrain transcription of $p18^{INK4c}$ (Figures 3.17 and 3.18). This is the first description of EBV mediated regulation of $p18^{INK4c}$ [now published (Styles et al., 2017)]. Furthermore, this is the first time an EBV-target has been shown to be

largely repressed by the expression of either EBNA3A or EBNA3C. This implies there are further genes regulated by both EBNA3A and EBNA3C where individual inactivation has not yet revealed the regulatory control induced by these proteins. It would therefore be of interest to perform a microarray or RNA-seq to identify genes differentially regulated only when both EBNA3A and EBNA3C are simultaneously inactive. Regulation of $p18^{INK4c}$ by EBNA3A and EBNA3C is particularly interesting as, aside from being a CDKI, $p18^{INK4c}$ has been shown to have specific functions in B cells, the primary target of EBV. $p18^{INK4c}$ functions as B cell differentiation factor and is required for the generation of terminally differentiated PC (Morse et al., 1997; Tourigny et al., 2002). Therefore, the repression of $p18^{INK4c}$ by EBNA3A and EBNA3C was investigated further, and the link to EBV-mediated regulation of the B cell to PC differentiation pathway is explored in Chapter IV.

Direct EBNA3-mediated regulation of $p15^{INK4b}$, $p16^{INK4a}$, $p57^{KIP2}$ and $p27^{KIP1}$ has been established by genetic analyses using recombinant EBV with genetic modifications to the EBNA3 genes. However, the precise mechanism employed by EBNA3A and EBNA3C to regulate CDKI $p21^{WAF1/CIP1}$ has not been conclusively demonstrated using recombinant EBV viruses within the context of infection. It has been suggested EBNA3C interacts with PIM-1 to target $p21^{WAF1/CIP1}$ for degradation. EBNA3C was shown to interact with PIM-1, and overexpression of EBNA3C in 293 cells enhanced PIM-1 mediated phosphorylation and subsequent degradation of $p21^{WAF1/CIP1}$ (Banerjee et al., 2014). Furthermore, shRNA mediated knock-down of EBNA3A in LCL and in a BL cell line which expressed a limited latency III profile lacking EBNA2, EBNA-LP and LMP proteins, was concurrent with elevated $p21^{WAF1/CIP1}$ protein expression (Tursiella et al., 2014). The results in this chapter do not identify the precise biological mechanisms employed by EBNA3A and EBNA3C in repression of $p21^{WAF1/CIP1}$. However, elevated levels of $p21^{WAF1/CIP1}$ protein were seen in in both newly infected B cells and in conditional LCL by western blot when EBNA3A, or both EBNA3A and EBNA3C, were non-functional. However, there was no difference in mRNA levels when EBNA3A or EBNA3C were active or inactive. This therefore further indicates that EBNA3A, and possibly EBNA3C, are employing post-transcriptional repressive mechanisms to regulate $p21^{WAF1/CIP1}$ during EBV infection. As with $p15^{INK4b}$,

p16^{INK4a} and p57^{KIP2}, regulation of p21$^{WAF1/CIP1}$ appears dependent on the continuous presence of functional EBNA3 proteins, as regulation can be reversed or induced by inactivation or activation of both EBNA3A and EBNA3C in conditional LCLs.

Consistent with p15^{INK4b}, p16^{INK4a}, p27^{KIP1} and p57^{KIP2}, the highest levels of p21$^{WAF1/CIP1}$ were identified in cells with simultaneously non-functional EBNA3A and EBNA3C. The levels of p18^{INK4c} were similarly highest in EBNA3A/EBNA3C-null cells. These elevated levels of EBNA3 regulated CDKI in cells with non-functional EBNA3A and EBNA3C are consistent with the findings of Section 3.2.2 which suggest a more extreme phenotype when both EBNA3A and EBNA3C are inactive. Here, reduced proliferation and increased cell death was seen in EBNA3A/EBNA3C-null cells compared to cells where EBNA3A or EBNA3C were independently inactive. It is likely the elevated levels of these cell cycle regulatory factors and tumour suppressors in cells with non-functional EBNA3A and EBNA3C are contributing to, if not responsible for, this phenotype.

The patterns of differential CDKI regulation during primary B cell infection where cells were never exposed to functional EBNA3A or EBNA3C expression, were largely reflected following inactivation of EBNA3A and EBNA3C in conditional LCLs (such as for p15^{INK4b}, p16^{INK4a}, p21$^{WAF1/CIP1}$ and p57^{KIP2}). However, EBNA3A- and EBNA3C-mediated regulation of p18^{INK4c} was only revealed by analysing CD19^{+ve} cells during primary infection with the double conditional EBV virus. It seems regulation of p18^{INK4c} may become independent of EBNA3A and EBNA3C, in that it was not consistently induced in conditional LCLs following inactivation of EBNA3A and EBNA3C. This contrasts with the reliably reversible regulation of p15^{INK4b}, p16^{INK4a}, p21$^{WAF1/CIP1}$ and p57^{KIP2} in conditional LCLs. It is likely other genes are regulated during primary infection in a similar manner to p18^{INK4c}, also leading to largely irreversible repression in conditional LCLs. Regulation was therefore only revealed in EBNA3A/EBNA3C-null cells rather than in LCLs with inactivated EBNA3A and EBNA3C. This demonstrates the importance of assessing both cell populations. Differential gene regulation by EBNA3 proteins may be missed when solely using LCLs as a model of EBV infection, highlighting the

importance of also assessing B cells during primary infection with EBV. Assessing both cell models will aid identification of EBNA3A and EBNA3C target genes.

As EBV have been shown to transcriptionally regulate the INK4 protein family members $p15^{INK4b}$, $p16^{INK4a}$ and $p18^{INK4c}$, it would also be of interest to investigate whether EBV is also targeting the remaining INK4 family member $p19^{INK4d}$ (Hirai et al., 1995). Furthermore, it is also likely EBV is targeting other cell cycle regulatory factors such as those within the DDR pathways, as EBNA3C has been shown attenuate this response by inhibition of CHK2 and ATM (Nikitin et al., 2010). Considering EBV mediates regulation through transcriptional, translational and proteasomal mechanisms, these cell cycle factors could be regulated by any of these EBV mediated processes. Further assessment of cells with non-functional EBNA3A and EBNA3C would likely reveal further complexities of EBV-mediated circumvention of cell cycle regulation.

3.4.3. Limits of reduced expression of modified EBNA3 proteins during ERT2 EBV infections

In interpreting results from cells infected with conditional EBV recombinant viruses, it must be noted that the levels of EBNA3A, and to a lesser extent EBNA3C, are lower than in cells with untagged WT EBNA3A or EBNA3C proteins (Figure 3.13). As EBNA3A and EBNA3C levels are lower in cells infected with conditional virus compared to when they are untagged, the active EBNA3 state (HT+) may be less repressive than WT. This could therefore result in less profound differential regulation, making it harder to conclusively identify targets of these proteins. Furthermore, for the qPCR analysis shown in this chapter, the CDKI mRNA levels are shown relative to those found in cells with active conditional EBNA3 proteins. This normalisation strategy may be misrepresenting EBNA3A-mediated regulation, as any changes in regulation may be from a lower base than from a WT infection, due to the substantially lower levels of EBNA3A in conditional cells. Despite the benefits of using these conditional systems, this highlights an inherent issue with using tagged proteins for analysis.

3.5. Final conclusions

In conclusion, a recombinant EBV virus with conditional expression of EBNA3A and EBNA3C was successfully constructed and validated. Using this double conditional virus, the results in this chapter highlights the overlapping and individual functions of EBNA3A and EBNA3C. There are extensive similarities and overlap in the functions of EBNA3A and EBNA3C, including shared target genes. A more extreme phenotype occurs in the absence of both EBNA3A and EBNA3C, compared to when they are individually inactive, with increased cell death and reduced proliferation. This indicates non-redundant independent functions within transformation and viral persistence. This is reflected in the regulation of CDKI, of which EBNA3A and EBNA3C co-operatively regulate. The highest levels of $p15^{INK4b}$, $p16^{INK4a}$, $p21^{WAF1/CIP1}$ and $p57^{KIP2}$ CDKIs were seen when both EBNA3A and EBNA3C were non-functional, indicating only partial loss of regulation when either EBNA3A or EBNA3C are inactivated. The use of this double conditional virus also revealed EBNA3A- and EBNA3C-mediated regulation of $p18^{INK4c}$, however in contrast to the other CDKI analysed, either EBNA3A or EBNA3C seem sufficient for repression. There were also inconsistencies in $p18^{INK4c}$ repression by EBNA3 proteins between newly infected cells and conditional LCLs, indicating the regulatory mechanisms differ to that of other CDKIs.

3.6. Remaining questions

There are still many unknowns regarding the combined and independent functions of the EBNA3A and EBNA3C oncogenes and questions to be addressed, including:

1. Why are the functions of the related oncogenes EBNA3A and EBNA3C so overlapping, yet distinct from the functionally divergent tumour suppressive activity of EBNA3B?

2. What are the mechanisms responsible for EBNA3A- and EBNA3C-mediated repression of the $p18^{INK4c}$? Why are there inconsistencies between newly infected cells and conditional LCLs? (Addressed in Chapter IV)

3. What are the mechanisms behind the apparent post-transcriptional regulation of $p21^{WAF1/CIP1}$ by EBNA3A and EBNA3C?

4. Do EBNA3A and EBNA3C restrain expression of other genes (such as those regulating the cell cycle or the DDR pathways), of which loss of regulation is only notable when both EBNA3A and EBNA3C are simultaneously non-functional?

4. Chapter IV: EBNA3A and EBNA3C suppress the B cell to plasma cell differentiation pathway during establishment of EBV latency

4.1. Introduction

This chapter will focus on the roles of EBNA3A and EBNA3C in the B cell-to-PC differentiation pathway. In the previous chapter I established that inactivation of EBNA3A and EBNA3C during primary infection of B cells with EBV results in a marked increase in $p18^{INK4c}$ expression, indicating a regulatory role for these EBNA3 proteins. As discussed in Chapter I, aside from being a CDKI, $p18^{INK4c}$ has also been linked with the B cell to PC differentiation pathway (Morse et al., 1997; Tourigny et al., 2002). Considering B cells are the primary target of EBV and the viral life cycle is intricately linked to that of B cell biology, EBNA3 mediated regulation of $p18^{INK4c}$ suggests EBNA3A and EBNA3C may play a role within EBV-mediated circumvention of B cell differentiation pathways. Currently, the GC model of EBV persistence suggests that upon primary infection of mature B cells, B cells are activated and enter the GC where they further differentiate and exit the GC as MBCs latently carrying the viral genome as episomes. It is unknown how the MBC pathway is favoured over the alternative PC differentiation pathway during the GC reaction (see Chapter I, Section 1.1.3).

In order to determine whether EBNA3-mediated regulation of $p18^{INK4c}$ is linked to its role in PC differentiation, the transcription factor BLIMP-1 was also chosen for further investigation as it is a key transcriptional regulator required for the B cell to PC differentiation pathway (see Chapter I, Section 1.1.4).

The majority of the results in this chapter have been published (Styles et al., 2017), and figures have been taken or adapted from this publication as per the Creative Commons Attribution (CC BY 4.0) License (http://creativecommons.org/licenses/by/4.0/). Figures from this publication are referenced accordingly.

4.2. Results

4.2.1. EBNA3A and EBNA3C are required to prevent activation of *CDKN2C* (p18^{INK4c}) and *PRDM1* (BLIMP-1) transcription after EBV infection

4.2.1.1. EBNA3-mediated regulation of PRDM1 (BLIMP-1) transcription resembles that of CDKN2C (p18^{INK4c})

EBNA3A and EBNA3C mediated regulation of *CDKN2C* (the gene encoding p18^{INK4c}, as seen in the previous chapter) was investigated further. CD19^{+ve} B cells were isolated from an independent donor and infected with EBV recombinant viruses with conditional expression of EBNA3A (3AERT2), EBNA3C (3CERT2), or conditional expression of both proteins (3A3CERT2). Cells were cultured for 30 days with or without HT and RNA samples harvested at 10, 15, 20 and 30 days pi for analysis by qPCR analysis. There was little difference seen in the level of p18^{INK4c} mRNA when EBNA3A was independently functional (HT+) or non-functional (HT-, Figure 4.1A). Analysis of cells from the same donor infected with 3CERT2 suggested that inactive EBNA3C (HT-) results in a small but sustained increase in p18^{INK4c} mRNA expression (Figure 4.1C). These results were consistent and reproducible in experiments with infection of primary B cells isolated from 3 independent donors (Figure 4.1D/E), leading to the conclusion that inactivating EBNA3A independently has little effect on the expression of p18^{INK4c} mRNA whereas inactivating EBNA3C has a modest but sustained effect. Analysis of cells from the same 3 independent donors infected with the double conditional 3A3CERT2 virus revealed that when EBNA3A and EBNA3C were simultaneously non-functional (HT-) there was substantial activation of p18^{INK4c} expression during the first 3 weeks of infection with recombinant EBV (Figure 4.1C/F). This further indicates EBNA3A- and EBNA3C-mediated regulation of *CDKN2C*.

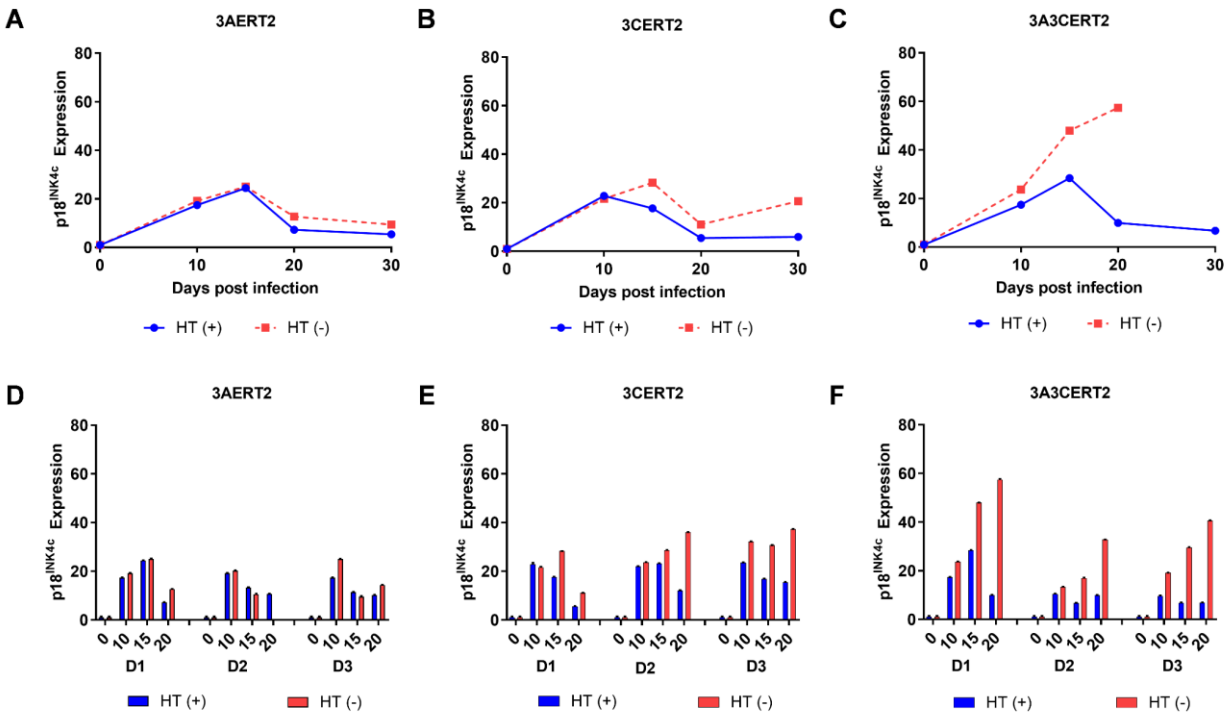


Figure 4.1. Activation of *CDKN2C* (p18^{INK4c}) transcription is prevented by EBNA3A and EBNA3C. CD19^{+ve} purified B cells were infected with 3AERT2 (**A** and **D**), 3CERT2 (**B** and **E**), or 3A3CERT2 (**C** and **F**) recombinant EBV and cultured for 30 days with (+) or without (-) 4-hydroxytamoxifen (HT). RNA samples were taken at the times indicated after infection and quantitative PCR (qPCR) analysis performed. *CDKN2C* (p18^{INK4c}) relative mRNA expression was normalised to the endogenous control *GNB2L1* and fold change is shown relative to uninfected B cells at day 0. Error bars show the standard deviation of qPCR triplicates for each sample. Analysis of HT (-) infected cells at later timepoints were not always possible due to large amounts of cell death in the culture. Similar analysis from 2 additional donors (D2 and D3) is shown for comparison (**D**, **E**, **F**) (Styles et al., 2017).

As p18^{INK4c} has been definitively linked with the B cell to PC differentiation pathway (see Chapter I, Section 1.1.4), I next wanted to assess whether BLIMP-1, a key transcriptional regulator of the PC pathway, was also a target of EBV. RNA isolated from the cells presented in Figure 4.1 were analysed for BLIMP-1 mRNA expression by qPCR as before. This revealed that BLIMP-1 is regulated by EBNA3 proteins in very similar manner to that of p18^{INK4c} (Figure 4.2), most notably in that simultaneous inactivation of EBNA3A and EBNA3C results in a robust activation of BLIMP-1 mRNA expression (3A3CERT2-, Figure 4.2C/F). This mirrors activation of p18^{INK4c} under the same conditions and is consistent across multiple donors (Figure 4.1C/F). Non-functional EBNA3A has a modest but

sustained effect with a small increase in BLIMP-1 mRNA (3AERT2-, Figure 4.2A/D), with inactivation of EBNA3C resulting in modest donor dependent increases in BLIMP-1 mRNA (3CERT2-, Figure 4.2B/E).

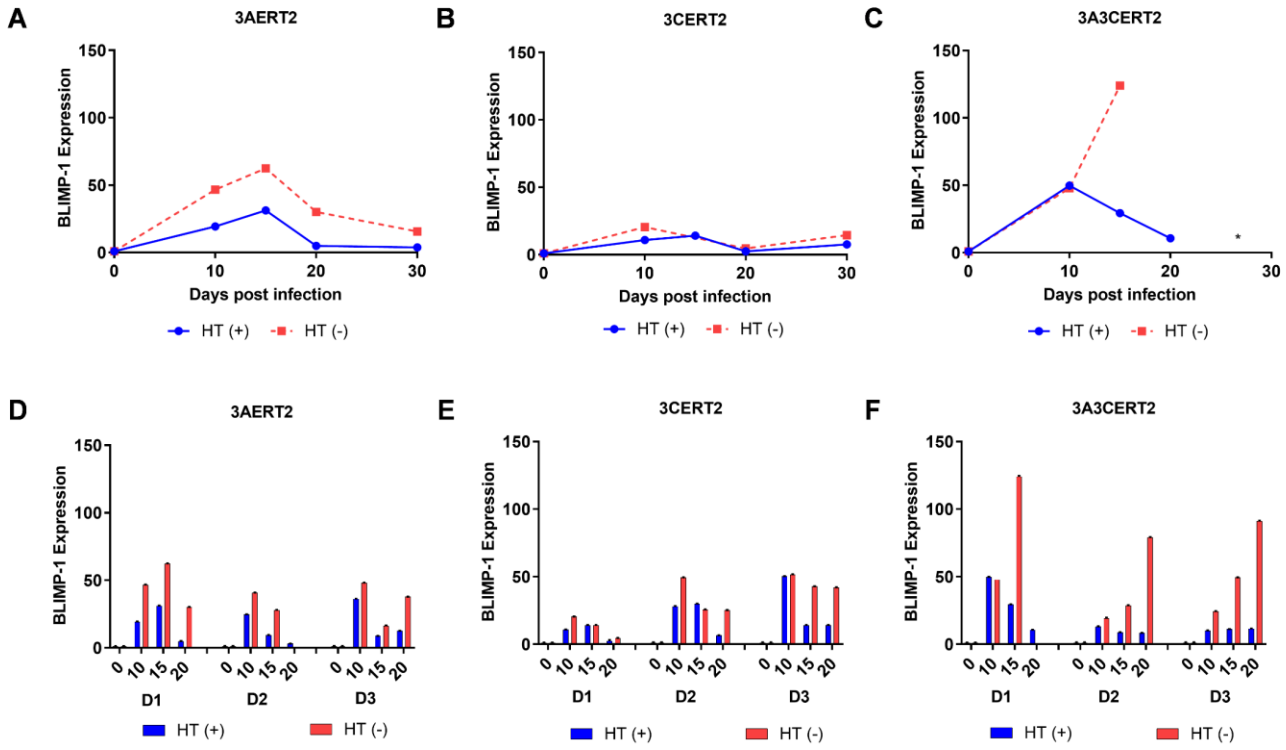


Figure 4.2. Activation of *PRDM1* (BLIMP-1) transcription is prevented by EBNA3A and EBNA3C. CD19^{+ve} purified B cells were infected with 3AERT2 (**A** and **D**), 3CERT2 (**B** and **E**), or 3A3CERT2 (**C** and **F**) recombinant EBV and cultured for 30 days with (+) or without (-) 4-hydroxytamoxifen (HT). RNA samples were taken at the times indicated after infection and quantitative PCR (qPCR) analysis performed. *PRDM1* (BLIMP-1) relative mRNA expression was normalised to the endogenous control *GNB2L1* and fold change is shown relative to uninfected B cells at day 0. Error bars show the standard deviation of qPCR triplicates for each sample. Analysis of HT (-) infected cells at later timepoints were not always possible due to large amounts of cell death in the culture. Similar analysis from 2 additional donors (D2 and D3) is shown for comparison (**D**, **E**, **F**) (Styles et al., 2017).

Similar analysis of the housekeeping gene *ALAS1* was used as a negative control in the cells presented in Figures 4.1/4.2 and showed no change in mRNA levels across the 30-day time course (Figure 4.3A-C). As previously established in this thesis and widely reported within the literature, p16^{INK4a} is regulated by EBNA3C and to a lesser extent EBNA3A, therefore regulation of the p16^{INK4a} encoding gene *CDKN2A* acted as a positive control for EBNA3A- and EBNA3C-mediated gene regulation. As expected, in these cells inactivation of EBNA3A resulted in a small increase in p16^{INK4a}

mRNA, with EBNA3C inactivation or simultaneous inactivation of EBNA3A and EBNA3C leading to a marked increase of $p16^{INK4a}$ expression (HT-, Figure 4.3D-F).

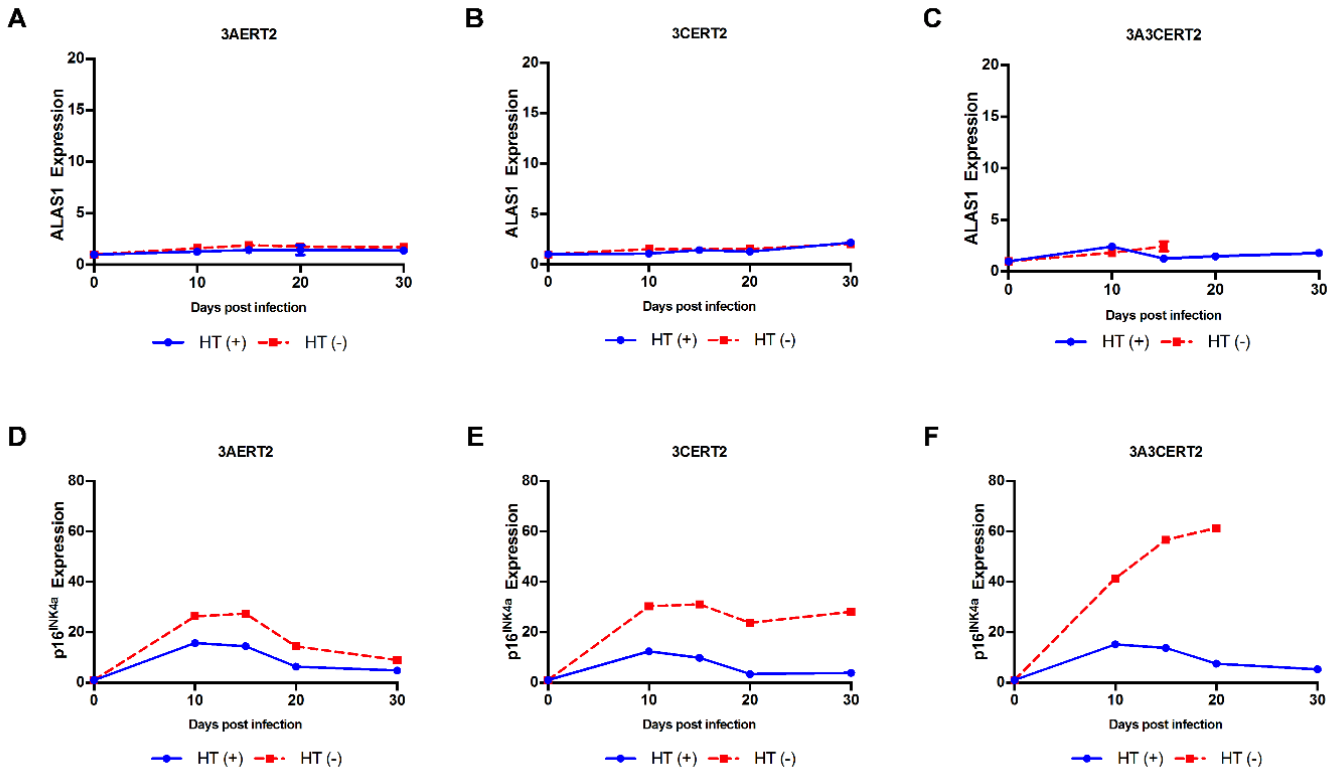


Figure 4.3. EBNA3A and EBNA3C repress *CDKN2C* ($p16^{INK4a}$) transcription but not *ALAS1*. $CD19^{+ve}$ purified B cells were infected with 3AERT2 (**A** and **D**), 3CERT2 (**B** and **E**), or 3A3CERT2 (**C** and **F**) recombinant EBV and cultured for 30 days with (+) or without (-) 4-hydroxytamoxifen (HT). RNA samples were taken at the times indicated after infection and quantitative PCR (qPCR) analysis performed. *ALAS1* (**A-C**) and *CDKN2A* ($p16^{INK4a}$, **D-E**) relative mRNA expression was normalised to the endogenous control *GNB2L1* and fold change is shown relative to uninfected B cells at day 0. Error bars show the standard deviation of qPCR triplicates for each sample. Analysis of HT (-) infected cells at later timepoints were not always possible due to large amounts of cell death in the culture (Styles et al., 2017).

To further assess EBNA3A and EBNA3C regulation of $p18^{INK4c}$ and BLIMP-1 transcription, mRNA levels were assessed in $CD19^{+ve}$ primary B cells derived from 3 independent donors infected with the triple knock-out virus (E3KO) in which the entire EBNA3 locus is deleted. This was compared with cells infected with the WT lab strain, where all EBNA3 proteins are expressed. Regulation of $p18^{INK4c}$ and BLIMP-1 transcription in primary B cells infected E3KO was consistent in magnitude and kinetics with

data from cells with conditionally inactive EBNA3A and EBNA3C (Figure 4.1/4.2), with a marked increase in both p18^{INK4c} and BLIMP-1 mRNA at 15-20 days pi when no EBNA3 proteins were expressed (E3KO, Figure 4.4A/B). This further confirms that a combination of EBNA3 proteins (namely EBNA3A and EBNA3C) is responsible for repression of p18^{INK4c} and BLIMP-1 transcription. As an EBNA3A and EBNA3C target gene, p16^{INK4a} expression acted as a positive control for EBNA3-mediated gene regulation (Figure 4.3C), with relative expression of the control housekeeping gene ALAS1 unaffected by the absence of the EBNA3 proteins (Figure 4.4D).

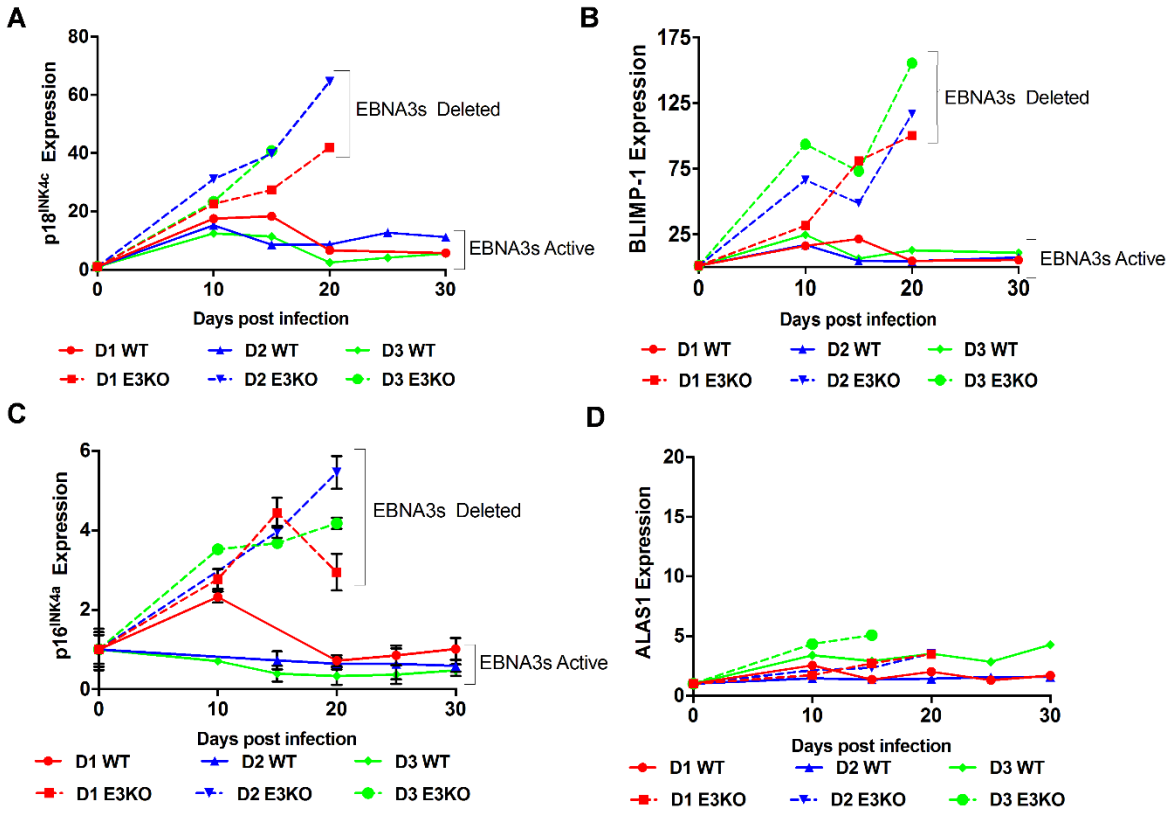


Figure 4.4. Activation of *CDKN2C* (p18^{INK4c}) and *PRDM1* (BLIMP-1) transcription is prevented by the EBNA3 proteins. CD19^{+ve} purified B cells from 3 independent donors (D1, D2, D3) were infected with WT (B95.8 BAC) or EBNA3KO recombinant EBV and cultured for 30 days. RNA samples were taken at the times indicated after infection and quantitative PCR (qPCR) analysis performed. *CDKN2C* (p18^{INK4c}, **A**), *PRDM1* (BLIMP-1, **B**), *CDKN2A* (EBNA3A/EBNA3C target control p16^{INK4a}, **C**) and *ALAS1* (housekeeping gene control, **D**) relative mRNA expression was normalised to the endogenous control *GNB2L1* and fold change is shown relative to uninfected cells at day 0. Error bars show the standard deviation of qPCR triplicates for each sample. Analysis of EBNA3KO cells at later time points was not possible due to large amounts of cell death in the culture. [Published in part (Styles et al., 2017)].

To determine whether EBNA3A- and EBNA3C-mediated transcriptional repression of *CDKN2C* ($p18^{INK4c}$) and *PRDM1* (BLIMP-1) is reflected at a protein level, western blot analysis was performed. Protein extracts were obtained from $CD19^{+ve}$ primary B cells derived from 2 independent donors (1°B D1, 1°B D2) infected with recombinant EBV with conditional expression of EBNA3A and EBNA3C (3A3CERT2) and cultured with (+) or without (-) HT for 20 days. Simultaneously inactive EBNA3A and EBNA3C resulted in elevated levels of both $p18^{INK4c}$ and BLIMP-1 protein in both donors and was therefore consistent with EBNA3A- and EBNA3C-mediated transcriptional regulation of the genes encoding $p18^{INK4c}$ and BLIMP-1 (Figure 4.5).

In conclusion, via the transcription factors EBNA3A and EBNA3C, EBV regulates both $p18^{INK4c}$ and BLIMP-1, two critical regulators of PC differentiation. This suggests a potentially pivotal role for EBNA3A and EBNA3C in preventing the B cell to PC differentiation pathway.

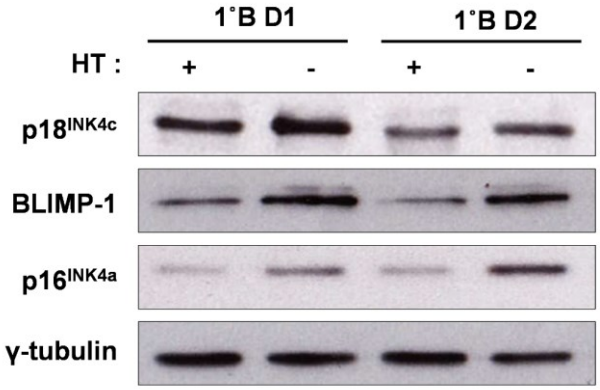


Figure 4.5. Elevated mRNA levels of $p18^{INK4c}$ and BLIMP-1 in EBNA3A/EBNA3C-null cells are consistent with protein levels. Expression of $p18^{INK4c}$, BLIMP-1 and $p16^{INK4a}$ (EBNA3A/EBNA3C target control) were shown by western blotting extracts from 3A3CERT2 infected $CD19^{+ve}$ primary B cells from 2 donors (1°B D1, 1°B D2) cultured with (+) or without (-) HT for 20 days. In each blot γ-tubulin was used as a loading control and was similarly consistent across all blots.

4.2.1.2. Activation of EBNA3A and EBNA3C reverses activation of p18^{INK4c} and BLIMP-1 transcription during primary B cell infection with EBV

Non-functional EBNA3A and EBNA3C results in elevated levels of p18^{INK4c} and BLIMP-1 transcription. Therefore, the ability of EBNA3A and EBNA3C to restrain the activation of p18^{INK4c} and BLIMP-1 transcription was investigated by activating the conditional EBNA3A and EBNA3C proteins during primary B cell infection.

To determine this, an experiment was performed using CD19^{+ve} B cells derived from a single donor infected with 3A3CERT2 recombinant EBV in which both EBNA3A and EBNA3C were expressed conditionally. Cells were either continuously grown in the absence (-) or presence of the activating ligand HT (+), or cells were initially grown without HT then HT added at either 4, 8 or 12 days pi and then cultured continuously with HT from this point onwards (ADD) to activate functional expression of EBNA3A and EBNA3C. Messenger RNA samples were taken every 4 days and expression of p18^{INK4c} and BLIMP1-1 mRNA was quantified by qPCR.

When EBNA3A and EBNA3C were activated at 4 days pi, BLIMP-1 mRNA levels rose initially over the first 12 days but then dropped to levels consistent with cells with continuously active EBNA3A and EBNA3C. In contrast, p18^{INK4c} mRNA levels did not rise when HT was added at this time point and levels remained consistent with cells with constitutively active EBNA3A and EBNA3C. Activation of EBNA3A and EBNA3C at 8- and 12-days pi led to repression of p18^{INK4c} (with reducing mRNA levels) but it appeared to take 10-15 days for levels to reduce to near that of cells with continuously functional EBNA3 proteins (Figure 4.6E/I). This is similar to BLIMP-1 repression, whereby activation of EBNA3A and EBNA3C at 8- or 12-days pi resulted in a reduction of BLIMP-1 mRNA to levels consistent to cells with continuously active EBNA3 proteins after 10-15 days (Figure 4.6F/J). This mirrored repression of p16^{INK4a} in the same cells under the same conditions (Figure 4.6G/K). Expression of the control housekeeping gene *ALAS1* was unaffected by the changes in EBNA3A and EBNA3C functionality (Figure 4.6D/H/L).

In conclusion, expression of both p18^{INK4c} and BLIMP-1 mRNA is repressed by the activation of EBNA3A and EBNA3C during primary B cell infection, further confirming EBV-mediated regulation of these PC differentiation associated factors.

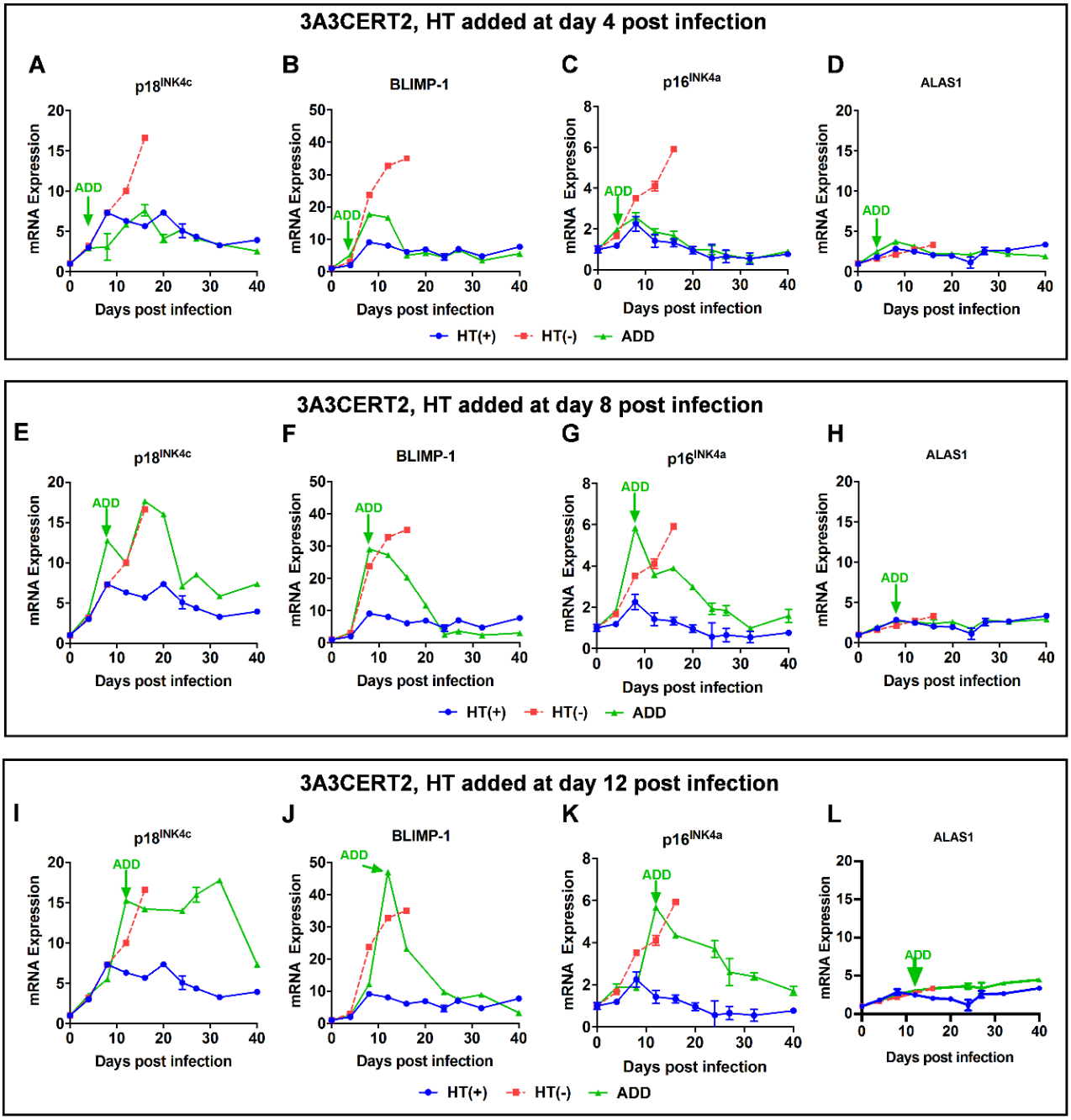


Figure 4.6. Elevated transcription of *CDKN2C* (p18^{INK4c}) and *PRDM1* (BLIMP-1) in 3A3CERT2 infected primary B cells is reversed by activation of EBNA3A and EBNA3C. CD19^{+ve} purified B cells from 1 independent donor were infected with 3A3CERT2 recombinant EBV and cultured for 30 days with 4-hydroxytamoxifen (HT) continuously (+), without HT (-), or HT was added after 4, 8 or 12 days (ADD) as indicated. *CDKN2C* (p18^{INK4c}; **A**, **E** and **I**), *PRDM1* (BLIMP-1; **B**, **F** and **J**), *CDKN2A* (EBNA3A/EBNA3C

target gene control; $p16^{INK4a}$; **C**, **G** and **K**) and *ALAS1* (control housekeeping gene; **D**, **H** and **L**) relative mRNA expression was normalised to the endogenous control *GNB2L1* with fold change shown relative to uninfected B cells at day 0. Error bars show the standard deviation of qPCR triplicates for each sample. Analysis of HT (-) at later time points was not possible because of large amounts of cell death in the culture. One representative example from two independent $CD19^{+ve}$ cell donors analysed.

4.2.1.3. EBNA3A and EBNA3C mediated repression of $p18^{INK4c}$ and BLIMP-1 becomes irreversible in primary B cells early after infection

It has been previously established by the Allday Laboratory and others that the genes encoding $p15^{INK4b}$ (*CDKN2B*) and $p16^{INK4a}$ (*CDKN2A*) are reversibly regulated by EBNA3A and EBNA3C. In conditional EBNA3A and EBNA3C cell lines, inactivation of EBNA3A and EBNA3C by removal of the activating ligand HT from the growth medium results in the reversal of EBNA3-mediated repression of $p15^{INK4b}$ and $p16^{INK4a}$, resulting in elevated mRNA and protein levels (Skalska et al., 2010, 2013; Styles et al., 2017). Reversible transcriptional regulation of the EBNA3A target STK39 (Bazot et al., 2018), EBNA3C target genes including COBLL1 and AICDA (Kalchschmidt et al., 2016a, 2016b) and combined EBNA3A and EBNA3C target genes including BIM (Paschos et al., 2012) has also been demonstrated. Therefore, the reversibility of EBNA3A- and EBNA3C-mediated transcriptional repression of $p18^{INK4c}$ and BLIMP-1 in LCLs was investigated.

LCLs derived from 3 independent donors with conditional expression of both EBNA3A and EBNA3C were assessed. Cells from the independent donors were infected with 3A3CERT2 recombinant EBV and grown continuously with HT for approximately 2 months (HT+), then half of the cells were washed and re-cultured in fresh media without HT (WASH) for 30 days, RNA and proteins samples were then harvested. In contrast to $p16^{INK4a}$, where expression was de-repressed by 30 days without HT (Figure 4.7A), qPCR analysis of the same cells reproducibly showed no increase in either $p18^{INK4c}$ or BLIMP-1 mRNA expression when EBNA3A and EBNA3C were inactivated for 30 days. This suggests repression of these 2 loci is not reversible under the same conditions, in contrast to *CDKN2A* and other EBNA3 target genes. Expression of the control housekeeping gene *ALAS1* was unaffected by inactivation EBNA3A and EBNA3C (Figure 4.7D). Western blot analysis of these cells confirmed the

same trend in p18^{INK4c} and BLIMP-1 expression at the protein level, with no increase in p18^{INK4c} or BLIMP-1 expression when EBNA3A and EBNA3C were non-functional for 30 days (Figure 4.7E).

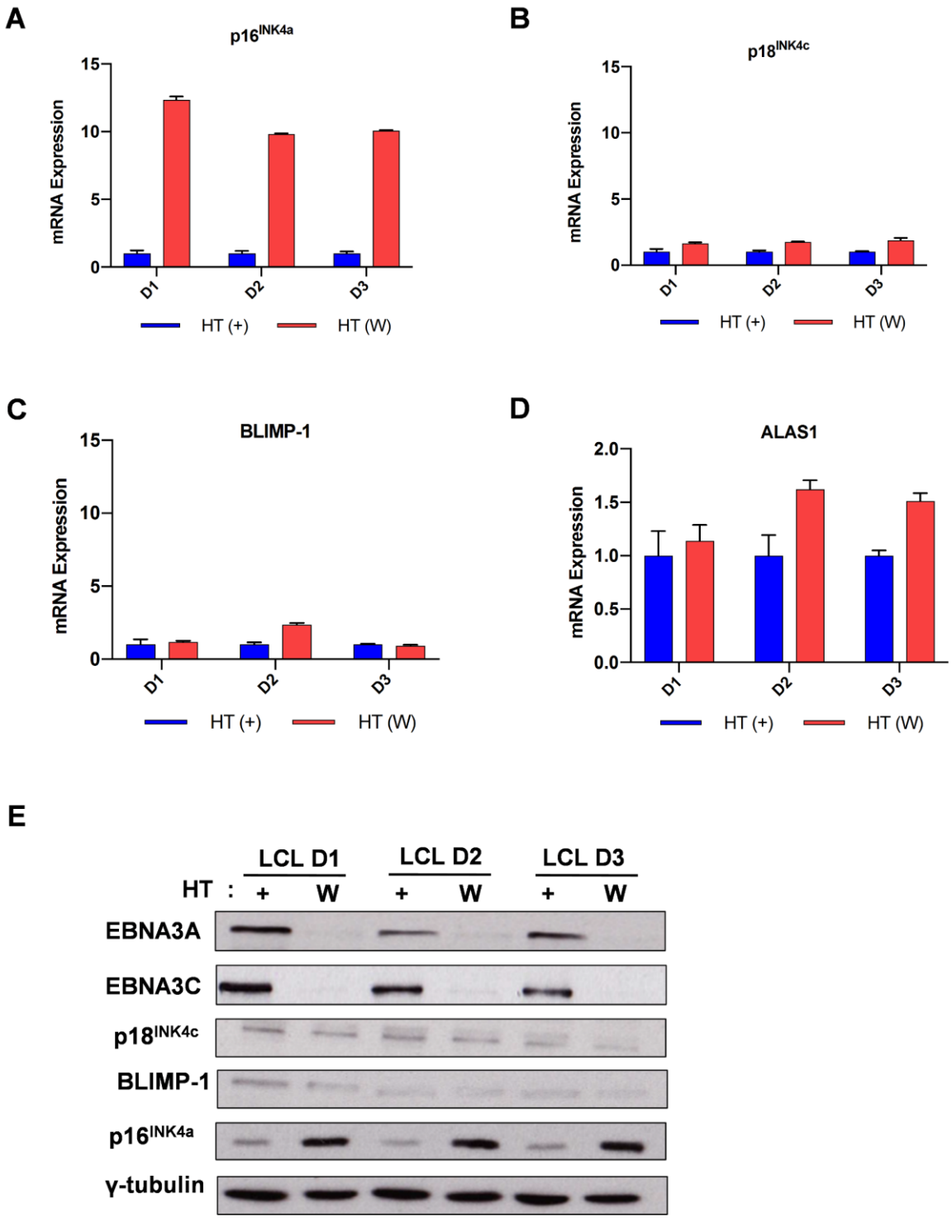


Figure 4.7. Repression of p18^{INK4c} and BLIMP-1 transcription is not reversible by inactivating EBNA3A/EBNA3C in newly established conditional LCLs. Newly established 3A3CERT2 cell lines (approximately 2 months post infection) derived from 3 independent donors (LCL D1, LCL D2, LCL D3)

were cultured with (+) or washed and grown without (W) 4-hydroxtamoxifen (HT) for 30 days. Analysis of expression of *CDKN2A* (EBNA3A/EBNA3C target gene control; $p16^{INK4a}$; **A**)*, CDKN2C* ($p18^{INK4c}$; **B**), *PRDM1* (BLIMP-1; **C**) and *ALAS1* (control housekeeping gene; **D**) mRNA was performed by quantitative PCR (qPCR) and relative mRNA expression was normalised to the endogenous control *GNB2L1,* with fold change shown relative to LCLs grown with (+) HT. Error bars indicate the standard deviation of qPCR triplicates for each sample. (**E**) Western blotting extracts of the same cells show expression of EBNA3A, EBNA3C, $p18^{INK4c}$, BLIMP-1 and $p16^{INK4a}$. In each blot γ-tubulin was used as a loading control and was similarly consistent across all blots. (Styles et al., 2017).

In contrast to the previous results, assessing established 3A3CERT2 LCLs which had been cultured in the continual presence of HT for over 6 months gave different results. Mirroring the data from newly established 3A3CERT2 conditional LCLs, repression of $p18^{INK4c}$ expression was maintained when EBNA3A and EBNA3C were inactivated by the removal of HT from long established 3A3CERT2 conditional LCLs for 30 days (W, Figure 4.8B). However, inactivation of EBNA3A and EBNA3C in these longer established LCL resulted in an increase in BLIMP-1 mRNA expression, mirroring the reversible regulation of $p16^{INK4a}$ (Figure 4.8A/C).

Western blot analysis of the same cells confirmed the trend in $p18^{INK4c}$ and BLIMP-1 mRNA expression. Elevated BLIMP-1 protein levels were seen following inactivation of EBNA3A and EBNA3C for 30 days, but the level of $p18^{INK4c}$ remained consistent regardless of EBNA3A and EBNA3C inactivation (Figure 4.8E). Taken together, these data suggest that, although BLIMP-1 may be reversibly regulated in established LCLs (cultured for over 6 months), this is not the same as newly established LCLs (cultured for 2 months) where it is irreversibly regulated. This suggests differential regulation to of $p16^{INK4a}$ (reversibly regulated under both conditions) and $p18^{INK4c}$ (irreversibly regulated under both conditions).

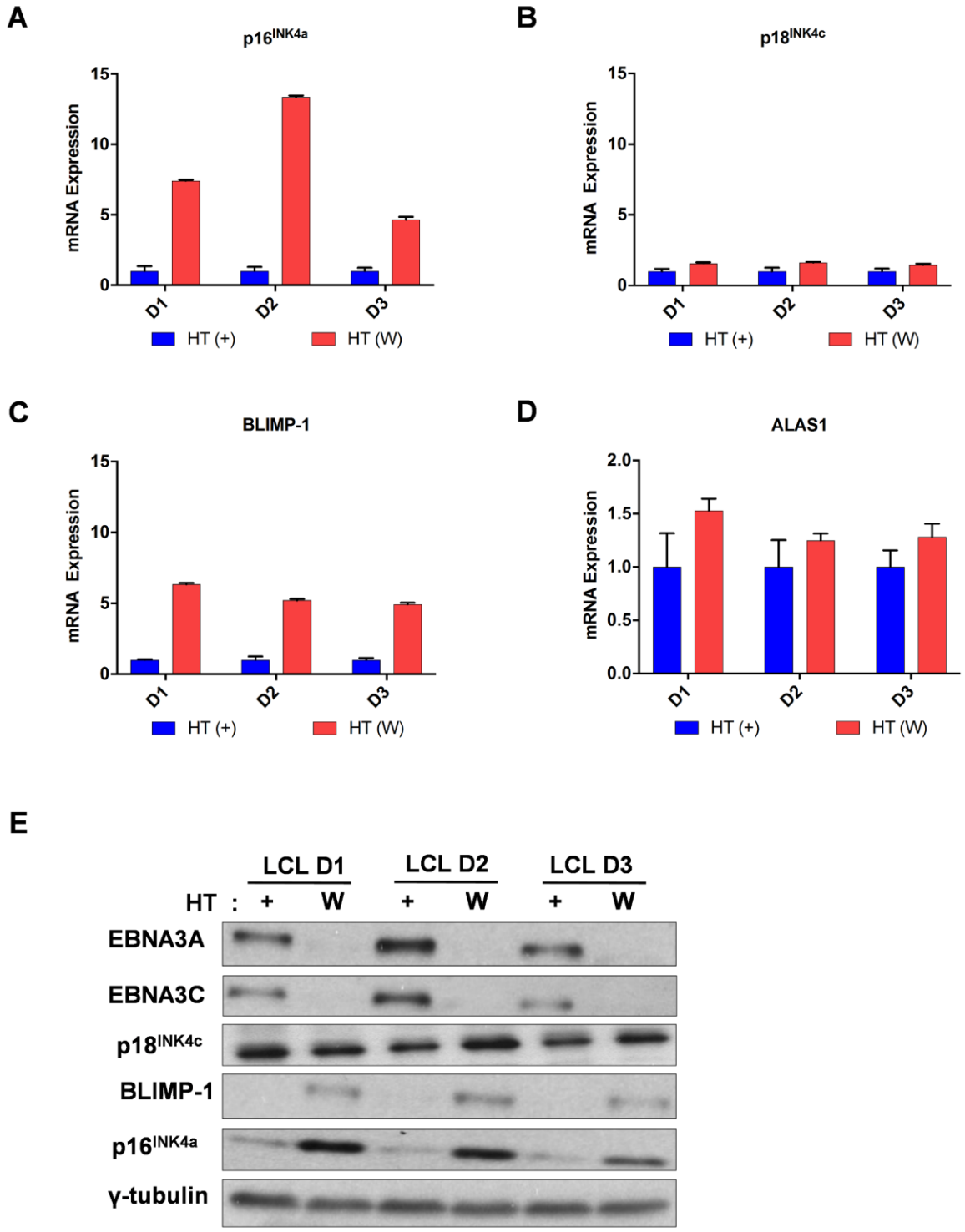


Figure 4.8. Repression of BLIMP-1, but not p18^{INK4c}, becomes reversible by inactivating EBNA3A/EBNA3C in well-established conditional LCLs. 3A3CERT2 cell lines established for 6 months derived from 3 independent donors (LCL D1, LCL D2, LCL D3) were cultured with (+) or washed and grown without (W) 4-hydroxtamoxifen (HT) for 30 days. Analysis of expression of *CDKN2A* (EBNA3A/EBNA3C target gene control; p16^{INK4a}; **A**), *CDKN2C* (p18^{INK4c}; **B**), *PRDM1* (BLIMP-1; **C**) and *ALAS1* (control housekeeping gene; **D**) mRNA was performed by quantitative PCR (qPCR) and relative mRNA expression was normalised to the endogenous control *GNB2L1,* with fold change shown relative

to LCLs grown with (+) HT. Error bars indicate the standard deviation of qPCR triplicates for each sample. (**E**) Western blotting extracts of the same cells show expression of EBNA3A, EBNA3C, $p18^{INK4c}$, BLIMP-1 and $p16^{INK4a}$. In each blot γ-tubulin was used as a loading control and was similarly consistent across all blots.

To further investigate the irreversible regulation of $p18^{INK4c}$ and BLIMP-1 in newly established LCLs, the time frame of irreversible repression occurrence within primary B cell infection with EBV was assessed. $CD19^{+ve}$ cells were infected with 3A3CERT2 conditional recombinant EBV and cultured with (+) or without (-) the activating ligand HT from the time of infection. HT was then washed out from the culture medium at 4, 8 or 12 days pi (WASH). mRNA samples were harvested every 4 days and qPCR analysis performed. When cells were grown in the presence of HT for 8 days pi then EBNA3A and EBNA3C inactivated by washing repression of $p18^{INK4c}$ and BLIMP-1 was no longer reversible, with mRNA levels remaining similar to that of cells where EBNA3A and EBNA3C were constitutively expressing (Figure 4.9E/F). This was consistent in data from cells where HT was washed out at 12 days pi, mirroring the results in newly established LCL (Figure 4.9I/J). By 8-12 days pi, cells appear to be committed to continual proliferation rather than differentiation, regardless of EBNA3 functionality. When HT was removed from the culture medium at 4 days pi there was an intermediate level of $p18^{INK4c}$ and BLIMP-1 mRNA expression compared to cells continuously grown in the absence of functional EBNA3 proteins. This demonstrates partial activation of $p18^{INK4c}$ and BLIMP-1, suggesting EBNA3A and EBNA3C act earlier in some cells (Figure 4.9A-D). Expression of the control housekeeping gene *ALAS1* was unaffected by the differing functionality of EBNA3A and EBNA3C (Figure 4.9D/H/L), and as expected $p16^{INK4a}$ was reversibly regulated under all conditions (Figure 4.9C/G/K).

These data indicate that irreversible regulation of $p18^{INK4c}$, and initially irreversible regulation of BLIMP-1 mediated by EBNA3A and EBNA3C occurs within 8-12 days of primary B cell infection with recombinant EBV.

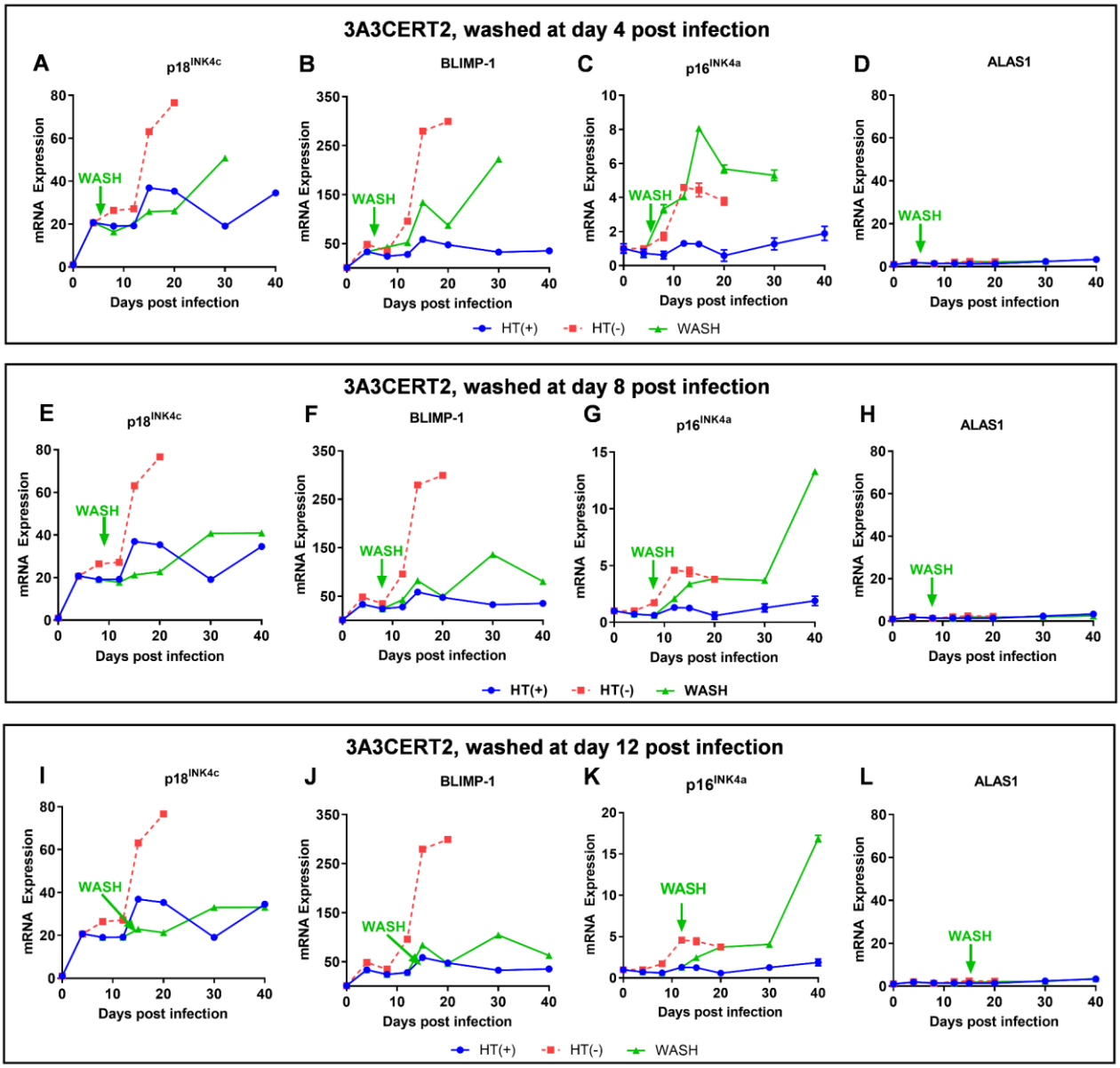


Figure 4.9. Repression of p18^{INK4c} and BLIMP-1 transcription occurs early after infection with EBV. CD19^{+ve} purified B cells from 1 independent donor were infected with 3A3CERT2 recombinant EBV and cultured for 30 days with 4-hydroxytamoxifen (HT) (+), without HT (-), or HT was removed after 4,8,12 or 16 days (WASH) as indicated. RNA samples were taken at the times after infection indicated and quantitative PCR (qPCR) analysis performed. *CDKN2C* (p18^{INK4c}; **A**, **E**, **I** and **M**), *PRDM1* (BLIMP-1; **B**, **F**, **J** and **N**), *CDKN2A* (p16^{INK4a}; **C**, **G**, **K** and **O**) and *ALAS1* (control housekeeping gene; **D**, **H**, **L** and **P**) relative mRNA expression was normalised to the endogenous control *GNB2L1* with fold change shown relative to uninfected B cells at day 0. Error bars show the standard deviation of qPCR triplicates for each sample. Analysis of HT (-) and day 4 washed cells at later time points was not possible because of large amounts of cell death in the culture. One representative example from three independent CD19^{+ve} cell donors analysed. [Published in part (Styles et al., 2017)].

4.2.2. EBNA3A/EBNA3C-null EBV infected primary B cells express a plasma-cell like phenotype

4.2.2.1. Expression of $p18^{INK4c}$ and BLIMP-1 in EBNA3A/EBNA3C-null cells is physiologically comparable to the levels found in two PC models

Since expression of both $p18^{INK4c}$ and BLIMP-1 is elevated in cells where EBNA3A and EBNA3C are non-functional, and both are associated with the PC differentiation pathway, the levels of $p18^{INK4c}$ and BLIMP-1 in EBNA3A/EBNA3C-null cells was compared to the physiological level found in 2 PC models. The first model utilized $CD19^{+ve}$ primary B cells isolated from 2 independent donors (PC1, PC2) which were incubated with CD40-L and IL21 for 7 days to induce PC differentiation [as described in (Deenick et al., 2013)]. Secondly, the myeloma/plasmacytoma-derived cell line U266 (Ikeyama et al., 1986) was used as a PC model as multiple myeloma cell lines are neoplasms arising from terminally differentiated PCs. It must be noted that there are limits to these models in comparison to true *in vivo* PC. *In vitro* induced differentiation of PC occurrs in only a subset of cells, with the absence of T cells and a GC reaction leading to short-lived PC rather than long lived PC (Deenick et al., 2013). Furthermore, U266 is a cancer cell line therefore contains aberrant mutations facilitating continuous proliferation not found in true *in vivo* PCs.

Expression of $p18^{INK4c}$ and BLIMP-1 mRNA was assessed in these PC systems and compared to those in $CD19^{+ve}$ cells (isolated from 3 independent donors; D1, D2, D3) infected with 3A3CERT2 recombinant EBV, and cultured with (+) or without HT (-) for 20 days. RNA was extracted and qPCR analysis performed.

The level of $p18^{INK4c}$ mRNA in EBNA3A/EBNA3C-null cells was generally higher than those in $CD19^{+ve}$ cells after 7 days induction of PC differentiation. In contrast, depending on the donor, the level in EBNA3A/EBNA3C-null cells were generally lower than the level in the U266 cell line (Figure 4.10A). Within the confines of the PC models, in which the levels of $p18^{INK4c}$ mRNA expression differed, the level of $p18^{INK4c}$ in EBNA3A/EBNA3C-null cells could be considered sufficient for PC differentiation.

BLIMP-1 mRNA levels were comparable (or higher depending on the donor) to CD19^{+ve} *in vitro* induced PCs and far exceed the level in U266 cells across all donors (Figure 4.10B). It can therefore be concluded that the elevated levels of the PC differentiation factor BLIMP-1, induced in EBV infected cells with non-functional EBNA3A and EBNA3C, are comparable to physiological levels found in the 2 PC models assessed. This suggests the level of p18^{INK4c} and BLIMP-1 in EBNA3A/EBNA3C-null cells could be considered appropriate to drive PC differentiation.

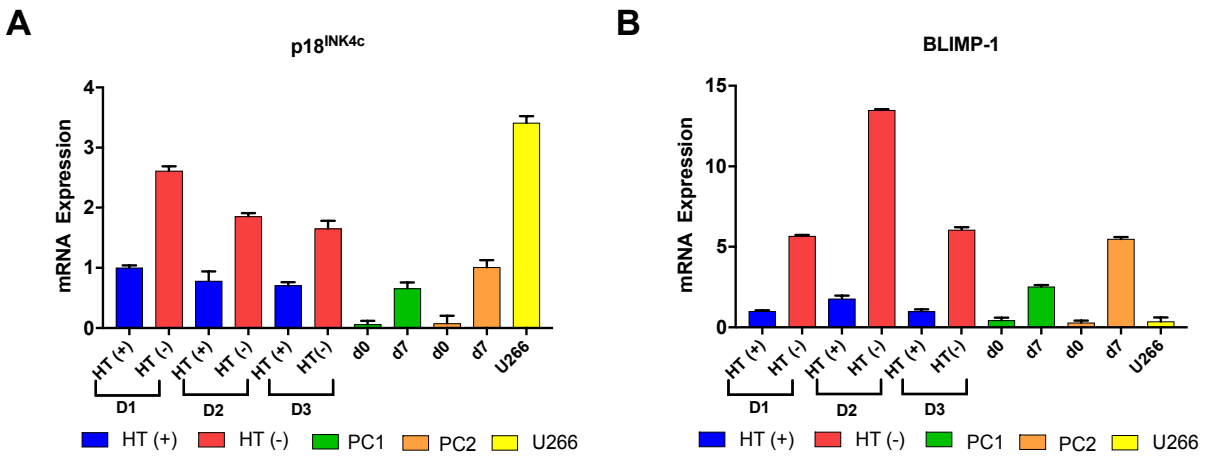


Figure 4.10. Expression of PC differentiation associated factors in EBNA3A/EBNA3C-null cells and PC models. RNA samples were taken from U266 cells, CD19^{+ve} purified B cells from 2 donors at day 0 (d0) and 7 days post induction (d7) with CD40-L/IL21 (PC1, PC2), and from CD19^{+ve} purified B cells from 3 independent donors (D1, D2, D3) infected with 3A3CERT2 recombinant EBV and grown for 20 days with (+) or without (-) HT, and qPCR performed. (**A**) *CDKN2C* (p18^{INK4c}) and (**B**) *PRDM1* (BLIMP-1) mRNA expression was normalized to the endogenous control *GNB2L1* with fold change shown relative to D1 grown with HT (+) 0. Error bars show the standard deviation of qPCR triplicates for each sample. [Published in part (Styles et al., 2017)].

4.2.2.2. BLIMP-1 target genes are differentially expressed in EBNA3A/EBNA3C-null cells

Since EBNA3A and EBNA3C regulate the PC differentiation transcriptional regulator BLIMP-1, differential expression of BLIMP-1 target genes was assessed in cells with non-functional EBNA3A and EBNA3C to determine whether the elevated levels of BLIMP-1 were functional. *SPIB* and *LMO2* are transcriptionally repressed by BLIMP-1, and *XBP1* is transcriptionally activated by BLIMP-1 (Cubedo et al., 2011; Minnich et al., 2016; Schmidlin et al., 2008). CD19^{+ve} primary B cells were isolated from a

single donor and infected with 3A3CERT2 recombinant EBV and then cultured with (+) or without HT (-), or infected with WT or infected with E3KO (EBNA3 locus deleted) and cultured for 30 days. From 10 days pi mRNA samples were harvested at 5 days intervals and expression of BLIMP-1 target genes quantified by RT-qPCR over the first 30 days of infection.

Consistent with progressively elevated levels of functional BLIMP-1 between 10-25 days pi in cells with inactive EBNA3A and EBNA3C (3A3CERT2-), transcription of the BLIMP-1 repressed genes *SPIB* and *LMO2* was concurrently substantially reduced over this time frame (Figure 4.11A/C/E). This indicates that the BLIMP-1 activated by EBV infection with non-functional EBNA3A and EBNA3C has retained its repressive functions. Furthermore, mRNA levels of the BLIMP-1 activated gene *XBP1* progressively increased over the time frame when EBNA3A and EBNA3C were non-functional in parallel with progressively elevated levels of BLIMP-1, demonstrating transcriptional activation by BLIMP-1 is sustained in these cells (Figure 4.11G). This phenotype was mirrored in cells where the entire EBNA3 locus has been deleted (E3KO) compared to cells expressing all EBNA3 proteins (WT, Figure 4.11B/D/F/H).

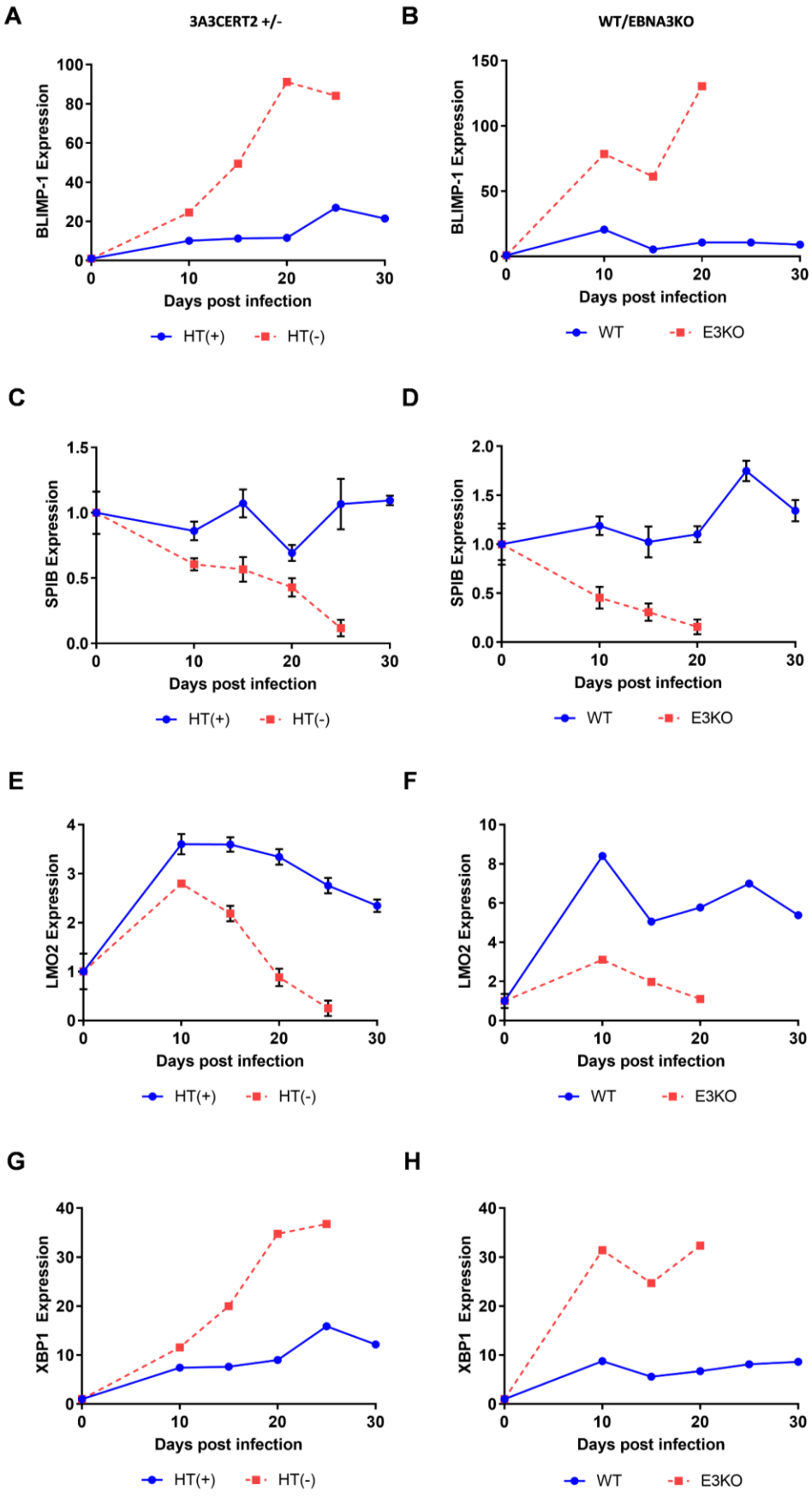

A
3A3CERT2 +/-
BLIMP-1 Expression
Days post infection
HT(+)
HT(-)
B
WT/EBNA3KO
BLIMP-1 Expression
Days post infection
WT
E3KO
C
SPIB Expression
Days post infection
HT(+)
HT(-)
D
SPIB Expression
Days post infection
WT
E3KO
E
LMO2 Expression
Days post infection
HT(+)
HT(-)
F
LMO2 Expression
Days post infection
WT
E3KO
G
XBP1 Expression
Days post infection
HT(+)
HT(-)
H
XBP1 Expression
Days post infection
WT
E3KO

Figure 4.11. Differential expression of BLIMP-1 target genes in EBNA3A/EBNA3C-null cells following primary B cell infection. CD19^{+ve} purified B cells were infected with 3A3CERT2 recombinant EBV and cultured with (+) or without (-) HT (**A**/**C**/**E**/**G**) for 30 days, or EBNA3 KO (E3KO) and 'WT' (B95.8-BAC) (**B**,**D**,**F**,**H**) and cultured for 30 days. RNA samples were taken at the times after infection indicated and qPCR analysis performed. *PRDM1* (BLIMP-1; **A** and **B**), *SPIB* (**C** and **D**), *LMO2* (**E** and **F**) and *XBP1* (**G** and **H**) relative mRNA expression was normalised to the endogenous control *GNB2L1* and fold change is shown relative to uninfected B cells at day 0. Error bars show the standard deviation of qPCR triplicates for each sample. Analysis of HT (-) infected cells at later time points was not possible because of large amounts of cell death in the culture**.** (Styles et al., 2017).

Elevated transcription of *XBP1*, and repression of *SPIB* and *LMO2*, was consistent across cells derived from 3 independent donors infected with 3A3CERT2 recombinant EBV when cultured in the absence (-) of HT for 20 days (Figure 4.12). Furthermore, when EBNA3A and EBNA3C are inactivated, levels of SPIB and LMO2 approached those seen in the PC model U266 (Figure 4.12A/B), whereas the level of XBP-1 mRNA in U266 cells is comparable to cells with functional EBNA3A and EBNA3C and far exceeds the level in U266 cells when EBNA3A and EBNA3C are inactive (Figure 4.12C). This indicates that the elevated levels of BLIMP-1 in EBNA3A/EBNA3C-null cells are transcriptionally functional.

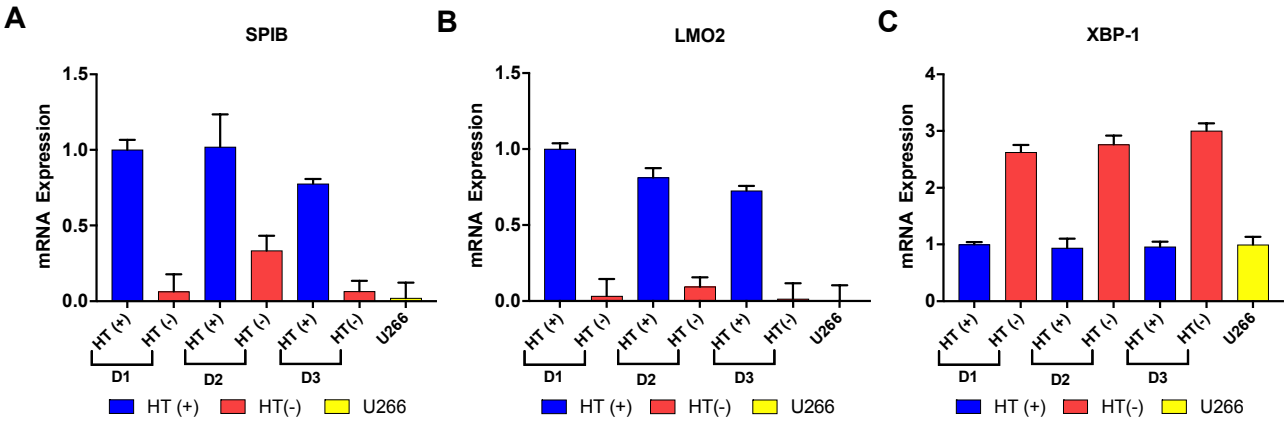


Figure 4.12. Expression of BLIMP-1 target genes in XBP-1, SPIB and LMO2 and in EBNA3A/EBNA3C-null cells and the plasmacytoma-derived cell line U266. RNA samples were taken from U266 cells and CD19^{+ve} purified B cells from 3 independent donors (D1, D2, D3) infected with 3A3CERT2 recombinant EBV and grown for 20 days with (+) or without (-) 4-hydroxtamoxifen (HT), and quantitative PCR (qPCR) performed. *SPIB* (**A**) LMO2 (**B**) and *XBP-1* (**C**) mRNA expression was normalized to the endogenous control *GNB2L1* with fold change shown relative to D1 grown with HT (+) 0. Error bars show the standard deviation of qPCR triplicates for each sample. (Published in part (Styles et al., 2017).

Aside from the transcriptional regulator BLIMP-1, IRF4 is another major transcription factor implicated in the PC differentiation pathway [see Chapter I, Section 1.1.4, (Nam and Lin, 2016)]. In contrast to BLIMP-1, IRF4 levels are unaffected by the functionality of EBNA3A and EBNA3C. Western blotting extracts from $CD19^{+ve}$ B cells infected with 3A3CERT2 recombinant EBV and cultured with (+) or without HT (-) for 20 days, alongside 3A3CERT2 conditional LCLs cultured with (+) or washed and grown without HT (W) for 30 days demonstrated consistent IRF4 levels irrespective of addition of HT and EBNA3 functionality. Levels in both newly infected cells and LCLs were comparable to the PC model U266 (Figure 4.13).

Together this data shows that the BLIMP-1 induced by EBV infection where EBNA3A and EBNA3C are non-functional is transcriptionally functional, and maintains its suppressive and activation transcriptional functions. Furthermore, the levels of the PC differentiation factors XBP-1, SPIB, LMO2 and IRF4 in EBNA3A/EBNA3C-null cells were comparable to levels in the PC model U266.

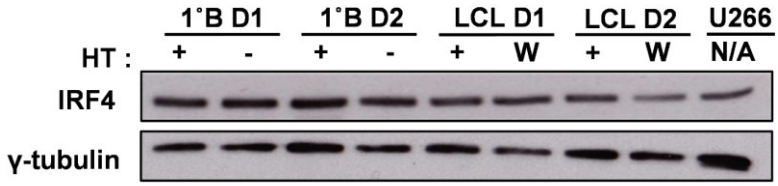


Figure 4.13. IRF4 protein levels are not affected by EBNA3A/EBNA3C functionality. Expression of IRF4 shown by western blotting extracts from 3A3CERT2 infected $CD19^{+ve}$ primary B cells from 2 donors (1˚B D1, 1˚B D2) grown with (+) or without (-) HT for 20 days and 3A3CERT2 conditional LCLs from 2 donors (LCL D1, LCL D2) grown with HT (+) or washed and grown without HT for 30 days (W). An extract from the myeloma/plasmacytoma cell line U266 is shown for comparison. In each blot γ-tubulin was used as a loading control and was similarly consistent across all blots. (Styles et al., 2017).

4.2.2.3. EBNA3A/EBNA3C-null cells express elevated levels of PC surface markers

With regards to the PC differentiation associated factors described above, EBNA3A/EBNA3C-null cells express a transcriptional profile similar to that of PCs. Therefore, the PC surface phenotype of $CD19^{+ve}$ B cells infected with 3A3CERT2 with inactive EBNA3A and EBNA3C was investigated further

and the presence of PC surface markers was assessed by flow cytometry. Expression of CD138 (Syndecan-1) and elevated CD38 levels, alongside absence or down-regulation of CD20 and expression of CD27 are considered to be the defining characteristics of PCs. Expression of these markers was therefore used to characterise a PC phenotype in EBV infected cells.

Following infection of $CD19^{+ve}$ primary B cells with 3A3ERT2 recombinant for 20 days pi, approximately 20% of cells with non-functional EBNA3A and EBNA3C could be described as exhibiting a PC-like phenotype, characterised by high levels of CD38 and expression of CD138 (Figure 4.14A). However, there is a distinct shift in expression of CD38 in the majority of cells with inactive EBNA3A and EBNA3C (HT-), compared to when the proteins are functional (HT+). This indicates that many cells with inactive EBNA3A and EBNA3C were responding to increases in expression of the PC differentiation associated factors $p18^{INK4c}$ and BLIMP-1 and are potentially progressing along a PC-like differentiation pathway, however cannot yet be considered PC-like.

Alongside CD38 and CD138, there was also a shift in expression of CD27 with elevated levels in cells with inactive EBNA3A and EBNA3C, with levels exceeding that in U266 cells (Figure 4.14D). Furthermore, there was a reduction in CD20 expression in cells with non-functional EBNA3A and EBNA3C, approaching levels seen in the PC model U266 (Figure 4.14E). Cells with reduced CD20 likely correspond to those exhibiting a PC phenotype when characterised by CD138 expression and high levels of CD38. The phenotypic analysis of cell surface markers shows that in the absence of EBNA3A and EBNA3C, concurrent with elevated levels of PC differentiation associated factors, EBV-infected cells express an increasingly PC-like phenotype. This further indicates EBNA3A and EBNA3C are functioning to prevent PC differentiation following infection of primary B cells by EBV.

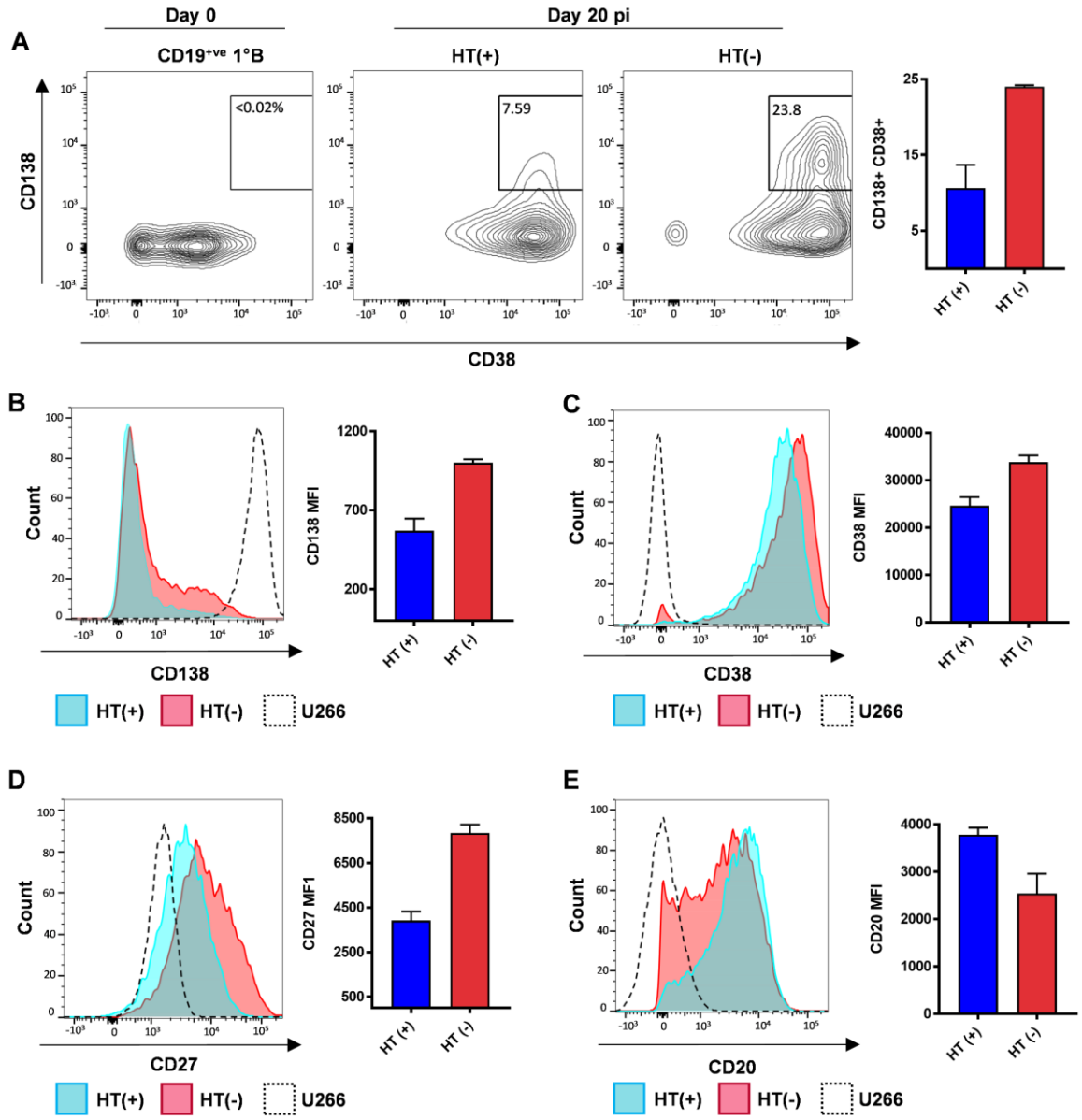


Figure 4.14. Flow cytometric analysis shows a plasmablast/PC-like phenotype in EBNA3A/EBNA3C-null cells. U266 cells (black) and CD19^{+ve} purified B cells infected with 3A3CERT2 recombinant EBV and cultured with (+, blue) or without (-, red) HT for 20 days, were analysed for CD138, CD38, CD27 and CD20 expression by flow cytometry. (**A**) Contour plots show CD38 and CD138 surface expression, the quadrant value represents the percentage of live single cells expressing both markers, mean percentage of CD138^{+} and CD38^{high} cells from 2 independent donors are also shown. Histograms show expression of CD138 (**B**), CD38 (**C**), CD27 (**D**) and CD20 (**E**) and corresponding mean fluorescence intensity of positive cells from 2 independent donors. Error bars show standard deviation from the 2 donors. Histograms and contour plots shown are one representative example from two independent experiments (Styles et al., 2017).

4.2.2.4. EBNA3A/EBNA3C-null cells express elevated immunoglobulin levels

Considering EBV infected cells with non-functional EBNA3A and EBNA3C express a PC-like phenotype, concurrent expression of Ig was assessed by flow cytometry. $CD19^{+ve}$ primary B cells treated with CD40-Ligand and IL21 for 7 days *in vitro* to induce PC differentiation were used a positive control for expression of Ig. Cells with inactive EBNA3A and EBNA3C at 20 days pi with 3A3CERT2 recombinant EBV exhibited a distinct shift in expression of IgG compared to cells with functional EBNA3 proteins. IgG expression in approximately 20% of cells with inactive EBNA3A and EBNA3C reached that of the CD40-L/IL21 treated induced PCs, corresponding to the 20% of cells with inactive EBNA3A and EBNA3C exhibiting a PC phenotype (Figure 4.15A). In addition, there was also a shift in IgM expression, with elevated levels in all cells with non-functional EBNA3A and EBNA3C with levels exceeding those in CD40-L/IL21 treated induced PCs (Figure 4.15B). Alongside PC surface markers, expression of Ig in EBV infected cells in the absence of EBNA3A and EBNA3C further indicates a role for EBNA3 proteins in suppression of the PC differentiation pathway.

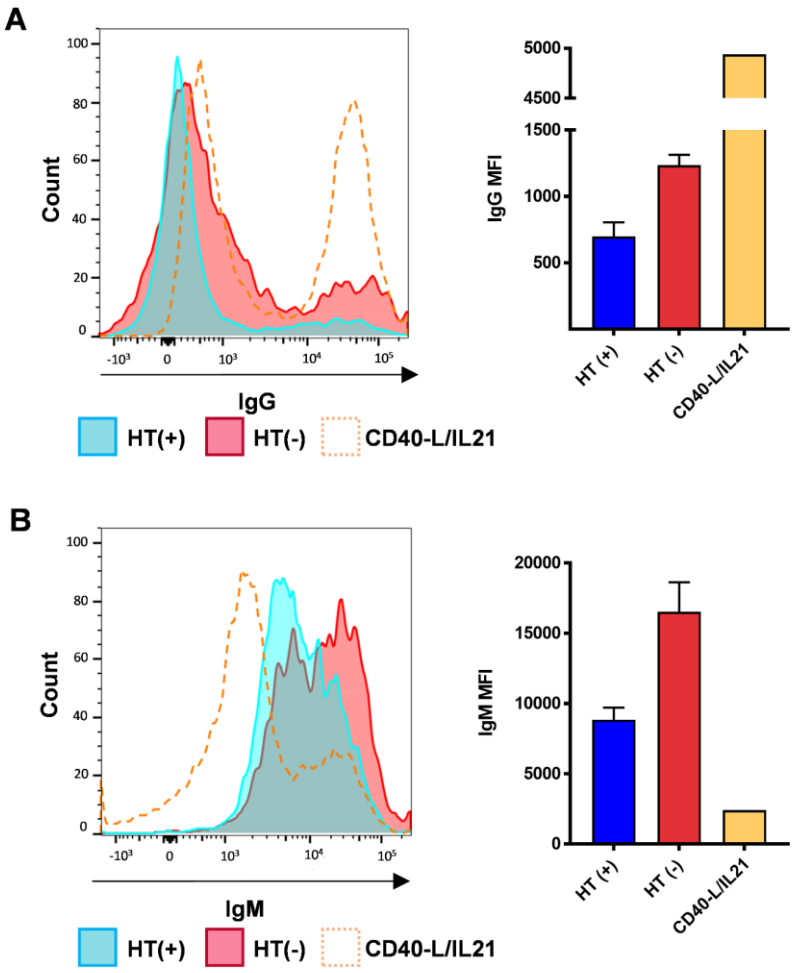


Figure 4.15. Primary B cells infected with 3A3CERT2 recombinant EBV express IgG and IgM. CD19^{+ve} purified B cells were infected with 3A3CERT2 recombinant EBV and cultured with (+, blue) or without (-, red) 4-hydroxtamoxifen (HT) for 20 days, then analysed for IgG and IgM expression by flow cytometry. Histograms show expression of IgG (**A**) and IgM (**B**) alongside corresponding mean fluorescence intensity of positive cells from 2 independent donors. PCs induced *in vitro* with CD40-ligand/IL21 were used as a control (orange). Error bars show standard deviation from 2 donors. Histograms shown are one representative example from two independent experiments (Styles et al., 2017).

4.2.3. Lytic cycle reactivation is not evident in EBNA3A/EBNA3C-null cells

The current GC model of EBV persistence suggests that the differentiation of latently infected MBC to PC is coupled with activation of the viral lytic cycle, with EBV replication demonstrated in rare cells during PC differentiation in the tonsils of healthy carriers (Laichalk and Thorley-Lawson, 2005). As it is suggested that PC differentiation of EBV infected cells results in lytic virus production, evidence of this process was assessed in cells with non-functional EBNA3A and EBNA3C which exhibit a PC-like phenotype.

Expression of mRNA of the lytic switch protein BZLF1 was assessed by qPCR in $CD19^{+ve}$ B cells purified from 4 independent donors (D1, D2, D3, D4) infected with 3A3CERT2 recombinant EBV and cultured with (+) or without HT (-) for 20 days. Although it could be predicted that BZLF1 would be activated concurrently with $p18^{INK4c}$ and BLIMP-1 transcription, no consistent correlation is seen in BZLF1 mRNA expression when EBNA3A and EBNA3C were inactive or active (Figure 4.16). Western blot analysis of protein extracts from $CD19^{+ve}$ B cells purified from 4 independent donors (1°B D1, 1°B D2, 1°B D3, 1°B D4) infected with 3A3CERT2 recombinant EBV and cultured with or without HT for 20 days did not reveal expression of the lytic protein BZLF1 despite the presence of BZLF1 mRNA. Furthermore, expression of the EBV lytic proteins BALF5 or p18-VCA was also not seen in cells with either active or inactive EBNA3A or EBNA3C (Figure 4.17). Despite exhibiting a PC-like phenotype, no evidence of lytic cycle activation was seen in cells with non-functional EBNA3A and EBNA3C.

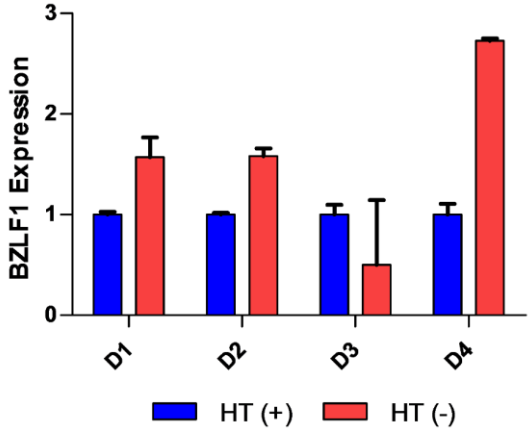


Figure 4.16. Evidence of activation of BZLF1 transcription is inconclusive in 3A3CERT2 infected cells. RNA samples were taken from CD19^{+ve} purified B cells from 4 independent donors (D1, D2, D3, D4) infected with 3A3CERT2 recombinant EBV and grown for 20 days with (+) or without (-) HT, and qPCR performed. *BZLF1* mRNA expression was normalized to the endogenous control *GNB2L1* with fold change shown relative to uninfected cells grown with HT. Error bars show the standard deviation of qPCR triplicates for each sample.

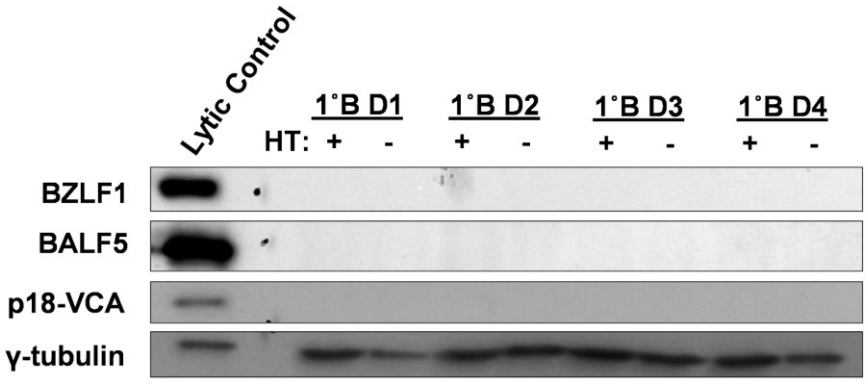


Figure 4.17. Lytic protein activation is not evident by western blot in 3A3CERT2 infected primary B cells. Expression of BZLF1, BALF5 and p18-VCA were demonstrated by western blotting extracts from a lytic control (293 virus producer cell line) and CD19^{+ve} purified B cells from 4 independent donors (D1, D2, D3, D4) infected with 3A3CERT2 recombinant EBV and cultured with 4-hydroxytamoxifen (HT) (+) or without (-) for 20 days. γ-tubulin was used as a loading control and was similarly consistent across all blots.

4.3. Summary

The results in this chapter provide a clear link between the EBV oncogenic transcription factors EBNA3A and EBNA3C, and the suppression of a transcription programme that results in the differentiation of B cells toward the phenotype of a terminally differentiated PC.

Inactivation of EBNA3A and EBNA3C through the use of the conditional 3A3CERT2 recombinant EBV virus resulted in elevated mRNA and protein levels of the CDKI and B cell differentiation factor $p18^{INK4c}$, and the major PC differentiation transcriptional regulator BLIMP-1. Expression of $p18^{INK4c}$ and BLIMP-1 in these cells could be restrained by the activation of EBNA3A and EBNA3C further indicating EBNA3A- and EBNA3C-mediated regulation of $p18^{INK4c}$ and BLIMP-1. Interestingly, inactivating EBNA3A and EBNA3C in newly established conditional LCLs did not result in loss of $p18^{INK4c}$ and BLIMP-1 repression, in contrast to the reversible repression of other EBNA3 target genes. Furthermore, repression of $p18^{INK4c}$ and BLIMP-1 by EBNA3A and EBNA3C was shown to be established by 8 days pi. However, in LCLs grown in prolonged culture for over 6 months, inactivation of EBNA3A and EBNA3C led to an increase in BLIMP-1, but not $p18^{INK4c}$. Together this indicates EBNA3A and EBNA3C are regulating transcription of $p18^{INK4c}$ and BLIMP-1, but by mechanisms independent of each other, and to other established EBNA3 target genes.

The levels of $p18^{INK4c}$ and BLIMP-1 in EBNA3A/EBNA3C-null cells was largely comparable to those found in two PC models, indicating these levels would be sufficient to drive PC differentiation. In addition, BLIMP-1 target genes responded accordingly to the increased levels of BLIMP-1 in cells with non-functional EBNA3A and EBNA3C. Elevated levels of the PC differentiation factors $p18^{INK4c}$ and BLIMP-1 in EBNA3A/EBNA3C-null cells corresponded with phenotypic expression of cell surface markers characteristic of PCs including CD138 and CD38, as well as elevated Ig production. However, although reactivation of the EBV lytic cycle is thought to occur following the differentiation of PC from latently infected MBC, no evidence of increased expression of EBV lytic genes were identified in EBNA3A/EBNA3C-null cells undergoing differentiation characteristic of PC.

4.4. Discussion

4.4.1. EBNA3A- and EBNA3C-mediated repression of $p18^{INK4c}$ and BLIMP-1

Deletion or biochemical inactivation by manipulation of the *EBNA3A* and *EBNA3C* genes in recombinant EBV viruses used to infected in $CD19^{+ve}$ primary B cells, reveals that EBNA3A and EBNA3C

both repress activation of the CDKI and PC differentiation factor p18^{INK4c} (encoded by *CDKN2C*) and the master regulator of PC differentiation BLIMP-1 (encoded by *PRDM1*) (Figures 4.1, 4.2 and 4.4). Activation of EBNA3A and EBNA3C in EBNA3A/EBNA3C-null cells by addition of the activating ligand HT at 4, 8 and 12 days pi restrains activation of p18^{INK4c} and BLIMP-1 transcription (Figure 4.6). Furthermore, the repression of p18^{INK4c} and BLIMP-1 did not require continuous expression of EBNA3A and EBNA3C and repression becomes independent of EBNA3A and EBNA3C by 8 days pi with EBV (Figure 4.9).

Following the result that EBNA3A and EBNA3C repress activation of both p18^{INK4c} and BLIMP-1, a recent ChIP-seq analysis performed on LCLs by Dr Paschos was interrogated. This revealed that EBV-recombinants expressing epitope-tagged EBNA3A or EBNA3C bind multiple sites on chromatin across the *CDKN2C* (p18^{INK4c}) and *PRDM1* (BLIMP-1) loci notably at regulatory elements, indicating that EBNA3A and EBNA3C play a direct repressive role and p18^{INK4} and BLIMP-1 (Styles et al., 2017). The targeting of EBNA3A and EBNA3C to regulatory elements within the *CDKN2C* and *PRDM1* loci was confirmed by ChIP-qPCR, where EBNA3A/EBNA3C-induced deposition of the repressive histone mark H3K27me3, catalysed by the EZH2 subunit of the PRC2 complex, was confirmed (Styles et al., 2017). This method of transcriptional repression is also seen in EBNA3A- and EBNA3C-mediated repression of the pro-apoptotic factor *BCL2L11* (BIM) and the CKDIs *CDKN2A* (p16^{INK4a}) and *CDKN2B* (p15^{INK4b}) (Jiang et al., 2017; Paschos et al., 2012; Skalska et al., 2010). However, the absence of sustained functional EBNA3A and EBNA3C leads to activation of p15^{INK4b}, p16^{INK4a} and BIM transcription (Paschos et al., 2012; Skalska et al., 2010; Styles et al., 2017). This contrasts regulation of p18^{INK4c} and BLIMP-1 which are the first, and currently only, genes identified as epigenetically repressed by EBNA3 proteins in newly established LCLs, whereby repression becomes independent of EBNA3 proteins (Figures 4.7 and 4.8). BLIMP-1 and p18^{INK4c} appear to be differentially regulated from each other, as well as from p16^{INK4a}, p15^{INK4b} and BIM. Whereas *CDKN2A* is reversibly repressed in newly established (2 months in culture, Figure 4.7) and in established conditional LCL (over 6 months in culture, Figure 4.8), and p18^{INK4c} consistently irreversibly repressed under both conditions, repression of BLIMP-1 is irreversible

in newly established LCL but becomes reversible in older established LCL. It would be of interest to determine the features of the $p18^{INK4c}$ and BLIMP-1 loci that permit the sustained repression of these B cell differentiation factors in the absence of EBNA3A and EBNA3C, and whether this irreversibility of $p18^{INK4c}$ or late stage reversibility of BLIMP-1 is related to requirements of gene expression during sustained infection.

The reversibility EBNA3A/EBNA3C-mediated regulation of BLIMP-1 in LCLs in prolonged culture compared to newly established LCLs is possibly reflective of the monoclonal nature of LCL cell lines. The progeny of a single B lymphocyte is primary represented in a long established LCL (Plagnol et al., 2008; Ryan et al., 2006). In contrast, EBV infection of primary B cells and newly established LCLs is more representative of a polyclonal B cell population. Alternatively, the secondary effects of prolonged LCL culture may be influencing gene regulation, with B cells undergoing primary EBV-mediated transformation and proliferation shown to have a growth and survival phenotype distinct from that of established LCLs (Price et al., 2012). Indeed, microarray analysis has indicated differential regulation of some EBNA3A target genes in newly established LCLs compared to long-term LCLs (Hertle et al., 2009). This is consistent with differential EBNA3-mediated regulation of BLIMP-1 between the LCLs of different ages. Alternatively, the reversibility of BLIMP-1 repression at a later point in EBV infection could be mediated by the virus. It is possible EBV represses BLIMP-1 during primary infection with EBV, then permits de-repression in cells where latency has been achieved, to prevent PC differentiation occurring before latent infection has been established. EBV may mediate activation of BLIMP-1 at a later stage of infection as it is essential for the differentiation of latently infected MBCs to PCs, which is required for reactivation of the EBV lytic cycle (Laichalk and Thorley-Lawson, 2005). The mechanisms surrounding the initially irreversible, then reversible, regulation of BLIMP-1 by EBNA3A and EBNA3C are presently unknown. It would be of interest to determine the novel EBNA3A and EBNA3C transcriptional regulatory mechanisms responsible for irreversible gene regulation, and whether it relates to the lytic reactivation stage of the EBV life cycle.

Interestingly, aside from their roles in PC differentiation, both p18^{INK4c} and BLIMP-1 have been identified as tumour suppressors. It has been shown p18^{INK4c} cooperates with the lymphoid differentiation regulator Gata3 to suppress B cell lymphomas (Liu et al., 2016). Furthermore, deletion of p18^{INK4c} is frequently observed in human B cell lymphomas (Beà et al., 2009; Mestre-Escorihuela et al., 2007; Sanchez-Aguilera, 2004) and deletion of one or both of the *p18^{INK4c}* alleles significantly promotes tumorigenesis in mice (Bai et al., 2003). In addition, nearly 50% of Reed-Sternberg cells in Hodgkin's lymphoma lack p18^{INK4c} expression, which is associated with an unfavourable prognosis (Sanchez-Aguilera, 2004). As with p18^{INK4c}, *PRDM1* is frequently deleted in human B cell lymphomas (Jackson et al., 2000; Pasqualucci et al., 2006; Thelander et al., 2008). In particular, *PRDM1* inactivation is often identified in cases of DLBCL and is thought to contribute to lymphomagenesis (Calado et al., 2010; Mandelbaum et al., 2010; Pasqualucci et al., 2006). Furthermore, deletion of mouse BLIMP-1 *in vivo* promotes lymphoproliferative disorders and mimics ABC-DLBCL pathology (Mandelbaum et al., 2010). It is likely that in B cell lymphomas resulting from EBV infection, the inactivation of these tumour suppressors by EBNA3A and EBNA3C enhances oncogenic progression.

4.4.2. Suppression of the B cell to PC pathway by EBNA3A and EBNA3C

The results in this chapter indicate that the biological aim of EBNA3A- and EBNA3C- mediated repression of the PC differentiation factors p18^{INK4c} and BLIMP-1 is to achieve suppression of the PC differentiation pathway. Unfortunately, the elevated levels of p18^{INK4c} and BLIMP-1 cannot be consequentially equated to physiological levels in PCs due to the limitations in PC models. Nonetheless, of the available PC models (ie the U266 plasmacytoma cell line and *in vitro* induced PC), levels of p18^{INK4c} and BLIMP-1 are largely comparable or exceed levels found in these 2 PC models (Figure 4.10). Furthermore, BLIMP-1 differentiation associated target genes responded as predicted to EBNA3A/EBNA3C-null EBV-induced BLIMP-1 activation (Figures 4.11 and 4.12). EBV-mediated suppression of the PC differentiation pathway was confirmed when flow cytometry identified the phenotypic consequences of elevated levels of these PC differentiation factors was shown to correlate with increased levels of markers characteristic of PC (namely CD138 expression and high levels of

CD38) and elevated IgG and IgM production in EBNA3A/EBNA3C-null cells at 20 days pi (Figures 4.14 and 4.15).

It is probable that the additional consequences of EBV infection compounded with the consequences of non-functional EBNA3A and EBNA3C are preventing the complete terminal differentiation of EBNA3A/EBNA3C-null EBV infected cells to PC. It is likely that the impaired proliferative capacity and elevating levels of $p16^{INK4a}$ in these cells, resulting in cell cycle arrest, is contributing to this (Skalska et al., 2010, 2013). It would be of interest to determine whether $p16^{INK4a}$-null cells are capable of complete terminal differentiation of PC in the absence of functional EBNA3A and EBNA3C.

EBV-mediated repression of $p18^{INK4c}$ and BLIMP-1 becomes independent of EBNA3A and EBNA3C in newly established LCLs, which likely relates to the establishment of EBV latency in MBCs (Roughan and Thorley-Lawson, 2009). It is thought that upon EBV infection of a quiescent, mature human B cells, the cell becomes activated and grows, and within a few days rapid proliferation begins. The GC model of persistence suggests that *in vivo,* depending on availability of T cells, or T cell-derived factors, cells differentiate and progress through the GC, a process through which viral gene expression is sequentially silenced. Infected cells leave the GC as latently infected MBC which do not express viral proteins. In the absence of EBV infection, when no T cell help is available antigen activated B cells can also progress down a PC differentiation route whereby they become plasmablasts and then functional short-lived Ig secreting PCs (Shi et al., 2015). Alternatively, when T cell help is available to antigen-activated B cells they can progress through the GC and follow the long-lived PC differentiation pathway rather than the alternative MBC pathway, a decision likely dependent on exogenous signals (Suan et al., 2017). However, it has not been established what happens to an EBV-infected B-blast in the absence of T cell help, or why MBC differentiation of EBV-infected cells is favoured in the GC. The results of this chapter suggest EBV has evolved to suppress the PC differentiation pathway, to favour long-term latency in MBC through EBNA3A- and EBNA3C-mediated repression of $p18^{INK4c}$ and BLIMP-1. As repression of these B cell differentiation factors becomes independent of EBNA3A and EBNA3C,

EBV has evolved to ensure transient expression of these viral proteins is sufficient to irreversibly repress $p18^{INK4c}$ and BLIMP-1 to avoid spontaneous PC differentiation of cells infected with EBV during progression through the GC, during which the EBNA3 genes are silenced. This mechanism favours the MBC differentiation pathway, therefore leading to long term viral persistence and latency.

Regulation of the B cell to PC differentiation pathway by EBNA3A- and EBNA3C-mediated repression of $p18^{INK4c}$ and BLIMP-1 appears to be independent of the tumour suppressive EBNA3 protein; EBNA3B. However, a distinct role for EBNA3B in the differentiation of B cells is indicated by microarray analysis of BL31 BL-derived cells, as deletion of EBNA3B results in an upregulation of a subset of genes usually repressed in the GC (White et al., 2010). This suggests EBNA3B may help facilitate MBC differentiation by contributing to the progression of EBV-infected cells through the GC reaction. Although the contribution of EBNA3B to this process has not been investigated, it is possible that all of the EBNA3 proteins are directing differentiation of EBV-infected cells toward the MBC compartment, and therefore the site of long-term latency.

4.4.3. EBV latency-associated proteins and B cell differentiation pathways

Aside from EBNA3A- and EBNA3C-mediated epigenetic repression of $p18^{INK4c}$ and BLIMP-1 (Styles et al., 2017), additional EBV factors have been associated with repression of BLIMP-1, the major regulatory transcription factor required for PC differentiation. Uninfected GC B cells transfected with the oncogenic EBV latency-associated protein LMP1 have been shown to express reduced levels of BLIMP-1 mRNA. This is speculated to occur due to LMP1 induced upregulation of c-MYC expression forming a reciprocal regulatory loop, rather than direct targeted repression of BLIMP-1 by LMP1 (Vrzalikova et al., 2011). This analysis of LMP1 repression of BLIMP-1 was performed by transfection of uninfected cells with only LMP1, rather than by genetic analysis using a recombinant EBV virus whereby all EBV latent proteins are expressed unless specifically inactivated. In addition, the EBV miR-BHRF1-2 has been shown to bind to the 3'UTR of *PRDM1* (BLIMP-1), and transfection of LCLs with an miR-BHRF1-2 inhibitor was shown to increase BLIMP-1 expression (Ma et al., 2016).

Although it is suggested these alternative EBV factors also repress BLIMP-1, evidence of significantly elevated levels of BLIMP-1 and differentiation of EBV-infected $CD19^{+ve}$ B cells along a PC differentiation pathway in EBNA3A/EBNA3C-null cells suggests EBNA3A and EBNA3C are vital for BLIMP-1 repression. Furthermore, EBNA3A and EBNA3C have been shown to bind to chromatin at regulatory elements in the vicinity of the $p18^{INK4c}$ and BLIMP-1 loci resulting in recruitment of chromatin modifications consistent with transcriptional repression. This indicates $p18^{INK4c}$ and BLIMP-1 are primary targets of EBV-mediated suppression of PC differentiation (Styles et al., 2017). Although EBNA3A and EBNA3C appear the dominant factors in repression of BLIMP-1, there appears to be a multi-faceted targeting of this vital PC differentiation factor. This indicates the importance of the repression of PC differentiation during the EBV life cycle. Suppression of PC differentiation likely promotes the alternative GC pathway of MBC differentiation, and consequentially long-term viral persistence and latency.

4.4.4. EBV lytic reactivation and the PC differentiation pathway

Lytic reactivation of EBV is thought to occur following the differentiation of a latently infected MBC to a PC. This *in vitro* model system could be ideal for investigating the switch between EBV latency and the EBV lytic cycle as it recapitulates PC differentiation of EBV infected cells. It has been shown that in the tonsils of healthy carriers, EBV replication occurs in rare cells undergoing differentiation of PC (Laichalk and Thorley-Lawson, 2005). Furthermore, a molecular link between these processes was shown when BLIMP-1 was demonstrated to induce reactivation of EBV in epithelial cells and a subset of B cells by activating transcription from the lytic switch promoters R and Z (Reusch et al., 2015). It was hypothesised elevated levels of BZLF1 would correlate with elevated levels of $p18^{INK4c}$ and BLIMP-1 and the PC phenotype of EBNA3A/EBNA3C-null cells seen at 20 days post pi. However, this work did not shed light on this stage of the EBV life cycle as there was no correlation between EBNA3A and EBNA3C functionality and expression of BZLF1, the earliest EBV lytic protein. There was no significant difference in BZLF1 mRNA expression in three of the four donors assessed, regardless of EBNA3A/EBNA3C functionality. Elevated levels of BZLF1 mRNA in the absence of EBNA3A and EBNA3C

in one of the four donors is therefore likely a result of donor dependent behaviour. Furthermore, western blotting extracts from EBNA3A/EBNA3C-null cells failed to identify BZLF1 indicating low or absent protein expression (Figure 4.16 and 4.17). In addition, expression of other lytic proteins was also not identified by western blot (Figure 4.17).

The absence of EBV lytic reactivation could be a consequence of incomplete terminal differentiation of PC, likely as a result of cell cycle arrest due to the absence of EBNA3A and EBNA3C (see above). Alternatively, rarity in which reactivation of EBV occurs (Laichalk and Thorley-Lawson, 2005) could be responsible for the lack of detectible BZLF1 protein. It is possible that difficulty in overcoming the stable repression of $p18^{INK4c}$ and BLIMP-1 induced by EBNA3A and EBNA3C may contribute to the rarity of PC differentiation and therefore rarity of EBV reactivation.

The differing genetic profile of B cells could also contribute to the apparent absence of EBV lytic activation (Shi et al., 2015). The PC-like cells resulting from infection with EBV in the absence of EBNA3A and EBNA3C more likely resemble GC-independent short-lived PC resulting from antigen activation in the absence of T cell help, as no T cells are available during the *in vitro* infection of purified $CD19^{+ve}$ cells with EBV. Furthermore, it is thought reactivation of EBV occurs when MBC differentiate into PC specifically in the tonsils (Laichalk and Thorley-Lawson, 2005). These MBC have progressed through the GC and travelled to the tonsils and likely have an altered genetic profile to GC-independent *in vitro* derived PC-like cells. Particularly as PC derived *in vitro* have been shown to lack features of *in vivo* PC (Shi et al., 2015). Reactivation of EBV may require certain molecules or transcriptional profiles that are only provided by the differentiation of MBC to PC rather than the GC-independent differentiation of B-blasts to PC as recapitulated in this *in vitro* system, or provided by the microenvironment of the tonsil. Indeed, the tonsillar PCs undergoing EBV lytic replication identified by Thorley-Lawson and colleagues, on which this aspect of the EBV life cycle is based, were shown to be $CD38^{high}$ but CD138 negative, contrasting bone marrow PC and those induced by EBNA3A/EBNA3C-null EBV infection *in vitro* (Laichalk and Thorley-Lawson, 2005; Styles et al., 2017).

Despite PC characteristics, the differences in these cells types could be responsible for the absence of EBV lytic reactivation in EBNA3A/EBNA3C-null EBV infected cells undergoing PC differentiation.

The absence of lytic activation could alternatively be a consequence of the lack of EBV latency. It has been shown that only latently infected cells transition into the lytic cycle, despite the presence of BZLF1 expression during primary infection, as a result of genome methylation (Kalla et al., 2010). This study focuses on primary B cell infection with EBV, therefore the cells have not progressed to latency and may be unable to induce the lytic cycle, despite the PC-like phenotype of the EBNA3A/EBNA3C-null cells. Challenges remain, but it would be of great interest to untangle the biochemistry linking PC differentiation and reactivation of the EBV lytic cycle.

4.5. Final conclusions

In conclusion, these results establish a formal link between the transcriptional regulation of EBV and the B cell to PC differentiation pathway. These results demonstrate that EBV-mediated repression of the PC differentiation factors $p18^{INK4c}$ and BLIMP-1, through the regulatory transcriptional mechanisms of EBNA3A and EBNA3C, suppresses the PC differentiation pathway following infection with EBV. This therefore favours establishment of long-term latency and persistence of EBV in MBCs.

4.6. Remaining questions

1. What are the different molecular mechanisms used by EBNA3A and EBNA3C to differentially regulate $p18^{INK4c}$ and BLIMP-1, from both each other and other EBNA3 target genes, despite PRC2 and H3K27me3 being involved in each case?

2. Are the EBNA3 proteins regulating any other B cell differentiation factors?

3. Can EBV-mediated suppression of the B cell to PC differentiation pathway be assessed *in vivo*?

5. Chapter V: EBV can persist in mice with human immune system components when EBNA3A and/or EBNA3C oncogenes are non-functional, but is less pathogenic

5.1. Introduction

Having looked at EBNA3A and EBNA3C *in vitro* in the previous chapters, this chapter will now focus on the roles of EBNA3A and EBNA3C in EBV persistence *in vivo.* EBNA3A and EBNA3C oncogenes promote transformation and increase cell survival *in vitro*, but until now the importance of these genes *in vivo* had not been determined. EBNA3C is essential for EBV-mediated transformation of primary B cells *in vitro*, with EBNA3C-null recombinant EBV viruses unable to establish continuously proliferating LCLs (Maruo et al., 2006; Skalska et al., 2010). EBNA3A is important in transformation, with EBNA3A-null LCL exhibiting reduced proliferative capacity *in vitro* (Bazot et al., 2015; Hertle et al., 2009; Maruo et al., 2003). In contrast, EBNA3B is dispensable for *in vitro* transformation, and is thought to have tumour suppressive activity *in vivo* (White et al., 2012).

It has already been established that mice reconstituted with human immune system components (hu-mice) are suitable models in which to study EBV infection *in vivo* (Fujiwara et al., 2015; Gujer et al., 2015; White et al., 2012). To investigate the roles of EBNA3A and EBNA3C in EBV persistence and latency *in vivo*, an NRG hu-mice model was established. These mice were then infected with recombinant EBV viruses with deletions in EBNA3A and EBNA3C independently, and a virus where the entire EBNA3 locus was deleted. Mice were followed over 6 weeks of infection, and assessed for EBV-mediated pathology and EBV DNA presence. During the write up of this study, EBV persistence in the absence of either EBNA3A and EBNA3C oncogenes was reported independently [(Murer et al., 2018); see Section 5.3 for discussion].

In addition to using recombinant EBV with deletions in EBNA3 proteins, the viability of using conditional ERT2 recombinant EBV viruses within the hu-mouse model was also analysed. These

viruses have been used *in vitro* to further determine the roles of EBNA3A and EBNA3C in viral latency and persistence (Bazot et al., 2015; Maruo et al., 2005, 2006; Skalska et al., 2013; Styles et al., 2017). As discussed in Chapter I (Section 1.4), these recombinant viruses contain an ER fused to the open reading frames of the EBNA3A and/or EBNA3C genes, making functional expression of these proteins dependent on the activating ligand HT (Bazot et al., 2015; Maruo et al., 2005, 2006; Skalska et al., 2013; Styles et al., 2017). As tamoxifen is metabolised in the liver to produce HT, tamoxifen-impregnated food (referred to hereafter as TMX-food) was used in combination with the conditional 3AERT2 recombinant EBV virus to establish whether a WT-like or KO-like phenotype would occur in the infected hu-mice depending on the presence or absence of the activating ligand HT. The ability to activate or deactivate functional EBNA3 protein expression *in vivo* would provide a useful tool to further investigate the intricate roles of EBNA3A and EBNA3C within viral persistence, pathogenesis and tumour development. This experiment was performed as a small-scale proof of concept, and requires further investigation.

Although performed with the aim of studying EBNA3A and EBNA3C in EBV persistence *in vivo*, the work described in this chapter was primarily done to explore the feasibility of studying EBV in a hu-mice model. Base-line protocols were established during these experiments, as it was the first time such work had been performed at Imperial College London. Six independent cohorts were infected during the course of this study; 5 cohorts focused on using EBNA3 KO viruses, and 1 cohort focused on assessing the conditional 3AERT2 virus *in vivo*. Different protocols were established over the duration of this study, therefore some experiments consider every mouse infected, whereas others represent a subset or specific cohort. This limits strong conclusions due to the different cohorts assessed.

5.2. Results

5.2.1. Generating a mouse model with human immune system components

5.2.1.1. Establishing a humanised mouse model and assessing engraftment of human immune system components in the peripheral blood and spleen

It has previously been established that mice with human immune system components support EBV infection, and model EBV associated diseases and lymphomagenesis *in vivo* (Fujiwara et al., 2015; Kohnken et al., 2017; White et al., 2012). Therefore, to investigate the importance of EBNA3A and EBNA3C *in vivo,* an NRG (NOD/Rag$^{-/-}$/IL2-Rγ^{null}) humanised mouse model with specific mutations resulting in severe immunodeficiency was used (see Chapter I, Section 1.5.4 for detail). To establish human immune system components in NRG mice, at 1-4 days old the mice were sub-lethally irradiated and injected with CD34^{+ve} haemopoietic stem cells purified from foetal liver (shown schematically in Figure 5.1). Engraftment was allowed to establish for a minimum of 3 months, before the reconstitution of human lymphocytes was assessed by flow cytometry.

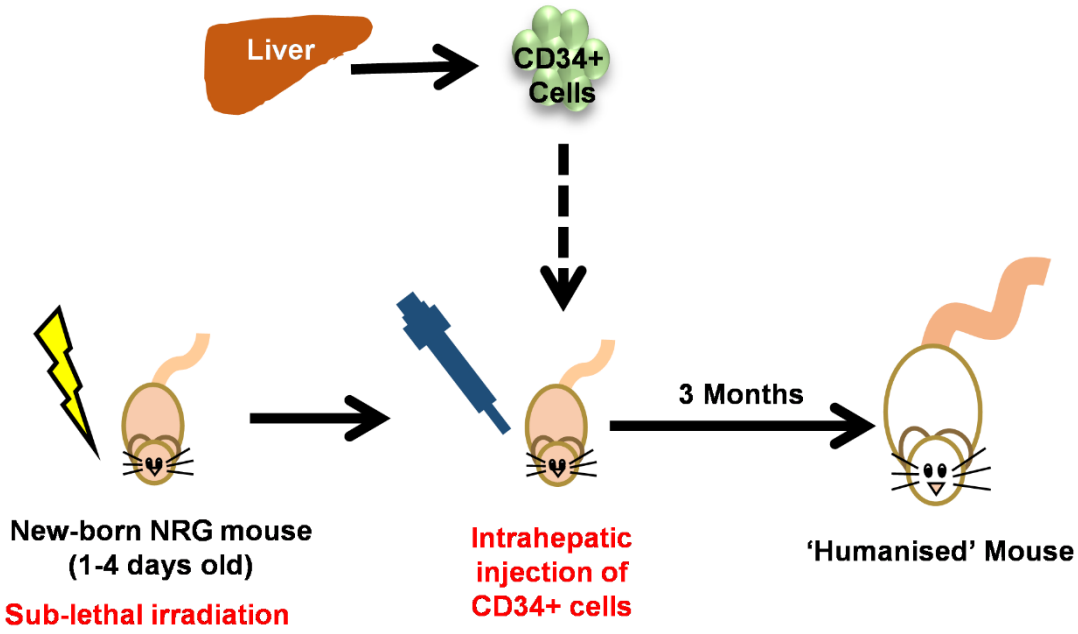


Figure 5.1. Schematic showing the process of humanisation of newborn mice. At 1-4 days old, NRG mice were sub-lethally irradiated and then injected with CD34^{+ve} cells isolated from foetal liver. Following 3 months of engraftment, mice are considered 'humanised' and assessed for the presence of human immune system components.

Engraftment of human lymphocytes within the peripheral blood of humanised mice was determined by flow cytometric analysis at 3-4 months post humanisation. Initially, levels of human CD45 (lymphocyte marker) and human CD19 (B cell marker) cell populations were measured (Figure 5.2A). The level of human CD45^{+ve} cells was compared with the level of mouse CD45^{+ve} to obtain the percentage of reconstitution. This revealed variable reconstitution levels between hu-mice. In order to more extensively assess the reconstitution of human immune system components in hu-mice, the engraftment of T cell populations was then included in later analysis of hu-mice engraftment. The presence of T cells was identified by the surface marker CD3, and distribution of these T cells between CD4^{+ve} and CD8^{+ve} cell populations was also assessed. This revealed that the majority of mice seem to engraft primarily with either more T cells or more B cells, with many mice expressing high levels of either T or B cells. Hu-mice also engrafted with notably more CD4^{+ve} T cells than CD8^{+ve} cells (Figure

5.2B). In addition, engraftment of human immune cells within the spleen of hu-mice was elevated compared to levels within the peripheral blood (Figure 5.3).

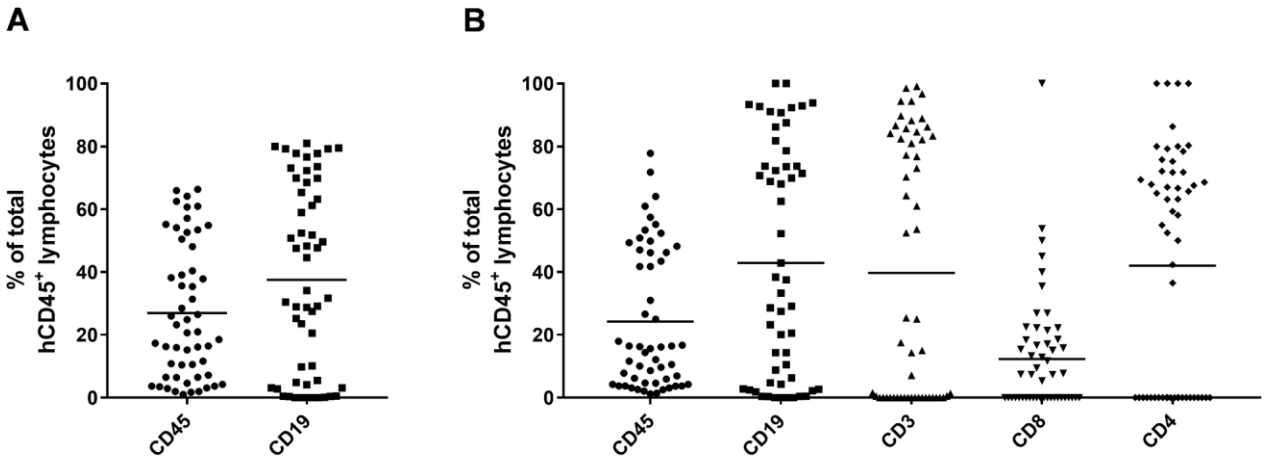


Figure 5.2. Composition of human lymphocytes in the peripheral blood of NRG mice engrafted with human immune system components. (**A**) Reconstitution levels of human $CD45^{+ve}$ human lymphocytes compared to mouse $CD45^{+ve}$ lymphocytes, and percentage of $CD19^{+ve}$ human cells in the peripheral blood of mice engrafted with human immune system components. (**B**) Reconstitution levels as in (**A**) alongside percentage of $CD3^{+ve}$, $CD4^{+ve}$ and $CD8^{+ve}$ human cells in the peripheral blood of mice engrafted with human immune system components. $CD19^{+ve}$ and $CD3^{+ve}$ cells are shown as a percentage of human $CD45^{+ve}$ cells. $CD4^{+ve}$ and $CD8^{+ve}$ cells are shown as a percentage of human $CD45^{+ve}$ $CD3^{+ve}$ cells. Flow cytometry was used to determine the frequencies of human lymphocytes. Each data point represents a single humanised mouse while horizontal bars represent the mean. Mice without detectible human cells are not shown.

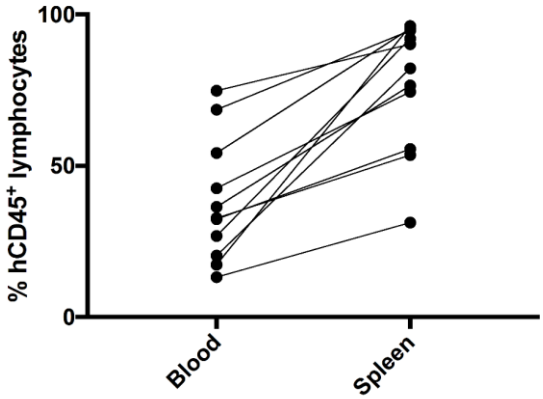


Figure 5.3. Engraftment of human CD45 immune cells in humanised mice is elevated in the spleen compared to peripheral blood. Reconstitution levels of $CD45^{+ve}$ human lymphocytes compared to mouse $CD45^{+ve}$ lymphocytes in the peripheral blood and spleen of mice engrafted with human immune system components. Flow cytometry was used to determine the frequencies of human and mouse $CD45^{+ve}$ lymphocytes. Each data point represents a single humanised mouse.

Following the humanisation process, some mice exhibited progressive alopecia (Figure 5.4). This may be a result of graft versus host disease (Ali et al., 2012) and was only evident in mice over approximately 4 months of age. There did not appear to be any correlation between sex, $CD34^{+ve}$ cell donor, level of $CD19^{+ve}$ B cells, reconstitution level, EBV infection or associated EBV pathology in mice presenting with fur loss. Furthermore, there was no weight loss associated with alopecia in the majority of mice. Hu-mice exhibiting alopecia in combination with severe weight loss or further indications of illness (such as hunched posture, low movement and isolation) were not included in analysis. The progressive alopecia seen in NRG hu-mice only occurred in mice with identifiable human $CD45^{+ve}$ cells in the peripheral blood, indicating it was a consequence of the engraftment of human lymphoid cells rather than the genetic background of the mice.

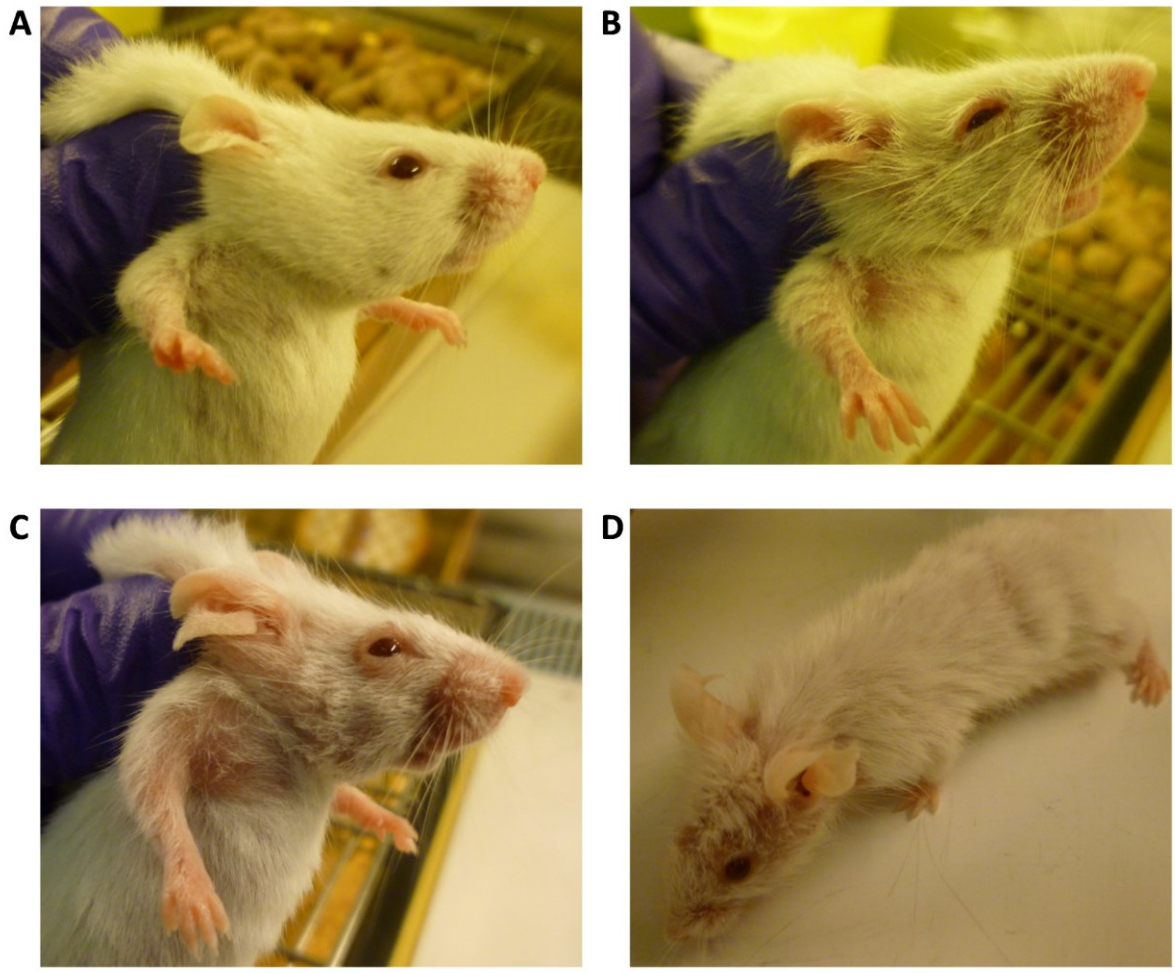


Figure 5.4. Humanisation of NOD/Rag$^{-/-}$/IL2-Rγ^{null} (NRG) mice can lead to progressive alopecia. A healthy adult NRG humanised mouse not exhibiting fur loss (**A**) is shown in comparison to humanised mice exhibiting advancing levels of alopecia (**B** and **C**) and a humanised mouse exhibiting severe alopecia (**D**).

5.2.1.2. Variables within the humanised mouse model

Variables within the NRG humanised mouse model were identified alongside differing levels of human CD45^{+ve} cells between mice engrafted with human immune system components. The CD34^{+ve} haemopoietic stem cell donor greatly affected the engraftment of human immune system components. Reconstitution levels of human CD45^{+ve} cells in the peripheral blood of hu-mice, engrafted with CD34^{+ve} cells isolated from different foetal liver donors, was assessed by flow cytometry. Some CD34^{+ve} donor cells resulted in a notable population of well-reconstituted mice (i.e. over 25% CD45^{+ve} cells), whereas other donors resulted in extremely low engraftment in all mice

(Figure 5.5). Conversely, other donor cells led to a range of reconstitution levels among humanised mice. Another notable variation among humanised mice was that there was a higher number of female mice engrafted with human cells compared to male mice. On average, female mice also exhibited a slightly higher average percentage of human $CD45^{+ve}$ cells (Figure 5.6). This is consistent with a previous report of higher levels of human engraftment in female NSG mice compared to males (McDermott et al., 2010).

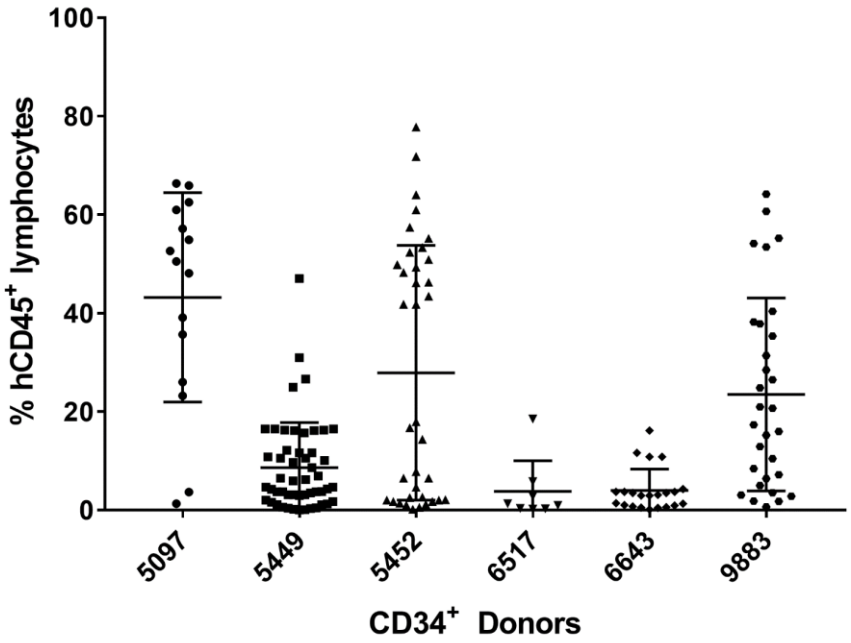


Figure 5.5. Engraftment of human immune system components in humanised mice is variable between $CD34^{+ve}$ cell donors. Reconstitution levels of human lymphocytes in the peripheral blood of mice humanised by injection of $CD34^{+ve}$ cells isolated from different donors. Reconstitution was assessed by flow cytometry to evaluate levels of human $CD45^{+ve}$ lymphocytes compared to mouse $CD45^{+ve}$ lymphocytes. Each data point represents a single humanised mouse, horizontal bars represent the mean and standard deviation.

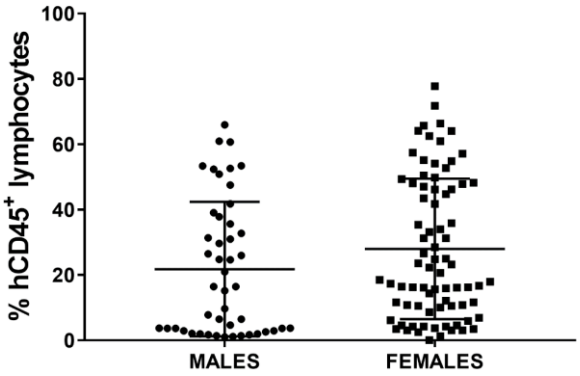


Figure 5.6. Female mice exhibit more effective engraftment of human immune system components than male mice following humanisation. Reconstitution levels of human lymphocytes in the peripheral blood of female and male NRG humanised mice infected with recombinant EBV viruses in the study of EBNA3 proteins *in vivo.* Reconstitution was assessed by flow cytometry to evaluate levels of human $CD45^{+ve}$ lymphocytes compared to mouse $CD45^{+ve}$ lymphocytes. Each data point represents a single humanised mouse with a minimum reconstitution of 1% human $CD45^{+ve}$ cells. Horizontal bars represent the mean and standard deviation. Mice lacking identifiable human $CD45^{+ve}$ cells are not shown.

5.2.2. Establishing protocols for investigating recombinant EBV infection in mice with human immune system components reveals EBV can persist in the absence of functional EBNA3 proteins, but is less pathogenic

5.2.2.1. Weekly and terminal analysis of humanised mice infected with EBV recombinant viruses

To assess the roles of EBNA3A and EBNA3C during EBV infection *in vivo,* mice engrafted with human immune system components were infected via intraperitoneal injection with 10^5 GRU of WT recombinant EBV or recombinant EBV with deletions in EBNA3A (3AKO), EBNA3C (3CKO) or a recombinant virus lacking all EBNA3 proteins (E3KO). Mice were infected for 6 weeks and then sacrificed for analysis. As a control, an uninfected 'MOCK' cohort was also analysed for comparison. The experimental plan for hu-mice infection with recombinant EBV is shown in Figure 5.7. To assess the viral load of EBV recombinant virus-infected mice during the 6-week infection, EBV infected hu-

mice were bled every week from 14 days pi, and DNA extracted to evaluate whether EBV DNA could be identified by qPCR (Figure 5.7A). At 6 weeks pi, hu-mice were sacrificed and the blood and the spleen from each mouse was isolated for analysis. DNA was extracted from both to assess EBV viral load. Spleens were additionally assessed for tumour development and splenomegaly, and a sample of spleens were fixed and mounted onto slides for immunohistochemical staining analysis. In addition, splenic lymphocytes were isolated and seeded to assess outgrowth of LCLs. In some mice flow cytometry was performed on splenic and peripheral blood lymphocytes to assess T cell responses and B cell composition (Figure 5.7B).

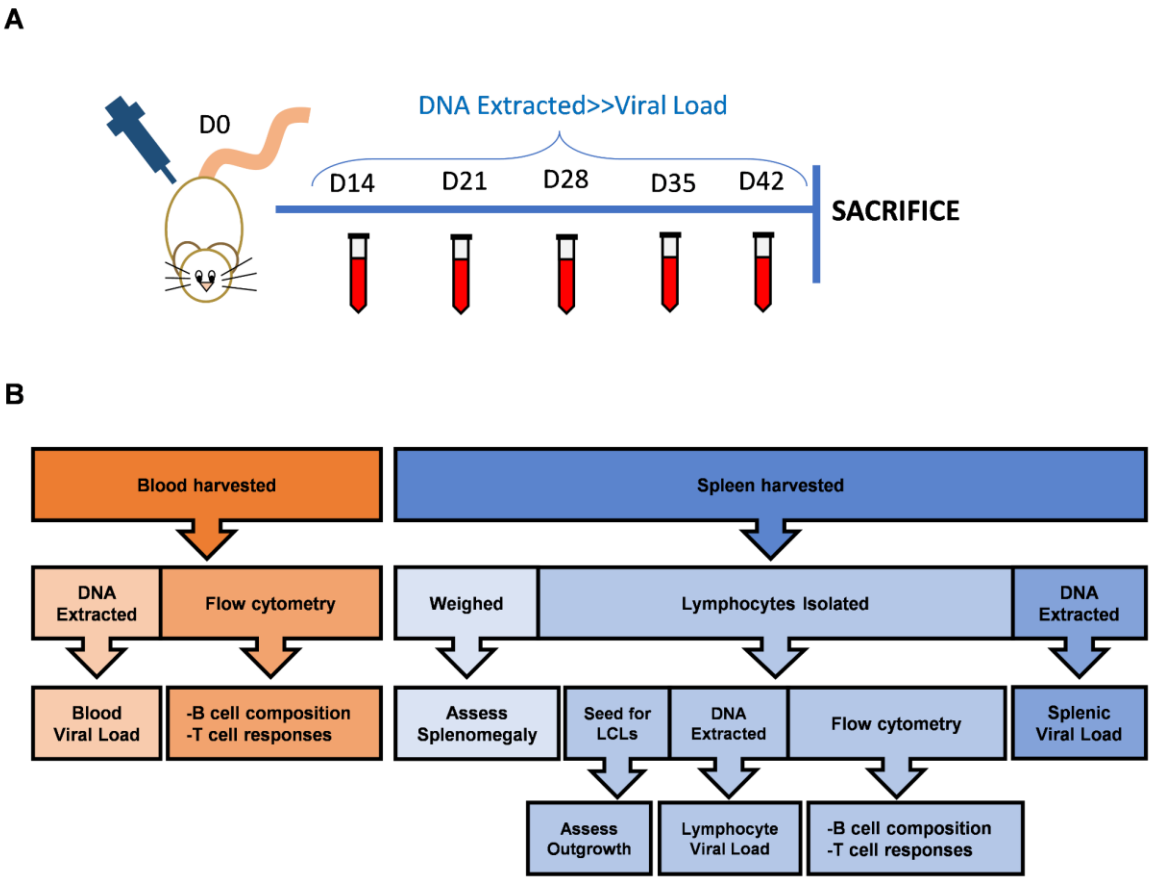


Figure 5.7. Schematic showing experimental procedure for EBV infection of humanised mice (**A**) Mice were bled weekly, DNA extracted from the peripheral blood and viral load analysed. At 6 weeks post infection mice were sacrificed. (**B**) Flow chart detailing terminal analysis of the blood and spleen isolated from humanised mice infected with recombinant EBV.

In addition to terminal analysis and weekly viral load, EBV recombinant infected mice were weighed twice weekly as a measure of overall health. There was no EBV infection-associated weight loss seen across the different recombinant EBV infections (Figure 5.8). Instead, mice gained weight at approximately the same rate over the course of the experiment. This is presumably due to ageing and growth of the mice. There was a tendency for the weight of uninfected 'MOCK' mice to increase at a higher rate than mice infected with recombinant EBV (Figure 5.8, purple line). The decreased weight gain in these mice could be a result of EBV infection, but the large error bars representing the standard deviation imply this is not significant.

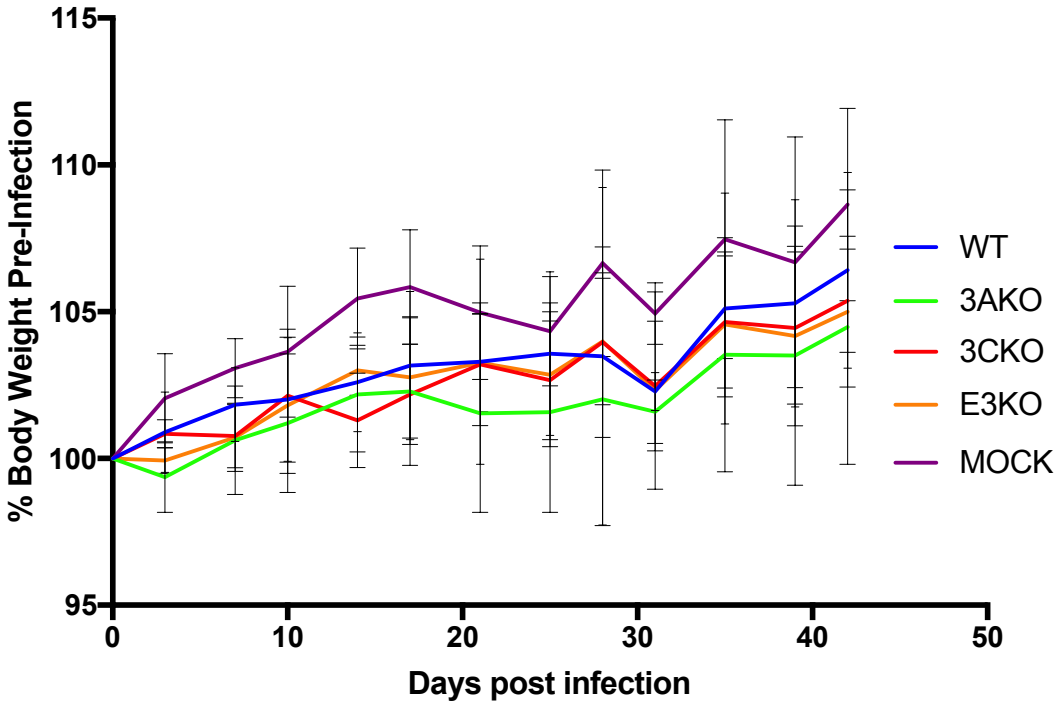


Figure 5.8. Humanised mice infected with recombinant EBV do not exhibit weight loss. Humanised NRG mice were weighed before infection with 10^5 GRU of WT, 3AKO, 3CKO or E3KO recombinant EBV (as indicated), and then twice weekly until sacrifice at 6 weeks post infection. Weight of mice was evaluated as a percentage loss or gain from the weight at the start of infection. Mean weight percentage change for mice infected with each recombinant EBV is shown. Uninfected 'MOCK' mice are shown for comparison.

5.2.2.2. EBV viral load in humanised mice is greater when EBNA3 proteins are functional

Hu-mice were infected with recombinant EBV where either EBNA3A and EBNA3C proteins were functional (WT), individually deleted (3AKO, 3CKO) or with a virus where the entire EBNA3 locus was deleted (E3KO). Blood was harvested weekly from 14 days pi from a cohort of the infected mice (WT=9, 3AKO=6, 3CKO=6, E3KO=6), and DNA extracted. EBV viral loads were then quantified by qPCR for the BALF5 DNA polymerase, a conserved EBV gene.

Across all infections there were some mice that did not exhibit any viral DNA in the peripheral blood and these were not plotted. The levels of EBV genomes identified across each EBV infection varied but was invariably higher in WT, and unexpectedly, also in mice infected with E3KO (Figure 5.9A). On average, E3KO infected mice at 5 weeks pi had the highest levels of EBV DNA (Figure 5.9B), greater even than the WT infected mice where all the EBNA3 proteins were functional (Figure 5.9). Although the average levels of EBV DNA across the different infections is presented (Figure 5.9B), this should be considered representative rather than definitive. The averages presented here only represent mice presenting with identifiable EBV DNA, and there was distinct variation between mice such that error bars were not plotted due to their excessive size.

EBNA3B-KO infections have been shown to result in elevated viral loads and tumorgenicity compared to WT infection (White et al., 2012). Therefore, the high levels of EBV DNA in mice infected with E3KO, may be a consequence of the absence of the tumour suppressive EBNA3B. However, despite the rising viral load levels in E3KO mice at 5 weeks of infection, levels of viral DNA then seem to drop dramatically. In some cases, viral DNA was undetectable at 6 weeks pi in either blood or the spleen (Figure 5.10). This may be a consequence of the concurrent absence of the oncogenic EBNA3A and EBNA3C with absence of the tumour-suppressive EBNA3B. This interplay between the absence of the EBNA3 proteins demonstrates the complex interactions and contradictions of the functions within this protein family. Alongside E3KO-infected hu-mice, EBV DNA was also identified in mice infected with the single KOs for EBNA3A or EBNA3C independently. The presence of EBV DNA in these mice indicates persistence of the virus, even in the absence of the EBNA3A and EBNA3C oncogenes.

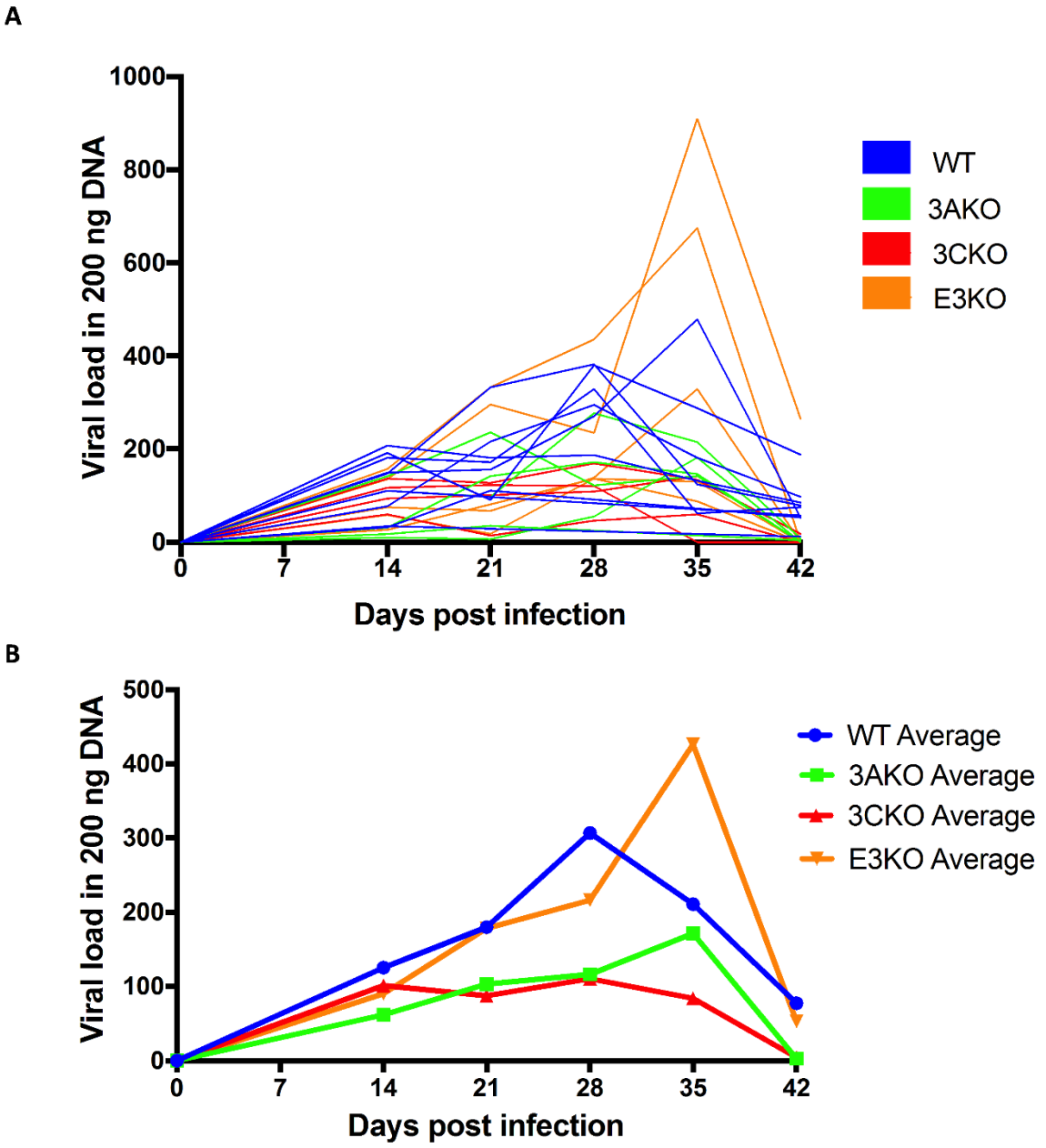


Figure 5.9. Viral load in humanised NRG mice following infection with recombinant EBV. (**A**) EBV DNA genome copies in the peripheral blood of humanised mice infected with 10^5 GRU of WT (blue), 3AKO (green), 3CKO (red) and E3KO (orange) recombinant EBV was determined by qPCR of 200 ng of DNA purified from the peripheral blood. EBV genome copies were assessed at 2 weeks post infection, then weekly until sacrifice at 6 weeks post infection. Recombinant EBV infected mice with no detectable EBV DNA were not plotted. Each data line represents a single recombinant EBV infected humanised mouse. (**B**) Averages of data presented in (**A**).

Mice were sacrificed at 6 weeks pi, and the peripheral blood and splenic tissue of every mouse analysed for presence of EBV DNA. The levels of EBV DNA identified in the blood of mice infected with WT EBV was higher than those found in mice infected with EBNA3 KO viruses, with the exception of a

single 3CKO infected mouse and single E3KO infected mouse (Figure 5.10A). However, overall there were significantly more mice infected with WT EBV with identifiable viral DNA in the blood compared to mice infected with viruses lacking EBNA3 genes, in which identification of EBV DNA was fairly low (Figure 5.10C). A higher level of EBV DNA was identified in the spleens of infected mice. At sacrifice, the highest levels of EBV DNA were found in WT infected mice, with 4 mice exhibiting far higher levels than those identified in mice infected with viruses with EBNA3 deletions (Figure 5.10B). These levels were notably higher than those infected with the E3KO recombinant virus, despite elevated levels seen in some of these mice at 5 weeks pi. Overall, EBV DNA was more readily identified in the spleen of infected mice compared to the blood, particularly in WT infected mice (Figures 5.10C and 5.10D). In addition, consistent with the blood results, there were significantly more WT infected mice presenting with identifiable EBV DNA compared to mice infected with 3AKO, 3CKO or E3KO (Figure 5.10D).

The levels of viral DNA were notably elevated in a number of WT infected mice compared to mice infected with EBV without the EBNA3A and/or the EBNA3C oncogenes, indicating EBNA3A and EBNA3C enhance infection and persistence. However, the presence of EBV DNA in the blood and spleens of some of the hu-mice infected with EBV recombinant viruses lacking EBNA3A, EBNA3C or the whole EBNA3 locus suggests persistence of EBV in the absence of these oncogenes. Albeit, at a lower level than in WT infection where the EBNA3 proteins are functional.

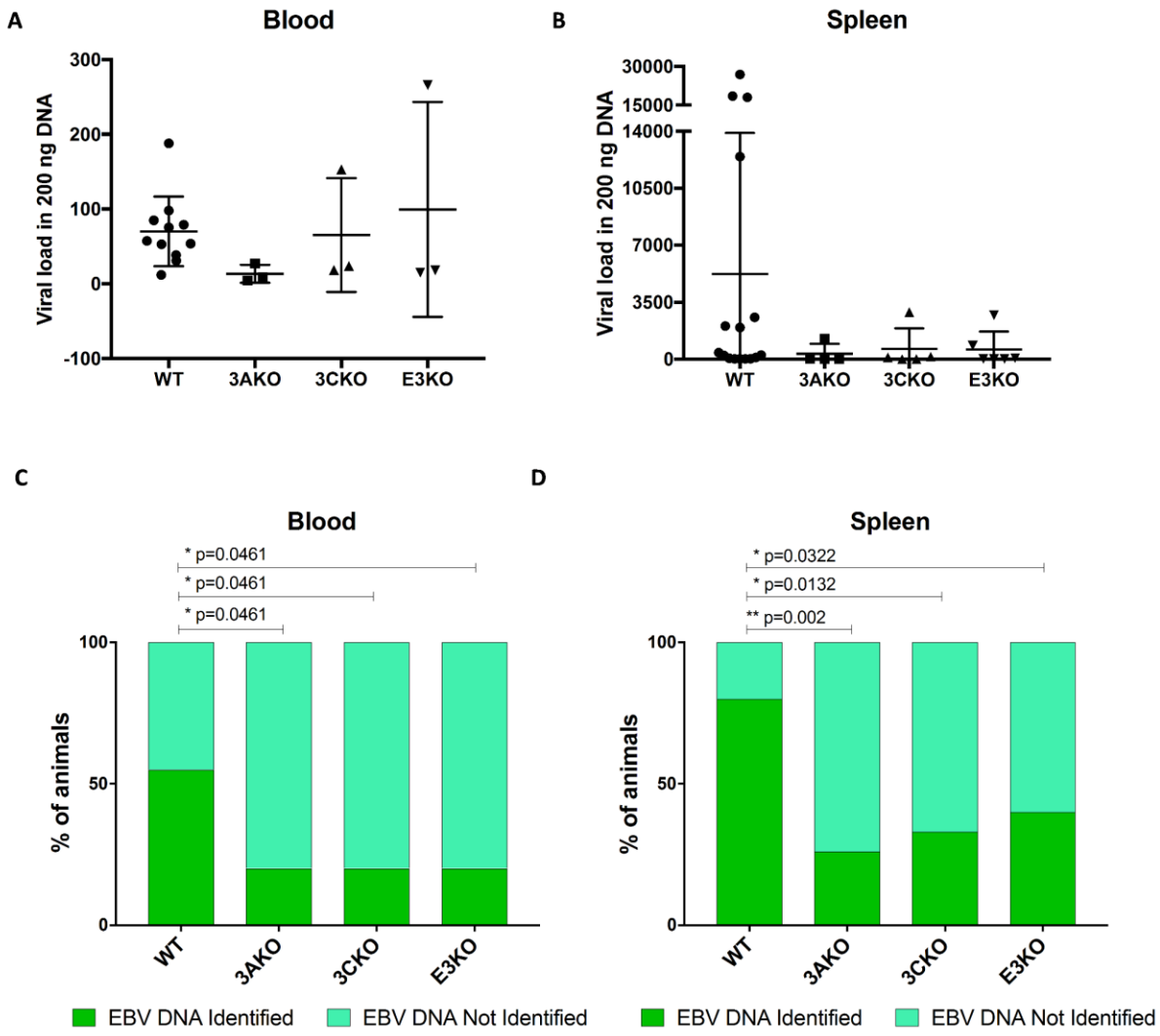


Figure 5.10. EBV DNA viral load in humanised NRG mice infected with recombinant EBV is higher in the spleen than in the peripheral blood. EBV DNA genome copies in the peripheral blood (**A**) and splenic tissue (**B**) of humanised mice infected with 10^5 GRU of WT, 3AKO, 3CKO and E3KO recombinant EBV at sacrifice at 6 weeks post infection (pi). EBV genome copies were determined by qPCR of 200 ng of DNA purified from peripheral blood or splenic tissue. Recombinant EBV infected mice with no detectable EBV DNA were not plotted. Each data point represents a single humanised mouse and horizontal bars represent the mean and standard deviation. (**C** and **D**) Percentage of humanised mice infected with 10^5 GRU of WT (n=20), 3AKO (n=15), 3CKO (n=15) and E3KO (n=15) recombinant EBV with identifiable EBV DNA at 6 weeks pi in the blood and spleen. Statistical significance was assessed by Fischer's Exact test, a p value of <0.05 was considered significant (*), a p value of <0.01 was considered more significant (**).

Some WT mice did not have identifiable EBV DNA, yet presented with macroscopically visible tumour development, where cells grew out that expressed EBV latency-associated proteins (See Sections 5.2.2.3 and 5.2.2.5). This implies there may be an issue with either the quality of DNA extracted or with the qPCR assay. However, both DNA extraction and qPCR amplification appeared successful as qPCR amplification of β2M (performed in duplex with the EBV gene BALF5 as a control) was successful. Therefore, the absence of detectable EBV DNA may reflect the limits of detection of the assay. This may also account for the low numbers of mice with identifiable viral DNA following infection with EBNA3 KO viruses, as they generally had lower levels of EBV DNA compared to WT infected mice.

5.2.2.3. Humanised mice infected with recombinant EBV viruses without the EBNA3A and/or EBNA3C oncogenes exhibit tumour development, but at a lower frequency than infection where EBNA3 genes are functional

Infection of hu-mice with WT recombinant EBV for 6 weeks resulted in macroscopically visible tumour development in just over 50% of mice (Figure 5.11B). Consistent with the presence of EBV DNA in the absence of EBNA3 oncogenes, splenic tumour development was also identified in some hu-mice at 6 weeks pi with 3AKO, 3CKO and E3KO recombinant EBV. Tumour development in the absence of the EBNA3 oncogenes occurred at a significantly lower frequency than in hu-mice infected with WT-recombinant EBV where the EBNA3 proteins were functional (Figure 5.12B). Furthermore, the splenic tumour development in mice where EBNA3A and/or EBNA3C were absent resembled the smaller tumour seen in Figure 5.11A (lower red arrow). In contrast, large splenic tumours such as seen in Figure 5.11A (upper red arrow) was only seen in some WT infected mice.

The level of engraftment of human $CD45^{+ve}$ and $CD19^{+ve}$ B cells in the peripheral blood of recombinant EBV infected hu-mice did not seem to affect the incidence of splenic tumour development (Figure 5.12A/B). Levels of human $CD45^{+ve}$ and $CD19^{+ve}$ cells in the spleen appeared only moderately elevated in mice exhibiting splenic tumour development following EBV infection (Figure 5.12C/D).

The number of mice presenting with splenic tumours was greater in 3AKO infected mice than either 3CKO or E3KO recombinant EBV infected mice. This correlates with the transforming ability of these viruses *in vitro.* Primary B cell infection *in vitro* where EBNA3A is non-functional can result in LCLs, but they have reduced proliferative capacity (Bazot et al., 2015; Hertle et al., 2009; Maruo et al., 2003). In contrast, transformation and LCL development does not occur in the absence of EBNA3C (Maruo et al., 2006; Skalska et al., 2013). The presence of both viral DNA and tumour development in some hu-mice infected with EBNA3A and EBNA3C KO viruses, and a recombinant virus lacking the entire EBNA3 locus, contrasts these established *in vitro* findings and suggests the oncogenic EBNA3 proteins may be dispensable for persistent EBV infection *in vivo.*

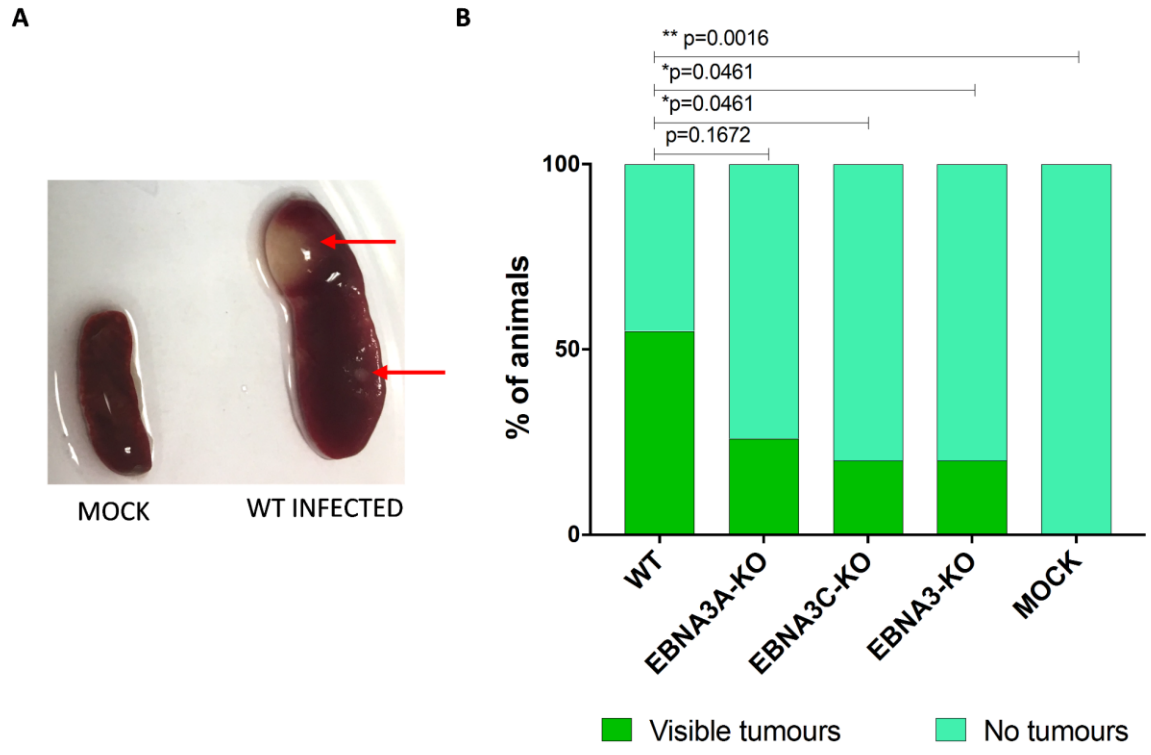


Figure 5.11. EBV mediated tumour development can occur in the absence of its EBNA3 oncogenes. (**A**) Example of a macroscopically visible tumour in the spleen of a humanised mouse 6 weeks post infection with WT recombinant EBV (WT INFECTED). A non-infected humanised mouse control ('MOCK') is shown for comparison**.** Red arrows indicate tumours. (**B**) Frequency of macroscopically visible splenic tumour development in humanised mice 6 weeks post infection with 10^5 GRU WT (11/20), 3AKO (4/15), 3CKO (3/15) or E3KO (3/15) recombinant EBV. Non-infected control humanised mice ('MOCK') are also shown (0/13). Statistical significance was assessed by Fischer's Exact test, a p value of <0.05 was considered significant (*), a p value of <0.01 was considered more significant (**).

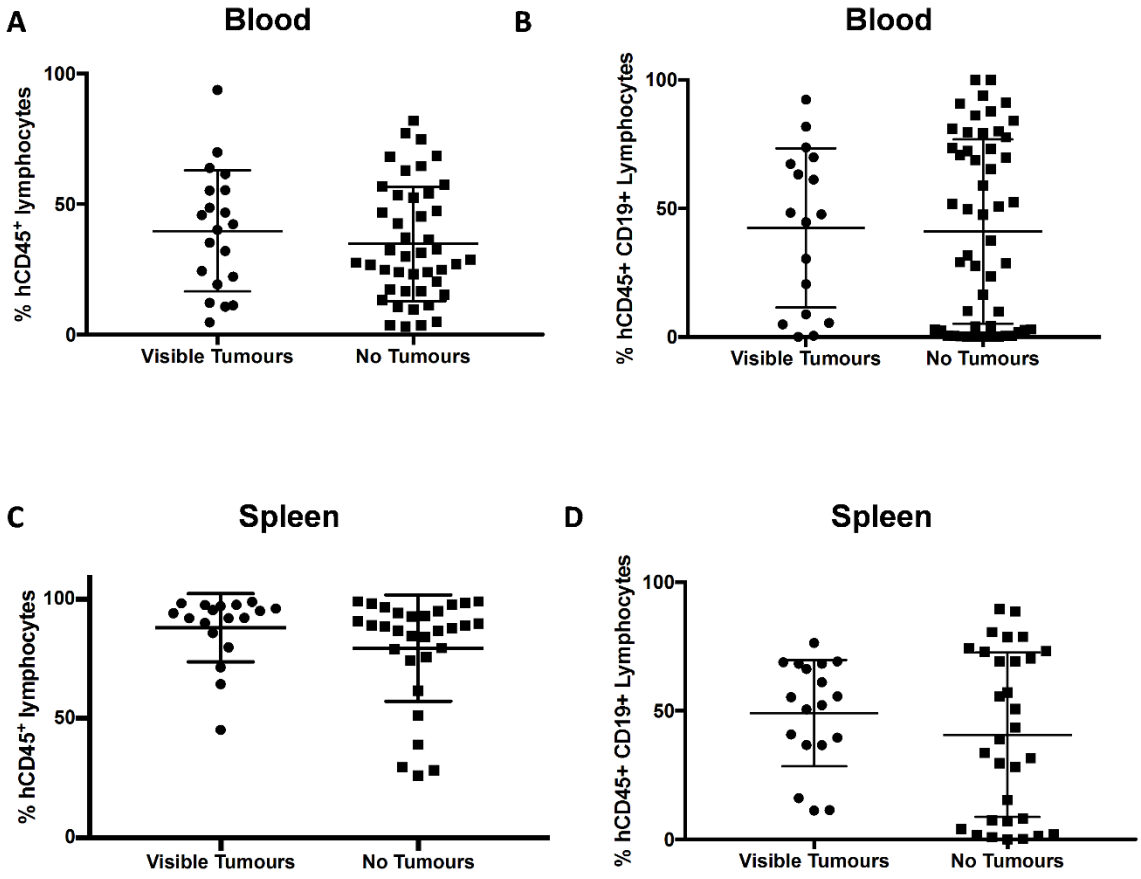


Figure 5.12. Tumour development in EBV infected humanised mice does not correlate with engraftment of human lymphocytes. Reconstitution levels of $CD45^+$ human lymphocytes (**A**) and $CD45^+$ $CD19^+$ human lymphocytes (**B**) in the peripheral blood in hu-mice lymphocytes either presenting with macroscopically visible tumour development (Visible Tumours) or not (No Tumours) at 6 weeks post infection with 10^5 GRU WT, 3AKO, 3CKO or E3KO recombinant EBV was assessed by flow cytometry. (**C** and **D**) As with **A** and **B** but splenic lymphocytes assessed. Each data point represents a single humanised mouse and horizontal bars represent the mean and standard deviation.

5.2.2.4. Humanised mice infected with recombinant EBV exhibit enhanced splenomegaly and elevated levels of proliferating cells when the EBNA3 proteins are functional

It has previously been established that infection of hu-mice with WT EBV can result in splenomegaly (Strowig et al., 2009). Therefore, this was used as an assessment of EBV pathogenesis in hu-mice infected with recombinant EBV lacking the EBNA3 and EBNA3C oncogenes. Splenomegaly was assessed by the weight of the spleen in comparison to the total weight of the individual mouse.

Mice with a spleen weight percentage greater than the average of uninfected 'MOCK' mice were considered as having splenomegaly. Splenomegaly is characteristic of infection of hu-mice with WT EBV where EBNA3 proteins are functional. As expected, splenomegaly was seen in a number of WT infected hu-mice, with spleen weights significantly higher than uninfected 'MOCK' mice. Overall, spleen sizes were not significantly increased in hu-mice infected with 3AKO, 3CKO and E3KO EBV compared to uninfected mice. However, splenomegaly was seen in some of these EBNA3-deficient EBV infected mice, indicating EBV-mediated pathology (Figure 5.13). Across all infections, there were mice exhibiting no splenomegaly, with spleen weight ratios comparable to those of uninfected 'MOCK' mice.

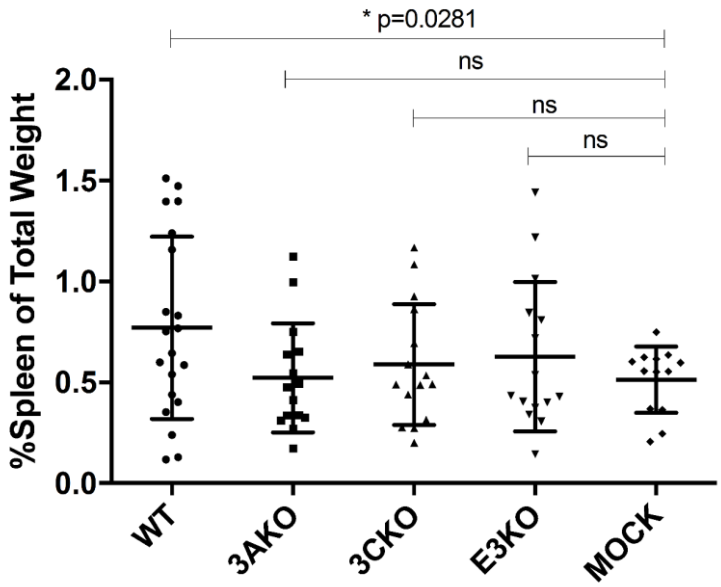


Figure 5.13. WT recombinant EBV infected humanised mice exhibit splenomegaly. Spleen weight as a percentage of total body weight of humanised mice 6 weeks post infection with 10^5 GRU WT (n=20), 3AKO (n=15), 3CKO (n=15) or E3KO (n=15) recombinant EBV. Non-infected control humanised mice ('MOCK', n=13) are also shown. Each data point represents a single humanised mouse and horizontal bars represent the mean and standard deviation. Statistical significance was assessed by an unpaired t-test with Welch's correction, a p value of <0.05 was considered significant (*).

Further assessment of the spleens of hu-mice infected with recombinant EBV was performed by immunohistochemistry. Sections of spleens were fixed in formaldehyde and mounted onto slides before staining for the B cell marker CD20, the proliferation marker Ki67 and the EBV latent protein EBNA2.

Assessment of the surface marker CD20 confirmed high numbers of B cells within the spleens of all hu-mice infected with recombinant EBV, with a slightly higher level seen in mice infected with WT EBV where the EBNA3A and EBNA3C oncogenes were functional. Furthermore, there was evidence of proliferating cells in the spleens of all mice infected with recombinant EBV, again with a modestly elevated level in hu-mice infected with WT recombinant EBV (Figure 5.14). However, it was not established whether the CD20 B cells or proliferating Ki67 expressing cells were EBV positive.

As expected, EBNA2 positive cells were readily identified in the spleens of hu-mice infected with WT recombinant EBV. However, low levels of EBNA2 expressing cells were also identified in the spleens of mice infected with recombinant EBV lacking the EBNA3A (3AKO) or EBNA3C oncogenes (3CKO), or the entire EBNA3 locus (E3KO) (Figure 5.14). These cells were much rarer than when EBNA3A and EBNA3C were functional in mice infected with WT EBV, indicating persistence is enhanced when EBNA3 proteins are expressed. Nevertheless, the presence of EBNA2 positive cells in the spleens of hu-mice infected with 3AKO, 3CKO and E3KO indicate EBV can persist in the absence of the EBNA3 oncogenes for 6 weeks in this model.

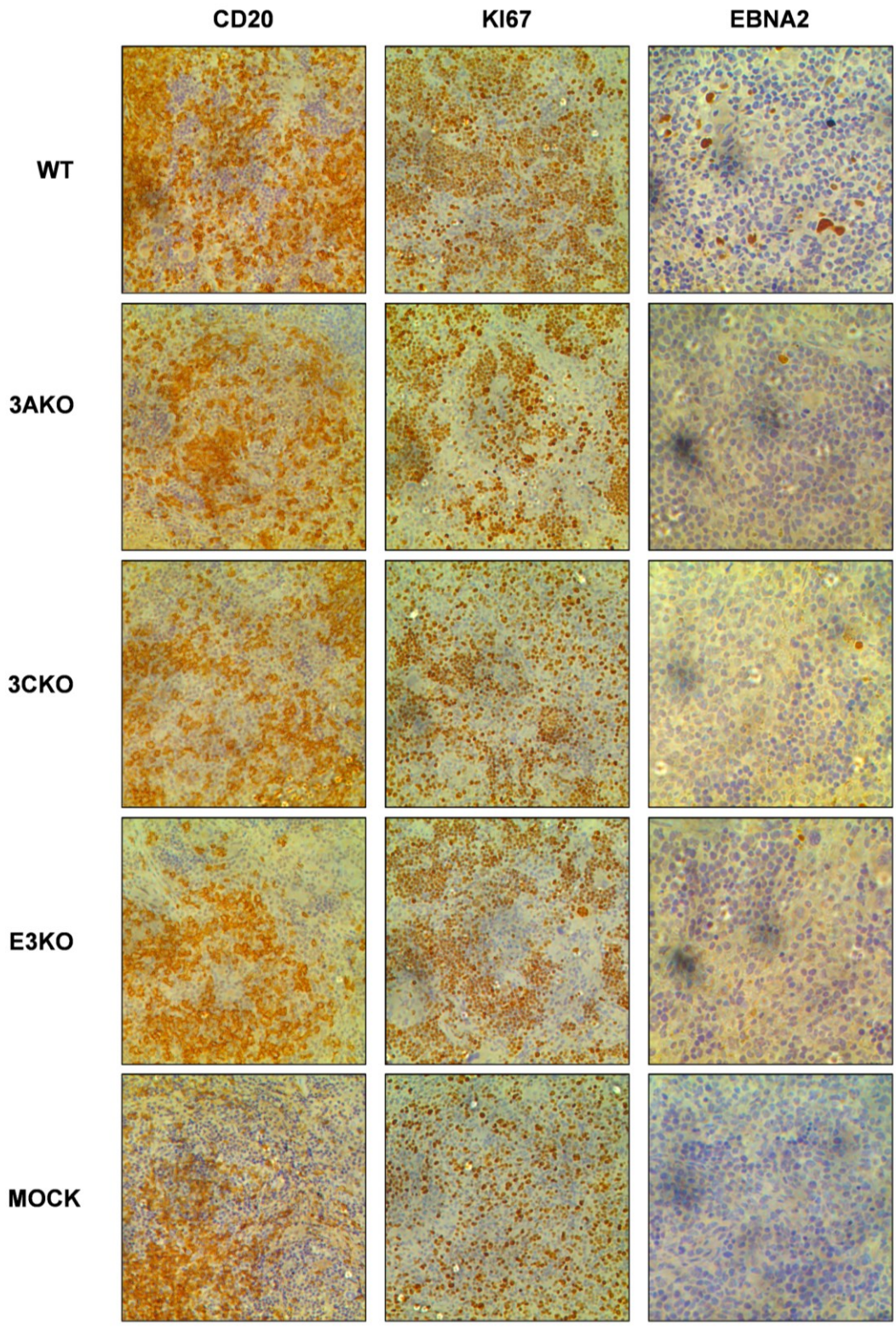


Figure 5.14. Immunohistological analysis of splenic sections from humanised mice infected with recombinant EBV viruses. Representative immunohistochemistry staining for CD20, Ki67 and EBNA2 in splenic sections isolated from humanised mice 6 weeks post infection with 10^5 GRU WT, 3AKO, 3CKO or E3KO recombinant EBV. Spleen sections from an uninfected 'MOCK' mouse is shown for comparison. A magnification of 20x for CD20 and Ki67 positive cells and 40x for EBNA2 positive cells is shown.

5.2.2.5. Cell lines can only be derived ex vivo from the spleens of humanised mice infected with EBV where EBNA3A and EBNA3C are functional

It has previously been established that EBV positive cells derived from WT EBV infected hu-mice can be grown out *ex vivo* to produce continuously proliferating LCLs (Strowig et al., 2009; White et al., 2012). *In vitro* cells infected with recombinant EBV with deleted or conditionally inactive EBNA3C are unable to establish LCLs, and EBNA3A-null cell lines exhibit reduced proliferative capacity (Bazot et al., 2015; Hertle et al., 2009; Maruo et al., 2003, 2006; Skalska et al., 2013). However, EBV positive cells were identified in the spleens of hu-mice infected with EBV lacking EBNA3A, EBNA3C or all three EBNA3 proteins at 6 weeks pi. Therefore, the ability of EBV infected cells from hu-mice infected with EBV with deletions in EBNA3A and/or EBNA3C to produce LCLs following *ex vivo* culturing of lymphocytes was assessed.

Splenic and peripheral blood lymphocytes derived from hu-mice infected with recombinant EBV were isolated on ficoll gradients and cultured to assess outgrowth of LCLs. Cyclosporin A was used to inhibit T cell activity. There was no cell expansion in any cells isolated from the peripheral blood of recombinant EBV infected humanised mice, likely as a result of low numbers of infected human $CD19^{+ve}$ cells (data not shown). However, approximately 70% of cell cultures derived from the spleens of humanised mice infected with WT recombinant EBV (where EBNA3 proteins are functional) expanded in culture, with cells exhibiting clumping characteristic of EBV transformation and LCL development. Of these cells around half expanded to establish continuously proliferating LCLs, quantified as expansion to over 10 ml of continually proliferating culture (Figure 5.15A). Western blot analysis of extracts from WT LCL derived from the hu-mice demonstrates expression of EBV latency-associated proteins in these cell lines (Figure 5.15B). No LCL-like cell clumping was evident in splenic lymphocytes isolated from humanised mice infected with either 3AKO, 3CKO or E3KO recombinant EBV, despite the presence of splenic tumour development and presence of proliferating and EBNA2 positive cells in the spleen (Figure 5.15A). This indicates endogenous factors *in vivo* may help facilitate

survival of EBV-infected cells without the EBNA3A and/or EBNA3C oncogenes, as cells are unable to survive in culture *ex vivo*.

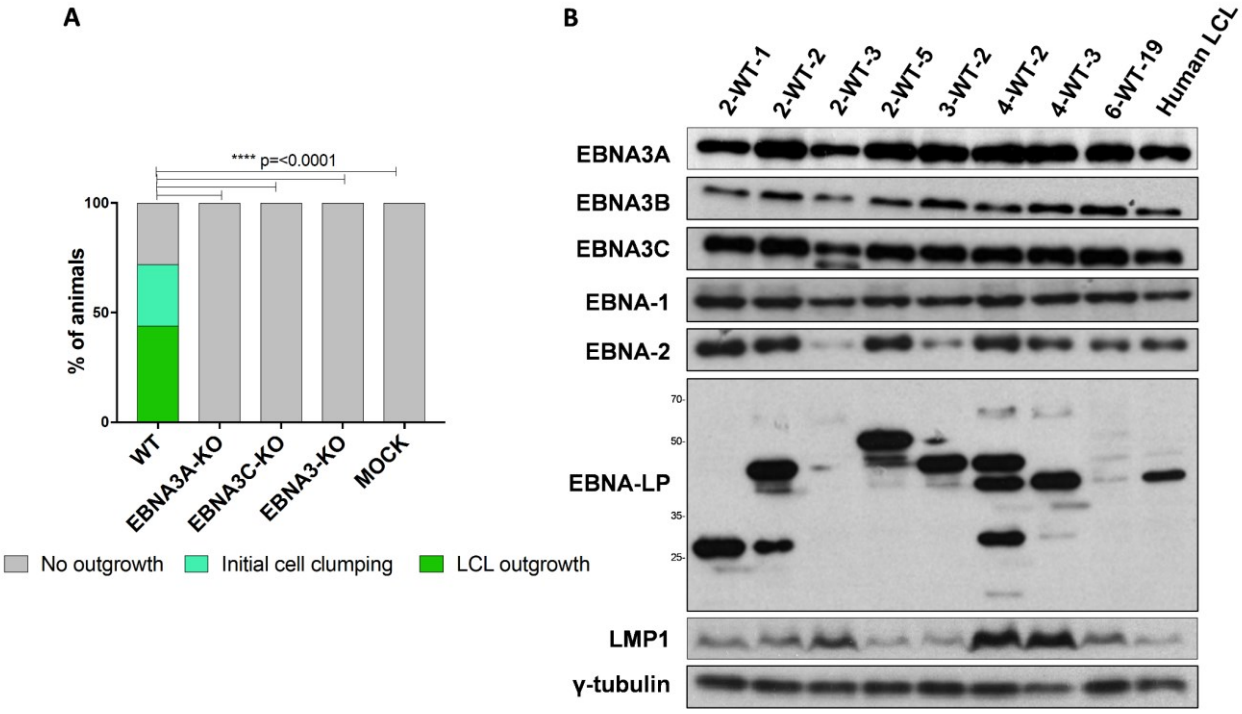


Figure 5.15. *Ex vivo* outgrowth of B cells derived from the spleens of humanised mice only occurs following infection with WT recombinant EBV. (**A**) Frequency of *ex vivo* outgrowth of B cells derived from the spleens of humanised mice 6 weeks post infection with 10^5 GRU WT (n=18), 3AKO (n=14), 3CKO (n=14) or E3KO recombinant EBV (n=14). Non-infected control humanised mice ('MOCK', n=13) are shown for comparison. Initial cell clumping was assessed by light microscopy and LCL outgrowth refers to cell expansion to over 10 ml of LCL culture. (**B**) Expression of EBV latency-associated proteins EBNA1, EBNA2, EBNA3A, EBNA3B, EBNA3C, EBNA-LP and LMP1 was demonstrated by western blotting extracts from LCL derived from the spleens of humanised mice 6 weeks post infection with WT recombinant EBV. In each blot γ-tubulin was used as a loading control and was similarly consistent across all blots. Statistical significance assessed by Fischer's Exact test, a p value of <0.0001 was considered highly significant (****).

Of the hu-mice infected with recombinant WT EBV, where splenic lymphocytes grew out *ex vivo*, outgrowth of continuously proliferating LCLs correlated with higher engraftment of human $CD45^{+ve}$ lymphocytes in the peripheral blood of mice at the point of sacrifice (Figure 5.16A). Engraftment of human lymphocytes in the spleen was consistently high in the majority of hu-mice (Figure 5.16B). LCLs were also more likely to grow out *ex vivo* from WT recombinant EBV-infected hu-mice with higher levels of human $CD19^{+ve}$ cells in the peripheral blood and particularly the spleen

(Figure 5.16 C/D). Furthermore, all but one of the B cell cultures derived from the spleens of hu-mice exhibiting macroscopically visible EBV-mediated tumour development led to LCL-like clumping. In most cases lymphocytes isolated from the spleen of a hu-mouse exhibiting splenic tumour development led to full LCL outgrowth *ex vivo*. However, there was still outgrowth of B cells derived from the spleens of hu-mice not presenting with macroscopically visible tumour development (Figure 5.16E). This indicates either tumour development that was not macroscopically visible in these mice, or EBV infected splenic B cells had oncogenic potential but had not yet developed into tumours. In addition, in some cases LCL outgrowth was seen in cells derived from the spleens of mice where EBV DNA was not identified by qPCR. The presence of EBV latency associated proteins (identified by western blot) indicates either an issue with assessment of EBV infection by qPCR of the BALF5 polymerase, or limits in the detection of EBV DNA using this method.

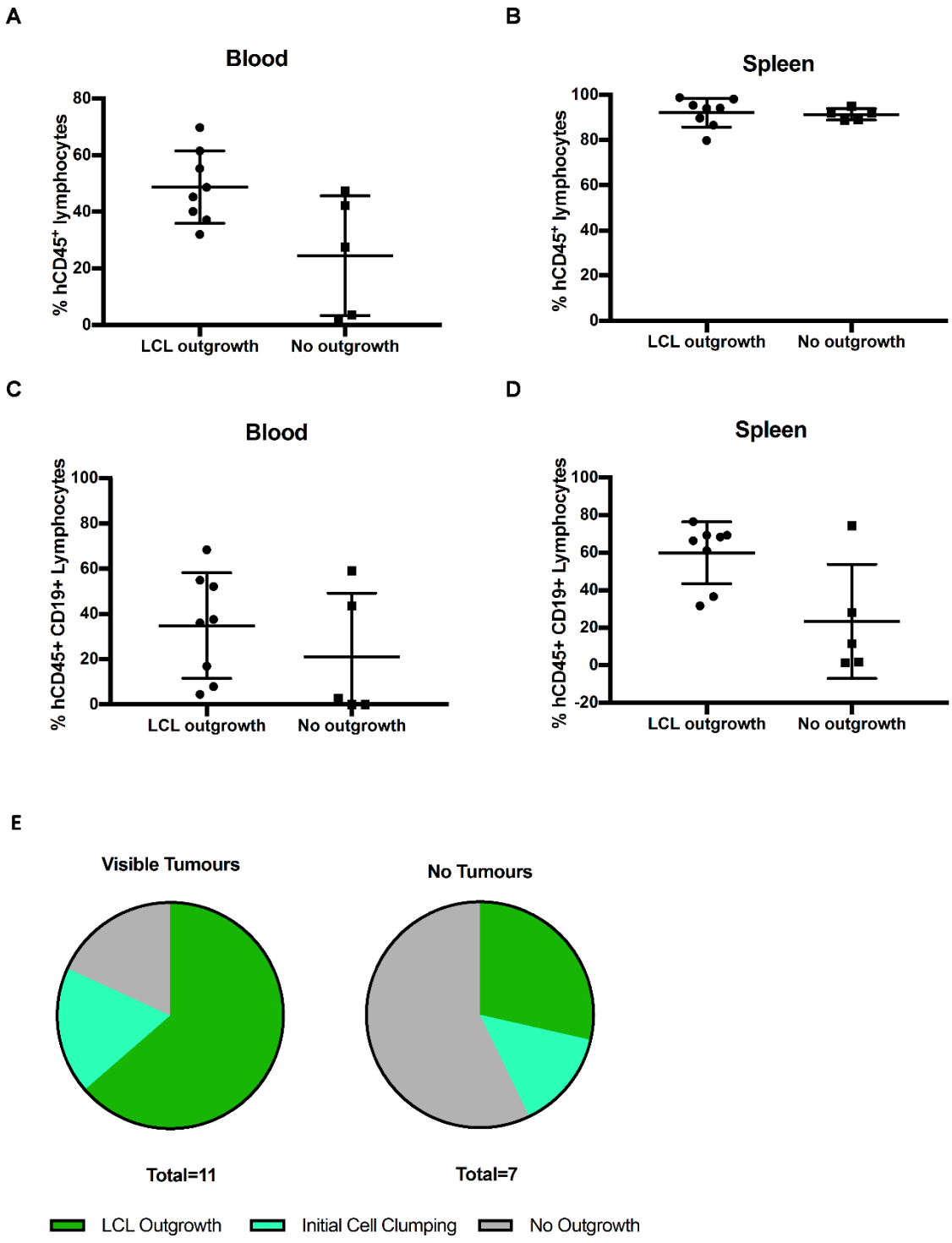


Figure 5.16. ***Ex vivo*** **outgrowth occurs more frequently when B cells are derived from the spleens of WT EBV infected humanised mice with higher levels of human lymphocytes.** Percentage of human $CD45^{+ve}$ (**A, B**) and $CD45^{+ve}$ $CD19^{+ve}$ (**C, D**) lymphocytes in the peripheral blood and spleen (as indicated) of humanised mice infected with 10^5 GRU WT recombinant EBV for 6 weeks. B cells were isolated from the spleens of these animals and assessed for cell expansion to continuously proliferating LCLs (LCL outgrowth, n=8) or no LCL-like clumping or expansion (No outgrowth, n=5). Cells which initially expanded but did not produce an LCL are not shown. CD45 and CD19 levels were assessed by flow

cytometry. Each data point represents a single humanised mouse and horizontal bars represent the mean and standard deviation. (**E**) Frequency of LCL outgrowth, initial cell clumping or no outgrowth from splenic lymphocytes isolated from humanised mice infected with 10^5 GRU WT recombinant EBV for 6 weeks either presenting with macroscopically visible tumours (Visible tumours) or not (No tumours).

5.2.2.6. Infection of humanised mice with recombinant EBV lacking EBNA3A and EBNA3C can lead to expansion of CD8^{+ve} T cells

Infection of hu-mice with WT EBV has been shown to result in expansion of human CD8^{+ve} T cells (Murer et al., 2018; Traggiai et al., 2004; White et al., 2012). Therefore, the levels of T cells in the peripheral blood and spleens of one cohort of hu-mice infected with recombinant EBV lacking the EBNA3A and EBNA3C oncogenes were assessed by flow cytometry.

The percentage of human CD45^{+ve} lymphocytes that were CD3^{+ve} varied among the recombinant EBV infected and uninfected hu-mice in the cohort of mice assessed, with considerable mouse-dependent distribution (Figure 5.17A/B). However, the mean percentage of CD3^{+ve} cells that were CD4^{+ve} was reduced in hu-mice infected with WT recombinant EBV compared to uninfected 'MOCK' mice, and there were individual mice infected with either 3AKO, 3CKO or E3KO which also exhibited reduced percentages of CD4^{+ve} cells (Figure 5.17C/D). The lower level percentage of CD3^{+ve} CD4^{+ve} cells was reflected in the increased percentage of CD3^{+ve} CD8^{+ve} cells in several hu-mice infected with WT recombinant EBV and in some mice following EBV infection where EBNA3A, EBNA3C or the entire EBNA3 locus was deleted (Figure 5.17E/F). Furthermore, the average level of CD8^{+ve} T cells was largely consistent between the peripheral blood and the spleen. In comparison to EBV infected hu-mice, uninfected 'MOCK' mice exhibit relatively low levels of CD8^{+ve} T cells in both the peripheral blood and spleen. The expansion of CD8^{+ve} T cells in the EBV infected mice could indicate a possible cellular immune response against 3AKO, 3CKO and E3KO recombinant EBV infection is being mounted, mirroring that of WT EBV infected mice. The average levels of CD8^{+ve} cells were slightly higher in mice infected with WT EBV, especially in the blood, indicating a stronger immune response may be

mounted when the EBNA3A and EBNA3C oncogenes are functional. This is consistent with evidence that EBNA3A and EBNA3C epitopes are targeted by human cytotoxic T cells (Khanna et al., 1992).

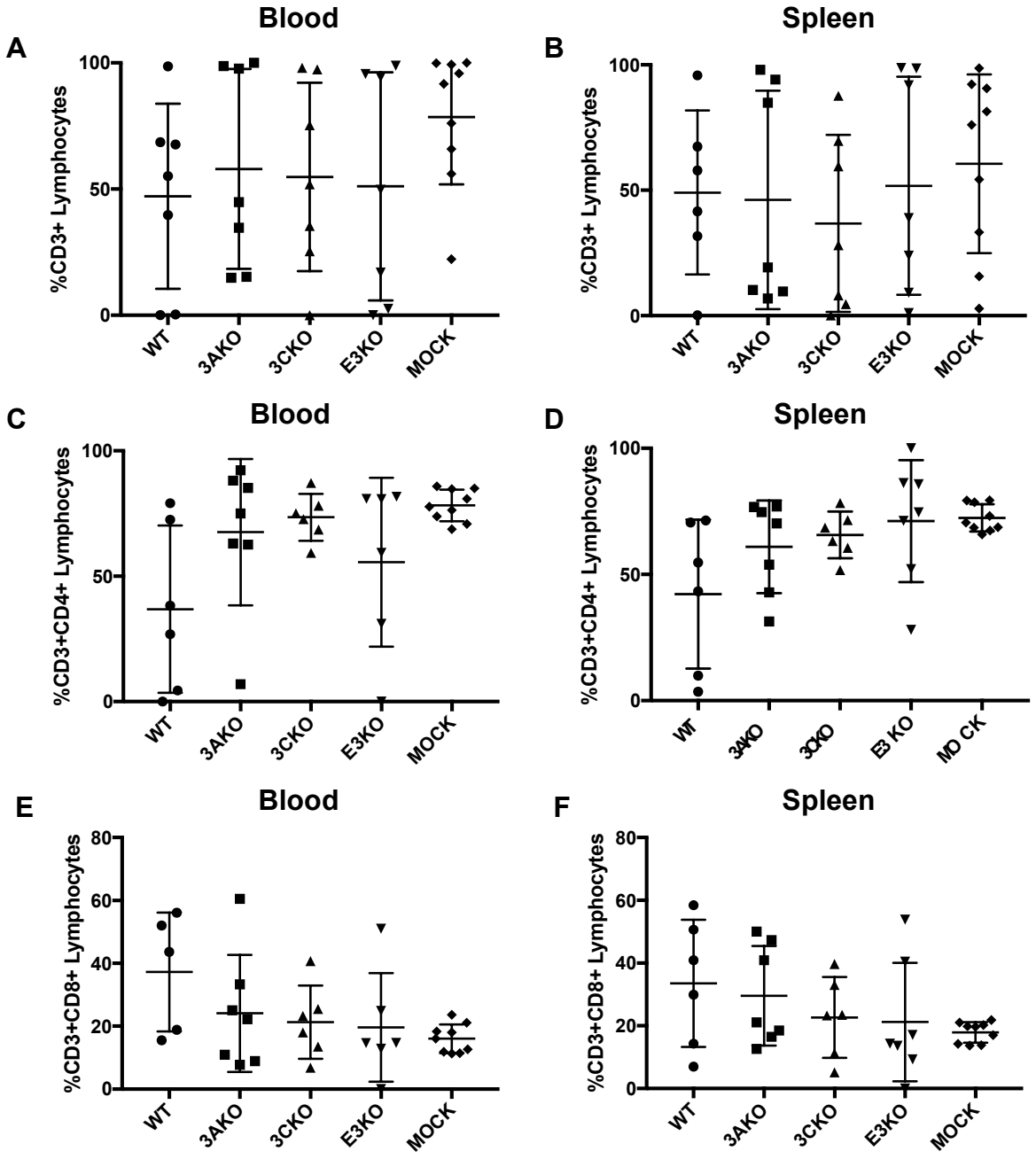


Figure 5.17. Hu-mice infected with recombinant EBV lacking the EBNA3 oncogenes can induce a cellular immune response. Percentage of $CD3^{+ve}$ (**A,B**) $CD3^{+ve}CD4^{+ve}$ (**C,D**) and $CD3^{+ve}CD8^{+ve}$ human $CD45^{+ve}$ lymphocytes in the peripheral blood or spleen (as indicated) of humanised mice infected with 10^5 GRU of WT (n=7), 3AKO (n=7), 3CKO (n=6) or E3KO (n=6) recombinant EBV for 6 weeks. Uninfected mice are shown as a comparison ('MOCK', n=9). Human CD45, CD3, CD4 and CD8 levels were assessed by flow cytometry. Each data point represents a single humanised mouse and horizontal bars represent the mean and standard deviation.

Consistent with enhanced EBV-mediated pathology, the average level of $CD8^{+ve}$ cells in the peripheral blood and the spleen in EBV infected hu-mice was elevated in mice presenting with macroscopically visible splenic tumours across all infections, compared to uninfected 'MOCK' mice and EBV-infected hu-mice not presenting with visible tumours (Figure 5.18).

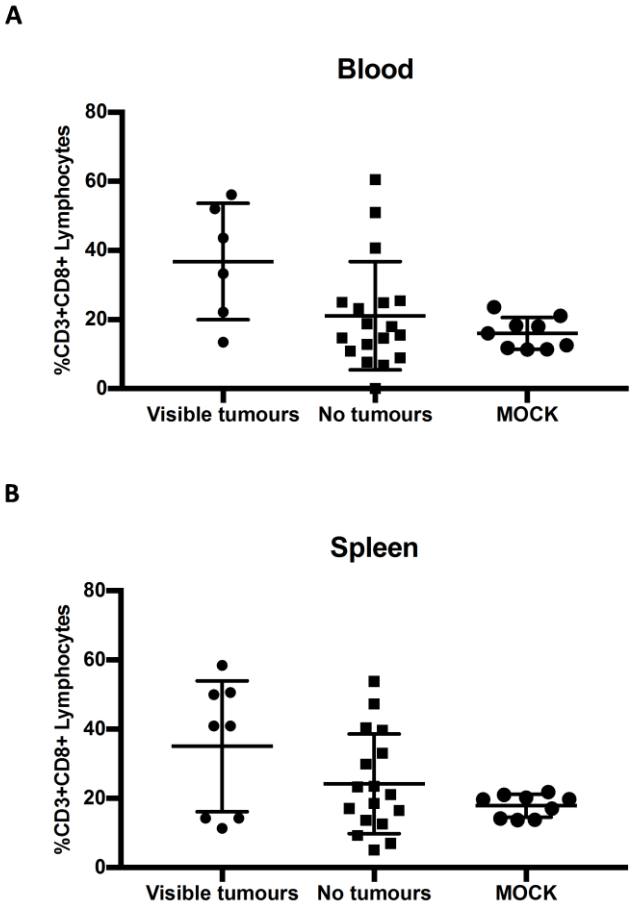


Figure 5.18. Mice exhibiting EBV-mediated tumour development have elevated levels of $CD8^{+ve}$ T cells. Percentage of $CD3^{+ve}$ $CD8^{+ve}$human lymphocytes in the peripheral blood (**A**) and spleen (**B**) of humanised mice infected with 10^5 GRU of WT, 3AKO, 3CKO or E3KO recombinant EBV for 6 weeks presenting with macroscopically visible tumour development (Visible tumours) or not (No tumours). Uninfected mice are shown as a comparison ('MOCK'). Human CD45, CD3 and CD8 levels were assessed by flow cytometry. Each data point represents a single humanised mouse and horizontal bars represent the mean and standard deviation.

5.2.2.7. Phenotypic analysis of B cell composition in humanised mice infected with EBV

The EBV life cycle is intimately linked with B cell biology. The GC model of EBV persistence suggests EBV infected cells transition through GC lymphoid structures and differentiate into MBC that

latently carry EBV as extra-chromosomal episomes (Babcock et al., 1998; Roughan and Thorley-Lawson, 2009). Furthermore, infection of $CD19^{+ve}$ primary B cells with EBV *in vitro* has demonstrated EBNA3A and EBNA3C repress the B cell to PC differentiation pathway likely as a mechanism to favour MBC differentiation and long-term persistence [(Styles et al., 2017); see Chapter IV]. Therefore, the composition of B cell populations in hu-mice infected with WT, 3AKO, 3CKO or E3KO recombinant EBV was assessed by flow cytometry. This was performed at a later stage in the study, therefore only a subset of mice was assessed.

Phenotypic analysis of the B cell composition in the peripheral blood of infected mice was inhibited due to low levels of human $CD19^{+ve}$ cells. Therefore, analysis was focused on lymphocytes isolated from the spleen of hu-mice infected with recombinant EBV. Splenic tissue was mechanically disrupted, and lymphocytes isolated by ficoll gradients prior to flow cytometric analysis for human B cell surface markers.

Cells positive for human CD45 were assessed for the percentage of $CD19^{+ve}$ cells (Figure 5.19A), which was variable within both EBV infected and uninfected 'MOCK' mice. Subsequent analysis of B cell surface markers to assess B cell populations was performed on these gated $CD19^{+ve}$ cells. Where less than 20% of the human lymphocytes identified were $CD19^{+ve}$, hu-mice were excluded from analysis as the low numbers could skew population percentages. However, this did reduce the number of mice within the analysis. The levels of $CD19^{+ve}$ cells were higher across all recombinant EBV infected hu-mice compared to uninfected 'MOCK' mice, possibly because of EBV-induced expansion of $CD19^{+ve}$ B cells. This subsequently hampered the phenotyping of B cell populations in uninfected 'MOCK' mice, as $CD19^{+ve}$ cells numbers were lower.

The majority of B cells isolated from the spleens of humanised mice both infected with recombinant EBV and uninfected mice were largely either transitional B cells (identified as $CD24^{high}$ and $CD38^{high}$ human lymphocytes) or were naïve B cells (identified as $CD27^{-ve}$ and IgD^{+ve} human lymphocytes) (Figure 5.19B/C). The dominance of immature transitional and naïve B cells in these hu-mice mirrors results in other humanized mouse models, as B cells in hu-mice are known to be severely

limited in their ability to undergo class switching and affinity maturation due to a lack of human secondary lymphoid organs (Jangalwe et al., 2016; Seung and Tager, 2013; Watanabe et al., 2009). Corresponding with these findings, no MBC (classified as $CD27^{+ve}$ and IgD^{+ve}) were identified in the uninfected or EBV recombinant infected hu-mice in this study (data not shown). This presents an issue in assessing EBV infection *in vivo* as the current model suggests EBV persistence in humans occurs in the MBC population.

Extremely low levels of plasmablast or PC characterised as $CD38^{high}$ and $CD138^{+ve}$ were identified in the majority of the hu-mice, with a small number of mice presenting with higher percentages of plasmablast or plasma cells, possibly skewed by low cell numbers (Figure 5.19D). These are likely short-lived PC due to the absence of GC maturation required for long-lived PC development. Cell numbers were not used due to the differing amounts of lymphocytes and B cells isolated from the spleens of different mice. There were no considerably elevated levels of plasmablasts or PC in E3KO infected hu-mice compared to hu-mice infected with EBV with functional EBNA3 proteins, despite evidence EBNA3 proteins repress the PC differentiation pathway (Styles et al., 2017). However, this could be a result of the limited ability of B cells to mature in humanised mice. It is possible EBV-mediated repression of PC differentiation is more important during the GC reaction which is not modelled in these mice.

Overall, there did not appear to be a difference in B cell populations between hu-mice infected with WT, compared to hu-mice infected with 3AKO, 3CKO or E3KO recombinant EBV or uninfected 'MOCK' mice. This suggests EBV does not affect the composition of B cell populations within the limits of this hu-mice model. Hu-mice models with advanced maturation of B cell populations, with secondary lymphoid organ development, may reveal EBV-associated B cell population diversity.

The overall distribution of B cell populations within these mice can be established by flow cytometry. However, the presence or absence of EBV infection within these B cells was not determined in the same manner. Therefore, gating of solely EBV positive cells was not possible. Presence of viral DNA and EBNA2 positive cells in the spleen and associated EBV pathology acts as an

assumption of successful EBV infection in these hu-mice. Advanced flow cytometric techniques to identify viral DNA alongside cell surface markers would enable analysis of the phenotypic analysis of B cells infected with EBV in humanised mice.

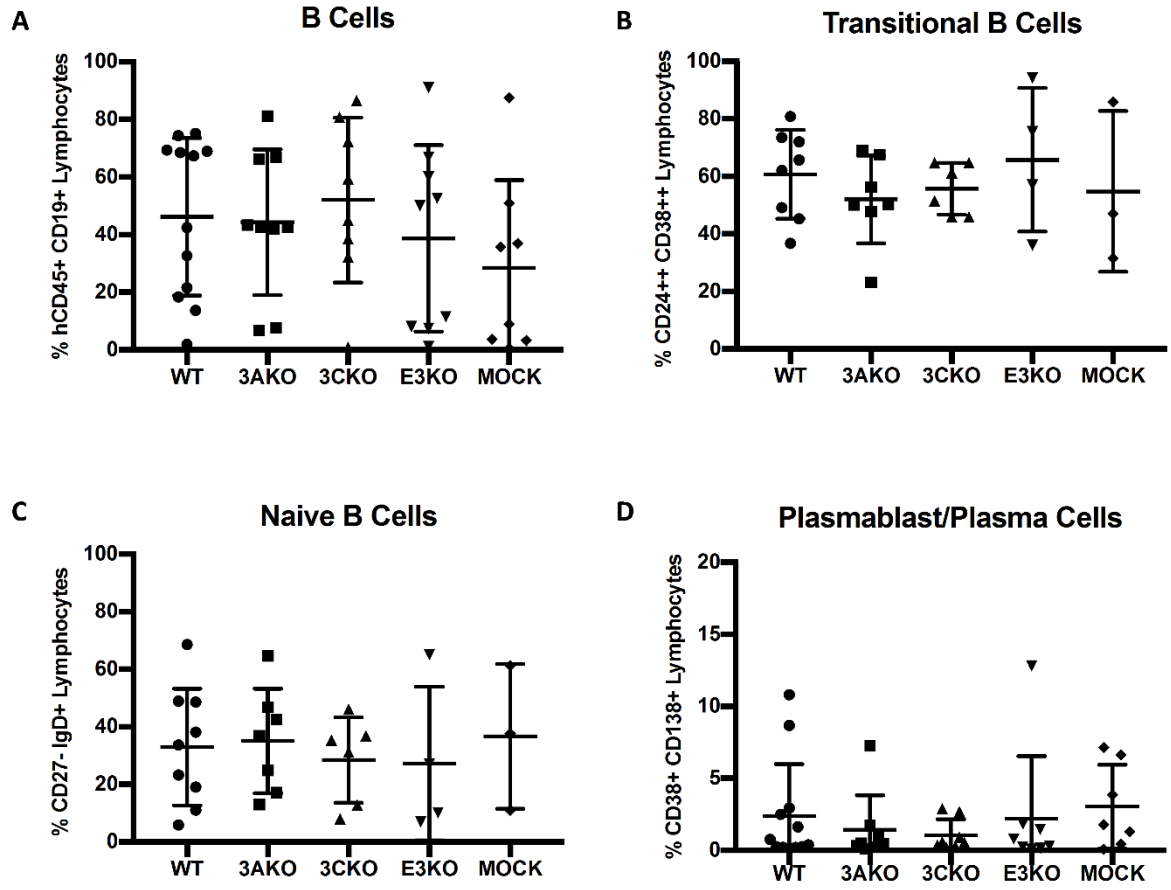


Figure 5.19. B cell populations in humanised mice infected with recombinant EBV lacking EBNA3 proteins. $CD19^{+ve}$ B lymphocytes (**A**), transitional B lymphocytes ($CD19^{+ve}$, $CD24^{high}$ and $CD38^{high}$, **B**) naïve B lymphocytes ($CD19^{+ve}$, $CD27^{-ve}$, IgD^{+ve}, **C**) and plasmablasts/plasma cells ($CD19^{+ve}$ $CD38^{+ve}$ $CD138^{+ve}$, **D**) as a percentage of live human $CD45^{+ve}$ lymphocytes in the spleen of humanised mice infected with 10^5 GRU of WT, 3AKO, 3CKO or E3KO recombinant EBV for 6 weeks. Uninfected mice are shown as a comparison ('MOCK'). Each data point represents a single humanised mouse and horizontal bars represent the mean and standard deviation. Cell surface markers were assessed by flow cytometry.

5.2.3. Determining the viability of using conditional ERT2 recombinant EBV viruses in humanised mice

Following successful analysis of hu-mice infected with EBV recombinant viruses containing EBNA3 deletions, the feasibility of using conditional ERT2 recombinant viruses in hu-mice was assessed. This was performed as a small-scale proof of concept experiment, as hu-mice have not previously been infected with ERT2 recombinant EBV viruses before. Therefore, only one small cohort of mice was used to establish feasibility of this system *in vivo*. This does therefore limit specific and robust conclusions. As a result of the small sample size statistical significance was not calculated.

5.2.3.1. Determining the viability of using tamoxifen-impregnated food

Following infection with ERT2 recombinant EBV, functional expression of the conditional protein relies upon introduction of HT. HT stabilises the fusion protein, allowing nuclear localisation and subsequent functional expression of the conditional fusion protein. *In vitro*, cells are exposed to HT to permit functional expression of conditional proteins, in the hu-mice TMX-food was utilized. Tamoxifen is metabolised in the liver of the mice to produce HT. It was hypothesised consumption of TMX-food and therefore HT would result in functional expression of the conditional protein and therefore a WT infection-like phenotype. The conditional ERT2 viruses that were generated in the lab used an ER that is not bound by endogenous mouse tamoxifen, enabling their use *in vivo* (Feil et al., 1997).

To acclimatise mice and determine predicted weight loss due to aversion to the TMX-food a feeding trial was performed prior to infection. Mice steadily lost weight over the first 4 days of ingesting TMX-food, such that severity levels were approached (15% loss of body weight). Regular food resumed over the next 2 days, which facilitated return to approximately the original weight prior to TMX-food (Figure 5.20, grey area). Upon replacement of regular food with TMX-food a second time, the weight of the mice dropped again but at a more rapid rate than seen previously. When food was weighed to determine how much was being consumed, the level of consumption of TMX-food was

seen to be negligible and far below that of food consumed in cages fed regular feed (data not shown). To increase palatability of TMX-food, it was mixed with water and placed in the bases of cages. This led to weight increase in approximately half of the mice and continued weight loss in the remaining mice. This suggests some, but not all, mice responded well to the wet food. To encourage sustained weight, alongside administration of tamoxifen, regular food and TMX-food were mixed 50:50 in water and placed in the base of the cage. Mice responded well to this food mix, but regular food was administered 2 days a week to allow weight recovery. Following stability of their weight on wet mix TMX-Food, hu-mice were infected with recombinant EBV viruses.

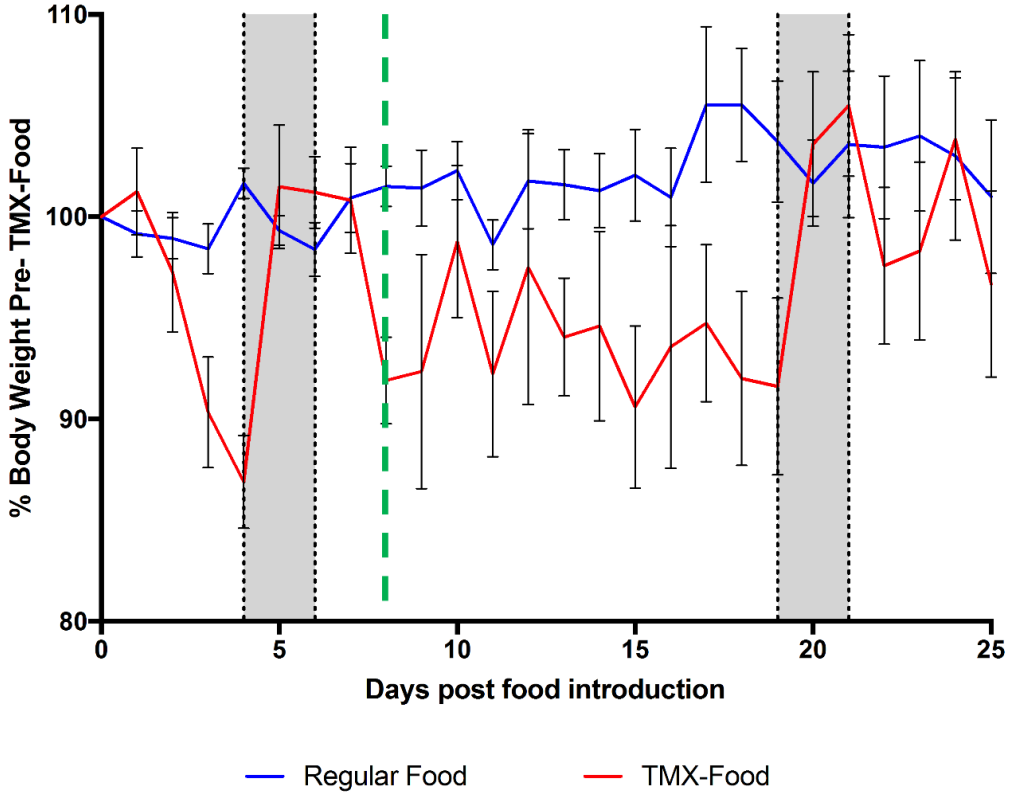


Figure 5.20. Humanised mice exhibit extensive weight loss when fed tamoxifen-impregnated food. Mice were weighed before introduction to tamoxifen-impregnated food (red, TMX-Food) and then weighed daily to evaluate percentage loss or gain of weight. To ensure weight gain, mice were fed regular food on select days (grey area). Wet food was started at 8 days post introduction of TMX-food (green dashed line). Mice fed regular food are shown for comparison (blue). Lines represent the mean weight percentage. Error bars represent standard deviation.

5.2.3.2. Weight analysis of humanised mice infected with conditional ERT2 recombinant EBV viruses

To assess the use of conditional EBV recombinant viruses *in vivo*, hu-mice were infected with 10^5 GRU of 3AERT2 whereby functional expression of EBNA3A is conditional upon the presence of the activating ligand HT. Half of the mice were not exposed to the activating ligand and fed regular mouse feed; the other half of the mice were exposed to tamoxifen (metabolised to HT in the liver) through the introduction of TMX-food. Uninfected 'MOCK' hu-mice and hu-mice infected with 10^5 GRU WT recombinant EBV were used as controls, with half fed with regular feed and half with TMX-food.

There was no notable difference in weight between EBV infected or uninfected 'MOCK' mice when fed regular food (Figure 5.21). As seen during previous experiments of KO-infected mice (Section 5.2.2.1), there was modest weight gain over the course of the experiment. However, weight of mice fed TMX-food was erratic, likely due to aversion to the modified feed and intermittent re-introduction of regular food. There was no notable difference in the weight of uninfected ('MOCK') mice fed TMX-food, to those infected with EBV and fed TMX-food (Figure 5.21), indicating weight changes across the 6-week infection was likely a result of food consumption, rather than disease burden. As weight loss could not be used as a measure of overall health, mice were inspected daily for signs of ill-health, such as isolation and hunched posture.

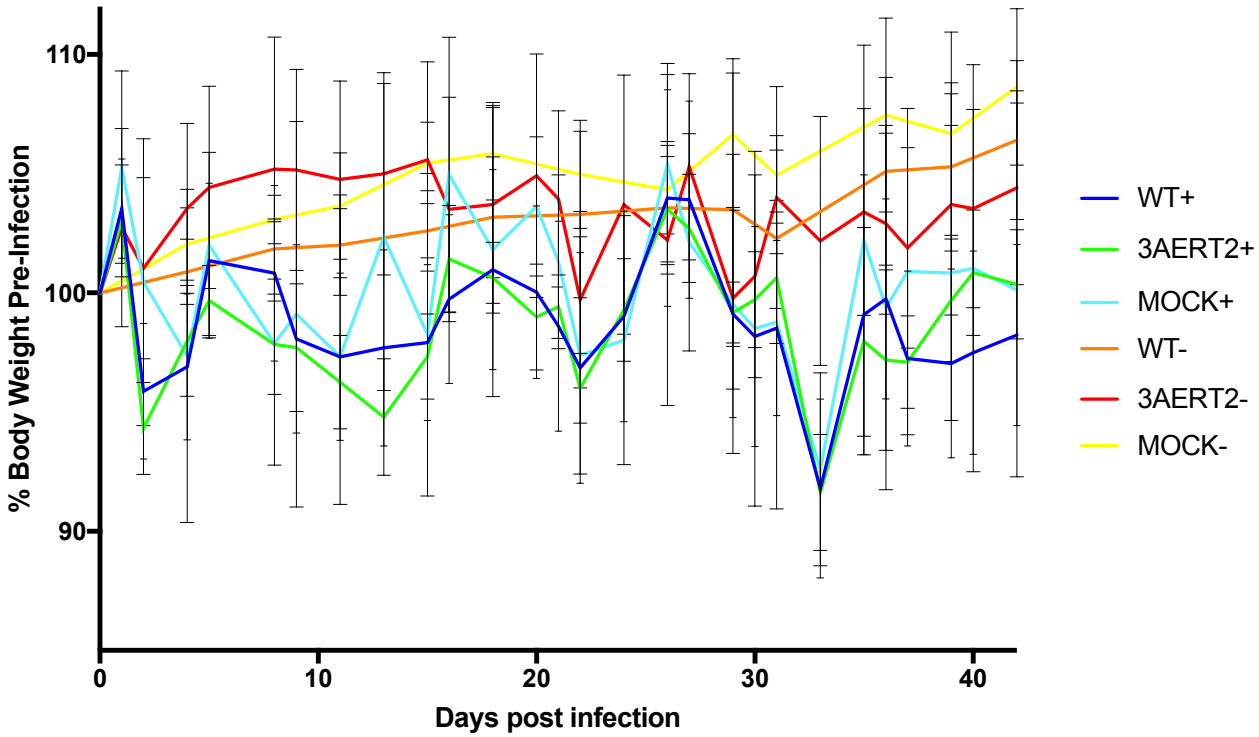


Figure 5.21. Humanised mice infected with recombinant EBV do not exhibit weight loss unless fed tamoxifen-impregnated food. Mice were weighed before the experiment and infected with 10^5 GRU WT or 3AERT2 recombinant EBV and every 1-2 days until sacrifice at 6 weeks post infection. Mice were fed either regular food (-) or tamoxifen-impregnated food (+) as indicated. For weight maintenance, mice were fed regular food on weekends. Weight of mice was evaluated as a percentage loss or gain from the weight at the start of infection. Lines represent the mean weight percentage change of mice in each category. Error bars represent standard deviation. Uninfected 'MOCK' mice are shown for comparison.

5.2.3.3. Splenic viral load in humanised mice infected with 3AERT2 conditional viruses is elevated when mice are exposed to tamoxifen, indicating functional EBNA3A expression

As a measure of EBV infection, DNA was extracted from the blood and spleen of hu-mice infected with WT or 3AERT2 at sacrifice (6 weeks pi) and qPCR for the EBV conserved gene BALF5 performed. No viral DNA was identified in the blood of mice infected with 3AERT2 (data not shown). This is likely a result of the small sample size, as viral DNA was only identified in blood of only a few mice infected with 3AKO (see Section 5.2.2.2).

Of the 6 hu-mice infected with 3AERT2 recombinant for 6 weeks and fed TMX-food, one exhibited a notably higher level of EBV DNA than mice fed regular food and infected with the same EBV recombinant virus (Figure 5.22). This suggests the TMX-food may be inducing functional expression of the conditional EBNA3A, as the higher level indicates a more WT-like phenotype. Only 2 mice infected with the 3AERT2 EBV without exposed to tamoxifen had identifiable EBV DNA, and at low levels, consistent with the 3AKO infected mice. The average level of EBV genomes were largely consistent in hu-mice infected with WT recombinant EBV and either fed regular food or TMX-food, with one mouse fed regular food exhibiting elevated levels of EBV DNA.

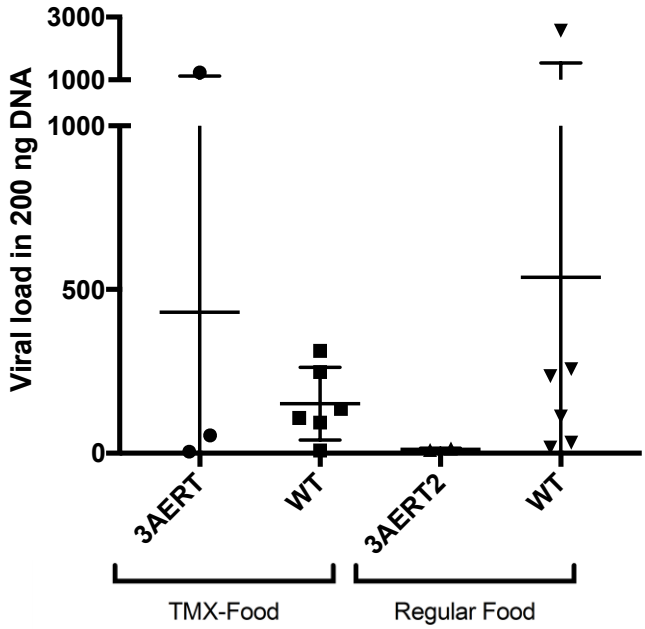


Figure 5.22. Tamoxifen can induce higher viral loads in the spleen of 3AERT2 infected hu-mice. EBV DNA genome copies in the splenic tissue of humanised mice infected with 10^5 GRU 3AERT2 or WT recombinant EBV and fed either regular food or tamoxifen impregnated food (TMX-Food) for 6 weeks. EBV genome copies were determined by qPCR of 200 ng of DNA purified from peripheral blood or splenic tissue. Recombinant EBV-infected mice with no detectable EBV DNA were not plotted. Horizontal bars represent the mean and standard deviation.

5.2.3.4. Tamoxifen-mediated conditional activation of EBNA3A in humanised mice infected with 3AERT2 recombinant EBV results in elevated tumour development

Consistent with functional EBNA3A expression and therefore a WT EBV phenotype, macroscopically visible splenic tumours were identified at a much higher frequency when hu-mice

were fed TMX-food following infection with 3AERT2 conditional recombinant EBV compared to mice with inactive EBNA3A (Figure 5.23). The number of hu-mice infected with 3AERT2 in the presence of tamoxifen presenting with visible tumour development was comparable to mice infected with WT EBV but not exposed to tamoxifen. In contrast, reduced tumour development was seen in mice infected with WT EBV that were not exposed to tamoxifen, which is likely a reflection of the lower viral load seen in these mice, or an artefact of the small cohort size (Figure 5.22).

Although it appears the introduction of tamoxifen through feed is inducing a WT EBV phenotype through activation of EBNA3A, tumour development was also seen in uninfected mice ('MOCK') when fed with TMX-Food. No tumour development had previously been seen in any uninfected 'MOCK' mice in previous experiments, when mice were not exposed to exogenous tamoxifen (n=13). This suggests that tamoxifen may be inducing tumour development in these mice. However, this contrasts the slight decrease in tumour development in WT EBV infected mice exposed to tamoxifen (although this could be attributable to the small sample size). Further experiments with a second cohort of mice may help illuminate whether tamoxifen is adversely affecting the hu-mice, or whether the small sample size is skewing these results. The presence of tumour development in the absence of EBV DNA in these 'MOCK' mice indicates that the use of TMX-food in this mouse model may not be suitable. Alternative methods of introducing HT or alternative conditional systems may be required to analyse EBNA3 proteins in a conditional manner *in vivo*.

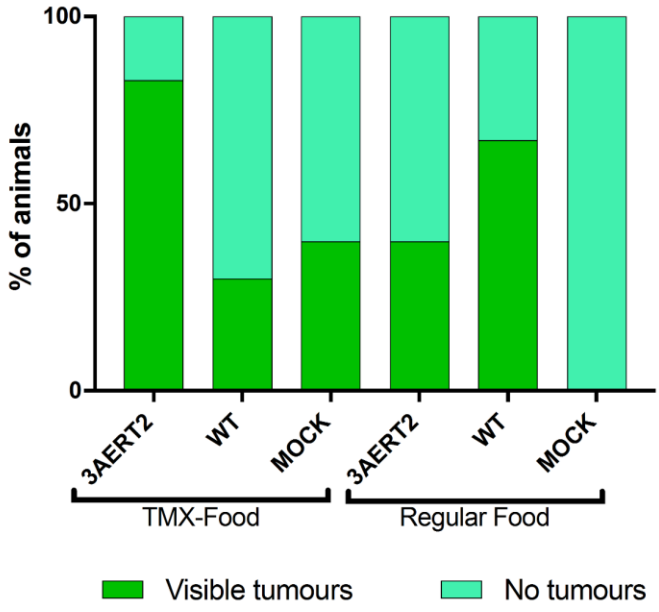


Figure 5.23. Tumour development in humanised mice infected with 3AERT2 recombinant EBV is elevated when tamoxifen is consumed. Frequency of macroscopically visible splenic tumour development in humanised mice 6 weeks post infection with 10^5 GRU of WT or 3AERT2 recombinant EBV and fed either regular food or tamoxifen-impregnated food (TMX-Food). Non-infected control humanised mice ('MOCK') are also shown. TMX-food; 3AERT2 n=5/6, WT=2/6, MOCK=2/5. Regular food; 3AERT2=2/5, WT=4/6, MOCK= 0/6.

5.2.3.5. Humanised mice infected with 3AERT2 conditional recombinant EBV exhibit elevated splenomegaly when EBNA3A is activated by exposure to tamoxifen

As a measure of EBV-associated pathology, splenomegaly was assessed in hu-mice infected with WT or 3AERT2 recombinant EBV for 6 weeks. When EBNA3A was assumed functionally active by the presence of tamoxifen following consumption of TMX-food, the average level of splenomegaly was notably higher than in hu-mice infected with the same 3AERT2 virus but not exposed to tamoxifen, and therefore presumed EBNA3A-null (Figure 5.24). Furthermore, consistent with the infection of mice with 3AKO, (see Section 5.2.2.4), one mouse did present with notable splenomegaly when EBNA3A was functionally inactive.

The level of splenomegaly in hu-mice infected with 3AERT2 EBV for 6 weeks was consistent with WT EBV-infected mice in the absence of TMX-food. This indicates that EBNA3A was indeed functional when TMX-food was consumed, resulting in a WT EBV-like infection phenotype. However, WT EBV-infected hu-mice exposed to tamoxifen did not exhibit splenomegaly with levels consistent with uninfected 'MOCK' mice with levels far lower that WT EBV infected hu-mice not exposed to tamoxifen (Figure 5.24). This is likely a result of the lower incidence of tumour development and lower viral loads seen in these hu-mice, and could be attributable to the small sample size assessed.

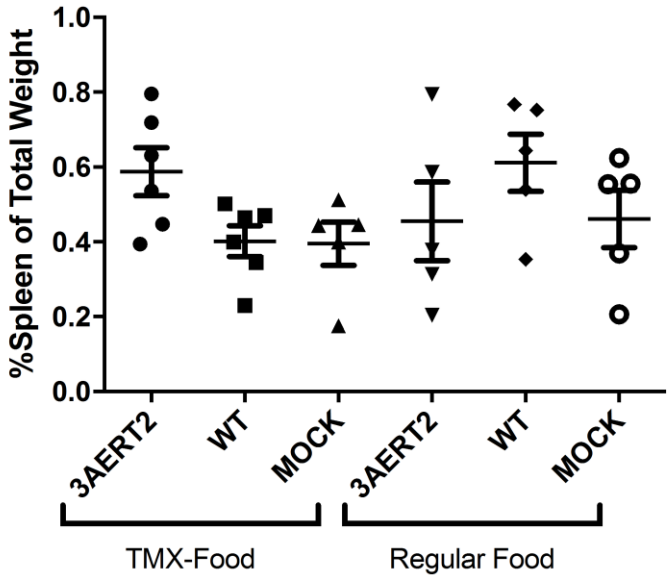


Figure 5.24. Splenomegaly in humanised mice infected with WT or 3AERT2 recombinant EBV in the presence and absence of tamoxifen. Spleen weight as a percentage of total body weight of humanised mice 6 weeks post infection with WT or 3AERT2 recombinant EBV and fed either regular food or tamoxifen-impregnated food (TMX-Food). Non-infected control humanised mice ('MOCK') are also shown. Each data point represents a single humanised mouse. Horizontal bars represent the mean.

5.2.3.6. Cell lines can be derived from the spleens of humanised mice infected with ERT2 conditional EBV in the presence of tamoxifen

It has previously been established that splenic lymphocytes derived from hu-mice infected with WT EBV can expand in culture and result in a continuously proliferating LCL [this study; (Strowig et al., 2009; White et al., 2012)]. Therefore, the ability of lymphocytes isolated from the spleens of hu-

mice infected with recombinant EBV with conditional expression of EBNA3A for 6 weeks to expand *ex vivo* was assessed. Spleens were mechanically disrupted, and lymphocytes were isolated by ficoll gradients then seeded to assess outgrowth in the presence of Cyclosporin A to inhibit T cell activity. Cells isolated from hu-mice infected with EBV with conditional expression of EBNA3A (3AERT2) only expanded in culture when hu-mice had been exposed to the activating ligand HT through consumption of TMX-food (Figure 5.25). Cells derived from half of the 3AERT2-infected mice in the presence of tamoxifen exhibited cell clumping characteristic of LCLs and EBV-mediated B cell transformation. Furthermore, cells isolated from one hu-mice infected with 3AERT2 recombinant EBV developed into a continuously proliferating LCL consistent with a WT EBV infection. Cells were classified as progressing to LCLs when they expanded to over 10 ml of continuously proliferating culture. This further indicates that the infection of hu-mice with 3AERT2 exposed to tamoxifen through TMX-food have induced functional expression of the conditional EBNA3A. This therefore allows *ex vivo* the outgrowth of splenic B cells characteristic of WT EBV infection.

B cells isolated from hu-mice infected with the conditional 3AERT2 and fed regular food did not expand in culture in either the presence or absence of HT. This resembles infection of hu-mice with 3AKO whereby EBNA3A is deleted, where no outgrowth of splenic lymphocytes was evident (see Section 5.2.2.5).

As expected, cells derived from the spleens of hu-mice infected with WT recombinant EBV and either exposed to, or not exposed to, tamoxifen expanded in culture with some exhibiting LCL-like clumping and others progressing into continuously proliferating LCLs (Figure 5.25).

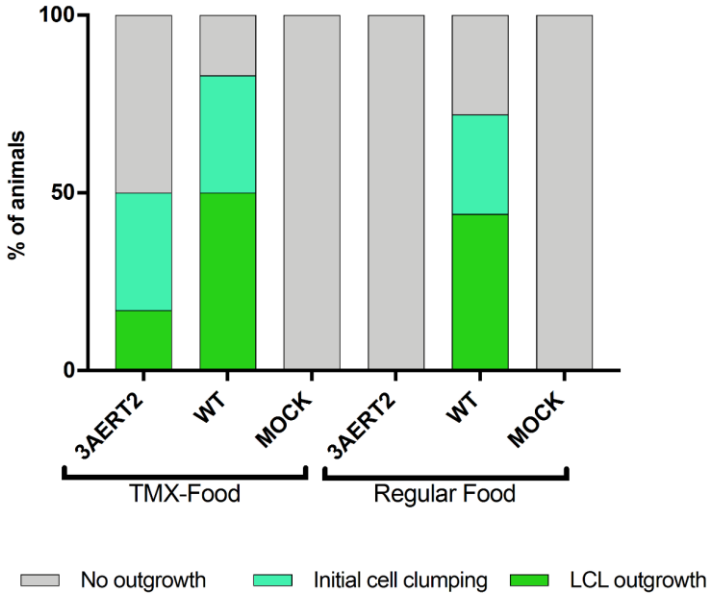


Figure 5.25. ***Ex vivo*** **outgrowth of B cells derived from the spleens of humanised mice infected with an 3AERT2 conditional recombinant EBV virus when EBNA3A was functional.** (**A**) Frequency of *ex vivo* outgrowth of B cells derived from the spleens of humanised mice 6 weeks post infection with WT or 3AERT2 recombinant EBV grown in the presence of 4-hydroxytamoxifen (+). Non-infected control humanised mice ('MOCK') are also shown. Initial cell clumping was assessed by light microscopy and LCL outgrowth refers to cell expansion to over 10 ml of LCL culture.

5.2.3.7. T cell populations in humanised mice infected with EBV with conditional expression of EBNA3A

As a measure of a possible EBV-mediated immune response, the level of CD4 and $CD8^{+ve}$ T cells in mice infected with WT or 3AERT2 recombinant EBV was assessed by flow cytometry. The level of $CD3^{+ve}$ T cells in the peripheral blood and spleens of hu-mice was variable between mice irrespective of EBV infection, or consumption of TMX-food (Figure 5.26).

The percentage of $CD8^{+ve}$ T cells in the blood and spleen was elevated in WT and 3AERT2 recombinant EBV-infected hu-mice compared to uninfected 'MOCK' mice fed regular food (Figure 5.26E/F). However, the level of $CD8^{+ve}$ T cells in uninfected mice fed TMX-food was comparable to EBV-infected mice. This may be a result of the EBV-independent tumour development seen in these mice, but prevents the firm conclusion of EBV-mediated increase of $CD8^{+ve}$ T cells in mice fed TMX-

food. Furthermore, despite elevated levels of viral DNA and tumour development, and therefore assumed EBV-induced disease in hu-mice infected with 3AERT2 with conditionally active EBNA3A (TMX-food) compared to those with inactive EBNA3A (regular food), there was no significant difference in the level of $CD8^{+ve}$ T cells. A larger sample size may reveal a more conclusive result.

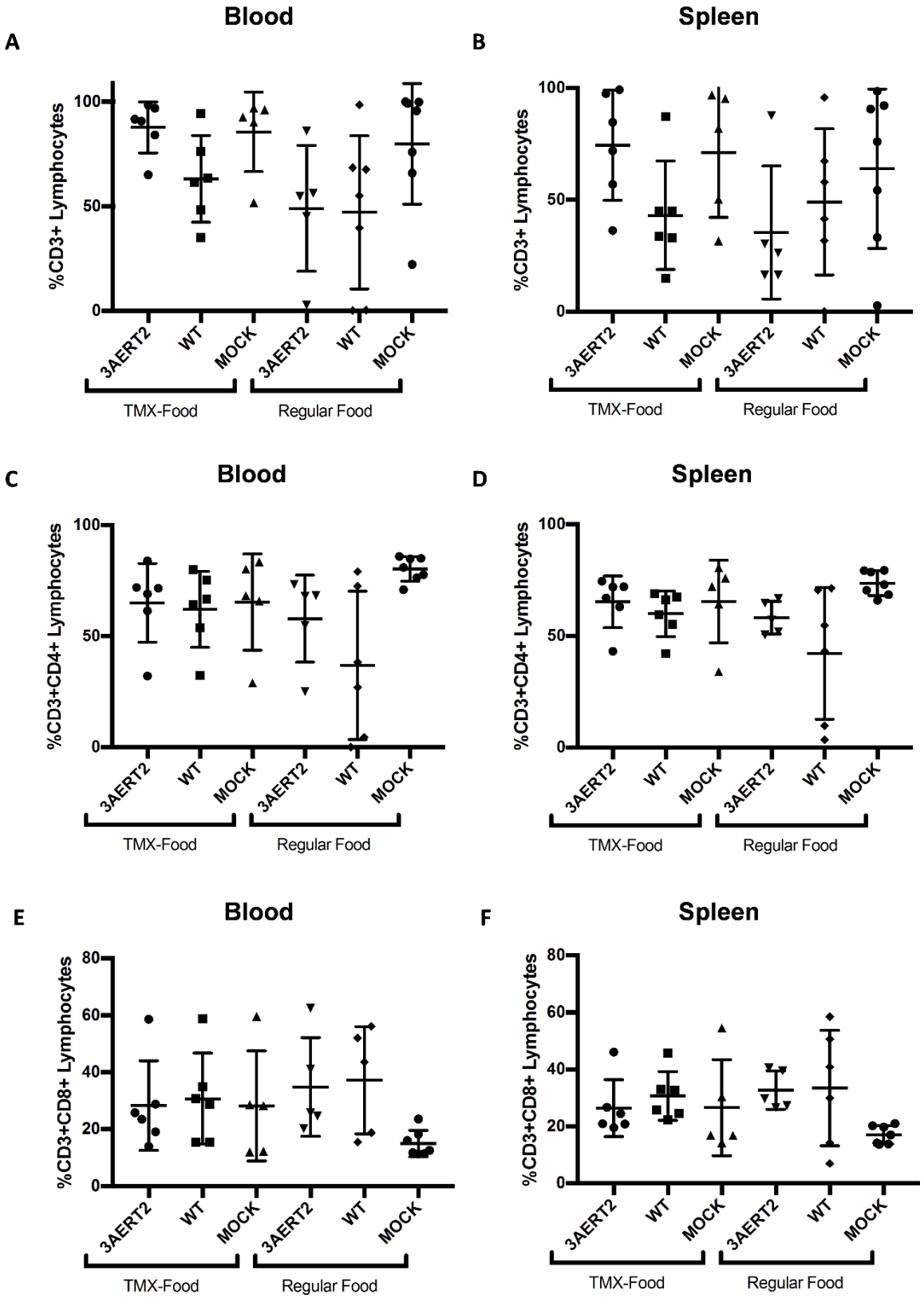


Figure 5.26. Hu-mice infected with recombinant EBV with conditional EBNA3A can induce a cellular immune response. Percentage of $CD3^{+ve}$ (**A,B**) $CD3^{+ve}CD4^{+ve}$ (**C,D**) and $CD3^{+ve}CD8^{+ve}$ (**E,F**) human $CD45^{+ve}$ lymphocytes in the peripheral blood or spleen (as indicated) of humanised mice infected with 10^5 GRU of WT or 3AERT2 recombinant EBV for 6 weeks. Uninfected mice are shown as a comparison

('MOCK'). Mice were fed either regular food or tamoxifen-impregnated food (TMX-Food). Human CD45, CD3, CD4 and CD8 levels were assessed by flow cytometry. Each data point represents a single humanised mouse and horizontal bars represent the mean and standard deviation.

5.3. Summary

This chapter details the establishment of a mouse model system with human immune system components in which to study the human-tropic virus EBV. Injection of human $CD34^{+ve}$ cells into new born mice led to adult hu-mice expressing human $CD45^{+ve}$ lymphocytes, including $CD19^{+ve}$ B cells and $CD3^{+ve}$ T cells in the peripheral blood and spleen.

The hu-mice model was permissive to EBV infection, and EBV was shown to persist in hu-mice for 6 weeks, even when mice were infected with EBV recombinant viruses deficient in EBNA3A, EBNA3C or the entire EBNA3 locus. Over the course of the 6-week infection, EBV DNA could be identified in the blood of some mice infected with WT, 3AKO, 3CKO and E3KO recombinant EBV. Unexpectedly, the highest levels of EBV DNA were identified in the blood of mice infected with E3KO at 5 weeks pi, where the entire EBNA3 locus (including the oncogenic EBNA3A and EBNA3C) were absent. However, at the point of sacrifice (6 weeks pi), EBV DNA levels in the blood and spleen were identified at a higher frequency in WT infected mice (and at higher levels) indicating a loss of EBV infected cells in E3KO infected hu-mice.

Analysis of the spleen and blood at the point of sacrifice showed infection of hu-mice with recombinant EBV lacking either EBNA3A, EBNA3C or the entire EBNA3 locus could lead to tumour development and splenomegaly in some mice, as well as elevated levels of $CD8^{+ve}$ T cells. However, the frequency of these aspects of disease were lower than those found in hu-mice infected with WT recombinant EBV where all EBNA3 proteins were functional. Furthermore, only splenic lymphocytes derived from mice infected with WT EBV exhibited LCL outgrowth *ex vivo*.

Hu-mice were also used in a small-scale experiment to assess the viability of using conditional recombinant EBV *in vivo*. The conditional EBNA3 proteins requires HT for stabilisation and subsequent function expression. Therefore TMX-food was utilized, as tamoxifen is metabolised in mice to produce

the activating ligand HT. Mice were infected with 3AERT2 recombinant EBV (or WT EBV as a control), and half exposed to the activating ligand through consumption of TMX-food. Mice infected with the conditional 3AERT2 virus exhibited elevated tumour development and higher EBV viral load when TMX-food was consumed, with a modest elevation in splenomegaly. Consistent with a WT phenotype, splenic lymphocytes isolated from 3AERT2 infected hu-mice exposed to tamoxifen exhibited LCL-like outgrowth *ex vivo,* whereas cells derived from hu-mice not exposed to tamoxifen did not. However, uninfected mock mice also presented with tumours following consumption of tamoxifen, indicating consumption of tamoxifen independent of EBV could be tumorigenic, and therefore has the potential to skew results.

5.4. Discussion

5.4.1. EBV persistence in the absence of EBNA3 proteins contrasts their central roles in B cell transformation *in vitro* and their role in favouring latency in memory B cells

Contrary to the requirement of EBNA3A and EBNA3C for efficient transformation of $CD19^{+ve}$ B cells, and maintenance of LCLs *in vitro* (Bazot et al., 2015; Hertle et al., 2009; Maruo et al., 2003, 2006, Skalska et al., 2010, 2013; Tomkinson et al., 1993), EBV was shown to persist in hu-mice for 6 weeks in the absence of the EBNA3A and EBNA3C oncogenes, and the absence of the entire EBNA3 locus.

Infection of hu-mice with 3AKO and 3CKO recombinant EBV led to identifiable EBV DNA in the peripheral blood and spleen of a number of mice (Figure 5.9 and 5.10), alongside EBNA2 positive cells in the spleen (Figure 5.14), indicating viral persistence in the absence of the EBNA3A and EBNA3C oncogenes for 6 weeks in hu-mice. This is consistent with Murer *et al*., who infected an NSG hu-mice model with 3AKO and 3CKO but used a higher viral titre compared to this study (10^6 GRU for 3AKO and 3CKO EBV viruses but 10^5 GRU for WT, compared to 10^5 GRU for all viruses in this study). This enabled detection of EBV DNA more clearly and strengthened the phenotype (Murer et al., 2018). Consistent with their study, EBV DNA was identified as a significantly higher level in both the blood

and spleen in WT infected mice, compared to mice infected with the KOs. This indicated infection is more productive when the oncogenic EBNA3 proteins are present.

Infection of hu-mice with EBV lacking the entire EBNA3 locus has not previously been performed. Identification of EBV DNA and EBNA2 positive cells in the spleen, with associated tumour development and splenomegaly, in some hu-mice infected with E3KO indicates EBV can also persist for 6 weeks without all three EBNA3 proteins. Unexpectedly, the highest levels of EBV DNA were identified in mice infected with E3KO at 5 weeks pi, with levels in 2 hu-mice clearly exceeding those of WT infected mice. However, the 5-week point appeared to represent a peak of infection, as the level of EBV DNA dropped dramatically at 6 weeks pi and was largely undetectable in the peripheral blood and spleen at sacrifice in E3KO infected hu-mice (Figures 5.9 and 5.10).

The increase in EBV viral load, and subsequent drop in E3KO infected hu-mice is possibly a result of the interplay between the absence of the oncogenic EBNA3A and EBNA3C, alongside the absence of the tumour suppressive EBNA3B. EBNA3B-deficient infections *in vivo* lead to elevated EBV DNA loads and have increased tumour development, and these tumours lack infiltrating T cells. Furthermore, *in vitro* the EBNA3B-deficient virus transforms B cells more readily and secretion of the T cell chemo-attractant CXCL10 is lower, resulting in reduced T cell recruitment (White et al., 2012). The absence of EBNA3B in the E3KO infection may be leading to a lack of T cell-mediated immune surveillance allowing the expansion of EBV infection for a period of time. Furthermore, the loss of all three of the EBNA3 proteins, which are all immunogenic and targeted by cytotoxic T cells [reviewed in (Rickinson and Moss, 1997)], could also be resulting in a dampened immune response against the virus. Following expanse of the virus, possibly due to a lack of immune control or absence of EBNA3B, it is possible that at a certain point the consequences of the absence of the oncogenes EBNA3A and EBNA3C may result in a loss of EBV infected cells, mirroring the cell cycle arrest and cell death seen *in vitro* in the absence of EBNA3A and EBNA3C (Maruo et al., 2003, 2011, Skalska et al., 2010, 2013). This would therefore lead to a reduction of EBV infected cells and consequentially an absence or reduction in identifiable EBV DNA. Although EBNA3 proteins are immunogenic, this theory could be confounded

by evidence that EBNA3C-deficient tumours in severely immunocompromised mice injected with 3CKO infected cord blood cells show increased T cell infiltration, and increased expression of T cell genes and chemokines (Romero-Masters et al., 2018). It would therefore be interesting to characterise EBNA3-KO infection in hu-mice with depleted $CD4^{+ve}$ and $CD8^{+ve}$ T cells to determine whether the increase in EBV DNA is a result of a lack of immune control, with T cell depletion shown to increase viral load and tumorigenesis (Strowig et al., 2009). It would also be of interest to determine the percentage of $CD4^{+ve}$ and $CD8^{+ve}$ T cells in E3KO infected mice on a weekly basis over the 6-week time course, rather than just at sacrifice, to determine whether this correlates with the levels of identifiable EBV DNA in infected mice.

A number of hu-mice infected with 3AKO, 3CKO or E3KO had identifiable macroscopically visible splenic tumours (Figure 5.11). This contrasts the findings of Murer *et al*., in which splenic tumours were not identified in NSG hu-mice infected with 3AKO or 3CKO, despite the higher amounts of EBV viruses administered to mice in this study (Murer et al., 2018). However, the presence of tumours in hu-mice infected with EBNA3C-deficient EBV have been identified in an alternative hu-mice system, also with reduced efficiency compared to WT infection and delayed kinetics (Romero-Masters et al., 2018). Here, EBNA3C-deficient tumour development was shown in severely immunocompromised adult NSG mice injected with CD34 depleted cord blood already infected with 3CKO EBV. This contrasts the method used in this study whereby new-born mice were humanised by engraftment of $CD34^{+ve}$ human cells prior to EBV infection of the hu-mice.

As EBNA3C-deficient tumours have been identified in severely immunocompromised mice humanised with 3CKO-infected $CD34^{+ve}$ cell depleted cord blood (Romero-Masters et al., 2018), it would be interesting to determine the phenotype of mice humanised with cord blood infected with either 3AKO or E3KO, and how this compares to 3CKO infection. The stronger phenotype seen in this model, in that almost 100% of mice humanised with WT infected cells and 40% of EBNA3C-deficient mice develop tumours (Romero-Masters et al., 2018), compared to around 50% of WT-infected and

20% of 3CKO-infected NRG hu-mice in this study, could help reveal further aspects of the combined and independent functions of EBNA3A and EBNA3C *in vivo*.

Similarly to infection of hu-mice with WT virus, which is known to result in expansion of $CD8^{+ve}$ T cells (Strowig et al., 2009; White et al., 2012), infection of hu-mice with 3AKO, 3CKO and E3KO viruses also saw an increase in $CD8^{+ve}$ cells in some mice (Figure 5.17), especially in mice presenting with macroscopically visible tumour development (Figure 5.18). Although this sample size was small and therefore significance could not be established with confidence, the expansion of $CD8^{+ve}$ T cells in some mice infected with 10^5 GRU EBV deficient in EBNA3A and EBNA3C was consistent with hu-mice infected with 10^6 GRU EBV infectious particles (Murer et al., 2018). EBV-specific T cell responses have previously been measured in EBV infected hu-mice using cell killing assays and ELISPOT assays enabling detection of IFN-γ production (Ma et al., 2011; Traggiai et al., 2004; Yajima et al., 2008). It would therefore be interesting to determine whether the elevated $CD8^{+ve}$ cell levels seen in some mice infected with 3AKO, 3CKO and E3KO are specific for EBV antigens to confirm an EBV-mediated immune response to these EBNA3-deficient viruses. Especially as EBNA3A- and EBNA3C-deficient EBV is thought to persist without elevated lytic replication (Murer et al., 2018); and T cells are thought to target lytic EBV antigens more frequently than latent antigens in hu-mice, with a greater response (Strowig et al., 2009).

The persistence of EBV *in vivo* in the absence of the EBNA3A or EBNA3C oncogenes, and the absence of the entire EBNA3 locus, indicates they are not vital for EBV infection *in vivo* despite their importance *in vitro*. *In vitro*, EBNA3A is considered important for transformation and EBNA3A-deficient LCLs have reduced proliferative capacity (Bazot et al., 2015; Hertle et al., 2009; Maruo et al., 2003; Tomkinson et al., 1993). EBNA3C is considered essential for primary B cell transformation and EBNA3C-deficient viruses are unable to establish LCLs (Maruo et al., 2006; Skalska et al., 2010, 2013; Tomkinson et al., 1993). Despite not being essential for persistence of EBV *in vivo*, in the absence of EBNA3A or EBNA3C oncogenes fewer mice presented with identifiable EBV in the peripheral blood and spleen than WT, and viral DNA levels were lower. In addition, WT infected mice presented with

significantly more tumour development and splenomegaly. Although EBNA3A and EBNA3C are not vital for persistence of EBV *in vivo*, they clearly promote infection with EBV, enhance viral persistence and promote oncogenic progression.

It is likely *in vivo* factors are enabling EBV to persist in the absence of EBNA3A and EBNA3C, as splenic lymphocytes were only able to outgrow when derived from hu-mice infected with WT EBV, where all EBNA3 proteins were expressed (Figure 5.15). Despite the presence of tumours in the spleens of 3AKO, 3CKO and E3KO infected mice [which increased the probability of outgrowth in cells from WT infected hu-mice (Figure 5.16)], no ex vivo LCL-like outgrowth occurred from splenic lymphocytes from KO infected mice. Murer *et al*., demonstrated that EBNA3A- and EBNA3C-deficient $CD19^{+ve}$ B cells can persist *in vitro* when CD40-L is provided by feeder cells (Murer et al., 2018). This indicates that *in vivo,* T cell-mediated CD40 stimulation of EBV infected cells lacking EBNA3A and EBNA3C may be supporting persistence of EBV in the absence of these oncogenes. As EBV DNA was more readily identified in the spleen than the peripheral blood following WT and KO infection of hu-mice (Figure 5.10), and has been found at higher levels in the spleen and lymph nodes following 3AKO and 3CKO infection (Murer et al., 2018), it is likely the microenvironment of these secondary lymphoid organs is aiding EBV persistence in the absence of EBNA3A and EBNA3C.

The similar experiments performed by Murer and colleagues to study EBNA3A and EBNA3C *in vivo* utilized an NSG hu-mice model, in contrast to the NRG model used in this study. The NRG hu-mice model has a Rag mutation instead of the scid mutation found in NSG mice. This may account for the discrepancy in the identification of tumours, as the mouse models used were not identical. However, these two models are phenotypically similar, with the only identified difference being NRG mice are considered more radioresistant than NSG mice. This is as the scid mutation is broadly expressed and involved in general DNA repair, whereas Rag genes are only involved in DNA recombination of the T and B cell receptors (Pearson et al., 2008).

Despite the presence of human $CD19^{+ve}$ B cells in the blood and spleen of hu-mice, some hu-mice did not present with identifiable EBV DNA in the blood or spleen, or associated pathology

following infection with an EBV recombinant virus. This leads to the assumption that they remained uninfected despite intraperitoneal introduction of infectious EBV virus. It may be that the level of EBV infection is not identified by qPCR analyses, or some mice simply do not get infected. The absence of EBV related pathology in a number of mice is somewhat similar to EBV infection in humans, as only a fraction of EBV-infected humans develop EBV-associated tumours. The biology behind this is largely uncharacterised, although clinical presentation of IM (symptomatic primary infection in adolescence) is thought to be a risk factor for EBV-mediated tumour development (Hjalgrim et al., 2000).

As baseline procedures were established during the course of these experiments, and optimisation of systems occurred throughout, some experiments had only a small sample size. This limits the ability to draw concise conclusions from this work, especially as infection with EBNA3-deficient viruses has a weaker phenotype than that of the WT. However, persistence of EBV in hu-mice in the absence of EBNA3A and EBNA3C is evident, and supports the conclusions of the recent publication also showing EBV persistence without the EBNA3A and EBNA3C oncogenes *in vivo* (Murer et al., 2018). Furthermore, for the first time, EBV was shown to persist for 6 weeks in the absence of all three EBNA3 proteins, leading to splenomegaly, tumour development and expansion of $CD8^{+ve}$ T cells in some hu-mice.

5.4.2. Conditional EBV in humanised mice

EBV recombinant viruses with conditional expression of EBNA3A, EBNA3C or both have revealed various aspects of EBV biology *in vitro* and provide a valuable system in which EBNA3 expression can be temporally controlled (Bazot et al., 2015; Maruo et al., 2003, 2006; Skalska et al., 2010; Styles et al., 2017). The ability to conditionally activate, inactivate or reactivate conditional EBNA3 oncogenes *in vivo* would enable assessment of the contributions and requirements of EBNA3A and EBNA3C to EBV-mediated tumorigenesis and pathogenesis.

A cohort of hu-mice were infected with recombinant EBV with conditional expression of EBNA3A (3AERT2) for 6 weeks. It was thought mice not exposed to the activating ligand HT would be EBNA3A-null and therefore mirror infection of hu-mice with 3AKO EBV, and mice exposed to the

activating ligand HT through consumption of TMX-food would exhibit a WT phenotype, due to activation of the conditional EBNA3A. The results from this small scale, proof of concept experiment provide merit to the further investigation this conditional system *in vivo*, with a higher number of mice required for more robust conclusions.

A mouse with EBV DNA levels comparable to WT following infection with 3AERT2 and exposure to tamoxifen was identified (Figure 5.22) and evidence of enhanced tumour development (Figure 5.23) and splenomegaly (Figure 5.24) in 3AERT2 infected hu-mice exposed to tamoxifen compared to mice not exposed to tamoxifen were found. This supports the hypothesis that tamoxifen metabolization is producing HT in 3AERT2 infected mice, leading to activation of EBNA3A protein expression, and therefore a more WT-like phenotype. Furthermore, LCL outgrowth from splenic lymphocytes was previously only possible from WT infected hu-mice, and no LCL-like clumping or outgrowth was seen from cell isolated from 3AKO infected mice (Figure 5.15). Splenic lymphocytes isolated from half of the 3AERT2 infected mice exposed to tamoxifen did exhibit LCL-like clumping ex vivo (with addition of HT), with full LCL outgrowth established from cells isolated from one of these mice. This indicates expression of active EBNA3A in the splenic lymphocytes of these hu-mice, and was therefore consistent with a WT phenotype [(Strowig et al., 2009; White et al., 2012), Figure 5.15]. The phenotype of hu-mice infected with WT EBV was largely unaffected by the consumption or absence of tamoxifen, although fewer tumours were seen. This indicates the different phenotypes observed between hu-mice infected with 3AERT2 is a result of the absence or consumption of TMX-food, which leads to the presence of the activating ligand HT and therefore seemingly active EBNA3A. However, a bigger cohort of mice is required to confirm this hypothesis.

Western blot or qPCR analysis of the conditional EBNA3 to quantify expression within the peripheral blood or secondary lymphoid organs of mice infected with 3AERT2 and exposed to tamoxifen would strengthen the theory that EBV is phenotypically WT in these mice. Especially as EBNA3 proteins with ERT2 fusions (particularly EBNA3A) have reduced expression compared to WT untagged EBNA3s (Chapter III). If the decreased levels of ERT2-tagged EBNA3A seen *in vitro* are

consistent in vivo, it may limit the use of this conditional system. Furthermore, it would be of benefit to know the time frame of exhaustion of the consumed tamoxifen and subsequent time frame of the inactivation of conditional proteins. *In vitro*, suspension of HT addition results in loss of conditional proteins at around 30-40 days post omission (Chapter III). However, quantifying this would require protein analysis of splenic cells over a time course, and the use of a large number of mice.

Administration of tamoxifen through TMX-food was problematic, with aversion to this alternative food leading to considerable weight loss. Therefore, alternative methods of administration could be employed upon expansion of this study. Injection of tamoxifen into transgenic Cre-lox mice has been shown to activate ER systems (Andersson et al., 2010; Kiermayer et al., 2007). However, as functional expression of conditional ERT2 fusion proteins requires continuous presence of HT, this would require daily injections. This is stressful and painful for the mice, and prohibitively labour intensive, therefore unfeasible. Increasing the palatability of the TMX-food, for example through introduction of sugar into the wet mix, may increase uptake and therefore possibly conditional protein activation. Alternatively, if a longer time period is available, a conditioning experiment where the composition of wet food is progressively altered from higher levels of regular food to higher levels of TMX-food could be performed to acclimatise the mice to TMX-food prior to infection.

Despite the widespread use of tamoxifen as an anti-cancer agent in humans [reviewed in (Jordan, 2003)], splenic tumours were identified independently of EBV infection in uninfected mice fed TMX-food, but not in uninfected mice not exposed to tamoxifen (Figure 5.23). This indicates the daily use of TMX-food may be inducing splenic tumours in hu-mice over the 6 week time course. Indeed, use of tamoxifen is associated with elevated risks of endometrial cancers in humans (Fornander et al., 1989) and daily doses was found to cause malignant liver tumours in rats (Gary et al., 1993). Alternatively, as this was a very small-scale experiment with mice of the same litters, the splenic tumours in these uninfected mice could have sporadically developed. Although tamoxifen induced tumours may skew results in EBV-infected mice, immunohistological staining of tumour samples to identify EBV proteins such as EBNA2 or LMP1, or EBER RNA *in situ* hybridisation on splenic

sections (Ma et al., 2017; Murer et al., 2018; Strowig et al., 2009; White et al., 2012), would characterise whether tumour development is a result of EBV infection rather than tamoxifen induced. Although EBNA3 immunohistochemical staining of splenic sections is not documented in the literature, if possible, staining for the conditional EBNA3 protein could also possibly help characterise expression and therefore WT phenotype in mice exposed to tamoxifen.

Although specific conclusions regarding the use of the conditional ERT2 recombinant virus system in hu-mice is limited by the small sample size, the results gained from this study add merit to the continued assessment of the feasibility of these viruses in hu-mice.

5.4.3. Expanding analysis of EBNA3-deficient EBV infection in humanised mice

The research performed in this chapter was primarily done to establish baseline protocols for the study of EBV in hu-mice, therefore there are many improvements and advances that could be made following the knowledge gained during these initial experiments, particularly overall expansion of the study.

Lymphoproliferative lesions have been identified in around 20-30% of hu-mice infected with WT EBV for 4 weeks (Chijioke et al., 2013). Following 6 weeks of WT EBV infection, tumour development was identified in 55% of hu-mice (Figure 5.11), consistent with other independent studies where over 50% of hu-mice developed splenic tumours after 6-8 weeks of EBV infection (Antsiferova et al., 2014; Ma et al., 2011). This suggests EBV-induced tumour incidence increases over time. Furthermore, using an alternative mouse model where EBV-infected CD34-depleted cord blood cells were injected into severely immunocompromised mice, the Kenney lab demonstrate EBV tumours resulting from an EBNA3C-deficient virus had delayed kinetics (Romero-Masters et al., 2018). Therefore, although splenic tumours were identified in 3AKO, 3CKO and E3KO infected mice (Figure 5.11), a higher incidence of tumours, and therefore a stronger identifiable phenotype, may result from

a longer infection period. Extending the time frame of the study may reveal further EBV mediated tumours in the lack of the EBNA3A and EBNA3C oncogenes, therefore enabling stronger conclusions.

It is also possible EBV can only persist in hu-mice for a shorter amount of time in the absence of the EBNA3 oncogenes, with EBV persistence in the absence of EBNA3A or EBNA3C shown for only 6 weeks in this study. This is indicated in the elevated levels of EBV DNA identified at 5 weeks pi in E3KO infected mice, which then becomes largely undetectable by 6 weeks pi in the peripheral blood and spleen (Figures 5.9 and 5.10). Furthermore, continuously proliferating LCLs could only be established from splenic lymphocytes derived from WT infected hu-mice (Figure 5.15). Although persistence of EBV in the absence of either EBNA3A or EBNA3C has been shown at 12 weeks pi, EBNA2 expression was decreased compared to levels at 5-6 weeks pi possibly indicating loss of EBV positive cells (Murer et al., 2018). It is possible EBV persistence in the absence of the entire EBNA3 locus could be lost after the 6-week infection time period. This would be more comparable to the situation *in vitro*, whereby $CD19^{+ve}$ B cells infected with EBNA3C-deficient viruses are not transformed into LCLs. EBNA3C-deficient cells proliferate in culture for around 10-15 days, at which point the consequences of the loss of EBNA3-mediated gene regulation begins to lead to cell cycle arrest and cell death at around 20 days pi (Skalska et al., 2013). However, there is a clear discrepancy in the time frames *in vitro* and *in vivo*. The time frame studied may be crucial to further assessing EBV persistence in the absence of the EBNA3A and EBNA3C oncogenes, with either an elevation of tumorigenesis and EBV pathogenesis, or loss of persistence possible. The spleens of EBV-infected hu-mice reveal more than the peripheral blood, in that they exhibit a higher frequency of identifiable EBV DNA, tumour development and immunohistochemical staining options. Therefore, a large-scale study in which splenic assessment is performed on a weekly basis in mice infected with either WT or EBNA3-deficient viruses could help further define EBV persistence in the absence of the EBNA3A and EBNA3C oncogenes.

It would also be beneficial to expand analysis of EBV infection hu-mice into alternative organs, particularly the lymph nodes which contain high levels of B cells, and have been shown previously to

contain EBV DNA at a higher level than the peripheral blood (Murer et al., 2018). Alongside the spleen and lymph nodes, EBV-mediated tumours have been identified in the kidney and liver (Strowig et al., 2009; Traggiai et al., 2004; Yajima et al., 2008), therefore EBV DNA load would likely also be identified in these organs. Expanding immunohistochemistry analysis to these organs as well, as well as to additional EBV proteins would also be beneficial. Staining for LMP-1 and EBNA2, alongside *in situ* hybridisation for EBER RNA, would enable classification of the latency stage of EBV-induced tumours (Ma et al., 2017, 2015; Murer et al., 2018; Strowig et al., 2009; White et al., 2012). Staining for T cells antigens including CD3, CD4 and CD8 could also help classify the immune response and infiltration of T cells into tumours induced by EBNA3-deficient EBV (Ma et al., 2017, 2015; Strowig et al., 2009; White et al., 2012). In addition, further expanding histological analysis using a double staining method would enable confirmation and quantification of EBV infected cells undergoing proliferation if stained for both EBNA2 and Ki67. EBNA3A- and EBNA3C-deficient cells have been shown to proliferate comparably to WT *in vivo* by immunofluorescence of EBNA2 and Ki67 (Murer et al., 2018), but this has not been established for EBV lacking expression of all three EBNA3 proteins.

Expanding analysis of hu-mice mediated immune control to innate responses may reveal further aspects of EBNA3-deficient infection. NK cells have been shown to control lytic EBV infection, with loss of NK cells resulting in enhanced IM symptoms and elevated tumorigenesis (Chijioke et al., 2013). However, mice infected with EBNA3A- and EBNA3C-deficient viruses have been found to persist in the absence of lytic replication, contrasting WT infected hu-mice who presented with viral DNA in the serum and BZLF1 positive cells in the spleen (Murer et al., 2018). Therefore, assessment of NK cells, particularly depletion, in EBNA3A- and EBNA3C-null mice could expand understanding of the innate immune response to EBV and whether EBNA3 proteins have a role in immune avoidance or as immunodominant epitopes.

EBV establishes latency in the MBC compartment, which requires progression and differentiation of B cells through GCs (Babcock et al., 1998). EBNA3A and EBNA3C are thought to repress PC differentiation to favour MBC differentiation during the GC reaction [Chapter IV, (Styles et

al., 2017)] and subsequent differentiation of latently infected MBC into PC results in lytic reaction of the virus (Laichalk and Thorley-Lawson, 2005). The lack of GC centre structures in the hu-mice model used in this study, and many others, prevents the assessment of this fundamental aspect of EBV biology due to the lack of class switching and affinity maturation of B cells (Jangalwe et al., 2016; Seung and Tager, 2013; Watanabe et al., 2009). Consistent with this, the majority of B cells identified in hu-mice following EBV infection in this study were naïve or translational (Figure 5.19). More advanced models, such as the BLT model which involves implantation of fetal thymic and liver tissues alongside injection of $CD34^{+ve}$ cells (from the same donor) into severely immunocompromised mice, do have rudimentary lymphoid structures containing human lymphocytes (Brainard et al., 2009; Lan et al., 2006; Melkus et al., 2006). These provide the required microenvironment for enhanced maturation of T and B cells in these hu-mice models and provide the potential to further study the EBV latency pathway in hu-mice. However, despite elevated maturation and differentiation, B cells at earlier developmental stages are still overrepresented in the spleen and bone marrow of BLT mice compared to adult humans (Brainard et al., 2009). Furthermore, terminally differentiated long lived PCs are not detected and short-lived plasmablasts are reduced compared to humans (Brainard et al., 2009). In addition, use of these models is limited due to the requirement of foetal tissues, and surgical facilities and expertise (Shultz et al., 2012). Further advanced hu-mice models with more representative B cell populations are still needed to fully model the EBV GC model of persistence *in vivo.*

5.5. Final conclusions

The most prominent conclusion from this work is that is it possible to generate a mouse model with human immune system components and infect them with EBV recombinant viruses to study EBV *in vivo.* Conclusions from this chapter regarding EBNA3A and EBNA3C *in vivo* are limited by the small cohorts of mice used for all experiments. This is as a result of the establishment of protocols and optimisation of experiments as they were performed for the first time over the course of this study. Nevertheless, EBV was shown to persist for 6 weeks in the absence of EBNA3A or EBNA3C, and for the first time it was shown EBV can persist in EBV infected hu-mice in the absence of all three EBNA3

proteins. In some mice, EBNA3-deficient EBV persistence correlated with tumour development, splenomegaly and elevated $CD8^{+ve}$ T cell levels. This indicates that although EBNA3A and EBNA3C are essential for B cell transformation and LCL maintenance *in vitro*, they are not vital for EBV persistence *in vivo*. Nevertheless, the elevated levels of EBV DNA and EBV-mediated pathology in WT infected mice indicate that viral persistence is enhanced when EBNA3A and EBNA3C are expressed.

A larger scale experiment is required to fully determine whether conditional ERT2 EBV viruses can be used *in vivo*. However, evidence of increase viral load, tumour development and splenomegaly in mice infected 3AERT2 and exposed to tamoxifen, compared to mice with not exposed to tamoxifen, suggests a WT-like phenotype and therefore the conditional activation of EBNA3A by tamoxifen. This indicates the ERT2 system could be used to investigate EBNA3 function in combination with TMX-food.

5.6. Remaining questions

This work was done to establish the feasibility of studying EBV in the hu-mice model, therefore there are various questions remaining. These include:

1. Why are EBV DNA levels so high in the blood of mice infected with E3KO at 5 weeks pi? And why do they decrease to almost undetectable levels by 6 weeks pi?

2. Why do some hu-mice get infected with EBV recombinant viruses and present with EBV DNA in the blood and spleen, whereas other mice do not get infected?

3. Would EBV persist in hu-mice infected with recombinant EBV lacking only EBNA3A and EBNA3C, rather than all EBNA3 proteins? Would the kinetics of EBV DNA presence mirror that of E3KO infected mice?

4. Can EBV persist in hu-mice the absence of the EBNA3 oncogenes for longer than 6 weeks?

5. What is the composition of EBV infected B cells in humanised mice? Does EBNA3A- and EBNA3C-mediated repression of the PC differentiation pathway lead to elevated PC development in E3KO infected mice? Would this be revealed in a hu-mice system with secondary lymphoid structures and therefore more matured B cells?

6. Could the GC model of EBV latency be investigated in a more sophisticated mouse model capable of generating GC and mature MBCs?

7. Why do uninfected mice fed TMX-food present with splenic tumour development?

8. Can introduction or withdrawal of TMX-Food allow the controlled activation or inactivation of conditional EBNA3 genes in the hu-mice model? What would be the time frame of inactivation or activation of modified EBNA3 expression?

6. Chapter VI: General discussion on the roles of EBNA3A and EBNA3C *in vitro* and *in vivo*

6.1. Translation of *in vitro* conclusions to results *in vivo*

Translation of the results gained from *in vitro* experiments to the biological complexities of *in vivo* studies is imperative in the understanding of pathogens and their associated diseases. Recently, the development of mice with human immune system components has allowed many aspects of EBV identified *in vitro* to be investigated within *in vivo* humanised mouse model systems. This not only expands EBV knowledge, but strengthens conclusions and confirmation of hypotheses.

In vitro, EBNA3A is considered important and EBNA3C essential for the efficient transformation of $CD19^{+ve}$ B cells into LCLs (Tomkinson et al., 1993). EBN3A-null LCLs can be produced, but they have reduced proliferative capacity (Bazot et al., 2015; Hertle et al., 2009). In contrast, in the absence of EBNA3C, LCLs cannot be produced, and infected cells undergo cell cycle arrest or cell death at around 3 weeks pi (Maruo et al., 2006; Skalska et al., 2013). The simultaneous absence of both EBNA3A and EBNA3C was shown to be cumulatively detrimental *in vitro* to both primary B cells and LCLs, with cell cycle arrest and cell death occurring at an elevated rate (Chapter III).

However, despite the importance of EBNA3A and EBNA3C for cell transformation and LCL maintenance *in vitro,* EBV was shown to persist in some hu-mice in the absence of either of the EBNA3A and EBNA3C oncogenes, and the absence of the entire EBNA3 locus, in hu-mice for 6 weeks [Chapter V, (Murer et al., 2018)]. This contradicts the critical expression of EBNA3A and EBNA3C *in vitro,* and indicates *in vivo* factors allow the persistence of EBV in the absence of the EBNA3A and EBNA3C oncogenes. In contrast, the assessment of an EBNA3B-deficient virus *in vivo* revealed its tumour suppressive activity, which corresponds to the increased transforming ability of EBNA3B-deficient viruses *in vitro* (White et al., 2012). This highlights that *in vivo* experiments reveal aspects of biology not captured by *in vitro* assessment, and are therefore important in the study of EBV. Although

EBV persistence in the absence of the EBNA3 oncogenes was shown, EBV-mediated pathology was found at a lower level indicating that, although they are not essential *in vivo*, EBNA3A and EBNA3C do enhance viral persistence. Nonetheless, further study is required to determine how EBV can persist in the absence of the EBNA3A and EBNA3C oncogenes in hu-mice for 6 weeks *in vivo*, when EBNA3A and EBNA3C are required for the transformation $CD19^{+ve}$ B cells and maintenance of LCLs *in vitro*.

Specific aspects of EBNA3A- and EBNA3C-mediated gene regulation identified *in vitro* have begun to be explored *in vivo,* such as EBNA3-mediated regulation of the CDKI $p16^{INK4c}$. *In vitro* studies have shown EBNA3A and EBNA3C transcriptionally repress $p16^{INK4a}$ by inducing deposition of the H3K27me3 repressive mark, mediated by PRC2, at the *CDKN2A* ($p16^{INK4a}$) locus (Maruo et al., 2006, 2011, Skalska et al., 2010, 2013). The translation of this finding to work performed *in vivo* was elegantly shown recently by immunohistochemistry. Here, double immunohistochemical staining of splenic sections of hu-mice infected with EBNA3A- or EBNA3C-KO recombinant EBV, were shown to have EBV positive cells with elevated levels of $p16^{INK4a}$ levels compared to mice infected with WT, whereby $p16^{INK4a}$ was repressed by the presence of functional EBNA3A and EBNA3C (Murer et al., 2018). In a separate system, also using immunohistochemistry, severely immunocompromised mice humanised by EBV infected cord blood also were shown to have elevated $p16^{INK4a}$ expression in EBV-induced lymphomas when EBNA3C was absent, further confirming the *in vitro* results (Romero-Masters et al., 2018). In addition, this cord blood system also demonstrated elevated BIM expression in EBV positive cells in the spleens of mice humanised with 3CKO-infected cord blood cells compared to WT infected cells (Romero-Masters et al., 2018). This corroborates *in vitro* findings which have shown that EBNA3C (alongside EBNA3A) transcriptionally represses BIM by PRC2 mediated deposition of H3K27me3 (Anderton et al., 2008; Paschos et al., 2012). Furthermore, RNA-seq of the EBNA3C-deficient tumours derived from cord-blood humanised mice has identified differential regulation of genes identified as directly regulated by EBNA3C by *in vitro* experiments (Romero-Masters et al., 2018). EBNA3C-deficient tumours had reduced *AICDA* expression [activated by EBNA3C (Kalchschmidt et al., 2016b)], and significantly increased expression of *CDKN2A, COBLL1, ADAMDEC1* and *ADAM28,*

which have been identified as targets for EBNA3C-mediated repression in *in vitro* studies (Kalchschmidt et al., 2016a; Maruo et al., 2011; Skalska et al., 2010, 2013). The consistency of EBNA3C-mediated regulation identified *in vitro,* within an *in vivo* EBV model, strengthens these hypothesises and enhances overall knowledge of the virus and its associated diseases.

Further studies assessing expression of other EBV-regulated genes, by double immunohistochemical staining of splenic sections derived from hu-mice infected with modified EBV recombinant viruses, and RNA-seq of EBNA3-deficient tumours would be beneficial. This would likely reveal further aspects of EBNA3A- and EBNA3C-mediated gene regulation.

6.2. Is evidence of EBNA3A- and EBNA3C-mediated suppression of PC differentiation *in vitro* recapitulated *in vivo*?

In vitro, the results in Chapter IV suggest EBNA3A- and EBNA3C-mediated suppression of the B cell to PC differentiation pathway. In $CD19^{+ve}$ primary B cells infected with an EBV recombinant virus where expression of both EBNA3A and EBNA3C was simultaneously inactive, increased mRNA and protein levels of the PC differentiation associated factors $p18^{INK4c}$ and BLIMP-1 were seen, indicating EBNA3A- and EBNA3C-mediated repression. Indeed, activation of $p18^{INK4c}$ and BLIMP-1 transcription could be restrained by the conditional activation of the EBNA3A and EBNA3C oncoproteins during primary infection. Elevated levels of these PC factors correlated with a PC-like cell surface phenotype and elevated Ig production in the absence of EBNA3A and EBNA3C. Suppression of PC differentiation likely favours the alternative MBC differentiation pathway during the GC reaction, and therefore persistence of EBV in latently infected MBC (Chapter IV, (Styles et al., 2017).

To assess this result *in vivo*, PC were assessed by flow cytometry for $CD138^{+ve}$ $CD38^{high}$ human B cells in hu-mice infected with EBV viruses with deletions in EBNA3A, EBNA3C and the entire EBNA3 locus (Chapter V). Unfortunately, despite EBNA3A- and EBNA3C-mediated repression of $p18^{INK4c}$ and BLIMP-1, and subsequent suppression of the PC differentiation pathway *in vitro*, there did not appear to be an increase in the presence of $CD138^{+ve}$ $CD38^{high}$ PC in hu-mice infected with E3KO virus for 6

weeks, compared to mice infected with WT EBV. Similarly, Murer *et al* did not identify an increase in $CD138^{+ve}$ cells in the spleens of hu-mice infected with 3AKO and 3CKO compared to WT when assessed by immunohistochemistry (Murer et al., 2018), despite an intermediate elevation of $p18^{INK4c}$ and BLIMP-1 in some EBNA3A-null and EBNA3C-null cells *in vitro* (Chapter IV).

Although the lack of evidence of PC differentiation suppression in WT EBV infected cells *in vivo* in this study is disappointing, it is possibly a result of inability to model the EBV GC model of persistence within the NRG hu-mice model, resulting from an absence of full B cell maturation due to the lack of human secondary lymphoid structures (discussed in Section 5.4.3). Repression of PC differentiation by EBV is theorised to promote differentiation of MBC from the GC reaction, therefore enhancing viral latency. But the absence of secondary lymphoid tissue inhibits the production of matured MBC and PC, therefore preventing assessment of EBV latency in many hu-mice models. Utilizing advanced hu-mice models such as the BLT model, where human thymic and liver tissue is introduced alongside $CD34^{+ve}$ cells which do generate rudimentary secondary lymphoid structures (Brainard et al., 2009; Lan et al., 2006; Melkus et al., 2006), may help to illuminate this phenomenon *in vivo.* However, even in these more advanced BLT hu-mice models, terminally differentiated long-lived PC were not identified, and the levels of short-lived plasmablasts were found to be lower than in adult humans (Brainard et al., 2009). Therefore, advanced hu-mice models with more representative PC populations, requiring full maturation in GCs, are required to fully determine EBNA3A- and EBNA3C-mediated repression of PC differentiation *in vivo*.

The propensity of the identified B cells populations in hu-mice to be EBV positive was not determined in the flow cytometry assays in this study. Flow cytometric analysis of specifically EBV positive B cells would aid study of the GC model of persistence and EBV-mediated suppression of PC differentiation *in vivo,* to conclusively identify the B cell compartments infected with EBV. *In situ* hybridisation using a peptide nucleic acid probe in combination with flow cytometry enabling detection of EBER has been shown in combination with cell surface markers (Kimura et al., 2009). However, the fixation step required may limit identification of surface antigens. Nevertheless, the

ability to quantify EBV infection and simultaneously characterise the phenotype of cell may reveal aspects of EBV latency if used in combination with advanced hu-mice models.

Alongside advanced flow cytometric analysis, other techniques could be employed to study the GC model of persistence and EBV-mediated repression of PC differentiation. Double immunohistochemical staining of EBV proteins, such as EBNA2 or LMP1, alongside PC cell factors such as the surface antigen CD138 or intracellular BLIMP-1, may identify the absence or presence of EBV positive PC in the spleens of EBV-infected hu-mice. Furthermore, it is possible RNA-seq of EBNA3KO tumours could reveal differential expression of genes associated with PC differentiation.

In addition, by injecting 3CKO infected CD34-depleted cord blood into immunosuppressed adult mice, EBV mediated tumours were found at an elevated level compared to the hu-mice model used in this study, where mice were humanised by $CD34^{+ve}$ cells before EBV infection [Chapter V, (Romero-Masters et al., 2018)]. If this 'stronger phenotype' also occurs following injection of E3KO-infected cord blood into immunosuppressed mice, it may reveal aspects of EBNA3A- and EBNA3C-mediated repression of PC differentiation.

Despite the lack of evidence of EBNA3A- and EBNA3C-mediated suppression of PC differentiation in infection models using hu-mice, mice with transgenic expression of EBV proteins do reveal evidence of EBNA3-mediated PC suppression. Using a Cre-lox mouse model system [described in (Wirtz et al., 2016)], transgenic expression of EBNA3A in murine $CD19^{+ve}$ B cells was shown to suppress the differentiation of B cells to PC (T. Sommerman et al*.,* unpublished). These *in vivo* results corroborate with the *in vitro* discovery of EBNA3A- and EBNA3C-mediated repression of the B cell to PC differentiation pathway.

6.3. Thesis summary

The extensive functions of the EBV oncogenic proteins EBNA3A and EBNA3C, encompassing the critical reprogramming of numerous host genes, are important for EBV persistence and latency. Determining the molecular mechanisms used by these proteins, and their functions during EBV infection, gives insight into how this ubiquitous and otherwise largely benign virus can lead to tumour development in a subset of infected hosts. The main findings of this thesis on the roles of EBV oncogenic proteins EBNA3A and EBNA3C *in vitro* and *in vivo* are summarised below:

1. A recombinant EBV virus was generated in which EBNA3A and EBNA3C are simultaneously conditionally expressed following fusion of an estrogen receptor to both genes, making functional expression dependent on the activating ligand HT:
    a. Infection of primary B cells with the newly constructed double conditional 3A3CERT2 virus revealed absence of both EBNA3A and EBNA3C results in a more extreme phenotype, with elevated cell death and reduced proliferation compared to when either EBNA3A or EBNA3C are expressed independently; this suggests independent and non-redundant functions alongside their overlapping roles.
    b. Loss of EBV-mediated regulation of CDKI was more profound in cells with simultaneously non-functional EBNA3A and EBNA3C, suggesting an overlap in EBNA3A- and EBNA3C-mediated repression of these cell cycle associated factors.

2. Infection of $CD19^{+ve}$ primary B cells with the double conditional 3A3CERT2 EBV virus revealed EBNA3A- and EBNA3C-mediated repression of the B cell to PC differentiation pathway:
    a. EBNA3A and EBNA3C were found to repress the CDKI and PC differentiation factor $p18^{INK4c}$, and the master regulator of PC differentiation, BLIMP-1.
    b. EBNA3A- and EBNA3C-mediated repression of $p18^{INK4c}$ and BLIMP-1 appeared to be regulated differently to each other and from the well-established reversible regulation of

the CDKI $p16^{INK4a}$, in that repression was irreversible in newly established LCLs, but repression of BLIMP-1 became reversible in LCLs cultured for over 6 months.

c. Concurrent with elevated levels of the PC differentiation factors $p18^{INK4c}$and BLIMP-1, the presence of PC cell surface markers and elevated Ig expression were identified in EBNA3A/EBNA3C-null cells at 20 days pi by flow cytometry, indicating progression along the PC differentiation pathway in the absence of EBNA3A and EBNA3C.

3. An NRG mouse model engrafted with human immune system components was established and shown to be permissive to infection with the human lymphotropic EBV. Base-line protocols for the study of EBV *in vivo* were developed.

4. Infection of hu-mice with recombinant EBV containing a deletion in either EBNA3A and EBNA3C, or a deletion in the entire EBNA3 locus, revealed:

   a. EBV can persist in hu-mice for 6 weeks in the absence of the oncogenic EBNA3 proteins, with the presence of EBV DNA in the blood and spleen established by qPCR and EBNA2 positive cells identified in the spleen by immunohistochemistry.

   b. EBV DNA levels were found to be highest in E3KO-infected hu-mice at 5 weeks pi, levels then dropped considerably at 6 weeks pi, indicating kinetics distinct from infection of hu-mice with 3AKO and 3CKO.

   c. Hallmarks of WT EBV infection of hu-mice (tumour development, splenomegaly and elevated $CD8^{+ve}$ T cell levels), were identified in some hu-mice infected with EBNA3-KO viruses but at a lower level. This indicates that although EBNA3A and EBNA3C oncoproteins are not required for EBV to persist for 6 weeks, they enhance viral persistence and therefore establishment of latency.

d. Evidence of EBNA3A- and EBNA3C-mediated repression of the PC differentiation pathway in EBV infected hu-mice was not seen by flow cytometric analysis of PC, likely due to the absence of B cell maturation in the humanised mouse model.

5. The viability of using conditional ERT2 recombinant EBV viruses in hu-mice models was assessed using selective introduction of food impregnated with tamoxifen to deliver the activating ligand HT:
    a. Although conclusions were limited by the small-scale of the experiment, mice infected with 3AERT2 and fed TMX-food had elevated tumour development and splenomegaly, and one had comparable EBV DNA levels to WT infected mice, indicating TMX-food was activating the conditional EBNA3A resulting in a WT-like phenotype.
    b. Some uninfected hu-mice developed splenic tumours when fed the TMX-food, suggesting daily administration of tamoxifen may be tumorigenic, therefore skewing assessment of EBV-induced tumours.

7. Bibliography

Abbot, S.D., Rowe, M., Cadwallader, K., Ricksten, A., Gordon, J., Wang, F., Rymo, L., and Rickinson, A.B. (1990). Epstein-Barr virus nuclear antigen 2 induces expression of the virus-encoded latent membrane protein. *Journal of virology*, *64*(5), 2126-2134.

Abbott, R.J.M., Quinn, L.L., Leese, A.M., Scholes, H.M., Pachnio, A., and Rickinson, A.B. (2013). CD8+ T Cell Responses to Lytic EBV Infection: Late Antigen Specificities as Subdominant Components of the Total Response. *The Journal of Immunology*, 1301629.

Albanese, M., Tagawa, T., Bouvet, M., Maliqi, L., Lutter, D., Hoser, J., Hastreiter, M., Hayes, M., Sugden, B., Martin, L., et al. (2016). Epstein–Barr virus microRNAs reduce immune surveillance by virus-specific CD8 $^{+}$ T cells. *Proceedings of the National Academy of Sciences*, *113*(42), E6467-E647

Albanese, M., Tagawa, T., Buschle, A., and Hammerschmidt, W. (2017). MicroRNAs of Epstein-Barr Virus Control Innate and Adaptive Antiviral Immunity. *Journal of virology*, *91*(16), e01667-16.

Alber, G., Kim, K.M., Weiser, P., Riesterer, C., Carsetti, R., and Reth, M. (1993). Molecular mimicry of the antigen receptor signalling motif by transmembrane proteins of the Epstein-Barr virus and the bovine leukaemia virus. *Current Biology*, *3*(6), 333-339.

Ali, N., Flutter, B., Sanchez Rodriguez, R., Sharif-Paghaleh, E., Barber, L.D., Lombardi, G., and Nestle, F.O. (2012). Xenogeneic Graft-versus-Host-Disease in NOD-scid IL-2Rγnull Mice Display a T-Effector Memory Phenotype. *PloS one*, *7*(8), e44219.

Alizadeh, a a, Eisen, M.B., Davis, R.E., Ma, C., Lossos, I.S., Rosenwald, a, Boldrick, J.C., Sabet, H., Tran, T., Yu, X., et al. (2000). Distinct types of diffuse large B-cell lymphoma identified by gene expression profiling. *Nature*, *403*(6769), 503.

Allday, M.J. (2009). How does Epstein-Barr virus (EBV) complement the activation of Myc in the pathogenesis of Burkitt's lymphoma? In *Seminars in cancer biology* (Vol. 19, No. 6, pp. 366-376). Academic Press.

Allday, M.J. (2013). EBV finds a polycomb-mediated, epigenetic solution to the problem of oncogenic stress responses triggered by infection. *Frontiers in genetics*, *4*, 212.

Allday, M.J., Crawford, D.H., and Griffin, B.E. (1989). Epstein-Barr virus latent gene expression during the initiation of B cell immortalization. *Journal of General Virology*, *70*(7), 1755-1764.

Allday, M.J., Bazot, Q., and White, R.E. (2015). The EBNA3 family: Two oncoproteins and a tumour suppressor that are central to the biology of EBV in B cells. In *Epstein Barr Virus Volume 2* (pp. 61-117). Springer, Cham.

Allen, C.D.C., Okada, T., and Cyster, J.G. (2007a). Germinal-Center Organization and Cellular Dynamics. *Immunity*, *27*(2), 190-202.

Allen, C.D.C., Okada, T., Tang, H.L., and Cyster, J.G. (2007b). Imaging of germinal center selection events during affinity maturation. *Science*, *315*(5811), 528-531.

Allen, M.D., Young, L.S., and Dawson, C.W. (2005). The Epstein-Barr virus-encoded LMP2A and LMP2B proteins promote epithelial cell spreading and motility. *Journal of virology*, *79*(3), 1789-1802.

Altmann, M., Pich, D., Ruiss, R., Wang, J., Sugden, B., and Hammerschmidt, W. (2006). Transcriptional activation by EBV nuclear antigen 1 is essential for the expression of EBV's transforming genes. *Proceedings of the National Academy of Sciences*, *103*(38), 14188-14193.

Ambinder, R.F., Shah, W. a, Rawlins, D.R., Hayward, G.S., and Hayward, S.D. (1990). Definition of the sequence requirements for binding of the EBNA-1 protein to its palindromic target sites in Epstein-Barr virus DNA. *Journal of virology*, *64*(5), 2369-2379.

Amyes, E., Hatton, C., Montamat-Sicotte, D., Gudgeon, N., Rickinson, A.B., McMichael, A.J., and Callan, M.F.C. (2003). Characterization of the CD4+ T cell response to Epstein-Barr virus during primary and persistent infection. *Journal of Experimental Medicine*, *198*(6), 903-911.

Andersson, K.B., Winer, L.H., Mørk, H.K., Molkentin, J.D., and Jaisser, F. (2010). Tamoxifen administration routes and dosage for inducible Cre-mediated gene disruption in mouse hearts. *Transgenic research*, *19*(4), 715-725.

Anderton, E., Yee, J., Smith, P., Crook, T., White, R.E., and Allday, M.J. (2008). Two Epstein-Barr virus (EBV) oncoproteins cooperate to repress expression of the proapoptotic tumour-suppressor Bim: Clues to the pathogenesis of Burkitt's lymphoma. *Oncogene*, *27*(4), 421.

Antsiferova, O., Müller, A., Rämer, P.C., Chijioke, O., Chatterjee, B., Raykova, A., Planas, R., Sospedra, M., Shumilov, A., Tsai, M.H., et al. (2014). Adoptive Transfer of EBV Specific CD8+T Cell Clones Can Transiently Control EBV Infection in Humanized Mice. *PLoS pathogens*, *10*(8), e1004333.

Aranda, S., Mas, G., and Di Croce, L. (2015). Regulation of gene transcription by Polycomb proteins. *Science advances*, *1*(11), e1500737.

Armitage, R.J., Fanslow, W.C., Strockbine, L., Sato, T.A., Clifford, K.N., Macduff, B.M., Anderson, D.M., Gimpel, S.D., Davis-Smith, T., and Maliszewski, C.R. (1992). Molecular and biological characterization of a murine ligand for CD40. *Nature*, *357*(6373), 80.

Ascherio, A., and Munger, K.L. (2015). EBV and autoimmunity. In Epstein Barr Virus. *Best practice & research Clinical rheumatology*, *22*(5), 883-896.

Ascherio, A., Munger, K.L., Lennette, E.T., Spiegelman, D., Hernán, M.A., Olek, M.J., Hankinson, S.E., and Hunter, D.J. (2001). Epstein-Barr virus antibodies and risk of multiple sclerosis: a prospective study. *Jama*, *286*(24), 3083-3088.

Babcock, G.J., Decker, L.L., Volk, M., and Thorley-Lawson, D.A. (1998). EBV persistence in memory B cells in vivo. *Immunity*, *9*(3), 395-404.

Babcock, G.J., Hochberg, D., and Thorley-Lawson, D.A. (2000). The expression pattern of Epstein-Barr virus latent genes in vivo is dependent upon the differentiation stage of the infected B cell. *Immunity*, *13*(4), 497-506.

Baer, R., Bankier, A.T., Biggin, M.D., Deininger, P.L., Farrell, P.J., Gibson, T.J., Hatfull, G., Hudson, G.S., Satchwell, S.C., Séguin, C., et al. (1984). DNA sequence and expression of the B95-8 Epstein—Barr virus genome. *Nature*, *310*(5974), 207.

Bai, F., Pei, X.-H., Godfrey, V.L., and Xiong, Y. (2003). Haploinsufficiency of p18(INK4c) sensitizes mice to carcinogen-induced tumorigenesis. *Molecular and cellular biology*, *23*(4), 1269-1277.

Bajaj, B.G., Murakami, M., Cai, Q., Verma, S.C., Lan, K., and Robertson, E.S. (2008). Epstein-Barr virus nuclear antigen 3C interacts with and enhances the stability of the c-Myc oncoprotein. *Journal of virology*, *82*(8), 4082-4090.

Balfour, H.H., Odumade, O.A., Schmeling, D.O., Mullan, B.D., Ed, J.A., Knight, J.A., Vezina, H.E., Thomas, W., and Hogquist, K.A. (2013). Behavioral, virologic, and immunologic factors associated with acquisition and severity of primary epstein-barr virus infection in university students. *The Journal of infectious diseases*, *207*(1), 80-88.

Balfour, H.H.J., Dunmire, S.K., and Hogquist, K.A. (2015). Infectious mononucleosis. *Clinical and Translational Immunology*

Banerjee, S., Lu, J., Cai, Q., Sun, Z., Jha, H.C., and Robertson, E.S. (2014). EBNA3C Augments Pim-1 Mediated Phosphorylation and Degradation of p21 to Promote B-Cell Proliferation. *PLoS pathogens*, *10*(8), e1004304.

Bartek, J., and Lukas, J. (2003). Chk1 and Chk2 kinases in checkpoint control and cancer. *Cancer cell*, *3*(5), 421-429.

Bartkova, J., Hořejší, Z., Koed, K., Krämer, A., Tort, F., Zleger, K., Guldberg, P., Sehested, M., Nesland, J.M., Lukas, C., et al. (2005). DNA damage response as a candidate anti-cancer barrier in early human tumorigenesis. *Nature*, *434*(7035), 864.

Bartkova, J., Rezaei, N., Liontos, M., Karakaidos, P., Kletsas, D., Issaeva, N., Vassiliou, L.V.F., Kolettas, E., Niforou, K., Zoumpourlis, V.C., et al. (2006). Oncogene-induced senescence is part of the tumorigenesis barrier imposed by DNA damage checkpoints. *Nature*, *444*(7119), 633.

Bazot, Q., Deschamps, T., Tafforeau, L., Siouda, M., Leblanc, P., Harth-Hertle, M.L., Rabourdin-Combe, C., Lotteau, V., Kempkes, B., Tommasino, M., et al. (2014). Epstein-Barr virus nuclear antigen 3A protein regulates CDKN2B transcription via interaction with MIZ-1. *Nucleic acids research*, *42*(15), 9700-9716.

Bazot, Q., Paschos, K., Skalska, L., Kalchschmidt, J.S., Parker, G.A., and Allday, M.J. (2015). Epstein-Barr Virus Proteins EBNA3A and EBNA3C Together Induce Expression of the Oncogenic MicroRNA

Cluster miR-221/miR-222 and Ablate Expression of Its Target $p57^{KIP2}$. *PLoS pathogens*, *11*(7), e1005031.

Bazot, Q., Paschos, K., and Allday, M.J. (2018). Epstein-Barr virus latent protein EBNA3A directly targets and silences the kinase *STK39* in B cells infected by EBV. *Journal of virology*, JVI-01918.

Beà, S., Salaverria, I., Armengol, L., Pinyol, M., Fernández, V., Hartmann, E.M., Jares, P., Amador, V., Hernández, L., Navarro, A., et al. (2009). Uniparental disomies, homozygous deletions, amplifications, and target genes in mantle cell lymphoma revealed by integrative high-resolution whole-genome profiling. *Blood*, *113*(13), 3059-3069.

Becker, J.L. (2007). The Cell Cycle. *XPharm: The Comprehensive Pharmacology Reference. 1-3*

Berges, B.K., and Tanner, A. (2014). Modelling of human herpesvirus infections in humanized mice. *Journal of General Virology*, *95*(10), 2106-2117.

Besson, A., Gurian-West, M., Chen, X., Kelly-Spratt, K.S., Kemp, C.J., and Roberts, J.M. (2006). A pathway in quiescent cells that controls p27Kip1 stability, subcellular localization, and tumor suppression. *Genes & development*, *20*(1), 47-64.

Besson, A., Dowdy, S.F., and Roberts, J.M. (2008). CDK Inhibitors: Cell Cycle Regulators and Beyond. *Developmental cell*, *14*(2), 159-169.

Bissig, K., Wieland, S.F., Tran, P., Isogawa, M., Le, T.T., Chisari, F. V, and Verma, I.M. (2010). Human liver chimeric mice provide a model for hepatitis B and C virus infection and treatment. *The Journal of clinical investigation*, *120*(3), 924-930.

Blackman, M.A., and Flaño, E. (2002). Persistent gamma-herpesvirus infections: what can we learn from an experimental mouse model? *Journal of Experimental Medicine*, *195*(7), F29-F32.

Blagosklonny, M. V., and Pardee, A.B. (2002). The restriction point of the cell cycle. *Cell cycle*, *1*(2), 102-109.

Blum, J.S., Wearsch, P.A., and Cresswell, P. (2013). Pathways of Antigen Processing. *Annual review of immunology*, *31*, 443-473.

Borza, C.M., and Hutt-Fletcher, L.M. (2002). Alternate replication in B cells and epithelial cells switches tropism of Epstein-Barr virus. *Nature medicine*, *8*(6), 594.

Bosma, G.C., Custer, R.P., and Bosma, M.J. (1983). A severe combined immunodeficiency mutation in the mouse. *Nature*, *301*(5900), 527.

Brady, G., MacArthur, G.J., and Farrell, P.J. (2007). Epstein-Barr virus and Burkitt lymphoma. *Postgraduate medical journal*, *84*(993), 372-377.

Brainard, D.M., Seung, E., Frahm, N., Cariappa, A., Bailey, C.C., Hart, W.K., Shin, H.-S., Brooks, S.F., Knight, H.L., Eichbaum, Q., et al. (2009). Induction of Robust Cellular and Humoral Virus-Specific Adaptive Immune Responses in Human Immunodeficiency Virus-Infected Humanized BLT Mice. *Journal of virology*, *83*(14), 7305-7321.

Bräuninger, A., Schmitz, R., Bechtel, D., Renné, C., Hansmann, M.L., and Küppers, R. (2006). Molecular biology of Hodgkin's and Reed/Sternberg cells in Hodgkin's lymphoma. *International journal of cancer*, *118*(8), 1853-1861.

Brink, A.A.T.P., Dukers, D.F., Van Den Brule, A.J.C., Oudejans, J.J., Middeldorp, J.M., Meijer, C.J.L.M., and Jiwa, M. (1997). Presence of Epstein-Barr virus latency type III at the single cell level in post-transplantation lymphoproliferative disorders and AIDS related lymphomas. *Journal of clinical pathology*, *50*(11), 911-918.

Brooks, L., Yao, Q.Y., Rickinson, A.B., and Young, L.S. (1992). Epstein-Barr virus latent gene transcription in nasopharyngeal carcinoma cells: coexpression of EBNA1, LMP1, and LMP2 transcripts. *Journal of virology*, *66*(5), 2689-2697.

Burkitt, D. (1958). A sarcoma involving the jaws in african children. *British Journal of Surgery*, *46*(197), 218-223.

Busson, P., McCoy, R., Sadler, R., Gilligan, K., Tursz, T., and Raab-Traub, N. (1992). Consistent transcription of the Epstein-Barr virus LMP2 gene in nasopharyngeal carcinoma. *Journal of virology*, *66*(5), 3257-3262.

Cahir-McFarland, E.D., Carter, K., Rosenwald, A., Giltnane, J.M., Henrickson, S.E., Staudt, L.M., and Kieff, E. (2004). Role of NF-kappa B in cell survival and transcription of latent membrane protein 1-expressing or Epstein-Barr virus latency III-infected cells. *Journal of virology*, *78*(8), 4108-4119.

Cai, X., Schäfer, A., Lu, S., Bilello, J.P., Desrosiers, R.C., Edwards, R., Raab-Traub, N., and Cullen, B.R. (2006). Epstein-Barr virus microRNAs are evolutionarily conserved and differentially expressed. *PLoS pathogens*, *2*(3), e23.

Calado, D.P., Zhang, B., Srinivasan, L., Sasaki, Y., Seagal, J., Unitt, C., Rodig, S., Kutok, J., Tarakhovsky, A., Schmidt-Supprian, M., et al. (2010). Constitutive Canonical NF-κB Activation Cooperates with Disruption of BLIMP1 in the Pathogenesis of Activated B Cell-like Diffuse Large Cell Lymphoma. *Cancer cell*, *18*(6), 580-589.

Caldwell, R.G., Wilson, J.B., Anderson, S.J., and Longnecker, R. (1998). Epstein-Barr virus LMP2A drives B cell development and survival in the absence of normal B cell receptor signals. *Immunity*, *9*(3), 405-411.

Callan, M.F., Steven, N., Krausa, P., Wilson, J.D., Moss, P.A., Gillespie, G.M., Bell, J.I., Rickinson, A.B., and McMichael, A.J. (1996). Large clonal expansions of CD8+ T cells in acute infectious mononucleosis. *Nature medicine*, *2*(8), 906.

Callan, M.F., Tan, L., Annels, N., Ogg, G.S., Wilson, J.D., O'Callaghan, C.A., Steven, N., McMichael, A.J., and Rickinson, A.B. (1998). Direct visualization of antigen-specific CD8+ T cells during the primary immune response to Epstein-Barr virus In vivo. *Journal of Experimental Medicine*, *187*(9), 1395-1402.

Cen, H., Breinig, M.C., Atchison, R.W., Ho, M., and McKnight, J.L. (1991). Epstein-Barr virus transmission via the donor organs in solid organ transplantation: polymerase chain reaction and restriction fragment length polymorphism analysis of IR2, IR3, and IR4. *Journal of virology*, *65*(2), 976-980.

Chaganti, S., Heath, E.M., Bergler, W., Kuo, M., Buettner, M., Niedobitek, G., Rickinson, A.B., and Bell, A.I. (2009). Epstein-Barr virus colonization of tonsillar and peripheral blood B-cell subsets in primary infection and persistence. *Blood*, *113*(25), 6372-6381.

Chang, K., Chen, Y., and Shibata, D. (1992). Description of an in situ hybridization methodology for detection of Epstein-Barr virus RNA in paraffin-embedded tissues, with a survey of normal and neoplastic. *Diagnostic molecular pathology: the American journal of surgical pathology, part B*, *1*(4), 246-255.

Chang, K.L., Albújar, P.F., Chen, Y.Y., Johnson, R.M., and Weiss, L.M. (1993). High prevalence of Epstein-Barr virus in the Reed-Sternberg cells of Hodgkin's disease occurring in Peru. *Blood*, *81*(2), 496-501

Chen, J., Sathiyamoorthy, K., Zhang, X., Schaller, S., Perez White, B.E., Jardetzky, T.S., and Longnecker, R. (2018). Ephrin receptor A2 is a functional entry receptor for Epstein-Barr virus. *Nature microbiology*, *3*(2), 172.

Cheng, M., Sexl, V., Sherr, C.J., and Roussel, M.F. (1998). Assembly of cyclin D-dependent kinase and titration of p27Kip1 regulated by mitogen-activated protein kinase kinase (MEK1). *Proceedings of the National Academy of Sciences*, *95*(3), 1091-1096.

Cheng, W.M., Chan, K.H., Chen, H.L., Luo, R.X., Ng, S.P., Luk, W., Zheng, B.J., Ji, M.F., Liang, J.S., Sham, J.S.T., et al. (2002). Assessing the risk of nasopharyngeal carcinoma on the basis of EBV antibody spectrum. *International journal of cancer*, *97*(4), 489-492.

Chijioke, O., Müller, A., Feederle, R., Barros, M.H.M., Krieg, C., Emmel, V., Marcenaro, E., Leung, C.S., Antsiferova, O., Landtwing, V., et al. (2013). Human natural killer cells prevent infectious mononucleosis features by targeting lytic epstein-barr virus infection. *Cell reports*, *5*(6), 1489-1498.

Chinnadurai, G. (2009). The transcriptional corepressor CtBP: A foe of multiple tumor suppressors. *Cancer research*, *69*(3), 731-734.

Chiu, Y., Lin, I.-Y., Su, S., Wang, K.-H., Yang, S., Tsai, D., Hsieh, Y., and Lin, K. (2014). Transcription factor ABF-1 suppresses plasma cell differentiation but facilitates memory B cell formation. *The Journal of Immunology*, 1400411.

Christophorou, M.A., Martin-Zanca, D., Soucek, L., Lawlor, E.R., Brown-Swigart, L., Verschuren, E.W., and Evan, G.I. (2005). Temporal dissection of p53 function in vitro and in vivo. *Nature genetics*, *37*(7), 718.

Cimprich, K.A., and Cortez, D. (2008). ATR: An essential regulator of genome integrity. *Nature reviews Molecular cell biology*, *9*(8), 616.

Cocco, M., Bellan, C., Tussiwand, R., Corti, D., Traggiai, E., Lazzi, S., Mannucci, S., Bronz, L., Palummo, N., Ginanneschi, C., et al. (2008). CD34+ cord blood cell-transplanted Rag2-/- gamma(c)-/- mice as a model for Epstein-Barr virus infection. *The American journal of pathology*, *173*(5), 1369-1378.

Coers, J., Starnbach, M.N., and Howard, J.C. (2009). Modeling infectious disease in mice: Co-adaptation and the role of host-specific IFNγ responses. *PLoS pathogens*, *5*(5), e1000333.

Cohen, J.I., Wang, F., Mannick, J., and Kieff, E. (1989). Epstein-Barr virus nuclear protein 2 is a key determinant of lymphocyte transformation. *Proceedings of the National Academy of Sciences*, *86*(23), 9558-9562.

Cotter, M.A., and Robertson, E.S. (2000). Modulation of histone acetyltransferase activity through interaction of epstein-barr nuclear antigen 3C with prothymosin alpha. *Molecular and cellular biology*, *20*(15), 5722-5735.

Crotty, S. (2015). A brief history of T cell help to B cells. *Nature Reviews Immunology*, *15*(3), 185.

Cubedo, E., Maurin, M., Jiang, X., Lossos, I.S., and Wright, K.L. (2011). PRDM1/Blimp1 downregulates expression of germinal center genes LMO2 and HGAL. *The FEBS journal*, *278*(17), 3065-3075.

Dang, C. V., O'Donnell, K.A., and Juopperi, T. (2005). The great MYC escape in tumorigenesis. *Cancer cell*, *8*(3), 177-178.

Dardari, R., Khyatti, M., Benider, A., Jouhadi, H., Kahlain, A., Cochet, C., Mansouri, A., Gueddari, B. El, Benslimane, A., and Joab, I. (2000). Antibodies to the Epstein-Barr virus transactivator protein (ZEBRA) as a valuable biomarker in young patients with nasopharyngeal carcinoma. *International journal of cancer*, *86*(1), 71-75.

Davies, M.L., Xu, S., Lyons-Weiler, J., Rosendorff, A., Webber, S.A., Wasil, L.R., Metes, D., and Rowe, D.T. (2010). Cellular factors associated with latency and spontaneous Epstein-Barr virus reactivation in B-lymphoblastoid cell lines. *Virology*, *400*(1), 53-67

Dawson, C.W., Tramountanis, G., Eliopoulos, A.G., and Young, L.S. (2003). Epstein-Barr virus latent membrane protein 1 (LMP1) activates the phosphatidylinositol 3-kinase/Akt pathway to promote cell survival and induce actin filament remodeling. *Journal of Biological Chemistry*, *278*(6), 3694-3704.

De-Thé, G., Geser, A., Day, N.E., Tukei, P.M., Williams, E.M., Beri, D.P., Smith, P.G., Dean, A.G., Bornkamm, G.W., Feorino, P., et al. (1978). Epidemiological evidence for causal relationship between Epstein-Barr virus and Burkitt's lymphoma from Ugandan prospective study. *Nature*, *274*(5673), 756.

De Silva, N.S., and Klein, U. (2015). Dynamics of B cells in germinal centres. *Nature reviews immunology*, *15*(3), 137.

Deenick, E.K., Avery, D.T., Chan, A., Berglund, L.J., Ives, M.L., Moens, L., Stoddard, J.L., Bustamante, J., Boisson-Dupuis, S., Tsumura, M., et al. (2013). Naive and memory human B cells have distinct requirements for STAT3 activation to differentiate into antibody-secreting plasma cells. *Journal of Experimental Medicine*, *210*(12), 2739-2753.

Dehay, C., and Kennedy, H. (2007). Cell-cycle control and cortical development. *Nature Reviews Neuroscience*, *8*(6), 438.

Delecluse, H.J., Hilsendegen, T., Pich, D., Zeidler, R., and Hammerschmidt, W. (1998). Propagation and recovery of intact, infectious Epstein-Barr virus from prokaryotic to human cells. *Proceedings of the National Academy of Sciences*, *95*(14), 8245-8250.

Dent, A.L., Shaffer, A.L., Yu, X., Allman, D., and Staudt, L.M. (1997). Control of inflammation, cytokine expression, and germinal center formation by BCL-6. *Science*, *276*(5312), 589-592.

Desai, S., Bolick, S.C.E., Maurin, M., and Wright, K.L. (2009). PU.1 Regulates Positive Regulatory Domain I-Binding Factor 1/Blimp-1 Transcription in Lymphoma Cells. *The Journal of Immunology*, jimmunol-0901120.

Dimri, G.P., Nakanishi, M., Desprez, P.Y., Smith, J.R., and Campisi, J. (1996). Inhibition of E2F activity by the cyclin-dependent protein kinase inhibitor p21 in cells expressing or lacking a functional retinoblastoma protein. *Molecular and cellular biology*, *16*(6), 2987-2997.

Dirmeier, U., Neuhierl, B., Kilger, E., Reisbach, G., Sandberg, M.L., and Hammerschmidt, W. (2003). Latent membrane protein 1 is critical for efficient growth transformation of human B cells by Epstein-Barr virus. *Cancer Research*, *63*(11), 2982-2989.

DiSanto, J.P., Muller, W., Guy-Grand, D., Fischer, A., and Rajewsky, K. (1995). Lymphoid development in mice with a targeted deletion of the interleukin 2 receptor gamma chain. *Proceedings of the National Academy of Sciences*, *92*(2), 377-381.

Doeing, D.C., Borowicz, J.L., and Crockett, E.T. (2003). Gender dimorphism in differential peripheral blood leukocyte counts in mice using cardiac, tail, foot, and saphenous vein puncture methods. *BMC clinical pathology*, *3*(1), 3.

Dontje, W., Schotte, R., Cupedo, T., Nagasawa, M., Scheeren, F., Gimeno, R., Spits, H., and Blom, B. (2006). Delta-like1-induced Notch1 signaling regulates the human plasmacytoid dendritic cell versus T-cell lineage decision through control of GATA-3 and Spi-B. *Blood*, *107*(6), 2446-2452.

Drake, A.C., Chen, Q., and Chen, J. (2012). Engineering humanized mice for improved hematopoietic reconstitution. *Cellular & molecular immunology*, *9*(3), 215.
Egle, A., Harris, A.W., Bouillet, P., and Cory, S. (2004). Bim is a suppressor of Myc-induced mouse B cell leukemia. *Proceedings of the National Academy of Sciences*, *101*(16), 6164-6169.
Enders, A., Bouillet, P., Puthalakath, H., Xu, Y., Tarlinton, D.M., and Strasser, A. (2003). Loss of the Pro-Apoptotic BH3-only Bcl-2 Family Member Bim Inhibits BCR Stimulation–induced Apoptosis and Deletion of Autoreactive B Cells. *Journal of Experimental Medicine*, *198*(7), 1119-1126.

Engels, N., Yigit, G., Emmerich, C.H., Czesnik, D., Schild, D., and Wienands, J. (2012). Epstein-Barr virus LMP2A signaling in statu nascendi mimics a B cell antigen receptor-like activation signal. *Cell Communication and Signaling*, *10*(1), 9.

Epstein, M.A., Achong, B.G., and Barr, Y.M. (1964). VIRUS PARTICLES IN CULTURED LYMPHOBLASTS FROM BURKITT'S LYMPHOMA. *Lancet*, *1*, 702-703

Epstein, M.A., Achong, B.G., Barr, Y.M., Zajac, B., Henle, G., and Henle, W. (1966). Morphological and virological investigations on cultured burkitt tumor lymphoblasts (strain raji). *Journal of the National Cancer Institute*, *37*(4), 547-559.

EPSTEIN, M.A., HENLE, G., ACHONG, B.G., and BARR, Y.M. (1965). MORPHOLOGICAL AND BIOLOGICAL STUDIES ON A VIRUS IN CULTURED LYMPHOBLASTS FROM BURKITT'S LYMPHOMA. *Journal of experimental medicine*, *121*(5), 761-770.

Epstein, A. (2015). Why and how epstein-barr virus was discovered 50 years ago. In *Epstein Barr Virus Volume 1* (pp. 3-15). Springer, Cham.

Eynon, E.E., and Flavell, R.A. (1999). Walking through the forest of transgenic models of human disease. *Immunological reviews*, *169*(1), 5-10.

Feederle, R., Kost, M., Baumann, M., Janz, A., Drouet, E., Hammerschmidt, W., & Delecluse, H. J. (2000). The Epstein–Barr virus lytic program is controlled by the co-operative functions of two transactivators. *The EMBO journal*, *19*(12), 3080-3089.

Feederle, R., Bartlett, E.J., and Delecluse, H.-J. (2010). Epstein-Barr virus genetics: talking about the BAC generation. *Herpesviridae*, *1*(1), 6.

Feil, R., Wagner, J., Metzger, D., and Chambon, P. (1997). Regulation of Cre recombinase activity by mutated estrogen receptor ligand-binding domains. *Biochemical and biophysical research communications*, *237*(3), 752-757.

Felsenfeld, G., and Groudine, M. (2003). Controlling the double helix. *Nature*, *421*(6921), 448.

Fero, M.L., Rivkin, M., Tasch, M., Porter, P., Carow, C.E., Firpo, E., Polyak, K., Tsai, L.H., Broudy, V., Perlmutter, R.M., et al. (1996). A syndrome of multiorgan hyperplasia with features of gigantism, tumorigenesis, and female sterility in p27Kip1-deficient Mice. *Cell*, *85*(5), 733-744.

Ferrari, K.J., Scelfo, A., Jammula, S.G., Cuomo, A., Barozzi, I., Stützer, A., Fischle, W., Bonaldi, T., and Pasini, D. (2014). Polycomb-Dependent H3K27me1 and H3K27me2 Regulate Active Transcription and Enhancer Fidelity. *Molecular cell*, *53*(1), 49-62.

Finke, J., Rowe, M., Kallin, B., Ernberg, I., Rosén, A., Dillner, J., and Klein, G. (1987). Monoclonal and polyclonal antibodies against Epstein-Barr virus nuclear antigen 5 (EBNA-5) detect multiple protein species in Burkitt's lymphoma and lymphoblastoid cell lines. *Journal of Virology*, *61*(12), 3870-3878.

Fischer, S.F., Bouillet, P., O'Donnell, K., Light, A., Tarlinton, D.M., and Strasser, A. (2007). Proapoptotic BH3-only protein Bim is essential for developmentally programmed death of germinal center-derived memory B cells and antibody-forming cells. *Blood*, *110*(12), 3978-3984.

Fornander, T., Rutqvist, L.E., Cedermark, B., Glas, U., Mattsson, a, Silfverswärd, C., Skoog, L., Somell, a, Theve, T., and Wilking, N. (1989). Adjuvant tamoxifen in early breast cancer: occurrence of new primary cancers. *The Lancet*, *333*(8630), 117-120.

Frappier, L., and O'Donnell, M. (1991). Overproduction, purification, and characterization of EBNA1, the origin binding protein of Epstein-Barr virus. *Journal of Biological Chemistry*, *266*(12), 7819-7826.

Fujiwara, S., Matsuda, G., and Imadome, K.-I. (2013). Humanized Mouse Models of Epstein-Barr Virus Infection and Associated Diseases. *Pathogens*, *2*(1), 153-176.

Fujiwara, S., Imadome, K.I., and Takei, M. (2015). Modeling EBV infection and pathogenesis in New-generation humanized mice. *Experimental & molecular medicine*, *47*(1), e135.

Fulop, G.M., and Phillips, R.A. (1990). The scid mutation in mice causes a general defect in DNA repair. *Nature*, *347*(6292), 479.

Gagrica, S., Brookes, S., Anderton, E., Rowe, J., and Peters, G. (2012). Contrasting behavior of the p18INK4c and p16INK4a tumor suppressors in both replicative and oncogene-induced senescence. *Cancer research*.

Gahn, T. a, and Sugden, B. (1995). An EBNA-1-dependent enhancer acts from a distance of 10 kilobase pairs to increase expression of the Epstein-Barr virus LMP gene. *Journal of virology*, *69*(4), 2633-2636.

Gary, W.M., Iatropoulos, M.J., Djordjevic, M. V., and Kaltenberg, O.P. (1993). The triphenylethylene drug tamoxifen is a strong liver carcinogen in the rat. *Carcinogenesis*, *14*(2), 315-317.

Giacinti, C., and Giordano, A. (2006). RB and cell cycle progression. *Oncogene*, *25*(38), 5220.

Gillman, A.C., Parker, G., Allday, M.J. and Bazot, Q., 2018. Epstein-Barr Virus (EBV) nuclear antigen 3C inhibits expression of COBLL1 and the ADAM28-ADAMDEC1 locus via interaction with the histone lysine demethylase KDM2B. *Journal of virology*, JVI-01362.

Gires, O., Zimber-Strobl, U., Gonnella, R., Ueffing, M., Marschall, G., Zeidler, R., Pich, D., and Hammerschmidt, W. (1997). Latent membrane protein 1 of Epstein-Barr virus mimics a constitutively active receptor molecule. *The EMBO journal*, *16*(20), 6131-6140.

Gloeckner, C.J., Boldt, K., Schumacher, A., Roepman, R., and Ueffing, M. (2007). A novel tandem affinity purification strategy for the efficient isolation and characterisation of native protein complexes. *Proteomics*, *7*(23), 4228-4234.

Goodnow, C.C., Vinuesa, C.G., Randall, K.L., MacKay, F., and Brink, R. (2010). Control systems and decision making for antibody production. *Nature immunology*, *11*(8), 681.

Greiner, D.L., Shultz, L.D., Yates, J., Appel, M.C., Perdrizet, G., Hesselton, R.M., Schweitzer, I., Beamer, W.G., Shultz, K.L., Pelsue, S.C., et al. (1995). Improved engraftment of human spleen cells in NOD/LtSz-scid/scid mice as compared with C.B-17-scid/scid mice. *The American journal of pathology*, *146*(4), 888.

Grogan, E. a, Summers, W.P., Dowling, S., Shedd, D., Gradoville, L., and Miller, G. (1983). Two Epstein-Barr viral nuclear neoantigens distinguished by gene transfer, serology, and chromosome binding. *Proceedings of the National Academy of Sciences*, *80*(24), 7650-7653.

Groves, H.T., McDonald, J.U., Langat, P., Kinnear, E., Kellam, P., McCauley, J., Ellis, J., Thompson, C., Elderfield, R., Parker, L., et al. (2018). Mouse models of influenza infection with circulating strains to test seasonal vaccine efficacy. *Frontiers in immunology*, *9*, 126.

Gu, Y., Turck, C.W., and Morgan, D.O. (1993). Inhibition of CDK2 activity in vivo by an associated 20K regulatory subunit. *Nature*, *366*(6456), 707.

Guan, K.L., Jenkins, C.W., Li, Y., Nichols, M.A., Wu, X., O'Keefe, C.L., Matera, A.G., and Xiong, Y. (1994). Growth suppression by p18, a p16INK4/MTS1- and p14INK4B/MTS2-related CDK6 inhibitor, correlates with wild-type pRb function. *Genes & development*, *8*(24), 2939-2952.

Gujer, C., Chatterjee, B., Landtwing, V., Raykova, A., McHugh, D., and Münz, C. (2015). Animal models of Epstein Barr virus infection. *Current opinion in virology*, *13*, 6-10.

Gunvén, P., Klein, G., Henle, G., Henle, W., and Clifford, P. (1970). Epstein-barr virus in burkitt's lymphoma and nasopharyngeal carcinoma: Antibodies to EBV associated membrane and viral capsid antigens in burkitt lymphoma patients. *Nature*, *228*(5276), 1053-1056.

Hadinoto, V., Shapiro, M., Sun, C.C., and Thorley-Lawson, D.A. (2009). The dynamics of EBV shedding implicate a central role for epithelial cells in amplifying viral output. *PLoS pathogens*, *5*(7), e1000496.

Hall, R.N., Meers, J., Fowler, E., and Mahony, T. (2012). Back to BAC: The use of infectious clone technologies for viral mutagenesis. *Viruses*, *4*(2), 211-235.

Hammerschmidt, W., and Sugden, B. (1988). Identification and characterization of oriLyt, a lytic origin of DNA replication of Epstein-Barr virus. *Cell*, *55*(3), 427-433.

Hanlon, P., Avenell, A., Aucott, L., and Vickers, M.A. (2014). Systematic review and meta-analysis of the sero-epidemiological association between Epstein-Barr virus and systemic lupus erythematosus. *Arthritis research & therapy*, *16*(1), R3.

Hannon, G.J., and Beach, D. (1994). p15INK4B is a potential effector of TGF-beta-induced cell cycle arrest. *Nature (Lond.)*, *371*.

Haque, T., Thomas, J.A., Parratt, R., Hunt, B.J., Yacoub, M.H., and Crawford, D.H. (1997). A prospective study in heart and lung transplant recipients correlating persistent Epstein-Barr virus infection with clinical events. *Transplantation*, *64*(7), 1028-1034.

Haque, T., Wilkie, G.M., Taylor, C., Amlot, P.L., Murad, P., Iley, A., Dombagoda, D., Britton, K.M., Swerdlow, A.J., and Crawford, D.H. (2002). Treatment of Epstein-Barr-virus-positive post-transplantation lymphoproliferative disease with partly HLA-matched allogeneic cytotoxic T cells. *The Lancet*, *360*(9331), 436-442.

Harada, S., and Kieff, E. (1997). Epstein-Barr virus nuclear protein LP stimulates EBNA-2 acidic domain-mediated transcriptional activation. *Journal of virology*, *71*(9), 6611-6618.

Hardwick, J.M., Lieberman, P.M., and Hayward, S.D. (1988). A new Epstein-Barr virus transactivator, R, induces expression of a cytoplasmic early antigen. *Journal of virology*, *62*(7), 2274-2284.

Harth-Hertle, M.L., Scholz, B.A., Erhard, F., Glaser, L. V., Dölken, L., Zimmer, R., and Kempkes, B. (2013). Inactivation of Intergenic Enhancers by EBNA3A Initiates and Maintains Polycomb Signatures across a Chromatin Domain Encoding CXCL10 and CXCL9. *PLoS pathogens*, *9*(9), e1003638.

Hausen, H. Zur, Schulte-Holthausen, H., Klein, G., Henle, W., Henle, G., Clifford, P., and Santesson, L. (1970). Epstein-barr virus in burkitt's lymphoma and nasopharyngeal carcinoma: EBV DNA in biopsies of burkitt tumours and anaplastic carcinomas of the nasopharynx. *Nature*, *228*(5276), 1056-1058.

He, G., Siddik, Z.H., Huang, Z., Wang, R., Koomen, J., Kobayashi, R., Khokhar, A.R., and Kuang, J. (2005). Induction of p21 by p53 following DNA damage inhibits both Cdk4 and Cdk2 activities. *Oncogene*, *24*(18), 2929.

Healy, J.A., and Dave, S.S. (2015). The role of EBV in the pathogenesis of diffuse large B cell lymphoma. In *Epstein Barr Virus Volume 1* (pp. 315-337). Springer, Cham.

Heintzman, N.D., and Ren, B. (2009). Finding distal regulatory elements in the human genome. *Current opinion in genetics & development*, *19*(6), 541-549.

Henkel, T., Ling, P.D., Hayward, S.D., and Peterson, M.G. (1994). Mediation of Epstein-Barr virus EBNA2 transactivation by recombination signal-binding protein Jκ. *Science*, *265*(5168), 92-95.

Henle, G., Henle, W., and Diehl, V. (1968). Relation of Burkitt'S Tumor-Associated Herpes-Ytpe Virus To Infectious Mononucleosis. *Proceedings of the National Academy of Sciences*, *59*(1), 94-101.
Henle, G., Henle, W., Clifford, P., Diehl, V., Kafuko, G.W., Kirya, B.G., Klein, G., Morrow, R.H., Munube, G.M.R., Pike, P., et al. (1969). Antibodies to epstein-barr virus in burkitt's lymphoma and control groups. *Journal of the National Cancer Institute*, *43*(5), 1147-1157.

Henle, W., Diehl, V., Kohn, G., Hausen, H. Zur, and Henle, G. (1967). Herpes-type virus and chromosome marker in normal leukocytes after growth with irradiated burkitt cells. *Science*, *157*(3792), 1064-1065.

Henle, W., Henle, G.E., and Horwitz, C.A. (1974). Epstein-barr virus specific diagnostic tests in infectous mononucleosis. *Human pathology*, *5*(5), 551-565.

Hertle, M.L., Popp, C., Petermann, S., Maier, S., Kremmer, E., Lang, R., Mages, J., and Kempkes, B. (2009). Differential gene expression patterns of EBV infected EBNA-3A positive and negative human B lymphocytes. P *PLoS pathogens*, *5*(7), e1000506.

Heslop, H.E. (2005). Biology and treatment of Epstein-Barr virus-associated non-Hodgkin lymphomas. *ASH Education Program Book*, *2005*(1), 260-266.

Hickabottom, M., Parker, G.A., Freemont, P., Crook, T., and Allday, M.J. (2002). Two nonconsensus sites in the epstein-barr virus oncoprotein EBNA3A cooperate to bind the co-repressor carboxyl-terminalbinding protein (CtBP). *Journal of Biological Chemistry*.

Hirai, H., Roussel, M.F., Kato, J.-Y., Ashmun, R.A., and Sherr, C.J. (1995). Novel INK4 proteins, p19 and p18, are specific inhibitors of the cyclin D-dependent kinases CDK4 and CDK6. *Molecular and cellular biology*, *15*(5), 2672-2681.

Hislop, A.D., Taylor, G.S., Sauce, D., and Rickinson, A.B. (2007). Cellular Responses to Viral Infection in Humans: Lessons from Epstein-Barr Virus. *Annu. Rev. Immunol.*, *25*, 587-617.

Hjalgrim, H., Askling, J., Sørensen, P., Madsen, M., Rosdahl, N., Storm, H.H., Hamilton-Dutoit, S., Eriksen, L.S., Frisch, M., Ekbom, A., et al. (2000). Risk of Hodgkin's disease and other cancers after infectious mononucleosis. *Journal of the National Cancer Institute*, *92*(18), 1522-1528.

Hjalgrim, H., Smedby, K.E., Rostgaard, K., Molin, D., Hamilton-Dutoit, S., Chang, E.T., Ralfkiaer, E., Sundström, C., Adami, H.O., Glimelius, B., et al. (2007). Infectious mononucleosis, childhood social environment, and risk of Hodgkin lymphoma. *Cancer research*, *67*(5), 2382-2388.

Ho, M., Miller, G., Atchison, R.W., Breinig, M.K., Dummer, J.S., Andiman, W., Starzl, T.E., Eastman, R., Griffith, B.P., Hardesty, R.L., et al. (1985). Epstein-Barr virus infections and DNA hybridization studies in posttransplantation lymphoma and lymphoproliferative lesions: The role of primary infection. *Journal of infectious Diseases*, *152*(5), 876-886.

Hochberg, D., Middeldorp, J.M., Catalina, M., Sullivan, J.L., Luzuriaga, K., and Thorley-Lawson, D.A. (2004). Demonstration of the Burkitt's lymphoma Epstein-Barr virus phenotype in dividing latently infected memory cells in vivo. *Proceedings of the National Academy of Sciences*, *101*(1), 239-244.

Hofelmayr, H., Strobl, L., Marschall, G., Bornkamm, G., and Zimber-Strobl, U. (2001). Activated Notch1 can transiently substitute for EBNA2 in the maintenance of proliferation of LMP1-expressing immortalized B cells. *Journal of virology*, *75*(5), 2033-2040.

Hoffman, W., Lakkis, F.G., and Chalasani, G. (2016). B cells, antibodies, and more. *Clinical Journal of the American Society of Nephrology*, CJN-09430915.

Hunter, T., and Pines, J. (1994). Cyclins and cancer II: Cyclin D and CDK inhibitors come of age. *Cell*, *79*(4), 573-582.

Huntington, N.D., Legrand, N., Alves, N.L., Jaron, B., Weijer, K., Plet, A., Corcuff, E., Mortier, E., Jacques, Y., Spits, H., et al. (2009). IL-15 trans-presentation promotes human NK cell development and differentiation in vivo. *Journal of Experimental Medicine*, *206*(1), 25-34.

Hurley, E.A., and Thorley-Lawson, D.A. (1988). B cell activation and the establishment of Epstein-Barr virus latency. *Journal of Experimental Medicine*, *168*(6), 2059-2075.

Iizasa, H., Nanbo, A., Nishikawa, J., Jinushi, M., and Yoshiyama, H. (2012). Epstein-barr virus (EBV)-associated gastric carcinoma. *Viruses*, *4*(12), 3420-3439.

Ikeyama, S., Nakagawa, S., Arakawa, M., Sugino, H., and Kakinuma, a (1986). Purification and characterization of IgE produced by human myeloma cell line, U266. *Molecular immunology*, *23*(2), 159-167.

Incrocci, R., McCormack, M., and Swanson-Mungerson, M. (2013). Epstein-barr virus LMP2A increases IL-10 production in mitogen-stimulated primary B-cells and B-cell lymphomas. *Journal of General Virology*, *94*(5), 1127-1133.

Islas-Ohlmayer, M., Padgett-Thomas, A., Domiati-Saad, R., Melkus, M.W., Cravens, P.D., Martin, M. del P., Netto, G., and Garcia, J.V. (2004). Experimental infection of NOD/SCID mice reconstituted with human CD34+ cells with Epstein-Barr virus. *Journal of virology*, *78*(24), 13891-13900.

Ito, M., Hiramatsu, H., Kobayashi, K., Suzue, K., Kawahata, M., Hioki, K., Ueyama, Y., Koyanagi, Y., Sugamura, K., Tsuji, K., et al. (2002). NOD/SCID/gamma(c)(null) mouse: an excellent recipient mouse model for engraftment of human cells. *Blood*, *100*(9), 3175-3182.

Iwakiri, D. (2014). Epstein-Barr virus-encoded RNAs: Key molecules in viral pathogenesis. *Cancers*, *6*(3), 1615-1630.

Jackson, S.P., and Bartek, J. (2010). The DNA-damage response in human biology and disease. *Nature*, *461*(7267), 1071.

Jackson, A., Carrara, P., Duke, V., Sinclair, P., Papaioannou, M., Harrison, C.J., and Foroni, L. (2000). Deletion of 6q16-q21 in human lymphoid malignancies: A mapping and deletion analysis. *Cancer research*, *60*(11), 2775-2779.

Jangalwe, S., Shultz, L.D., Mathew, A., and Brehm, M.A. (2016). Improved B cell development in humanized NOD-scid IL2Rg null mice transgenically expressing human stem cell factor, granulocyte-macrophage colony-stimulating factor and interleukin-3. *Immunity, inflammation and disease*, *4*(4), 427-440.

Jha, H.C., AJ, M.P., Saha, A., Banerjee, S., Lu, J., and Robertson, E.S. (2014). Epstein-Barr Virus Essential Antigen EBNA3C Attenuates H2AX Expression. *Journal of virology*, JVI-03568.

Ji, M.F., Wang, D.K., Yu, Y.L., Guo, Y.Q., Liang, J.S., Cheng, W.M., Zong, Y.S., Chan, K.H., Ng, S.P., Wei, W.I., et al. (2007). Sustained elevation of Epstein-Barr virus antibody levels preceding clinical onset of nasopharyngeal carcinoma. *British journal of cancer*, *96*(4), 623.

Jiang, S., Willox, B., Zhou, H., Holthaus, A.M., Wang, A., Shi, T.T., Maruo, S., Kharchenko, P. V., Johannsen, E.C., Kieff, E., et al. (2014). Epstein-Barr Virus Nuclear Antigen 3C binds to BATF/IRF4 or SPI1/IRF4 composite sites and recruits Sin3A to repress CDKN2A. *Proceedings of the National Academy of Sciences*, *111*(1), 421-426.

Jiang, S., Zhou, H., Liang, J., Gerdt, C., Wang, C., Ke, L., Schmidt, S.C.S., Narita, Y., Ma, Y., Wang, S., et al. (2017). The Epstein-Barr Virus Regulome in Lymphoblastoid Cells. *Cell host & microbe*, *22*(4), 561-573.

Johannsen, E., Miller, C.L., Grossman, S.R., and Kieff, E. (1996). EBNA-2 and EBNA-3C extensively and mutually exclusively associate with RBPJkappa in Epstein-Barr virus-transformed B lymphocytes. *Journal of virology*, *70*(6), 4179-4183.

Johnson, J.I., Decker, S., Zaharevitz, D., Rubinstein, L. V., Venditti, J.M., Schepartz, S., Kalyandrug, S., Christian, M., Arbuck, S., Hollingshead, M., et al. (2001). Relationships between drug activity in NCI preclinical in vitro and in vivo models and early clinical trials. *British journal of cancer*, *84*(10), 1424.

Jordan, V.C. (2003). Tamoxifen: A most unlikely pioneering medicine. *Nature reviews Drug discovery*, *2*(3), 205.

Kaiser, C., Laux, G., Eick, D., Jochner, N., Bornkamm, G.W., and Kempkes, B. (1999). The proto-oncogene c-myc is a direct target gene of Epstein-Barr virus nuclear antigen 2. *Journal of virology*, *73*(5), 4481-4484.

Kalchschmidt, J.S., Gillman, A.C.T., Paschos, K., Bazot, Q., Kempkes, B., and Allday, M.J. (2016a). EBNA3C Directs Recruitment of RBPJ (CBF1) to Chromatin during the Process of Gene Repression in EBV Infected B Cells. *PLoS pathogens*, *12*(1), e1005383.

Kalchschmidt, J.S., Bashford-Rogers, R., Paschos, K., Gillman, A.C.T., Styles, C.T., Kellam, P., and Allday, M.J. (2016b). Epstein-Barr virus nuclear protein EBNA3C directly induces expression of AID and somatic mutations in B cells. *Journal of Experimental Medicine*, jem-20160120.

Kalla, M., and Hammerschmidt, W. (2012). Human B cells on their route to latent infection - Early but transient expression of lytic genes of Epstein-Barr virus. *European journal of cell biology*, *91*(1), 65-69.

Kalla, M., Schmeinck, A., Bergbauer, M., Pich, D., and Hammerschmidt, W. (2010). AP-1 homolog BZLF1 of Epstein-Barr virus has two essential functions dependent on the epigenetic state of the viral genome. *Proceedings of the National Academy of Sciences*, *107*(2), 850-855.

Kallies, A., Hasbold, J., Fairfax, K., Pridans, C., Emslie, D., McKenzie, B.S., Lew, A.M., Corcoran, L.M., Hodgkin, P.D., Tarlinton, D.M., et al. (2007). Initiation of Plasma-Cell Differentiation Is Independent of the Transcription Factor Blimp-1. *Immunity*, *26*(5), 555-566.

Kamel-Reid, S., and Dick, J.E. (1988). Engraftment of immune-deficient mice with human hematopoietic stem cells. *Science*, *242*(4886), 1706-1709.

Kanda, T., Otter, M., and Wahl, G.M. (2001). Coupling of Mitotic Chromosome Tethering and Replication Competence in Epstein-Barr Virus-Based Plasmids. *Molecular and cellular biology*, *21*(10), 3576-3588.

Kanda, T., Yajima, M., Ahsan, N., Tanaka, M., and Takada, K. (2004). Production of High-Titer Epstein-Barr Virus Recombinants Derived from Akata Cells by Using a Bacterial Artificial Chromosome System. *Journal of virology*, *78*(13), 7004-7015.

Kang, J., and Coles, M. (2012). IL-7: The global builder of the innate lymphoid network and beyond, one niche at a time. In *Seminars in immunology* (Vol. 24, No. 3, pp. 190-197). Academic Press

Kang, I., Quan, T., Nolasco, H., Park, S.-H., Hong, M.S., Crouch, J., Pamer, E.G., Howe, J.G., and Craft, J. (2004). Defective Control of Latent Epstein-Barr Virus Infection in Systemic Lupus Erythematosus. *The Journal of Immunology*, *172*(2), 1287-1294.

Kastan, M.B., and Bartek, J. (2004). Cell-cycle checkpoints and cancer. *Nature*, *432*(7015), 316.

Kaye, K.M., Izumi, K.M., and Kieff, E. (1993). Epstein-Barr virus latent membrane protein 1 is essential for B-lymphocyte growth transformation. *Proceedings of the National Academy of Sciences*, *90*(19), 9150-9154.

Kempkes, B., and Ling, P.D. (2015). EBNA2 and its coactivator EBNA-LP. In *Epstein Barr Virus Volume 2* (pp. 35-59). Springer, Cham.

Kempkes, B., Spitkovskyl, D., Jansen-Durr ', P., Ellwart2, J.W., Kremmer3, E., Delecluse4, H.-J., Rottenberger, C., Bornkamm5, G.W., and Hammerschmidt, W. (1995). B-cell proliferation and

induction of early G1-regulating proteins by Epstein-Barr virus mutants conditional for EBNA2. *The EMBO journal*, *14*(1), 88-96.

Khan, G., and Hashim, M. (2014). Global burden of deaths from Epstein-Barr virus attributable malignancies 1990-2010. I *Infectious agents and cancer*, *9*(1), 38.

Khanna, R., Burrows, S.R., Kurilla, M.G., Jacob, C. a, Misko, I.S., Sculley, T.B., Kieff, E., and Moss, D.J. (1992). Localization of Epstein-Barr virus cytotoxic T cell epitopes using recombinant vaccinia: implications for vaccine development. *Journal of Experimental Medicine*, *176*(1), 169-176.

Kiermayer, C., Conrad, M., Schneider, M., Schmidt, J., and Brielmeier, M. (2007). Optimization of spatiotemporal gene inactivation in mouse heart by oral application of tamoxifen citrate. *genesis*, *45*(1), 11-16.

Kieser, A., and Sterz, K.R. (2015). The latent membrane protein 1 (LMP1). In *Epstein Barr Virus Volume 2* (pp. 119-149). Springer, Cham.

Kieser, A., Kilger, E., Gires, O., Ueffing, M., Kolch, W., and Hammerschmidt, W. (1997). Epstein-Barr virus latent membrane protein-1 triggers AP-1 activity via the c-Jun N-terminal kinase cascade. *The EMBO journal*, *16*(21), 6478-6485.

Kimura, H., Miyake, K., Yamauchi, Y., Nishiyama, K., Iwata, S., Iwatsuki, K., Gotoh, K., Kojima, S., Ito, Y., and Nishiyama, Y. (2009). Identification of Epstein-Barr Virus (EBV)–Infected Lymphocyte Subtypes by Flow Cytometric In Situ Hybridization in EBV-Associated Lymphoproliferative Diseases. *The Journal of infectious diseases*, *200*(7), 1078-1087.

Kitagawa, N., Goto, M., Kurozumi, K., Maruo, S., Fukayama, M., Naoe, T., Yasukawa, M., Hino, K.I., Suzuki, T., Todo, S., et al. (2000). Epstein-Barr virus-encoded poly(A)-RNA supports Burkitt's lymphoma growth through interleukin-10 induction. *The EMBO journal*, *19*(24), 6742-6750.

Klein, G., Dombos, L., and Gothoskar, B. (1972). Sensitivity of Epstein-Barr virus (EBV) producer and non-producer human lymphoblastoid cell lines to superinfection with EB-virus. *International journal of cancer*, *10*(1), 44-57.

Klein, U., Klein, G., Ehlin-Henriksson, B., Rajewsky, K., and Küppers, R. (1995). Burkitt's lymphoma is a malignancy of mature B cells expressing somatically mutated V region genes. *Molecular Medicine*, *1*(5), 495.

Knight, J.S., and Robertson, E.S. (2004). Epstein-Barr virus nuclear antigen 3C regulates cyclin A/p27 complexes and enhances cyclin A-dependent kinase activity. *Journal of virology*, *78*(4), 1981-1991.

Knight, J.S., Lan, K., Subramanian, C., and Robertson, E.S. (2003). Epstein-Barr virus nuclear antigen 3C recruits histone deacetylase activity and associates with the corepressors mSin3A and NCoR in human B-cell lines. *Journal of virology*, *77*(7), 4261-4272.

Knight, J.S., Sharma, N., and Robertson, E.S. (2005a). SCFSkp2 complex targeted by Epstein-Barr virus essential nuclear antigen. *Molecular and cellular biology*, *25*(5), 1749-1763.

Knight, J.S., Sharma, N., and Robertson, E.S. (2005b). Epstein-Barr virus latent antigen 3C can mediate the degradation of the retinoblastoma protein through an SCF cellular ubiquitin ligase. *Proceedings of the National Academy of Sciences*, *102*(51), 18562-18566.

Kohnken, R., Porcu, P., and Mishra, A. (2017). Overview of the Use of Murine Models in Leukemia and Lymphoma Research. *Frontiers in oncology*, *7*, 22.

Komano, J., Maruo, S., Kurozumi, K., Oda, T., and Takada, K. (1999). Oncogenic role of Epstein-Barr virus-encoded RNAs in Burkitt's lymphoma cell line Akata. *Journal of virology*, *73*(12), 9827-9831.

Kräutler, N.J., Suan, D., Butt, D., Bourne, K., Hermes, J.R., Chan, T.D., Sundling, C., Kaplan, W., Schofield, P., Jackson, J., et al. (2017). Differentiation of germinal center B cells into plasma cells is initiated by high-affinity antigen and completed by Tfh cells. *Journal of Experimental Medicine*, jem-20161533.

Kulwichit, W., Edwards, R.H., Davenport, E.M., Baskar, J.F., Godfrey, V., and Raab-Traub, N. (1998). Expression of the Epstein-Barr virus latent membrane protein 1 induces B cell lymphoma in transgenic mice. *Proceedings of the National Academy of Sciences*, *95*(20), 11963-11968.

Kuppers, R. (2003). B cells under influence: transformation of B cells by Epstein-Barr virus. *Nature Reviews Immunology*, *3*(10), 801.

Küppers, R. (2009). The biology of Hodgkin's lymphoma. *Nature Reviews Cancer*, *9*(1), 15.

Kurosaki, T., Kometani, K., and Ise, W. (2015). Memory B cells. *Nature Reviews Immunology*, *15*(3), 149.

Kuzmichev, A., Nishioka, K., Erdjument-Bromage, H., Tempst, P., and Reinberg, D. (2002). Histone methyltransferase activity associated with a human multiprotein complex containing the Enhancer of Zeste protein. *Genes & development*, *16*(22), 2893-2905.

Laichalk, L.L., and Thorley-Lawson, D.A. (2005). Terminal Differentiation into Plasma Cells Initiates the Replicative Cycle of Epstein-Barr Virus In Vivo. *Journal of virology*, *79*(2), 1296-1307.

Laichalk, L.L., Hochberg, D., Babcock, G.J., Freeman, R.B., and Thorley-Lawson, D.A. (2002). The dispersal of mucosal memory B cells: Evidence from persistent EBV infection. *Immunity*, *16*(5), 745-754.

Lalioti, M., and Heath, J. (2001). A new method for generating point mutations in bacterial artificial chromosomes by homologous recombination in Escherichia coli. *Nucleic acids research*, *29*(3), e14-e14.

Lan, P., Tonomura, N., Shimizu, A., Wang, S., and Yang, Y.G. (2006). Reconstitution of a functional human immune system in immunodeficient mice through combined human fetal thymus/liver and CD34+ cell transplantation. *Blood*, *108*(2), 487-492.
Lane, P.J.L., Gaspal, F.M., McConnell, F.M., Withers, D.R., and Anderson, G. (2012). Lymphoid tissue inducer cells: Pivotal cells in the evolution of CD4 immunity and tolerance? *Frontiers in immunology*, *3*, 24.

Lanzavecchia, A. (1985). Antigen-specific interaction between T and B cells. *Nature*, *314*(6011), 537.

Lassnig, C., Sanchez, C.M., Egerbacher, M., Walter, I., Majer, S., Kolbe, T., Pallares, P., Enjuanes, L., and Muller, M. (2005). Development of a transgenic mouse model susceptible to human coronavirus 229E. *Proceedings of the National Academy of Sciences*, *102*(23), 8275-8280.

Laux, G., Perricaudet, M., and Farrell, P.J. (1988). A spliced Epstein-Barr virus gene expressed in immortalized lymphocytes is created by circularization of the linear viral genome. *The EMBO journal*, *7*(3), 769-774.

Laux, G., Economou, A., and Farrell, P.J. (1989). The terminal protein gene 2 of Epstein-Barr virus is transcribed from a bidirectional latent promoter region. *Journal of general virology*, *70*(11), 3079-3084.

Lee, E.K., Joo, E.H., Song, K.-A., Choi, B., Kim, M., Kim, S.-H., Kim, S.J., and Kang, M.-S. (2015). Effects of lymphocyte profile on development of EBV-induced lymphoma subtypes in humanized mice. *Proceedings of the National Academy of Sciences*, *112*(42), 13081-13086.

Lee, M.A., Diamond, M.E., and Yates, J.L. (1999). Genetic evidence that EBNA-1 is needed for efficient, stable latent infection by Epstein-Barr virus. *Journal of virology*, *73*(4), 2974-2982.

Lee, M.H., Reynisdottir, I., and Massague, J. (1995). Cloning of p57(KIP2), a cyclin-dependent kinase inhibitor with unique domain structure and tissue distribution. *Genes & development*, *9*(6), 639-649.

Lee, S., Sakakibara, S., Maruo, S., Zhao, B., Calderwood, M.A., Holthaus, A.M., Lai, C.-Y., Takada, K., Kieff, E., and Johannsen, E. (2009). Epstein-Barr Virus Nuclear Protein 3C Domains Necessary for Lymphoblastoid Cell Growth: Interaction with RBP-J Regulates TCL1. *Journal of virology*, *83*(23), 12368-12377.

Leonard, W.J. (2001). Cytokines and immunodeficiency diseases. *Nature Reviews Immunology*, *1*(3), 200.

Levin, L.I., Munger, K.L., Rubertone, M. V, Peck, C. a, Lennette, E.T., Spiegelman, D., and Ascherio, A. (2005). Temporal relationship between elevation of epstein-barr virus antibody titers and initial onset of neurological symptoms in multiple sclerosis. *Jama*, *293*(20), 2496-2500.

Levin, L.I., Munger, K.L., O'Reilly, E.J., Falk, K.I., and Ascherio, A. (2010). Primary infection with the Epstein-Barr virus and risk of multiple sclerosis. *Annals of neurology*, *67*(6), 824-830.

Levitskaya, J., Coram, M., Levitsky, V., Imreh, S., Steigerwald-Mullen, P.M., Klein, G., Kurilla, M.G., and Masucci, M.G. (1995). Inhibition of antigen processing by the internal repeat region of the epstein-barr virus nuclear antigen-1. *Nature*, *375*(6533), 685

Li, Y.Y., Chung, G.T.Y., Lui, V.W.Y., To, K.F., Ma, B.B.Y., Chow, C., Woo, J.K.S., Yip, K.Y., Seo, J., Hui, E.P., et al. (2017). Exome and genome sequencing of nasopharynx cancer identifies NF-? B pathway activating mutations. *Nature communications*, *8*, 14121.

Lindberg, D., Åkerström, G., and Westin, G. (2008). Evaluation of CDKN2C/p18, CDKN1B/p27 and CDKN2B/p15 mRNA expression, and CpG methylation status in sporadic and MEN1-associated pancreatic endocrine tumours. *Clinical endocrinology*, *68*(2), 271-277.

Liu, P., and Speck, S.H. (2003). Synergistic autoactivation of the Epstein-Barr virus immediate-early BRLF1 promoter by Rta and Zta. *Virology*, *310*(2), 199-206.

Liu, S., Chan, H.L., Bai, F., Ma, J., Scott, A., Robbins, D.J., Capobianco, A.J., Zhu, P., Pei, X.-H., Liu, S., et al. (2016). Gata3 restrains B cell proliferation and cooperates with p18INK4c to repress B cell lymphomagenesis. *Oncotarget*, *7*(39), 64007.

Liu, Y.J., Johnson, G.D., Gordon, J., and MacLennan, I.C.M. (1992). Germinal centres in T-cell-dependent antibody responses. *Immunology today*, *13*(1), 17-21.

Loebel, M., Strohschein, K., Giannini, C., Koelsch, U., Bauer, S., Doebis, C., Thomas, S., Unterwalder, N., Von Baehr, V., Reinke, P., et al. (2014). Deficient EBV-specific B- and T-cell response in patients with Chronic Fatigue Syndrome. *PloS one*, *9*(1), e85387.

Long, H.M., Leese, A.M., Chagoury, O.L., Connerty, S.R., Quarcoopome, J., Quinn, L.L., Shannon-Lowe, C., and Rickinson, A.B. (2011). Cytotoxic CD4+ T Cell Responses to EBV Contrast with CD8 Responses in Breadth of Lytic Cycle Antigen Choice and in Lytic Cycle Recognition. *The Journal of Immunology*, 1100590.

Lu, F., Chen, H.S., Kossenkov, A. V., DeWispeleare, K., Won, K.J., and Lieberman, P.M. (2016). EBNA2 Drives Formation of New Chromosome Binding Sites and Target Genes for B-Cell Master Regulatory Transcription Factors RBP-jκ and EBF1. *PLoS pathogens*, *12*(1), e1005339.

Luckow, V. a, Lee, S.C., Barry, G.F., and Olins, P.O. (1993). Efficient generation of infectious recombinant baculoviruses by site-specific transposon-mediated insertion of foreign genes into a baculovirus genome propagated in Escherichia coli. *Journal of virology*, *67*(8), 4566-4579.

Lukas, J., Parry, D., Aagaard, L., Mann, D.J., Bartkova, J., Strauss, M., Peters, G., and Bartek, J. (1995). Retinoblastoma-protein-dependent cell-cycle inhibition by the tumour suppressor p16. *Nature*, *375*(6531), 503.

Ma, J., Nie, K., Redmond, D., Liu, Y., Elemento, O., Knowles, D.M., and Tam, W. (2016). EBV-miR-BHRF1-2 targets PRDM1/Blimp1: Potential role in EBV lymphomagenesis. *Leukemia*, *30*(3), 594.

Ma, S.-D., Hegde, S., Young, K.H., Sullivan, R., Rajesh, D., Zhou, Y., Jankowska-Gan, E., Burlingham, W.J., Sun, X., Gulley, M.L., et al. (2011). A new model of Epstein-Barr virus infection reveals an important role for early lytic viral protein expression in the development of lymphomas. *Journal of virology*, *85*(1), 165-177.

Ma, S.-D., Tsai, M.-H., Romero-Masters, J.C., Ranheim, E.A., Huebner, S.M., Bristol, J.A., Delecluse, H.-J., and Kenney, S.C. (2017). Latent Membrane Protein 1 (LMP1) and LMP2A Collaborate To Promote Epstein-Barr Virus-Induced B Cell Lymphomas in a Cord Blood-Humanized Mouse Model but Are Not Essential. *Journal of Virology*, JVI-01928.

Ma, S.D., Xu, X., Plowshay, J., Ranheim, E.A., Burlingham, W.J., Jensen, J.L., Asimakopoulos, F., Tang, W., Gulley, M.L., Cesarman, E., et al. (2015). LMP1-deficient Epstein-Barr virus mutant requires T cells for lymphomagenesis. *The Journal of clinical investigation*, *125*(1), 304-315.

MacLennan, I.C. (1994). Germinal centers. *Annual review of immunology*, *12*(1), 117-139.

Malumbres, R., Fresquet, V., Roman-Gomez, J., Bobadilla, M., Robles, E.F., Altobelli, G.G., Calasanz, M.J., Smeland, E.B., Aznar, M.A., Agirre, X., et al. (2011). LMO2 expression reflects the different stages of blast maturation and genetic features in B-cell acute lymphoblastic leukemia and predicts clinical outcome. *Haematologica.*

Mancao, C., and Hammerschmidt, W. (2007). Epstein-Barr virus latent membrane protein 2A is a B-cell receptor mimic and essential for B-cell survival. *Blood*, *110*(10), 3715-3721.

Mandelbaum, J., Bhagat, G., Tang, H., Mo, T., Brahmachary, M., Shen, Q., Chadburn, A., Rajewsky, K., Tarakhovsky, A., Pasqualucci, L., et al. (2010). BLIMP1 Is a Tumor Suppressor Gene Frequently Disrupted in Activated B Cell-like Diffuse Large B Cell Lymphoma. *Cancer cell*, *18*(6), 568-579.

Mannick, J.B., Cohen, J.I., Birkenbach, M., Marchini, A., and Kieff, E. (1991). The Epstein-Barr virus nuclear protein encoded by the leader of the EBNA RNAs is important in B-lymphocyte transformation. *Journal of virology*, *65*(12), 6826-6837.

Manolov, G., and Manolova, Y. (1972). Marker band in one chromosome 14 from burkitt lymphomas. *Nature*, *237*(5349), 33.

Maruo, S., Johannsen, E., Illanes, D., Cooper, A., and Kieff, E. (2003). Epstein-Barr Virus nuclear protein EBNA3A is critical for maintaining lymphoblastoid cell line growth. *Journal of virology*, *77*(19), 10437-10447.

Maruo, S., Johannsen, E., Illanes, D., Cooper, A., Zhao, B., and Kieff, E. (2005). Epstein-Barr virus nuclear protein 3A domains essential for growth of lymphoblasts: transcriptional regulation through RBP-Jkappa/CBF1 is critical. *Journal of virology*, *79*(16), 10171-10179.

Maruo, S., Wu, Y., Ishikawa, S., Kanda, T., Iwakiri, D., and Takada, K. (2006). Epstein-Barr virus nuclear protein EBNA3C is required for cell cycle progression and growth maintenance of lymphoblastoid cells. *Proceedings of the National Academy of Sciences*, *103*(51), 19500-19505.

Maruo, S., Zhao, B., Johannsen, E., Kieff, E., Zou, J., and Takada, K. (2011). Epstein-Barr virus nuclear antigens 3C and 3A maintain lymphoblastoid cell growth by repressing p16 ^{INK4A} and p14 ^{ARF} expression. *Proceedings of the National Academy of Sciences*, *108*(5), 1919-1924.

Matsumura, T., Kametani, Y., Ando, K., Hirano, Y., Katano, I., Ito, R., Shiina, M., Tsukamoto, H., Saito, Y., Tokuda, Y., et al. (2003). Functional CD5+ B cells develop predominantly in the spleen of NOD/SCID/gammac(null) (NOG) mice transplanted either with human umbilical cord blood, bone marrow, or mobilized peripheral blood CD34+ cells. *Experimental hematology*, *31*(9), 789-797.

Maunders, M.J., Petti, L., and Rowe, M. (1994). Precipitation of the Epstein-Barr virus protein EBNA 2 by an EBNA 3c-specific monoclonal antibody. *Journal of general virology*, *75*(4), 769-778.

McClain, M.T., Heinlen, L.D., Dennis, G.J., Roebuck, J., Harley, J.B., and James, J.A. (2005). Early events in lupus humoral autoimmunity suggest initiation through molecular mimicry. *Nature medicine*, *11*(1), 85.

McClellan, M.J., Khasnis, S., Wood, C.D., Palermo, R.D., Schlick, S.N., Kanhere, A.S., Jenner, R.G., and West, M.J. (2012). Downregulation of Integrin Receptor-Signaling Genes by Epstein-Barr Virus EBNA 3C via Promoter-Proximal and -Distal Binding Elements. *Journal of virology*, JVI-07161.

McClellan, M.J., Wood, C.D., Ojeniyi, O., Cooper, T.J., Kanhere, A., Arvey, A., Webb, H.M., Palermo, R.D., Harth-Hertle, M.L., Kempkes, B., et al. (2013). Modulation of Enhancer Looping and Differential Gene Targeting by Epstein-Barr Virus Transcription Factors Directs Cellular Reprogramming. *PLoS pathogens*, *9*(9), e1003636.

McCune, J.M., Namikawa, R., Kaneshima, H., Shultz, L.D., Lieberman, M., and Weissman, I.L. (1988). The SCID-hu mouse: Murine model for the analysis of human hematolymphoid differentiation and function. *Science*, *241*(4873), 1632-1639.

McDermott, S.P., Eppert, K., Lechman, E.R., Doedens, M., and Dick, J.E. (2010). Comparison of human cord blood engraftment between immunocompromised mouse strains. *Blood*.

Melkus, M.W., Estes, J.D., Padgett-Thomas, A., Gatlin, J., Denton, P.W., Othieno, F.A., Wege, A.K., Haase, A.T., and Garcia, J.V. (2006). Humanized mice mount specific adaptive and innate immune responses to EBV and TSST-1. *Nature medicine*, *12*(11), 1316.

Merchant, M., Swart, R., Katzman, R.B., Ikeda, M., Ikeda, a, Longnecker, R., Dykstra, M.L., and Pierce, S.K. (2001). The effects of the Epstein-Barr virus latent membrane protein 2A on B cell function. *International reviews of immunology*, *20*(6), 805-835.

Messerle, M., Crnkovic, I., Hammerschmidt, W., Ziegler, H., and Koszinowski, U.H. (1997). Cloning and mutagenesis of a herpesvirus genome as an infectious bacterial artificial chromosome. *Proceedings of the National Academy of Sciences*, *94*(26), 14759-14763.

Mestre-Escorihuela, C., Rubio-Moscardo, F., Richter, J.A., Siebert, R., Climent, J., Fresquet, V., Beltran, E., Agirre, X., Marugan, I., Marín, M., et al. (2007). Homozygous deletions localize novel tumor suppressor genes in B-cell lymphomas. *Blood*, *109*(1), 271-280.

Middeldorp, J.M. (2015). Epstein-barr virus-specific humoral immune responses in health and disease. In *Epstein Barr Virus Volume 2* (pp. 289-323). Springer, Cham.

Middeldorp, J.M., and Pegtel, D.M. (2008). Multiple roles of LMP1 in Epstein-Barr virus induced immune escape. In *Seminars in cancer biology* (Vol. 18, No. 6, pp. 388-396). Academic Press.

Miller, C.L., Burkhardt, A.L., Lee, J.H., Stealey, B., Longnecker, R., Bolen, J.B., and Kieff, E. (1995). Integral membrane protein 2 of Epstein-barr virus regulates reactivation from latency through dominant negative effects on protein-tyrosine kinases. *Immunity*, *2*(2), 155-166.

Miller, G., Shope, T., Lisco, H., Stitt, D., and Lipman, M. (1972). Epstein-Barr virus: transformation, cytopathic changes, and viral antigens in squirrel monkey and marmoset leukocytes. *Proceedings of the National Academy of Sciences*, *69*(2), 383-387.

Mimura, N., Fulciniti, M., Gorgun, G., Tai, Y.T., Cirstea, D., Santo, L., Hu, Y., Fabre, C., Minami, J., Ohguchi, H., et al. (2012). Blockade of XBP1 splicing by inhibition of IRE1α is a promising therapeutic option in multiple myeloma. *Blood*.

Minnich, M., Tagoh, H., Bönelt, P., Axelsson, E., Fischer, M., Cebolla, B., Tarakhovsky, A., Nutt, S.L., Jaritz, M., and Busslinger, M. (2016). Multifunctional role of the transcription factor Blimp-1 in coordinating plasma cell differentiation. *Nature immunology*, *17*(3), 331.

Mombaerts, P., Iacomini, J., Johnson, R.S., Herrup, K., Tonegawa, S., and Papaioannou, V.E. (1992). RAG-1-deficient mice have no mature B and T lymphocytes. *Cell*, *68*(5), 869-877.

Monroe, J.G. (2006). ITAM-mediated tonic signalling through pre-BCR and BCR complexes. *Nature Reviews Immunology*, *6*(4), 283.

Morse, L., Chen, D., Franklin, D., Xiong, Y., and Chen-Kiang, S. (1997). Induction of cell cycle arrest and B cell terminal differentiation by CDK inhibitor p18(INK4c) and IL-6. *Immunity*, *6*(1), 47-56.

Mosier, D.E., Gulizia, R.J., Baird, S.M., and Wilson, D.B. (1988). Transfer of a functional human immune system to mice with severe combined immunodeficiency. *Nature*, *335*(6187), 256.

Mueller, N., Evans, A., Harris, N.L., Comstock, G.W., Jellum, E., Magnus, K., Orentreich, N., Polk, B.F., and Vogelman, J. (1989). Hodgkin's disease and Epstein-Barr virus. Altered antibody pattern before diagnosis. *New England Journal of Medicine*, *320*(11), 689-695.

Murer, A., McHugh, D., Caduff, N., Kalchschmidt, J., Barros, M., Zbinden, A., Capaul, R., Niedobitek, G., Allday, M., Chijioke, O., et al. (2018). EBV persistence without its EBNA3A and 3C oncogenes in vivo. *PLoS pathogens*, *14*(4), e1007039.

Murphy, D.J., Junttila, M.R., Pouyet, L., Karnezis, A., Shchors, K., Bui, D.A., Brown-Swigart, L., Johnson, L., and Evan, G.I. (2008). Distinct Thresholds Govern Myc's Biological Output In Vivo. *Cancer cell*, *14*(6), 447-457.

Murray, P., and Bell, A. (2015). Contribution of the epstein-barr virus to the pathogenesis of hodgkin lymphoma. In *Epstein Barr Virus Volume 1* (pp. 287-313). Springer, Cham.

Nanbo, A., Inoue, K., Adachi-Takasawa, K., and Takada, K. (2002). Epstein-Barr virus RNA confers resistance to interferon-alpha-induced apoptosis in Burkitt's lymphoma. *The EMBO journal*, *21*(5), 954-965.

de Napoles, M., Mermoud, J.E., Wakao, R., Tang, Y.A., Endoh, M., Appanah, R., Nesterova, T.B., Silva, J., Otte, A.P., Vidal, M., et al. (2004). Polycomb group proteins ring1A/B link ubiquitylation of histone H2A to heritable gene silencing and X inactivation. *Developmental cell*, *7*(5), 663-676.

Ngampasutadol, J., Ram, S., Gulati, S., Agarwal, S., Li, C., Visintin, A., Monks, B., Madico, G., and Rice, P.A. (2008). Human Factor H Interacts Selectively with Neisseria gonorrhoeae and Results in Species-Specific Complement Evasion. *The Journal of Immunology*, *180*(5), 3426-3435.

Nguyen, L., Papenhausen, P., and Shao, H. (2017). The Role of c-MYC in B-Cell Lymphomas: Diagnostic and molecular aspects. *Genes*, *8*(4), 116.

Nikitin, P.A., Yan, C.M., Forte, E., Bocedi, A., Tourigny, J.P., White, R.E., Allday, M.J., Patel, A., Dave, S.S., Kim, W., et al. (2010). An ATM/Chk2-mediated DNA damage-responsive signaling pathway suppresses Epstein-Barr virus transformation of primary human B cells. *Cell host & microbe*, *8*(6), 510-522.

Nilsson, K., Bennich, H., Johansson, S.G.O., and Pontén, J. (1970). Established immunoglobulin producing myeloma (IgE) and Lymphoblastoid (IgG) cell lines from an IgE myeloma patient. *Clinical and experimental immunology*, *7*(4), 477.

Nonkwelo, C., Skinner, J., Bell, A., Rickinson, A., and Sample, J. (1996). Transcription start sites downstream of the Epstein-Barr virus (EBV) Fp promoter in early-passage Burkitt lymphoma cells define a fourth promoter for expression of the EBV EBNA-1 protein. *ournal of virology*, *70*(1), 623-627.

Nurieva, R.I., Chung, Y., Martinez, G.J., Yang, X.O., Tanaka, S., Matskevitch, T.D., Wang, Y.-H., and Dong, C. (2009). Bcl6 mediates the development of T follicular helper cells. *Science*, *325*(5943), 1001-1005.

Nutt, S.L., Taubenheim, N., Hasbold, J., Corcoran, L.M., and Hodgkin, P.D. (2011). The genetic network controlling plasma cell differentiation. In *Seminars in immunology* (Vol. 23, No. 5, pp. 341-349). Academic Press.

Nutt, S.L., Hodgkin, P.D., Tarlinton, D.M., and Corcoran, L.M. (2015). The generation of antibody-secreting plasma cells. *Nature Reviews Immunology*, *15*(3), 160.

O'Connor, M., Peifer, M., and Bender, W. (1989). Construction of large DNA segments in Escherichia coli. *Science*, *244*(4910), 1307-1312.

O'Nions, J., and Allday, M.J. (2004). Proliferation and differentiation in isogenic populations of peripheral B cells activated by Epstein-Barr virus or T cell-derived mitogens. *Journal of general virology*, *85*(4), 881-895.

Ochiai, K., Muto, A., Tanaka, H., Takahashi, S., and Igarashi, K. (2008). Regulation of the plasma cell transcription factor Blimp-1 gene by Bach2 and Bcl6. *International immunology*, *20*(3), 453-460.

Okuda, T., Hirai, H., Valentine, V.A., Shurtleff, S.A., Kidd, V.J., Lahti, J.M., Sherr, C.J., and Downing, J.R. (1995). Molecular cloning, expression pattern, and chromosomal localization of human CDKN2D/INK4d, an inhibitor of cyclin D-dependent kinases. *Genomics*, *29*(3), 623-630.

Palendira, U., and Rickinson, A.B. (2015). Primary immunodeficiencies and the control of Epstein-Barr virus infection. *Annals of the New York Academy of Sciences*, *1356*(1), 22-44.

Papavasiliou, F.N., and Schatz, D.G. (2002). Somatic hypermutation of immunoglobulin genes: Merging mechanisms for genetic diversity. *Cell*, *109*(2), S35-S44.

Parker, B.D., Bankier, A., Satchwell, S., Barrell, B.T., and Farrell, P.J. (1990). Sequence and transcription of Raji Epstein-Barr virus DNA spanning the B95-8 deletion region. *Virology*, *179*(1), 339-346.

Parker, G.A., Crook, T., Bain, M., Sara, E.A., Farrell, P.J., and Allday, M.J. (1996). Epstein-Barr virus nuclear antigen (EBNA)3C is an immortalizing oncoprotein with similar properties to adenovirus E1A and papillomavirus E7. *Oncogene*, *13*(12), 2541-2549.

Paschos, K., Smith, P., Anderton, E., Middeldorp, J.M., White, R.E., and Allday, M.J. (2009). Epstein-Barr virus latency in B cells leads to epigenetic repression and CpG methylation of the tumour suppressor gene Bim. *PLoS pathogens*, *5*(6), e1000492.

Paschos, K., Parker, G.A., Watanatanasup, E., White, R.E., and Allday, M.J. (2012). BIM promoter directly targeted by EBNA3C in polycomb-mediated repression by EBV. *Nucleic acids research*, *40*(15), 7233-7246.

Paschos, K., Bazot, Q., Ho, G., Parker, G.A., Lees, J., Barton, G., and Allday, M.J. (2017). Core binding factor (CBF) is required for Epstein-Barr virus EBNA3 proteins to regulate target gene expression. *Nucleic acids research*, *45*(5), 2368-2383.

Pasqualucci, L., Compagno, M., Houldsworth, J., Monti, S., Grunn, A., Nandula, S. V., Aster, J.C., Murty, V. V., Shipp, M.A., and Dalla-Favera, R. (2006). Inactivation of the PRDM1/BLIMP1 gene in diffuse large B cell lymphoma. *Journal of Experimental Medicine*, *203*(2), 311-317.

Pathmanathan, R., Prasad, U., Sadler, R., Flynn, K., and Raab-Traub, N. (1995). Clonal Proliferations of Cells Infected with Epstein–Barr Virus in Preinvasive Lesions Related to Nasopharyngeal Carcinoma. *New England Journal of Medicine*, *333*(11), 693-698.

Pearson, T., Shultz, L.D., Miller, D., King, M., Laning, J., Fodor, W., Cuthbert, A., Burzenski, L., Gott, B., Lyons, B., et al. (2008). Non-obese diabetic-recombination activating gene-1 (NOD-Rag1null) interleukin (IL)-2 receptor common gamma chain (IL2rγnull) null mice: A radioresistant model for human lymphohaematopoietic engraftment. *Clinical & Experimental Immunology*, *154*(2), 270-284.

Pei, Y., Singh, R.K., Shukla, S.K., Lang, F., Zhang, S., and Robertson, E.S. (2018). Epstein–Barr Virus nuclear antigen 3C facilitates cell proliferation by regulating Cyclin D2. *Journal of virology*, JVI-00663.

Peng, R., Moses, S.C., Tan, J., Kremmer, E., and Ling, P.D. (2005). The Epstein-Barr virus EBNA-LP protein preferentially coactivates EBNA2-mediated stimulation of latent membrane proteins expressed from the viral divergent promoter. *Journal of virology*, *79*(7), 4492-4505.

Pfeffer, S., Zavolan, M., Grässer, F.A., Chien, H., Russo, J.J., Ju, J., John, B., Enright, A.J., Marks, D., Sander, C., et al. (2004). Identification of Virus-Encoded MicroRNAs. *Science*, *304*(5671), 734-736.

Pillai, S., and Cariappa, A. (2009). The follicular versus marginal zone B lymphocyte cell fate decision. *Nature Reviews Immunology*, *9*(11), 767.

Pippa, R., Espinosa, L., Gundem, G., García-Escudero, R., Dominguez, A., Orlando, S., Gallastegui, E., Saiz, C., Besson, A., Pujol, M.J., et al. (2012). P27Kip1represses transcription by direct interaction with p130/E2F4 at the promoters of target genes. *Oncogene*, *31*(38), 4207.

Plagnol, V., Uz, E., Wallace, C., Stevens, H., Clayton, D., Ozcelik, T., and Todd, J.A. (2008). Extreme clonality in lymphoblastoid cell lines with implications for allele specific expression analyses. *PLoS One*, *3*(8), e2966.

Polyak, K., Kato, J.Y., Solomon, M.J., Sherr, C.J., Massague, J., Roberts, J.M., and Koff, A. (1994a). p27Kip1, a cyclin-Cdk inhibitor, links transforming growth factor-beta and contact inhibition to cell cycle arrest. *Genes & development*, *8*(1), 9-22.

Polyak, K., Lee, M.-H., Erdjument-Bromage, H., Koff, A., Roberts, J.M., Tempst, P., and Massagué, J. (1994b). Cloning of $p27^{Kip1}$, a cyclin-dependent kinase inhibitor and a potential mediator of extracellular antimitogenic signals. *Cell*, *78*(1), 59-66.

Pope, J.H., Horne, M.K., and Scott, W. (1968). Transformation of foetal human leukocytes in vitro by filtrates of a human leukaemic cell line containing herpes-like virus. *International journal of cancer*, *3*(6), 857-866.

Popov, N., and Gil, J. (2010). Epigenetic regulation of the INK4B-ARF-INK4a locus: In sickness and in health. *Epigenetics*, *5*(8), 685-690.

Portal, D., Zhao, B., Calderwood, M.A., Sommermann, T., Johannsen, E., and Kieff, E. (2011). EBV nuclear antigen EBNALP dismisses transcription repressors NCoR and RBPJ from enhancers and EBNA2 increases NCoR-deficient RBPJ DNA binding. *Proceedings of the National Academy of Sciences*, 201104991.

Portal, D., Zhou, H., Zhao, B., Kharchenko, P. V., Lowry, E., Wong, L., Quackenbush, J., Holloway, D., Jiang, S., Lu, Y., et al. (2013). Epstein-Barr virus nuclear antigen leader protein localizes to promoters and enhancers with cell transcription factors and EBNA2. *Proceedings of the National Academy of Sciences*, 201317608.

Price, A.M., Tourigny, J.P., Forte, E., Salinas, R.E., Dave, S.S., and Luftig, M.A. (2012). Analysis of Epstein-Barr Virus-Regulated Host Gene Expression Changes through Primary B-Cell Outgrowth Reveals Delayed Kinetics of Latent Membrane Protein 1-Mediated NF- B Activation. *Journal of virology*, JVI-01069.

Qiu, J., Smith, P., Leahy, L., and Thorley-Lawson, D.A. (2015). The Epstein-Barr Virus Encoded BART miRNAs Potentiate Tumor Growth In Vivo. *PLoS pathogens*, *11*(1), e1004561.

Quinn, L.L., Zuo, J., Abbott, R.J.M., Shannon-Lowe, C., Tierney, R.J., Hislop, A.D., and Rowe, M. (2014). Cooperation between Epstein-Barr Virus Immune Evasion Proteins Spreads Protection from CD8+T Cell Recognition across All Three Phases of the Lytic Cycle. *PLoS pathogens*, *10*(8), e1004322.

Raab-Traub, N. (2015). Nasopharyngeal carcinoma: An evolving role for the epstein–barr virus. n *Epstein Barr Virus Volume 1* (pp. 339-363). Springer, Cham.

Raab-Traub, N., and Flynn, K. (1986). The structure of the termini of the Epstein-Barr virus as a marker of clonal cellular proliferation. *Cell*, *47*(6), 883-889.

Raab-Traub, N., Dambaugh, T., and Kieff, E. (1980). DNA of Epstein-Barr virus VIII: B95-8, the previous prototype, is an unusual deletion derivative. *Cell*, *22*(1), 257-267.

Raab-Traub, N., Hood, R., Yang, C.S., Henry, B. d, and Pagano, J.S. (1983). Epstein-Barr virus transcription in nasopharyngeal carcinoma. *Journal of virology*, *48*(3), 580-590.

Rabson, M., Gradoville, L., Heston, L., and Miller, G. (1982). Non-immortalizing P3J-HR-1 Epstein-Barr virus: a deletion mutant of its transforming parent, Jijoye. *ournal of virology*, *44*(3), 834-844.

Reedman, B.M., and Klein, G. (1973). Cellular localization of an Epstein-Barr virus (EBV)-associated complement-fixing antigen in producer and non-producer lymphoblastoid cell lines. *International Journal of Cancer*, *11*(3), 499-520.

Reimold, a M., Ponath, P.D., Li, Y.S., Hardy, R.R., David, C.S., Strominger, J.L., and Glimcher, L.H. (1996). Transcription factor B cell lineage-specific activator protein regulates the gene for human X-box binding protein 1. *Journal of Experimental Medicine*, *183*(2), 393-401.

Reisman, D., Yates, J., and Sugden, B. (1985). A putative origin of replication of plasmids derived from Epstein-Barr virus is composed of two cis-acting components. *Molecular and cellular biology*, *5*(8), 1822-1832.

Reusch, J.A., Nawandar, D.M., Wright, K.L., Kenney, S.C., and Mertz, J.E. (2015). Cellular Differentiation Regulator BLIMP1 Induces Epstein-Barr Virus Lytic Reactivation in Epithelial and B Cells by Activating Transcription from both the R and Z Promoters. *Journal of virology*, *89*(3), 1731-1743.

Rezaee, R., and Abdollahi, M. (2017). The importance of translatability in drug discovery. *Expert Opin. Drug Discov.* 237-239.
Rickinson, a B., and Moss, D.J. (1997). Human cytotoxic T lymphocyte responses to Epstein-Barr virus infection. *Annual review of immunology*, *15*(1), 405-431.

Rivailler, P., Cho, Y.-G., and Wang, F. (2002). Complete genomic sequence of an Epstein-Barr virus-related herpesvirus naturally infecting a new world primate: a defining point in the evolution of oncogenic lymphocryptoviruses. *Journal of virology*, *76*(23), 12055-12068.

Robertson, E.S., Lin, J., and Kieff, E. (1996). The amino-terminal domains of Epstein-Barr virus nuclear proteins 3A 3B and 3C interact with RBPJ(kappa). *Journal of virology*, *70*(5), 3068-3074.

Rogers, R.P., Woisetschlaeger, M., and Speck, S.H. (1990). Alternative splicing dictates translational start in Epstein-Barr virus transcripts. *The EMBO journal*, *9*(7), 2273-2277.

Romero-Masters, J. C., Ohashi, M., Djavadian, R., Eichelberg, M. R., Hayes, M., Bristol, J. A., ... & Kenney, S. C. (2018). An EBNA3C-deleted Epstein-Barr virus (EBV) mutant causes B-cell lymphomas with delayed onset in a cord blood-humanized mouse model. *PLoS pathogens*, *14*(8), e1007221

Rongvaux, A., Takizawa, H., Strowig, T., Willinger, T., Eynon, E.E., Flavell, R.A., and Manz, M.G. (2013). Human Hemato-Lymphoid System Mice: Current Use and Future Potential for Medicine. *Annual review of immunology*, *31*.

Rooney, C.M., Rowe, D.T., Ragot, T., and Farrell, P.J. (1989). The spliced BZLF1 gene of Epstein-Barr virus (EBV) transactivates an early EBV promoter and induces the virus productive cycle. *Journal of virology*, *63*(7), 3109-3116.

Rosenthal, N., and Brown, S. (2007). The mouse ascending: Perspectives for human-disease models. *Nature cell biology*, *9*(9), 993.
Roughan, J.E., and Thorley-Lawson, D.A. (2009). The Intersection of Epstein-Barr Virus with the Germinal Center. *Journal of virology*, *83*(8), 3968-3976.

Le Roux, A., Kerdiles, B., Walls, D., Dedieu, J.F., and Perricaudet, M. (1994). The Epstein-Barr virus determined nuclear antigens EBNA-3A, -3B, and -3C repress EBNA-2-mediated transactivation of the viral terminal protein 1 gene promoter. *Virology*, *205*(2), 596-602.

Rovedo, M., and Longnecker, R. (2007). Epstein-Barr Virus Latent Membrane Protein 2B (LMP2B) Modulates LMP2A Activity. *Journal of virology*, *81*(1), 84-94.

Rowe, D.T., Rowe, M., Evan, G.I., Wallace, L.E., Farrell, P.J., and Rickinson, A.B. (1986). Restricted expression of EBV latent genes and T-lymphocyte-detected membrane antigen in Burkitt's lymphoma cells. *The EMBO journal*, *5*(10), 2599-2607.

Rowe, M., Rooney, C.M., Rickinson, A.B., Lenoir, G.M., Rupani, H., Moss, D.J., Stein, H., and Epstein, M.A. (1985). Distinctions between endemic and sporadic forms of epstein-barr virus-positive burkitt's lymphoma. *International journal of cancer*, *35*(4), 435-441.

Rowe, M., Rowe, D.T., Gregory, C.D., Young, L.S., Farrell, P.J., Rupani, H., and Rickinson, A.B. (1987). Differences in B cell growth phenotype reflect novel patterns of Epstein-Barr virus latent gene expression in Burkitt's lymphoma cells. *The EMBO journal*, *6*(9), 2743-2751.

Rowell, E.A., Wang, L., Chunder, N., Hancock, W.W., and Wells, A.D. (2014). Regulation of T cell differentiation and alloimmunity by the cyclin-dependent kinase inhibitor p18ink4c. *PloS one*, *9*(3), e91587.

Russell WMS, B.K. (1992). The principles of humane experimental technique. *UFAW, London.*

Ryan, J.L., Kaufmann, W.K., Raab-Traub, N., Oglesbee, S.E., Carey, L. a, and Gulley, M.L. (2006). Clonal evolution of lymphoblastoid cell lines. *Laboratory investigation*, *86*(11), 1193.

Saha, A., Murakami, M., Kumar, P., Bajaj, B., Sims, K., and Robertson, E.S. (2009). Epstein-Barr Virus Nuclear Antigen 3C Augments Mdm2-Mediated p53 Ubiquitination and Degradation by Deubiquitinating Mdm2. *Journal of virology*, *83*(9), 4652-4669.

Saha, A., Lu, J., Morizur, L., Upadhyay, S.K., AJ, M.P., and Robertson, E.S. (2012). E2F1 mediated apoptosis induced by the DNA damage response is blocked by EBV nuclear antigen 3C in lymphoblastoid cells. *PLoS pathogens*, *8*(3), e1002573.

Sample, J., Liebowitz, D., and Kieff, E. (1989). Two related Epstein-Barr virus membrane proteins are encoded by separate genes. *Journal of virology*, *63*(2), 933-937.

Sample, J., Henson, E.B., and Sample, C. (1992). The Epstein-Barr virus nuclear protein 1 promoter active in type I latency is autoregulated. *Journal of virology*, *66*(8), 4654-4661.

Sanchez-Aguilera, A. (2004). Silencing of the p18INK4c gene by promoter hypermethylation in Reed-Sternberg cells in Hodgkin lymphomas. *Blood*, *103*(6), 2351-2357.

Schaefer, B.C., Strominger, J.L., and Speck, S.H. (1995). Redefining the Epstein-Barr virus-encoded nuclear antigen EBNA-1 gene promoter and transcription initiation site in group I Burkitt lymphoma cell lines. *Proceedings of the National Academy of Sciences*, *92*(23), 10565-10569.

Schmidlin, H., Diehl, S.A., Nagasawa, M., Scheeren, F.A., Schotte, R., Uittenbogaart, C.H., Spits, H., and Blom, B. (2008). Spi-B inhibits human plasma cell differentiation by repressing BLIMP1 and XBP-1 expression. *Blood*, *112*(5), 1804-1812.
Schmidt, S.C.S., Jiang, S., Zhou, H., Willox, B., Holthaus, A.M., Kharchenko, P. V., Johannsen, E.C., Kieff, E., and Zhao, B. (2015). Epstein–Barr virus nuclear antigen 3A partially coincides with EBNA3C genome-wide and is tethered to DNA through BATF complexes. *Proceedings of the National Academy of Sciences*, *112*(2), 554-559.

Sciammas, R., Shaffer, A.L., Schatz, J.H., Zhao, H., Staudt, L.M., and Singh, H. (2006). Graded Expression of Interferon Regulatory Factor-4 Coordinates Isotype Switching with Plasma Cell Differentiation. *Immunity*, *25*(2), 225-236.

Sellin, C.I., and Horvat, B. (2009). Current animal models: Transgenic animal models for the study of measles pathogenesis. n *Measles* (pp. 111-127). Springer, Berlin, Heidelberg.

Serrano, M., Hannon, G.J., and Beach, D. (1993). A new regulatory motif in cell-cycle control causing specific inhibition of cyclin D/CDK4. *nature*, *366*(6456), 704.

Seto, E., Moosmann, A., Grömminger, S., Walz, N., Grundhoff, A., and Hammerschmidt, W. (2010). Micro RNAS of epstein-barr virus promote cell cycle progression and prevent apoptosis of primary human B cells. *PLoS pathogens*, *6*(8), e1001063.

Seung, E., and Tager, A.M. (2013). Humoral immunity in humanized mice: a work in progress. *The Journal of infectious diseases*, *208*(suppl_2), S155-S159.

Shaffer, A.L., Lin, K.I., Kuo, T.C., Yu, X., Hurt, E.M., Rosenwald, A., Giltnane, J.M., Yang, L., Zhao, H., Calame, K., et al. (2002). Blimp-1 orchestrates plasma cell differentiation by extinguishing the mature B cell gene expression program. *Immunity*, *17*(1), 51-62.

Shannon-Lowe, C., and Rowe, M. (2014). Epstein Barr virus entry; Kissing and conjugation. *Current opinion in virology*, *4*, 78-84.

Shannon-Lowe, C., Adland, E., Bell, A.I., Delecluse, H.-J., Rickinson, A.B., and Rowe, M. (2009). Features distinguishing Epstein-Barr virus infections of epithelial cells and B cells: viral genome expression, genome maintenance, and genome amplification. *Journal of virology*, *83*(15), 7749-7760.

Shapiro-Shelef, M., Lin, K.I., McHeyzer-Williams, L.J., Liao, J., McHeyzer-Williams, M.G., and Calame, K. (2003). Blimp-1 is required for the formation of immunoglobulin secreting plasma cells and pre-plasma memory B cells. *Immunity*, *19*(4), 607-620.

Sherr, C.J. (1996). Cancer cell cycles. *Science*, *274*(5293), 1672-1677.

Sherr, C.J., and Roberts, J.M. (1995). Inhibitors of mammalian G1 cyclin-dependent kinases. *Genes & development*, *9*(10), 1149-1163.

Sherr, C.J., and Roberts, J.M. (1999). CDK inhibitors: Positive and negative regulators of G1-phase progression. *Genes & development*, *13*(12), 1501-1512.

Shetab-Boushehri, S.V., and Abdollahi, M. (2012). Current concerns on the validity of in vitro models that use transformed neoplastic cells in pharmacology and toxicology. *Int. J. Pharmacol.* 594-595.

Shi, W., Liao, Y., Willis, S.N., Taubenheim, N., Inouye, M., Tarlinton, D.M., Smyth, G.K., Hodgkin, P.D., Nutt, S.L., and Corcoran, L.M. (2015). Transcriptional profiling of mouse B cell terminal differentiation defines a signature for antibody-secreting plasma cells. *Nature immunology*, *16*(6), 663.

Shiloh, Y. (2003). ATM and related protein kinases: Safeguarding genome integrity. *Nature Reviews Cancer*, *3*(3), 155.

Shinkai, Y., Rathbun, 0Gary, Lam, K.P., Oltz, E.M., Stewart, V., Mendelsohn, M., Charron, J., Datta, M., Young, F., Stall, A.M., et al. (1992). RAG-2-deficient mice lack mature lymphocytes owing to inability to initiate V(D)J rearrangement. *Cell*, *68*(5), 855-867.

Shlomchik, M.J., and Weisel, F. (2012). Germinal center selection and the development of memory B and plasma cells. *Immunological reviews*, *247*(1), 52-63.

Shulman, Z., Gitlin, A.D., Weinstein, J.S., Lainez, B., Esplugues, E., Flavell, R.A., Craft, J.E., and Nussenzweig, M.C. (2014). Dynamic signaling by T follicular helper cells during germinal center B cell selection. *Science*, *345*(6200), 1058-1062.

Shultz, L.D., Ishikawa, F., and Greiner, D.L. (2007). Humanized mice in translational biomedical research. *Nature Reviews Immunology*, *7*(2), 118.

Shultz, L.D., Saito, Y., Najima, Y., Tanaka, S., Ochi, T., Tomizawa, M., Doi, T., Sone, A., Suzuki, N., Fujiwara, H., et al. (2010). Generation of functional human T-cell subsets with HLA-restricted immune responses in HLA class I expressing NOD/SCID/IL2rγnull humanized mice. *Proceedings of the National Academy of Sciences*, *107*(29), 13022-13027.

Shultz, L.D., Brehm, M.A., Victor Garcia-Martinez, J., and Greiner, D.L. (2012). Humanized mice for immune system investigation: Progress, promise and challenges. *Nature Reviews Immunology*, *12*(11), 786.

Siouda, M., Frecha, C., Accardi, R., Yue, J., Cuenin, C., Gruffat, H., Manet, E., Herceg, Z., Sylla, B.S., and Tommasino, M. (2014). Epstein-Barr Virus Down-Regulates Tumor Suppressor DOK1 Expression. *PLoS pathogens*, *10*(5), e1004125.

Sjoblom, A., Jansson, A., Yang, W., Lain, S., Nilsson, T., and Rymo, L. (1995). PU box-binding transcription factors and a POU domain protein cooperate in the Epstein-Barr virus (EBV) nuclear

antigen 2-induced transactivation of the EBV latent membrane protein 1 promoter. *Journal of general virology*, *76*(11), 2679-2692.

Skalska, L., White, R.E., Franz, M., Ruhmann, M., and Allday, M.J. (2010). Epigenetic repression of p16INK4A by latent epstein-barr virus requires the interaction of EBNA3A and EBNA3C with CtBP. *PLoS pathogens*, *6*(6), e1000951.

Skalska, L., White, R.E., Parker, G.A., Sinclair, A.J., Paschos, K., and Allday, M.J. (2013). Induction of p16INK4a Is the Major Barrier to Proliferation when Epstein-Barr Virus (EBV) Transforms Primary B Cells into Lymphoblastoid Cell Lines. *PLoS pathogens*, *9*(2), e1003187.

Sorrentino, J.A., Krishnamurthy, J., Tilley, S., Alb, J.G., Burd, C.E., and Sharpless, N.E. (2014). P16INK4a reporter mice reveal age-promoting effects of environmental toxicants. *The Journal of clinical investigation*, *124*(1), 169-173.

Speck, P., Kline, K.A., Cheresh, P., and Longnecker, R. (1999). Epstein-Barr virus lacking latent membrane protein 2 immortalizes B cells with efficiency indistinguishable from that of wild-type virus. *Journal of general virology*, *80*(8), 2193-2203.

Speck, S.H., Pfitzner, A., and Strominger, J.L. (1986). An Epstein-Barr virus transcript from a latently infected, growth-transformed B-cell line encodes a highly repetitive polypeptide. *Proceedings of the National Academy of Sciences*, *83*(24), 9298-9302.

Strasser, A. (2005). The role of BH3-only proteins in the immune system. *Nature Reviews Immunology*, *5*(3), 189.

Strowig, T., Gurer, C., Ploss, A., Liu, Y.-F., Arrey, F., Sashihara, J., Koo, G., Rice, C.M., Young, J.W., Chadburn, A., et al. (2009). Priming of protective T cell responses against virus-induced tumors in mice with human immune system components. *Journal of Experimental Medicine*, *206*(6), 1423-1434.

Styles, C., Paschos, K., White, R., and Farrell, P. (2018). The Cooperative Functions of the EBNA3 Proteins Are Central to EBV Persistence and Latency. *Pathogens*, *7*(1), 31.

Styles, C.T., Bazot, Q., Parker, G.A., White, R.E., Paschos, K., and Allday, M.J. (2017). EBV epigenetically suppresses the B cell-to-plasma cell differentiation pathway while establishing long-term latency. *PLoS biology*, *15*(8), e2001992.

Su, S., Zhang, M., Li, L., and Wu, M. (2014). Polycomb group genes as the key regulators in gene silencing. *Wuhan University Journal of Natural Sciences*, *19*(1), 1-7.

Suan, D., Sundling, C., and Brink, R. (2017). Plasma cell and memory B cell differentiation from the germinal center. *Current opinion in immunology*, *45*, 97-102.

Sugden, B., and Warren, N. (1989). A promoter of Epstein-Barr virus that can function during latent infection can be transactivated by EBNA-1, a viral protein required for viral DNA replication during latent infection. *Journal of virology*, *63*(6), 2644-2649.

Swaminathan, S., Tomkinson, B., and Kieff, E. (1991). Recombinant Epstein-Barr virus with small RNA (EBER) genes deleted transforms lymphocytes and replicates in vitro. *Proceedings of the National Academy of Sciences*, *88*(4), 1546-1550.

Szymula, A., Palermo, R.D., Bayoumy, A., Groves, I.J., Ba abdullah, M., Holder, B., and White, R.E. (2018). Epstein-Barr virus nuclear antigen EBNA-LP is essential for transforming naïve B cells, and facilitates recruitment of transcription factors to the viral genome. *PLoS pathogens*, *14*(2), e1006890.

Tagawa, T., Albanese, M., Bouvet, M., Moosmann, A., Mautner, J., Heissmeyer, V., Zielinski, C., Lutter, D., Hoser, J., Hastreiter, M., et al. (2016). Epstein-Barr viral miRNAs inhibit antiviral CD4 $^{+}$ T cell responses targeting IL-12 and peptide processing. *Journal of Experimental Medicine*, *213*(10), 2065-2080.

Takenaka, K., Prasolava, T.K., Wang, J.C.Y., Mortin-Toth, S.M., Khalouei, S., Gan, O.I., Dick, J.E., and Danska, J.S. (2007). Polymorphism in Sirpa modulates engraftment of human hematopoietic stem cells. *Nature immunology*, *8*(12), 1313.

Taub, R., Kirsch, I., Morton, C., Lenoir, G., Swan, D., Tronick, S., Aaronson, S., and Leder, P. (1982). Translocation of the c-myc gene into the immunoglobulin heavy chain locus in human Burkitt lymphoma and murine plasmacytoma cells. *Proceedings of the National Academy of Sciences*, *79*(24), 7837-7841.

Taylor, J.J., Pape, K.A., and Jenkins, M.K. (2012). A germinal center–independent pathway generates unswitched memory B cells early in the primary response. *Journal of Experimental Medicine*, *209*(3), 597-606.

Tellier, J., Shi, W., Minnich, M., Liao, Y., Crawford, S., Smyth, G.K., Kallies, A., Busslinger, M., and Nutt, S.L. (2016). Blimp-1 controls plasma cell function through the regulation of immunoglobulin secretion and the unfolded protein response. *Nature immunology*, *17*(3), 323.

Tempera, I., and Lieberman, P.M. (2010). Chromatin organization of gammaherpesvirus latent genomes. *Biochimica et Biophysica Acta (BBA)-Gene Regulatory Mechanisms*, *1799*(3), 236-245.

Temple, R.M., Zhu, J., Budgeon, L., Christensen, N.D., Meyers, C., and Sample, C.E. (2014). Efficient replication of Epstein–Barr virus in stratified epithelium in vitro. *Proceedings of the National Academy of Sciences*, *111*(46), 16544-16549.

Thacker, E.L., Mirzaei, F., and Ascherio, A. (2006). Infectious mononucleosis and risk for multiple sclerosis: A meta-analysis. *Annals of neurology*, *59*(3), 499-503.

Thelander, E.F., Ichimura, K., Corcoran, M., Barbany, G., Nordgren, A., Heyman, M., Berglund, M., Mungall, A., Rosenquist, R., Collins, V.P., et al. (2008). Characterization of 6q deletions in mature B cell lymphomas and childhood acute lymphoblastic leukemia. *Leukemia & lymphoma*, *49*(3), 477-487.

Thomas, M.D., Srivastava, B., and Allman, D. (2006). Regulation of peripheral B cell maturation. *Cellular immunology*, *239*(2), 92-102.

Thorley-Lawson, D.A. (2001). Epstein-Barr virus: Exploiting the immune system. *Nature Reviews Immunology*, *1*(1), 75.

Thorley-Lawson, D.A. (2015). EBV persistence-introducing the virus. In *Epstein Barr Virus Volume 1* (pp. 151-209). Springer, Cham.

Thorley-Lawson, D., and Babcock, G. (1999). A model for persistent infection with Epstein-Barr virus: the stealth virus of human B cells. *Life sciences*, *65*(14), 1433-1453.

Thorley-Lawson, D.A., and Allday, M.J. (2008). The curious case of the tumour virus: 50 years of Burkitt's lymphoma. *Nature Reviews Microbiology*, *6*(12), 913.

Thullberg, M., Bartkova, J., Khan, S., Hansen, K., Rönnstrand, L., Lukas, J., Strauss, M., and Bartek, J. (2000). Distinct versus redundant properties among members of the INK4 family of cyclin-dependent kinase inhibitors. *FEBS letters*, *470*(2), 161-166.

Tomkinson, B., and Kieff, E. (1992). Use of second-site homologous recombination to demonstrate that Epstein-Barr virus nuclear protein 3B is not important for lymphocyte infection or growth transformation in vitro. *Journal of virology*, *66*(5), 2893-2903.

Tomkinson, B., Robertson, E., and Kieff, E. (1993). Epstein-Barr virus nuclear proteins EBNA-3A and EBNA-3C are essential for B-lymphocyte growth transformation. *Journal of virology*, *67*(4), 2014-2025.

Touitou, R., Hickabottom, M., Parker, G., Crook, T., and Allday, M.J. (2001). Physical and functional interactions between the corepressor CtBP and the Epstein-Barr virus nuclear antigen EBNA3C. *Journal of virology*, *75*(16), 7749-7755.

Touitou, R., O'Nions, J., Heaney, J., and Allday, M.J. (2005). Epstein-Barr virus EBNA3 proteins bind to the C8/α7 subunit of the 20S proteasome and are degraded by 20S proteasomes in vitro, but are very stable in latently infected B cells. *Journal of general virology*, *86*(5), 1269-1277.

Tourigny, M.R., Ursini-Siegel, J., Lee, H., Toellner, K.-M., Cunningham, A.F., Franklin, D.S., Ely, S., Chen, M., Qin, X.-F., Xiong, Y., et al. (2002). CDK inhibitor $p18^{INK4c}$ is required for the generation of functional plasma cells. *Immunity*, *17*(2), 179-189.

Traggiai, E., Chicha, L., Mazzucchelli, L., Bronz, L., Piffaretti, J.C., Lanzavecchia, A., and Manz, M.G. (2004). Development of a Human Adaptive Immune System in Cord Blood Cell-Transplanted Mice. *Science*, *304*(5667), 104-107.

Tunyaplin, C., Shaffer, A.L., Angelin-Duclos, C.D., Yu, X., Staudt, L.M., and Calame, K.L. (2004). Direct Repression of prdm1 by Bcl-6 Inhibits Plasmacytic Differentiation. *The Journal of Immunology*, *173*(2), 1158-1165.

Turner, C.A., Mack, D.H., and Davis, M.M. (1994). Blimp-1, a novel zinc finger-containing protein that can drive the maturation of B lymphocytes into immunoglobulin-secreting cells. *Cell*, *77*(2), 297-306.

Tursiella, M.L., Bowman, E.R., Wanzeck, K.C., Throm, R.E., Liao, J., Zhu, J., and Sample, C.E. (2014). Epstein-Barr Virus Nuclear Antigen 3A Promotes Cellular Proliferation by Repression of the Cyclin-Dependent Kinase Inhibitor p21WAF1/CIP1. *PLoS pathogens*, *10*(10), e1004415.

Uchida, J., Yasui, T., Takaoka-Shichijo, Y., Muraoka, M., Kulwichit, W., Raab-Traub, N., and Kikutani, H. (1999). Mimicry of CD40 signals by Epstein-Barr virus LMP1 in B lymphocyte responses. *Science*, *286*(5438), 300-303.

Ulff-Møller, C.J., Nielsen, N.M., Rostgaard, K., Hjalgrim, H., and Frisch, M. (2010). Epstein-Barr virus-associated infectious mononucleosis and risk of systemic lupus erythematosus. *Rheumatology*, *49*(9), 1706-1712.

Vereide, D.T., Seto, E., Chiu, Y.F., Hayes, M., Tagawa, T., Grundhoff, A., Hammerschmidt, W., and Sugden, B. (2014). Epstein-Barr virus maintains lymphomas via its miRNAs. *Oncogene*, *33*(10), 1258.

Victora, G.D., and Nussenzweig, M.C. (2012). Germinal Centers. *Annual review of immunology*, *30*, 429-457.

Victora, G.D., Schwickert, T.A., Fooksman, D.R., Kamphorst, A.O., Meyer-Hermann, M., Dustin, M.L., and Nussenzweig, M.C. (2010). Germinal center dynamics revealed by multiphoton microscopy with a photoactivatable fluorescent reporter. *Cell*, *143*(4), 592-605.

Vizán, P., Beringer, M., Ballaré, C., and Di Croce, L. (2015). Role of PRC2-associated factors in stem cells and disease. *The FEBS journal*, *282*(9), 1723-1735.

Vrzalikova, K., Vockerodt, M., Leonard, S., Bell, A., Wei, W., Schrader, A., Wright, K.L., Kube, D., Rowe, M., Woodman, C.B., et al. (2011). Down-regulation of BLIMP1 by the EBV oncogene, LMP-1, disrupts the plasma cell differentiation program and prevents viral replication in B cells: implications for the pathogenesis of EBV-associated B-cell lymphomas. *Blood*.

Waga, S., Hannon, G.J., Beach, D., and Stillman, B. (1994). The p21 inhibitor of cyclin-dependent kinases controls DNA replication by interaction with PCNA. *Nature*, *369*(6481), 574.

Wang, A., Welch, R., Zhao, B., Ta, T., Keleş, S., and Johannsen, E. (2015). EBNA3 proteins regulate EBNA2 binding to distinct RBPJ genomic sites. *Journal of virology*, *90*(6), 2906-2919.

Wang, F., Tsang, S.F., Kurilla, M.G., Cohen, J.I., and Kieff, E. (1990). Epstein-Barr virus nuclear antigen 2 transactivates latent membrane protein LMP1. *Journal of virology*, *64*(7), 3407-3416.

Wang, H., Wang, L., Erdjument-Bromage, H., Vidal, M., Tempst, P., Jones, R.S., and Zhang, Y. (2004). Role of histone H2A ubiquitination in Polycomb silencing. *nature*, *431*(7010), 873.

Wang, H., Beyer, I., Persson, J., Song, H., Li, Z., Richter, M., Cao, H., van Rensburg, R., Yao, X., Hudkins, K., et al. (2012). A new human DSG2-transgenic mouse model for studying the tropism and pathology of human adenoviruses. *Journal of virology*, JVI-00205.

Wang, S., Medeiros, L.J., Xu-Monette, Z.Y., Zhang, S., O'Malley, D.P., Orazi, A., Zuo, Z., Bueso-Ramos, C.E., Yin, C.C., Liu, Z., et al. (2014). Epstein-Barr virus-positive nodular lymphocyte predominant Hodgkin lymphoma. *Annals of diagnostic pathology*, *18*(4), 203-209.

Wardemann, H., Yurasov, S., Schaefer, A., Young, J.W., Meffre, E., and Nussenzweig, M.C. (2003). Predominant autoantibody production by early human B cell precursors. *Science*, *301*(5638), 1374-1377.

Washburn, M.L., Bility, M.T., Zhang, L., Kovalev, G.I., Buntzman, A., Frelinger, J.A., Barry, W., Ploss, A., Rice, C.M., and Su, L. (2011). A humanized mouse model to study hepatitis C virus infection, immune response, and liver disease. *Gastroenterology*, *140*(4), 1334-1344.

Watanabe, Y., Takahashi, T., Okajima, A., Shiokawa, M., Ishii, N., Katano, I., Ito, R., Ito, M., Minegishi, M., Minegishi, N., et al. (2009). The analysis of the functions of human B and T cells in humanized NOD/shi-scid/gammac(null) (NOG) mice (hu-HSC NOG mice). *International immunology*, *21*(7), 843-858.

Waterston, R.H., Lindblad-Toh, K., Birney, E., Rogers, J., Abril, J.F., Agarwal, P., Agarwala, R., Ainscough, R., Alexandersson, M., An, P., et al. (2002). Initial sequencing and comparative analysis of the mouse genome. *Nature*, *420*(6915), 520.

Weinberg, R.A. (1995). The retinoblastoma protein and cell cycle control. *Cell*, *81*(3), 323-330.

Weinreb, M., Day, P.J., Niggli, F., Green, E.K., Nyong'o, A.O., Othieno-Abinya, N.A., Riyat, M.S., Raafat, F., and Mann, J.R. (1996). The consistent association between Epstein-Barr virus and Hodgkin's disease in children in Kenya. *Blood*, *87*(9), 3828-3836.

Weisel, F.J., Zuccarino-Catania, G. V., Chikina, M., and Shlomchik, M.J. (2016). A Temporal Switch in the Germinal Center Determines Differential Output of Memory B and Plasma Cells. *Immunity*, *44*(1), 116-130.

West, M.J. (2017). Chromatin reorganisation in Epstein-Barr virus-infected cells and its role in cancer development. *Current opinion in virology*, *26*, 149-155.

White, R.E., Calderwood, M.A., and Whitehouse, A. (2003). Generation and precise modification of a herpesvirus saimiri bacterial artificial chromosome demonstrates that the terminal repeats are

required for both virus production and episomal persistence. *Journal of General Virology*, *84*(12), 3393-3403.

White, R.E., Groves, I.J., Turro, E., Yee, J., Kremmer, E., and Allday, M.J. (2010). Extensive co-operation between the Epstein-Barr virus EBNA3 proteins in the manipulation of host gene expression and epigenetic chromatin modification. *PloS one*, *5*(11), e13979.

White, R.E., Rämer, P.C., Naresh, K.N., Meixlsperger, S., Pinaud, L., Rooney, C., Savoldo, B., Coutinho, R., Bödör, C., Gribben, J., et al. (2012). EBNA3B-deficient EBV promotes B cell lymphomagenesis in humanized mice and is found in human tumors. *The Journal of clinical investigation*, *122*(4).

Whitfield, J., Littlewood, T., Evan, G.I., and Soucek, L. (2015). The estrogen receptor fusion system in mouse models: a reversible switch. *Cold Spring Harbor Protocols*, *2015*(3), pdb-top069815.

Whyte, W.A., Orlando, D.A., Hnisz, D., Abraham, B.J., Lin, C.Y., Kagey, M.H., Rahl, P.B., Lee, T.I., and Young, R.A. (2013). Master transcription factors and mediator establish super-enhancers at key cell identity genes. *Cell*, *153*(2), 307-319.

Williams, H., McAulay, K., Macsween, K.F., Gallacher, N.J., Higgins, C.D., Harrison, N., Swerdlow, A.J., and Crawford, D.H. (2005). The immune response to primary EBV infection: A role for natural killer cells. *British journal of haematology*, *129*(2), 266-274.

Wilson, C.H., Gamper, I., Perfetto, A., Auw, J., Littlewood, T.D., and Evan, G.I. (2014). The kinetics of ER fusion protein activation in vivo. *Oncogene*, *33*(40), 4877.

Wirtz, T., Weber, T., Kracker, S., Sommermann, T., Rajewsky, K., and Yasuda, T. (2016). Mouse model for acute Epstein-Barr virus infection. *Proceedings of the National Academy of Sciences*, *113*(48), 13821-13826.

Woisetschlaeger, M., Yandava, C.N., Furmanski, L.A., Strominger, J.L., and Speck, S.H. (1990). Promoter switching in Epstein-Barr virus during the initial stages of infection of B lymphocytes. *Proceedings of the National Academy of Sciences*, *87*(5), 1725-1729.

Woisetschlaeger, M., Jin, X.W., Yandava, C.N., Furmanski, L. a, Strominger, J.L., and Speck, S.H. (1991). Role for the Epstein-Barr virus nuclear antigen 2 in viral promoter switching during initial stages of infection. *Proceedings of the National Academy of Sciences*, *88*(9), 3942-3946.

Wood, C.D., Veenstra, H., Khasnis, S., Gunnell, A., Webb, H.M., Shannon-Lowe, C., Andrews, S., Osborne, C.S., and West, M.J. (2016). MYC activation and BCL2L11 silencing by a tumour virus through the large-scale reconfiguration of enhancer-promoter hubs. *Elife*, *5*, e18270.

Wysokenski, D. a, and Yates, J.L. (1989). Multiple EBNA1-binding sites are required to form an EBNA1-dependent enhancer and to activate a minimal replicative origin within oriP of Epstein-Barr virus. *Journal of virology*, *63*(6), 2657-2666.

Xiong, Y., Hannon, G.J., Zhang, H., Casso, D., Kobayashi, R., and Beach, D. (1993). P21 is a universal inhibitor of cyclin kinases. *nature*, *366*(6456), 701.

Yajima, M., Kanda, T., and Takada, K. (2005). Critical role of Epstein-Barr Virus (EBV)-encoded RNA in efficient EBV-induced B-lymphocyte growth transformation. *Journal of virology*, *79*(7), 4298-4307.

Yajima, M., Imadome, K., Nakagawa, A., Watanabe, S., Terashima, K., Nakamura, H., Ito, M., Shimizu, N., Honda, M., Yamamoto, N., et al. (2008). A New Humanized Mouse Model of Epstein-Barr Virus Infection That Reproduces Persistent Infection, Lymphoproliferative Disorder, and Cell-Mediated and Humoral Immune Responses. *The Journal of infectious diseases*, *198*(5), 673-682.

Yan, Y., Frisén, J., Lee, M.H., Massagué, J., and Barbacid, M. (1997). Ablation of the CDK inhibitor p57(Kip2) results in increased apoptosis and delayed differentiation during mouse development. *Genes & development*, *11*(8), 973-983.

Yates, J., Warren, N., Reisman, D., and Sugden, B. (1984). A cis-acting element from the Epstein-Barr viral genome that permits stable replication of recombinant plasmids in latently infected cells. *Proceedings of the National Academy of Sciences*, *81*(12), 3806-3810.

Yates, J.L., Warren, N., and Sugden, B. (1985). Stable replication of plasmids derived from Epstein-Barr virus in various mammalian cells. *Nature*, *313*(6005), 812.

Yee, J., White, R.E., Anderton, E., and Allday, M.J. (2011). Latent Epstein-Barr virus can inhibit apoptosis in B cells by blocking the induction of NOXA expression. *PLoS One*, *6*(12), e28506.

Yenamandra, S.P., Sompallae, R., Klein, G., and Kashuba, E. (2009). Comparative analysis of the Epstein-Barr virus encoded nuclear proteins of EBNA-3 family. *Computers in biology and medicine*, *39*(11), 1036-1042.

Yi, F., Saha, A., Murakami, M., Kumar, P., Knight, J.S., Cai, Q., Choudhuri, T., and Robertson, E.S. (2009). Epstein-Barr virus nuclear antigen 3C targets p53 and modulates its transcriptional and apoptotic activities. *Virology*, *388*(2), 236-247.

Young, L.S., and Rickinson, A.B. (2004). Epstein-Barr virus: 40 Years on. *Nature Reviews Cancer*, *4*(10), 757.

Young, K.A., Chen, X.S., Holers, V.M., and Hannan, J.P. (2007). Isolating the Epstein-Barr virus gp350/220 binding site on complement receptor type 2 (CR2/CD21). *Journal of biological chemistry*, *282*(50), 36614-36625.

Yu, Y.H., and Lin, K.I. (2016). Factors That Regulate the Generation of Antibody-Secreting Plasma Cells. In *Advances in immunology* (Vol. 131, pp. 61-99). Academic Press.

Zhang, B., Kracker, S., Yasuda, T., Casola, S., Vanneman, M., Hömig-Hölzel, C., Wang, Z., Derudder, E., Li, S., Chakraborty, T., et al. (2012). Immune surveillance and therapy of lymphomas driven by Epstein-Barr virus protein LMP1 in a mouse model. *Cell*, *148*(4), 739-751

Zhang, H., Li, Y., Wang, H.B., Zhang, A., Chen, M.L., Fang, Z.X., Dong, X.D., Li, S.B., Du, Y., Xiong, D., et al. (2018a). Ephrin receptor A2 is an epithelial cell receptor for Epstein-Barr virus entry. *Nature microbiology*, *3*(2), 164.

Zhang, P., Liégeois, N.J., Wong, C., Finegold, M., Hou, H., Thompson, J.C., Silverman, A., Harper, J.W., DePinho, R.A., and Elledge, S.J. (1997). Altered cell differentiation and proliferation in mice lacking p57(KIP2) indicates a role in Beckwith-Wiedemann syndrome. *Nature*, *387*(6629), 151-158.

Zhang, Y., Xiong, Y., and Yarbrough, W.G. (1998). ARF promotes MDM2 degradation and stabilizes p53: ARF-INK4a locus deletion impairs both the Rb and p53 tumor suppression pathways. *Cell*, *92*(6), 725-734.

Zhang, Y., Tech, L., George, L.A., Acs, A., Durrett, R.E., Hess, H., Walker, L.S.K., Tarlinton, D.M., Fletcher, A.L., Hauser, A.E., et al. (2018b). Plasma cell output from germinal centers is regulated by signals from Tfh and stromal cells. *Journal of Experimental Medicine*, *215*(4), 1227-1243.

Zhao, B., Marshall, D.R., and Sample, C.E. (1996). A conserved domain of the Epstein-Barr virus nuclear antigens 3A and 3C binds to a discrete domain of Jkappa. *Journal of virology*, *70*(7), 4228-4236.

Zhou, W., Zhu, P., Wang, J., Pascual, G., Ohgi, K.A., Lozach, J., Glass, C.K., and Rosenfeld, M.G. (2008). Histone H2A Monoubiquitination Represses Transcription by Inhibiting RNA Polymerase II Transcriptional Elongation. *Molecular cell*, *29*(1), 69-80.

Zhu, H.Z., Chen, J.Q., Cheng, G.X., and Xue, J.L. (2003). Generation and characterization of transgenic mice expressing tamoxifen-inducible cre-fusion protein specifically in mouse liver. *World Journal of Gastroenterology: WJG*, *9*(8), 1844.

8. Appendix

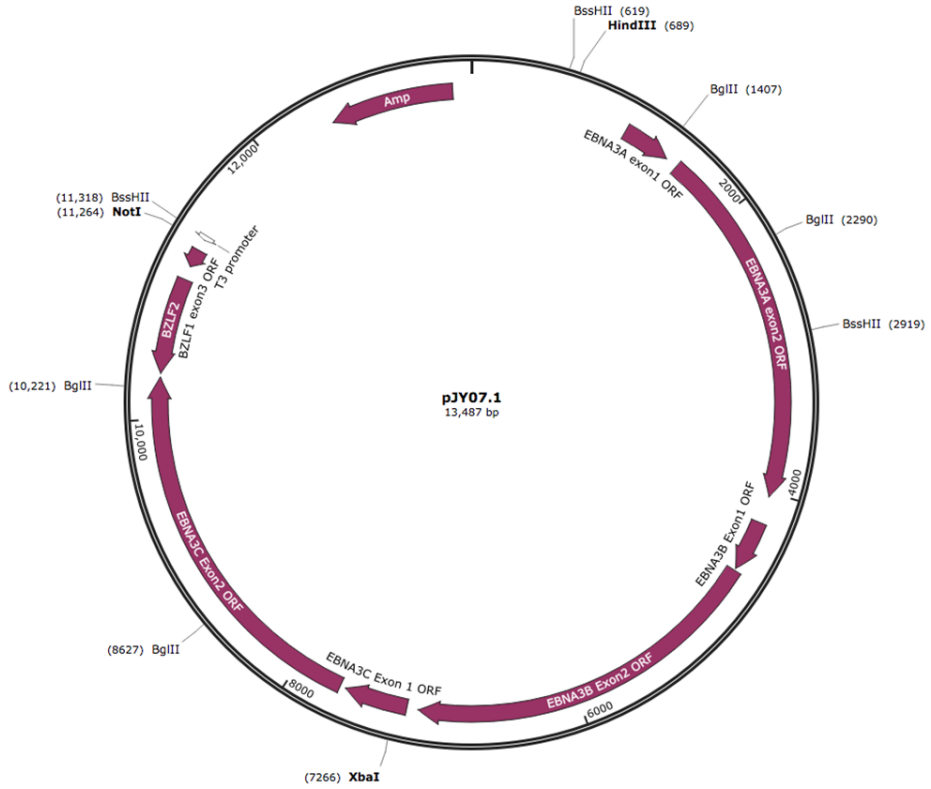


Figure 8.1. Map of pJY07.1 and restriction digest sites used for the generation of the 3A3CERT2 EBV-BAC. pJY07.1 was used as the source of the EBNA3 genes for the construction of the 3A3CERT2 EBV-BAC as detailed in Chapter III.

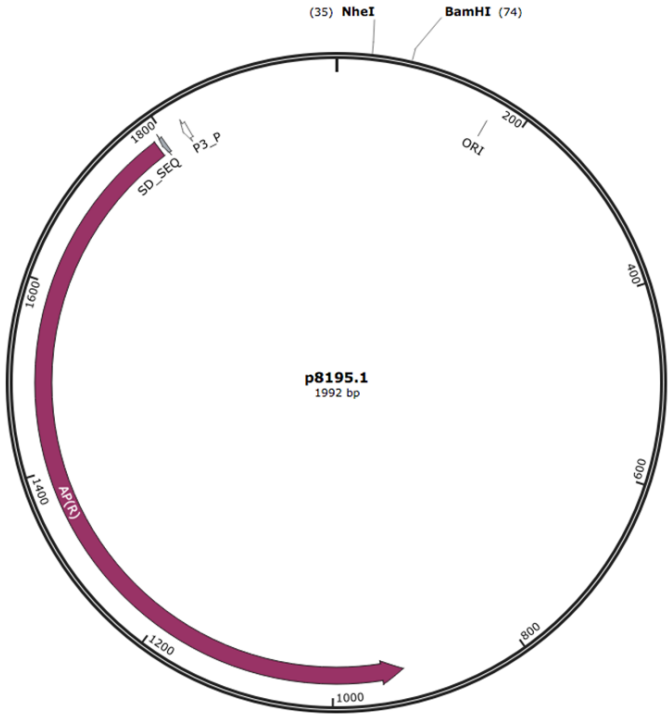


Figure 8.2. Map of p8195.1 and restriction digest sites used for the generation of the 3A3CERT2 EBV-BAC. p8195.7 was used as shuttle vector during the early stages of 3A3CERT2 EBV-BAC construction as described in Chapter III, due to multiple cloning sites and ampicillin resistance.

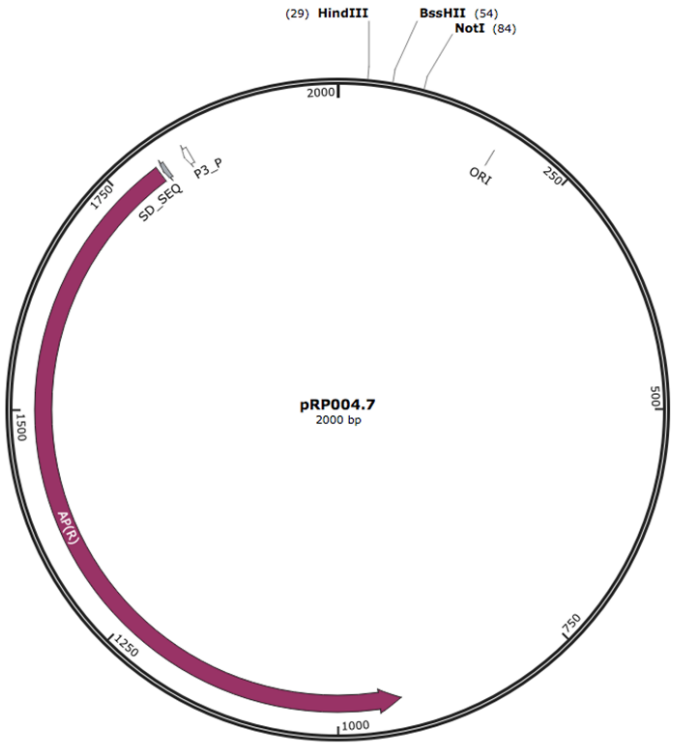


Figure 8.3. Map of pRP004.7 and restriction digest sites used for the generation of the 3A3CERT2 EBV-BAC. pRP004.7 was used as shuttle vector during the early stages of 3A3CERT2 EBV-BAC construction as described in Chapter III, due to multiple cloning sites and ampicillin resistance.

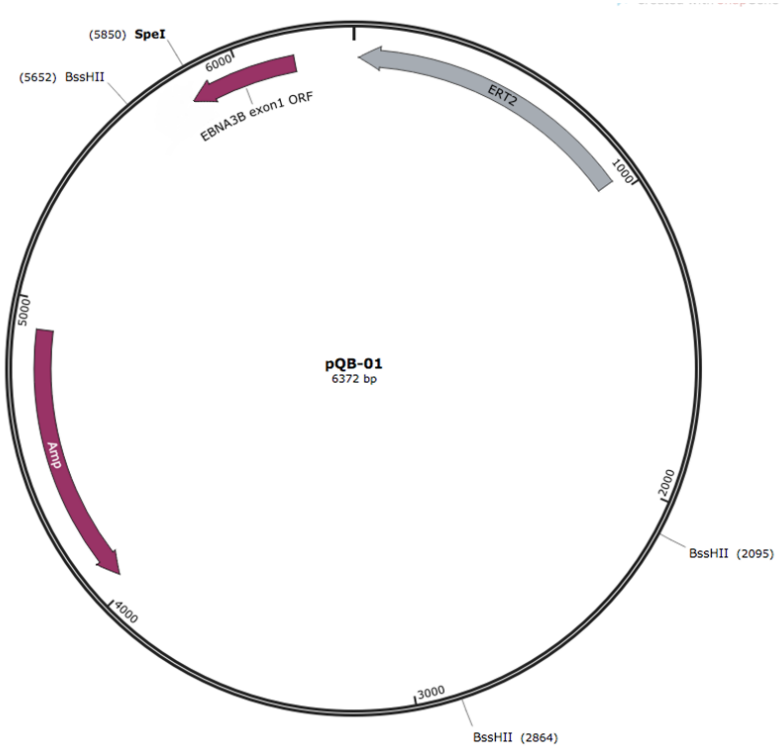


Figure 8.4. Map of pQB-01 and restriction digest sites used for the generation of the 3A3CERT2 EBV-BAC. pQB-01 was used as a source of the ERT2 gene for the construction of the 3A3CERT2 EBV-BAC as detailed in Chapter III.

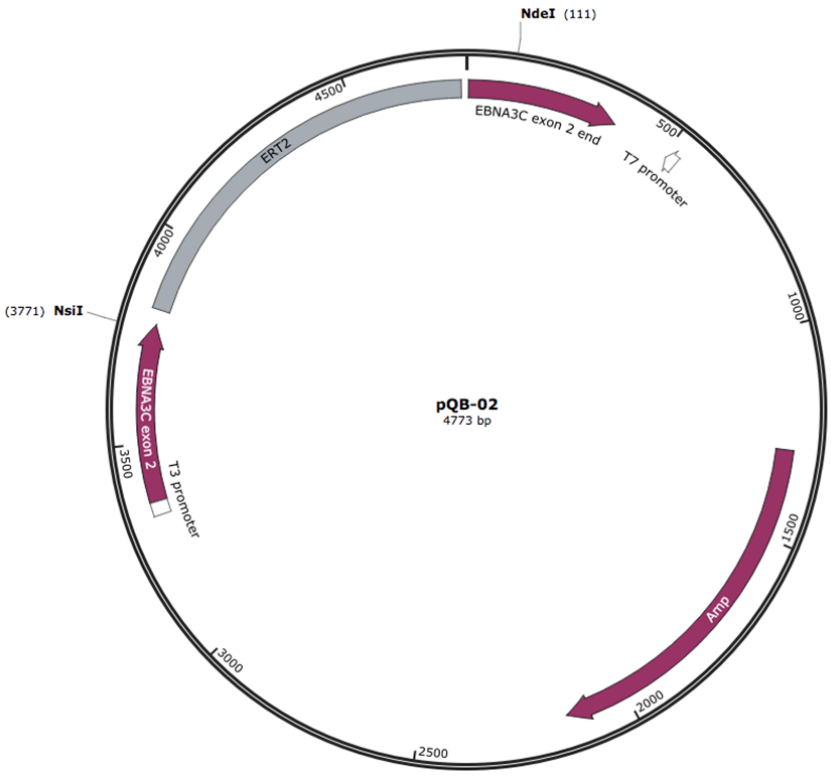


Figure 8.5. Map of pQB-02 and restriction digest sites used for the generation of the 3A3CERT2 EBV-BAC. pQB-02 was used as a source of the ERT2 gene for the construction of the 3A3CERT2 EBV-BAC as detailed in Chapter III.

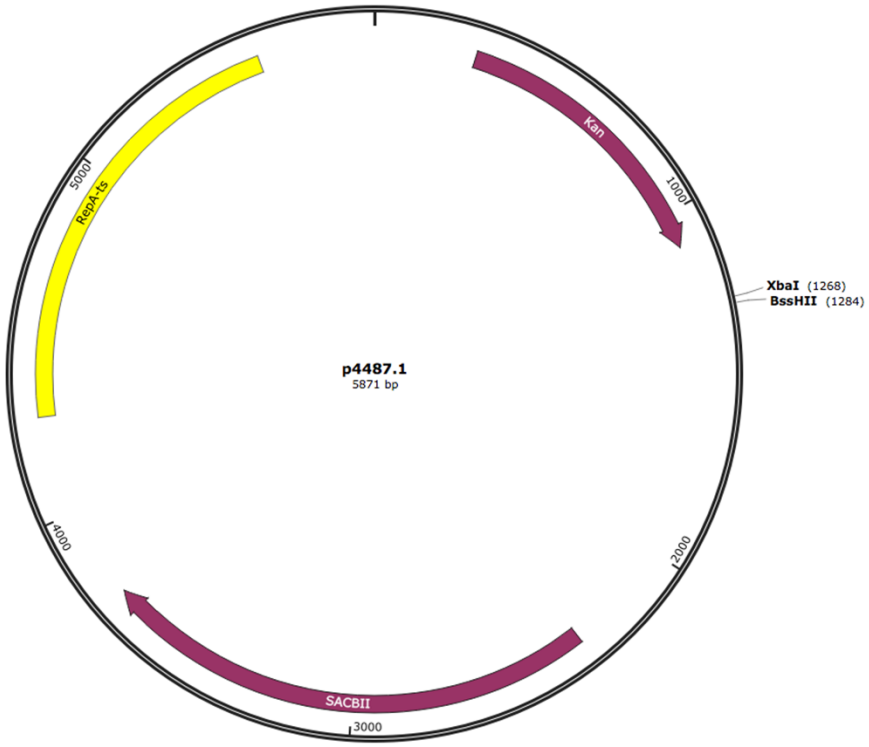


Figure 8.6. Map of p4487.1 and restriction digest sites used for the generation of the 3A3CERT2 EBV-BAC. p4487.1 was used as a shuttle vector for insertion of modified EBNA3 genes into the E3KO BAC to create the 3A3CERT2 EBV-BAC as detailed in Chapter III.